NASA TECHNICAL NOTE

NASA TN D-5333

NASA TN D-5333

EFFECTS OF JET-EXHAUST LOCATION ON THE LONGITUDINAL AERODYNAMIC CHARACTERISTICS OF A JET V/STOL MODEL

by Arthur W. Carter

Langley Research Center
Langley Station, Hampton, Va.

NATIONAL AERONAUTICS AND SPACE ADMINISTRATION • WASHINGTON, D. C. • JULY 1969

1. Report No. NASA TN D-5333	2. Government Accession No.	3. Recipient's Catalog No.
4. Title and Subtitle EFFECTS OF JET-EXHAUST LOCATION ON THE LONGITUDINAL AERODYNAMIC CHARACTERISTICS OF A JET V/STOL MODEL		5. Report Date July 1969 6. Performing Organization Code
7. Author(s) Arthur W. Carter		8. Performing Organization Report No. L-6479
9. Performing Organization Name and Address NASA Langley Research Center Langley Station Hampton, Va. 23365		10. Work Unit No. 721-01-00-18-23 11. Contract or Grant No. 13. Type of Report and Period Covered Technical Note
12. Sponsoring Agency Name and Address National Aeronautics and Space Administration Washington, D.C. 20546		14. Sponsoring Agency Code

15. Supplementary Notes

16. Abstract

A wind-tunnel investigation of the jet-location interference effects on the longitudinal aerodynamic characteristics of a jet V/STOL model has been made for an unswept, untapered wing with an aspect ratio of 6 and 30-percent-chord slotted flaps. The effects of jet location were explored systematically from several wing-chord lengths ahead to several chord lengths behind the wing. Various vertical locations were also investigated. Aerodynamic and pressure data are presented.

17. Key Words Suggested by Author(s) Jet interference V/STOL Aerodynamic characteristics	18. Distribution Statement Unclassified – Unlimited		
19. Security Classif. (of this report) Unclassified	20. Security Classif. (of this page) Unclassified	21. No. of Pages 133	22. Price* $3.00

*For sale by the Clearinghouse for Federal Scientific and Technical Information
Springfield, Virginia 22151

Page Intentionally Left Blank

EFFECTS OF JET-EXHAUST LOCATION ON THE LONGITUDINAL AERODYNAMIC CHARACTERISTICS OF A JET V/STOL MODEL

By Arthur W. Carter
Langley Research Center

SUMMARY

A wind-tunnel investigation of the jet-location interference effects on the longitudinal aerodynamic characteristics of a jet V/STOL model has been made for an unswept, untapered wing with an aspect ratio of 6 and 30-percent-chord slotted flaps. The effects of jet location were explored systematically from several wing-chord lengths ahead to several chord lengths behind the wing. Various vertical locations of the jets were also investigated.

The results indicated that all locations of the jet exhaust ahead of the wing resulted in a detrimental effect on the wing lift. This detrimental lift interference reached a minimum at approximately 0.8 chord below the wing. Locations of the jet exhaust above this plane resulted in an increase in the detrimental interference effect on the lift which rose rapidly with upward vertical movement of the jets above the wing chord line. Minimum interference of the jets on wing lift occurred for jet locations below the wing near the wing midchord. Aft of the wing midchord, favorable lift interference was obtained. The favorable lift interference was more pronounced near the lower surface of the wing, especially near the wing flap. At jet locations aft of the wing, the favorable lift interference was relatively unaffected by vertical movement of the jets. The effect of the jet exhaust was less pronounced on the drag and pitching moment of the wing than on the lift. Pressure-distribution data for the wing and flaps indicated that the interference effects of the jet exhaust on the aerodynamic characteristics of the model resulted largely from a change in the effective angle of attack of the wing.

Reducing the jet deflection from 90° to 60° reduced the magnitude of the detrimental as well as the magnitude of the favorable interference on the wing lift. Retraction of the wing flaps from 40° to 0° resulted in an increase in the detrimental lift interference, and the results indicated that the jet must be located near the trailing edge of the wing before favorable lift interference can be obtained for zero flap deflection.

INTRODUCTION

Jet V/STOL aircraft experience aerodynamic interference effects during hovering and in the transition-speed regime between hovering and conventional flight. Some of the jet-induced effects in transitional flight are discussed in references 1 to 5. These results indicated that jets located in front of the wing result in an unfavorable lift interference, whereas jets located behind the wing result in a favorable lift interference. Within limitations imposed by adequate pitching moment and other considerations, proper location of the jets with respect to the wing can produce a favorable lift interference or at least minimize the loss in lift due to interference during transition.

In order to determine the effects of jet location systematically, an exploratory investigation of jet locations several wing-chord lengths ahead to several chord lengths behind an unswept wing has been made in the Langley 300-MPH 7- by 10-foot tunnel. Various vertical locations of the jets were also investigated. The main purpose of the investigation was to explore a rather large number of jet-exhaust locations to determine in a generalized manner the favorable and/or unfavorable effects of the various jet locations on the forces and moments on the wing and to indicate trends rather than provide performance data. The unswept, untapered wing had an aspect ratio of 6 and was equipped with a 30-percent-chord slotted Fowler-type flap. The two jets, one on either side of the simple fuselage, were located spanwise at the 25-percent semispan station and were mounted independently of the wing so that only the aerodynamic forces and interference effects were measured on the wing.

SYMBOLS

The units used for the physical quantities defined in this paper are given both in U.S. Customary Units and in the International System of Units (SI). Factors relating these two systems of units are presented in reference 6.

A_j total area of jet exit nozzles, 2π in^2 (12.9π centimeters^2)

c wing chord, 0.667 ft (0.2032 meter)

C_D drag coefficient, $\dfrac{\text{Drag}}{q_\infty S}$

C_L lift coefficient, $\dfrac{\text{Lift}}{q_\infty S}$

C_m pitching-moment coefficient, $\dfrac{\text{Pitching moment}}{q_\infty Sc}$

C'_p pressure coefficient, $\frac{p_{t,\infty} - p_l}{q_\infty}$

C_T thrust coefficient, $\frac{\text{Thrust}}{q_\infty S}$

p_l local static pressure, lbf/ft^2 (newtons/meter^2)

$p_{t,\infty}$ free-stream total pressure, lbf/ft^2 (newtons/meter^2)

q_∞ free-stream dynamic pressure, lbf/ft^2 (newtons/meter^2)

S wing area, 2.667 ft^2 (0.24774 meter^2)

V_e effective velocity ratio, $\sqrt{\rho_\infty V_\infty^2 / \rho_j V_j^2}$

V_j velocity at jet exhaust exit, ft/sec (meter/sec)

V_∞ free-stream velocity, ft/sec (meter/sec)

x longitudinal distance from leading edge of wing (positive when measured aft of leading edge of wing), ft (meters)

z vertical distance from wing chord line (positive when measured above chord line), ft (meters)

z_o vertical distance from wing chord line wind-off (positive when measured above chord line), ft (meters)

α angle of attack, deg

δ_f flap deflection (positive when deflected down), deg

δ_j jet exhaust deflection from horizontal direction, deg

ΔC_D incremental drag coefficient due to power (power-on C_D minus power-off C_D)

ΔC_L incremental lift coefficient due to power (power-on C_L minus power-off C_L)

ΔC_m incremental pitching-moment coefficient due to power (power-on C_m minus power-off C_m)

$\Delta C_p'$ incremental pressure coefficient due to power (power-on C_p' minus power-off C_p')

ρ_j mass density of air at jet exhaust exit, slugs/ft^3 (kilograms/meter^3)

ρ_∞ free-stream mass density of air, slugs/ft^3 (kilograms/meter^3)

MODEL AND APPARATUS

A drawing of the model is shown in figure 1. The wing was unswept and untapered and had an aspect ratio of 6 with a 30-percent wing-chord slotted Fowler-type flap deflected 40°. The wing and flap had NACA 4415 airfoil sections. The wing was mounted at zero incidence at the top of a cylindrical fuselage which had a faired nose section. In order to determine the pressure distributions on the wing and flap, pressure orifices were located on the upper and lower surfaces of the right wing and flap at the same spanwise location as the jet-exhaust nozzles (25-percent-semispan station). Measurements of the pressures were obtained by the use of pressure transducers.

The model was mounted on a sting-supported six-component strain-gage balance for direct measurement of the total forces and moments on the model. The balance was located in the center of the fuselage with the moment center of the balance located at the 25-percent-chord station of the wing. An electronic clinometer was located in the nose section of the fuselage for use in determining the geometric angle of attack of the wing during the investigation.

The two jet-exhaust nozzles, one on either side of the fuselage, were located at the 25-percent-semispan station as shown in figure 2. The apparatus which supported the two nozzles was attached to the ceiling of the tunnel test section in such a manner that the jets could be placed at various longitudinal and vertical locations with respect to the wing of the model. The nozzles were mounted independently of the model so that only the aerodynamic forces and moments and the jet-exhaust interference effects were measured on the balance. Each jet was powered by an ejector which was operated by cold, dry, compressed air. A detailed description of the ejector units is given in reference 7. Sectional views of the ejector unit and exhaust nozzle are shown in figure 3. Rings were installed at the periphery of each ejector through which water was injected into the secondary airflow through the ejector in order to provide flow visualization of the jet exhaust.

Photographs of the model and the support apparatus for the nozzles are shown as figure 4. As shown in the photographs, the supports for the nozzles were located behind

the wing with the ejector inlets facing downstream. The supports were located in this manner for jet locations aft of the 25-percent-chord station of the wing. For jet locations from the wing trailing edge forward, the support apparatus was moved in front of the wing, and the ejector inlets were then facing upstream. An overlap of jet locations from the 25-percent-chord station to the trailing edge of the wing was obtained by the two methods of locating the support apparatus.

TEST CONDITIONS

The investigation was made in the Langley 300-MPH 7- by 10-foot tunnel. The Reynolds number based on the maximum free-stream dynamic pressure of 60 lbf/ft^2 (2870 newtons/meter^2) and wing chord of 0.667 foot (0.2032 meter) was 0.9×10^6.

Aerodynamic and pressure data were obtained for the wing with flaps deflected 40° and with the jets directed vertically downward $(\delta_j = 90^\circ)$ and directed aft 30° from the vertical position $(\delta_j = 60^\circ)$. In addition, data were obtained for the wing with the flaps retracted $(\delta_f = 0^\circ)$ and with the jets directed vertically downward. The various longitudinal and vertical locations of the jets for the investigation are shown schematically in figure 5. The locations shown refer to the center line of the jet at the exhaust nozzle exit and were measured with respect to the leading edge of the wing for zero angle of attack of the wing at the wind-off condition. The data were obtained at a geometric angle of attack of 0°, with a constant level of thrust, through a range of values of free-stream dynamic pressure from 0 to approximately 60 lbf/ft^2 (2870 newtons/meter^2) in order to simulate effective velocity ratios from 0 to approximately 0.25. Because the support apparatus for the ejectors was located in the flow field of the model, power-off and power-on tests were made at each jet location in order to make direct measurements of the jet-exhaust interference effects on the aerodynamic characteristics of the model.

Because of sting bending and deflection of the strain-gage balance, the geometric angle of attack of the wing changed slightly throughout the range of tunnel free-stream dynamic pressures used during the investigation. The change in angle of attack was recorded along with the aerodynamic data. The maximum change was approximately 1.5° and occurred at the maximum free-stream dynamic pressure. However, for a given dynamic pressure, the angle of attack was approximately the same for the power-off and power-on data. The jet-support apparatus was attached rigidly to the tunnel ceiling and the position and angle of the jet-exhaust nozzles did not change during the test run. Therefore, because of sting bending, the vertical location of the wing with respect to the jet exhaust did change during the test run. The change in vertical location of the wing was calculated by use of the sting-bending calibration. The calculated change in vertical location of the wing is reflected in the data presented to show the effect of vertical location of the jets on the aerodynamic characteristics of the model.

The thrust from the two ejectors was determined from the difference between the total and static pressure measurements in the jet exits, in a manner similar to that used in reference 7. The total thrust of the two jets at 90° deflection was approximately 81 lbf (360 newtons) at the wind-off condition and increased to approximately 87 lbf (387 newtons) at the free-stream dynamic pressure of 60 lbf/ft^2 (2870 newtons/meter^2). The total thrust of the two jets at 60° deflection was approximately 80 pounds (356 newtons) at the wind-off condition and increased to approximately 84 pounds (374 newtons) at the free-stream dynamic pressure of 60 lbf/ft^2 (2870 newtons/meter^2). Thrust coefficients and effective velocity ratios were determined from the total thrust measurements by use of the following equations:

$$C_T = \frac{\text{Thrust}}{q_\infty S} \tag{1}$$

$$V_e = \sqrt{\frac{\rho_\infty V_\infty^2}{\rho_j V_j^2}} = \sqrt{\frac{q_\infty}{\text{Thrust}/2A_j}} \tag{2}$$

$$C_T = \frac{2A_j/S}{\left(\frac{\rho_\infty V_\infty^2}{\rho_j V_j^2}\right)} \tag{3}$$

The variation of thrust coefficient with effective velocity ratio determined from equation (3) is presented in figure 6.

When the pressure data were reduced to the nondimensional pressure coefficient, the pressures on the surface of the wing were divided by the tunnel free-stream dynamic pressure, which increased with increase in effective velocity ratio.

No corrections were made to the data for model blockage or jet boundary. However, the jet-boundary corrections were calculated for several typical locations of the jets, and the effect of the jet boundary on the lift and drag of the model is discussed subsequently.

PRESENTATION OF RESULTS

Results of the present investigation are presented in the following figures:

DISCUSSION

Power-Off Aerodynamic Characteristics

The effects of an upstream installation of the jet nozzles and their supporting apparatus on the aerodynamic characteristics of the model are shown in figure 7 for the nozzle exit located 0.25 chord ahead of the leading edge of the wing and 0.64 chord below the wing chord line for flap deflections of 0^o and 40^o. The interference from the jet-nozzle

installation apparently produced a downwash over the wing which reduced the effective angle of attack and resulted in a reduction in lift for a given angle of attack. As shown in figure 7(b), the effect of the downwash from the strut installation on the lift of the model was small compared with the effect of the jet-nozzle installation. The change in flow at the wing leading edge caused by the strut installation apparently delayed the leading-edge separation on the wing and produced a small increase in maximum lift; whereas, addition of the jet-nozzle installation to the struts resulted in an increase in the stall angle of about 3° and an increase in the maximum lift coefficient of 0.1, compared with the data when only the model was installed in the tunnel. The jet-nozzle installation had a negligible effect on the drag and pitching moment (at a given lift) when the flaps were retracted except at high angles of attack near the stall (fig. 7(a)). With flaps deflected 40° (fig. 7(b)), the jet-nozzle installation resulted in an increase in drag and a reduction in negative pitching moment.

Power-On Aerodynamic Characteristics

Flow visualization of jet efflux.- Wind-tunnel investigations reported in references 2 and 4 have shown that interference between the jets and the free stream caused significant changes in the aerodynamic characteristics of jet V/STOL configurations. The magnitude and distribution of this interference have been attributed (ref. 4) primarily to the rolling up of the wake into a vortex pair downstream from the jet exit nozzle. The photographs of figures 8 and 9 show the effect of an increase in effective velocity ratio on the wake from the jet-exhaust nozzles. At low effective velocity ratios (below 0.05), the jet efflux appeared unaffected by the tunnel free stream. As the effective velocity ratio was increased, the jet exhaust was deflected toward the direction of the free stream. The free stream appeared to have a greater influence on the jet deflected 90° than on the jet deflected 60° with an increase in effective velocity ratio, and at a velocity ratio of 0.25, both jet wakes approached the free-stream direction a short distance downstream of the nozzle exit.

Incremental forces and moments.- The basic force and moment data have been plotted as variations of incremental lift, drag, and pitching-moment coefficients due to power through a range of effective velocity ratios for a number of locations of the jet exit nozzle. As shown in figures 10, 11, and 12 for the three jet and flap configurations investigated, the incremental forces and moments generally increased with effective velocity ratio. The magnitude and direction of the forces and moments resulted from mixing of the jet exhaust and the free stream and deflection of the jet exhaust by the free stream.

Jet-boundary corrections.- The effects of applying jet-boundary corrections to typical lift and drag data are shown in figures 10(g concluded) and 11(d) for jet deflections of 90° and 60°, respectively. The corrections reduced the increments due to power slightly. However, the corrections to the data for the jet deflection of 60° were less than those for

the jet deflection of 90°. It should be noted that the jets were not connected to the model, and therefore, the drag of the installation and the thrust vector were not included in the drag measurements on the balance. The main purpose of this paper is to present trends in the interference effects due to jet-exhaust locations relative to the wing and, as shown in figures 10 and 11, the jet-boundary corrections did not change the trends or conclusions which may be drawn relative to the jet-exhaust interference effects; therefore, the data presented in the remaining figures of this paper have not been corrected for jet-boundary interference.

Pressure distributions.- As shown in figures 13, 14, and 15, the basic pressure distributions on the wing and flaps of the model varied with changes in effective velocity ratio. The magnitude and changes in the shape of the pressure-distribution plots depend upon the deflection of the jet exhaust by the free stream and, in some instances, upon impingement of the jet exhaust on the aerodynamic surfaces. These pressure distributions indicate that the jet exhaust changed the airflow over the wing and thereby resulted in a change in the effective angle of attack of the wing. Depending upon the location of the jet-exit nozzle, the interference from the jet exhaust increased or decreased the effective angle of attack of the wing and thereby produced favorable or unfavorable interference effects on the aerodynamic characteristics of the model.

Effect of Location of Jet Exhaust

Aerodynamic forces and moments.- The data of figure 16 summarize the effect of the longitudinal location of the jet exhaust on the incremental lift, drag, and pitching-moment coefficients due to power at several different vertical locations. The data of figure 17 summarize the effect of the vertical location of the jet exhaust on the same incremental coefficients at several longitudinal locations. These data show that all locations of the jet exhaust ahead of the wing resulted in a detrimental effect on the wing lift. The data of figure 17 show that the detrimental interference effect of the jet exhaust on the lift of the wing reached a minimum at locations approximately 0.8 chord below the wing. Movement of the jet exhaust below the 0.8-chord location increased the detrimental effect on the lift, but the increase was negligible below effective velocity ratios of 0.20. Movement of the jet exhaust to locations above 0.8 chord below the wing resulted in an increase in the detrimental interference effect on the lift. At vertical locations of the jets above the wing chord line, the detrimental effect on the lift increased rapidly, and as the jets approached locations 0.8 chord above the wing, the detrimental jet interference on the lift was extremely large, especially at the higher effective velocity ratios. At these locations of the jets, the loss in lift exceeded one-third of the power-off wing lift. As shown in figure 16, longitudinal movement of the jet exhaust had little effect at locations ahead of the wing except at those above the wing chord line.

Data obtained for jet locations from 0.25 wing chord to the trailing edge with the jet support apparatus located behind the wing as well as ahead of the wing (fig. 16) indicated no conclusive effects of the location of the apparatus on the incremental forces and moments due to power, and an average fairing of the two sets of data was made. At both planes below the wing, the longitudinal location of the jet exhaust for minimum interference on wing lift ranged from 0.45 to 0.65 wing chord through the range of effective velocity ratios from 0.10 to 0.25. In general, locations of the jet exhaust aft of the wing midchord resulted in a favorable interference effect on the wing lift which increased as the jet exhaust was moved toward the wing trailing edge and flap. The favorable interference effect was more pronounced in the plane nearer the undersurface of the wing. The increase in favorable lift interference apparently resulted from an effect similar to that of a jet-augmented flap which would produce an even larger increase in the induced lift of the wing. Movement of the jet-exit nozzle aft of the flaps reduced the favorable interference on the wing lift which became approximately constant at locations between 2 and 3 chords aft of the leading edge of the wing. At the three vertical locations of the jets 3 chord lengths behind the leading edge of the wing (fig. 17), favorable interference on the wing lift was obtained with relatively small variations in the lift increment throughout the range of vertical locations investigated.

The effect of the location of the jet exhaust on the incremental drag was less pronounced than on the lift increments (figs. 16 and 17). The jet exhaust resulted in an interference drag at all vertical locations of the jet nozzles below the wing, although the variation in this drag with vertical location of the jets was small. At jet-nozzle locations ahead of the wing, the drag remained approximately constant throughout the range of longitudinal locations of the jet exit nozzles except when the jet exhaust was located in planes above the wing. At locations above the wing, the detrimental drag increments decreased with aft movement of the jets and resulted in a favorable or thrust increment. Longitudinal locations of the jets from the leading edge of the wing aft produced a nearly constant drag increment except in locations near the flaps where the drag increment increased. The interference drag for jet locations 3 chords aft of the wing leading edge was less than that for the jet locations ahead of the wing. This interference drag was not affected appreciably by changes in vertical locations of the jets (fig. 17).

The effect of the location of the jet exhaust on the incremental pitching moment was also less pronounced than on the incremental lift (figs. 16 and 17). Longitudinal locations of the jets ahead of the wing resulted in small variations in the negative pitching-moment increments in planes below the wing. These negative pitching-moment increments decreased as the jet location was moved vertically upward and became positive for locations above the wing chord line. When the jet exhaust was located above the wing, these positive pitching-moment increments increased in magnitude with movement of the jets from locations 2 chords ahead of the wing to locations about 0.8 chord ahead of the wing.

Further aft movement of the jets resulted in a small decrease in the magnitude of the positive pitching-moment increment as the leading edge of the wing was approached. Relatively large positive pitching-moment increments were obtained at the higher vertical locations of the jets ahead of the wing. Longitudinal locations of the jet nozzles from the leading edge of the wing to 3 chords aft produced a nearly constant negative pitching moment except at locations near the wing flap where the pitching-moment increment became more negative.

Pressure distributions.- The diagrams of incremental pressure distribution in figure 18 show that at longitudinal locations of the jet nozzles ahead of the wing midchord, the jet exhaust produced a net down load over most of the wing surface which resulted in a lift loss, or unfavorable lift interference, from the jet exhaust. The incremental pressures at the trailing edge of the wing ($x/c = 1.0$) show a net increase in lift, or a favorable lift interference. At all of the jet locations shown in figure 18, the incremental pressure distributions indicate an increase in lift on the flaps which resulted in a drag increase and a negative pitching-moment increment due to interference from the jet exhaust.

The data of figure 19 show a net down load on the wing at the six vertical locations of the jet nozzles ahead of the wing. The incremental pressures indicate a large loss in lift at the highest vertical location of the jets $\left(z_o/c = 0.86\right)$. As was shown in the force data of figure 17, the lift loss decreased as the jet nozzles were moved from above the wing to below the wing.

The data of figure 20 for jet-nozzle locations 3 chords aft of the wing leading edge show a favorable, although small, lift interference from the jet exhaust at all three vertical locations of the nozzles.

Effect of Deflection of Jet Exhaust

Forces and moments.- As shown in figure 21, a change in deflection of the jets to 60^o throughout the range of longitudinal locations of the jets from 0.5 chord ahead of the wing to the trailing edge of the wing resulted in interference effects similar to those obtained with jet deflections of 90^o. At effective velocity ratios from 0.10 to 0.20, the change in the jet deflection reduced the magnitude of the detrimental as well as the favorable interference on the wing lift. At effective velocity ratios near 0.25, the change in the deflection of the jets increased the detrimental interference effects on the wing lift, and the favorable lift interference was reduced in magnitude by the change in jet deflection. The location of the jets for minimum lift interference moved from 0.4 chord for the 90^o deflection to 0.65 chord for the 60^o deflection. As shown in figure 22, the effects of the vertical location of the jets on the aerodynamic characteristics were not appreciably changed by a change in jet deflection.

As shown in figure 21, the change in deflection of the jet exhaust from 90° to 60° reduced the drag interference and the nose-down pitching moments over the range of longitudinal locations of the investigation at an effective velocity ratio near 0.25, although the change in jet deflection had little effect on the drag and pitching-moment increments at the lower velocity ratios. The drag and pitching-moment increments were not appreciably different for jet deflections of 60° and 90° with vertical movement of the exhaust nozzle as shown in figure 22.

Pressure distributions.- Comparison of the incremental pressure distributions due to power for the jet-nozzle deflection of 60° (figs. 23 and 24) with the data for the jet-nozzle deflection of 90° (figs. 18 and 19) indicate the relatively small effects of the change in jet deflection and support the force and moment data presented in figures 21 and 22.

Effect of Retraction of Wing Flaps

Forces and moments.- Retraction of the wing flaps from 40° to 0° resulted in a decrease in the favorable lift interference and an increase in the detrimental lift interference at all effective velocity ratios (fig. 25). The favorable lift interference was obtained only near the trailing edge of the wing at effective velocity ratios above 0.20. As shown in figure 26, at vertical locations of the jets below the wing, the detrimental effect on the wing lift was not appreciably different for flap deflections of 0° and 40° at effective velocity ratios below 0.20; whereas at effective velocity ratios near 0.25, the detrimental effect on lift was increased by retraction of the flaps. When the jets were located above the wing, the jets produced a detrimental effect on wing lift, but the magnitude was considerably less at a flap deflection of 0° than at a flap deflection of 40°.

The drag interference effects were considerably reduced by retraction of the flaps from 40° to 0°, and as shown in figure 25, drag interference for the wing with a flap deflection of 0° was small throughout the range of longitudinal jet-exhaust locations. At vertical locations of the jets below the wing (fig. 26), the jets produced a small thrust increment for the model with flaps at 0° but a much larger drag increment when the flaps were deflected to 40°. At vertical locations of the jets above the wing, the jets produced a thrust increment which increased with upward movement of the jets.

The pitching-moment interference effects were small, and from the wing leading edge aft to the trailing edge, the increments due to power were positive for a flap deflection of 0°, whereas the pitching-moment increments were negative at all longitudinal locations of the jets for flap deflections of 40°. At vertical locations of the jets below the wing, the effect of the jets on the pitching-moment increment was not appreciably different for flap deflections of 0° and 40°. However, at vertical locations of the jets above the wing, the pitching-moment increment was decreased by retraction of the wing flaps.

Pressure distributions.- From a comparison of the incremental pressure distributions due to power for the wing with flaps retracted (figs. 27 and 28) with those for flaps deflected 40° (figs. 18 and 19), the differences in the loading on the wing for the two flap conditions is indicated.

CONCLUSIONS

An exploratory wind-tunnel investigation of the jet location interference effects on the longitudinal aerodynamic characteristics of a jet V/STOL model has been made for an unswept, untapered wing with an aspect ratio of 6 and 30-percent-chord slotted flaps. The results of the investigation led to the following conclusions:

1. All locations of the jet exhaust ahead of the wing resulted in a detrimental effect on the wing lift. Minimum interference of the jets on wing lift occurred below the wing for jet locations near the wing midchord. For jet locations aft of the wing midchord, favorable lift interference was obtained.

2. The favorable lift interference was more pronounced near the lower surface of the wing, especially near the wing flap.

3. Pressure-distribution data for the wing and flaps indicated that the interference effects of the jet exhaust on the aerodynamic characteristics of the model resulted largely from the change in the effective angle of attack of the wing.

4. For jet exhaust locations ahead of the wing, the detrimental lift interference reached a minimum when the jets were approximately 0.8 chord below the wing. Locations of the jet exhaust above this plane resulted in an increase in the detrimental interference effect on the lift which rose rapidly with upward vertical movement of the jets above the wing chord and became extremely large at locations approaching 0.8 chord above the wing.

5. For jet locations aft of the wing, the favorable lift interference was relatively unaffected by vertical movement of the jets.

6. The effects of the location of the jet exhaust were less pronounced on the drag and pitching moment of the wing than on the lift.

7. Reducing the jet deflection from 90° to 60° reduced the magnitude of the detrimental as well as the magnitude of the favorable interference on the wing lift. This change in jet deflection moved the location of the jet for minimum lift interference from 0.4 wing chord for the 90° jets to 0.65 wing chord for the 60° jets.

8. Retraction of the wing flaps from 40° to 0° resulted in an increase in the detrimental lift interference, and the results indicated the jet must be located near the trailing edge of the wing before favorable lift interference can be obtained for zero flap deflection.

Jet exhaust interference effects on the drag and pitching moment of the wing were relatively small compared with those for the wing with a flap deflection of 40°.

Langley Research Center,
National Aeronautics and Space Administration,
Langley Station, Hampton, Va., May 2, 1969,
721-01-00-18-23.

REFERENCES

1. Margason, Richard J.; and Gentry, Garl L., Jr.: Aerodynamic Characteristics of a Five-Jet VTOL Configuration in the Transition Speed Range. NASA TN D-4812, 1968.

2. Margason, Richard J.: Jet-Induced Effects in Transition Flight. Conference on V/STOL and STOL Aircraft. NASA SP-116, 1966, pp. 177-189.

3. Hammond, Alexander D.; and McLemore, H. Clyde: Hot-Gas Ingestion and Jet Interference Effects for Jet V/STOL Aircraft. Integration of Propulsion Systems in Airframes, AGARD Conf. Proc. No. 27, Sept. 1967, pp. 8-1 – 8-27.

4. Williams, John; and Wood, Maurice N.: Aerodynamic Interference Effects With Jet Lift Schemes on V/STOL Aircraft at Forward Speeds. Aerodynamics of Power Plant Installation, Pt. II, AGARDograph 103, Oct. 1965, pp. 619-652.

5. Seidel, M.: Der Einfluss eines geneigten Strahles auf das Strömungsfeld in der Umgebung eines Leitwerks sowie auf dessen Luftkraftbeiwerte – Teil I: Versuchseinrichtung, Vorversuche und Kraftmessungen mit horizontalem und vertikalem Strahl. DFL-Ber. Nr. 0487, 1968.

6. Mechtly, E. A.: The International System of Units – Physical Constants and Conversion Factors. NASA SP-7012, 1964.

7. Margason, Richard J.; and Gentry, Garl L.: Static Calibration of an Ejector Unit for Simulation of Jet Engines in Small-Scale Wind-Tunnel Models. NASA TN D-3867, 1967.

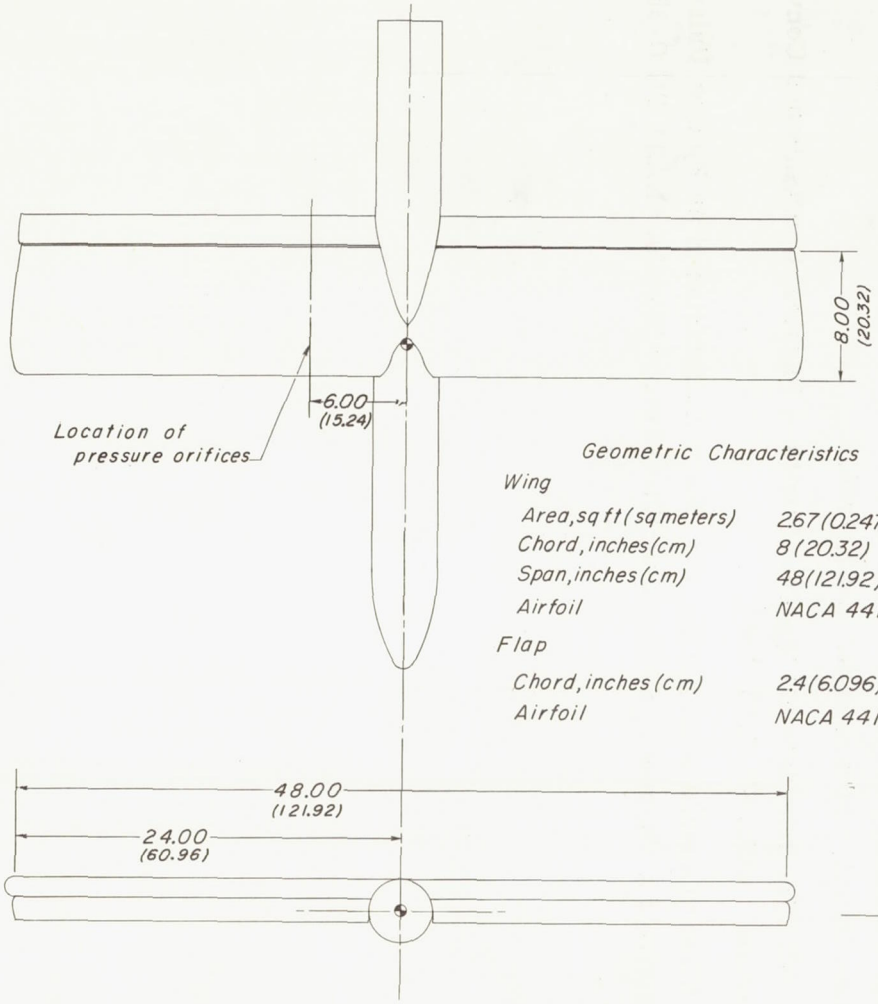

Geometric Characteristics

Wing	
Area, sq ft (sq meters)	2.67 (0.2477)
Chord, inches (cm)	8 (20.32)
Span, inches (cm)	48 (121.92)
Airfoil	NACA 4415
Flap	
Chord, inches (cm)	2.4 (6.096)
Airfoil	NACA 4415

Location of pressure orifices	
Wing station, percent chord	Flap station, percent chord
0	
0.50	
1.00	1.0
1.75	
5.0	5.0
7.5	
10.0	10.0
20.0	
30.0	30.0
40.0	
50.0	50.0
60.0	
70.0	70.0
80.0	
90.0	90.0
100.0	100.0

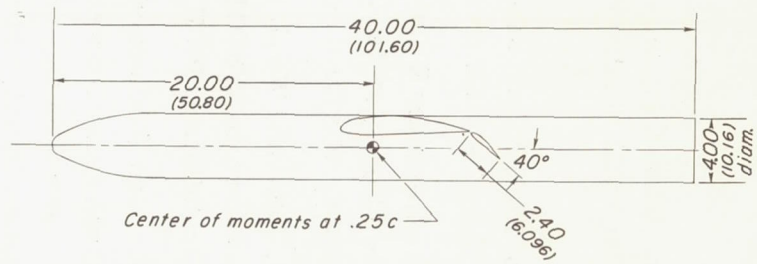

Figure 1.- Three-view drawing of model. Dimensions are given in inches and parenthetically in centimeters.

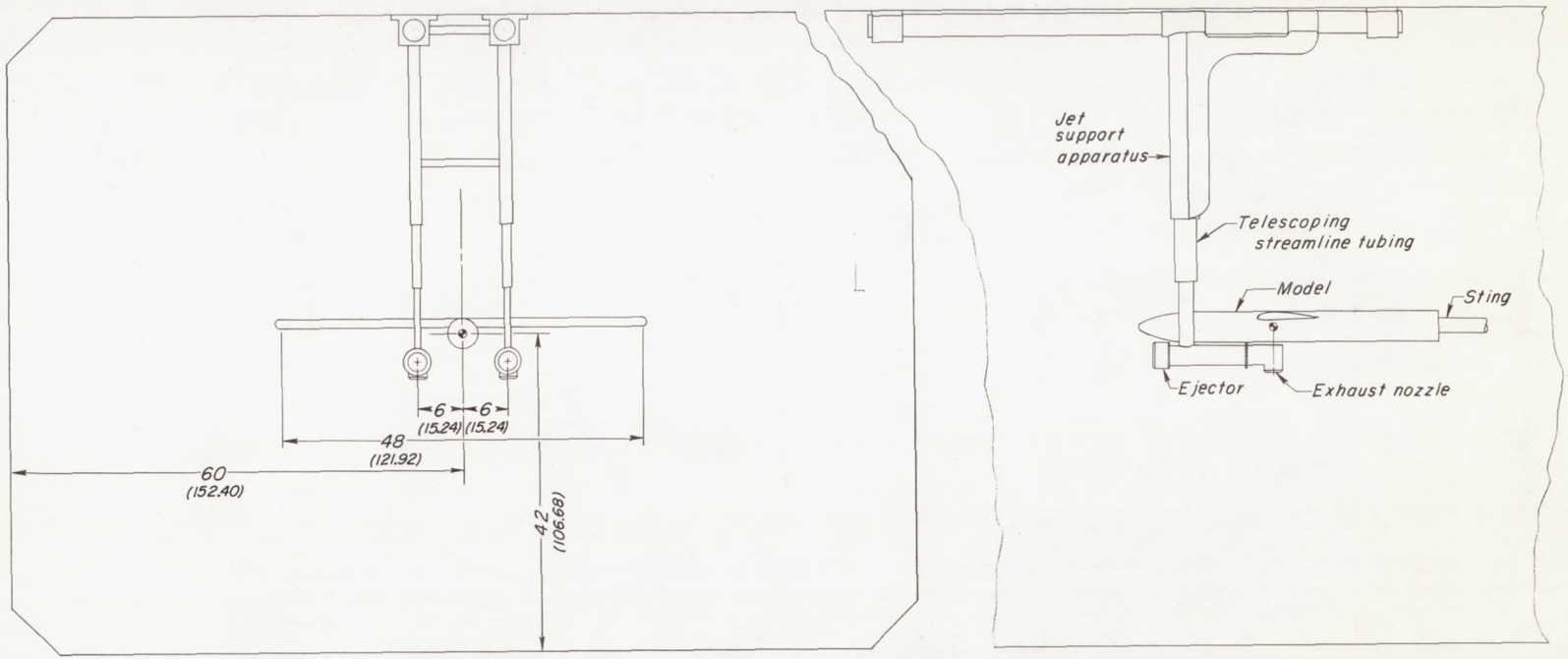

Figure 2.- Sketch showing setup of model, ejectors, and jet support apparatus in test section of the Langley 300-MPH 7- by 10-foot tunnel. Dimensions are given in inches and parenthetically in centimeters.

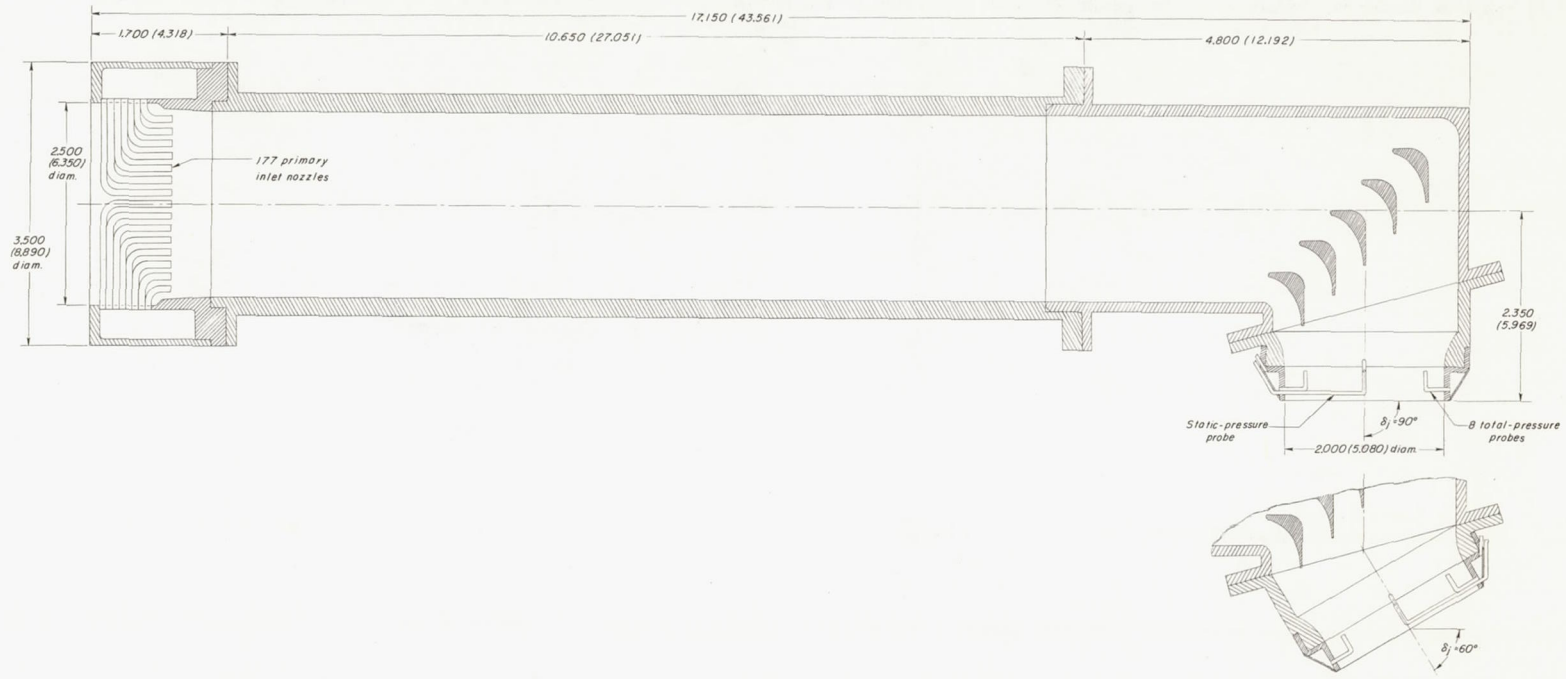

Figure 3.- Sectional views of the ejector unit and exhaust nozzle for simulating jet engines deflected 90^0 and 60^0. Dimensions are in inches and parenthetically in centimeters.

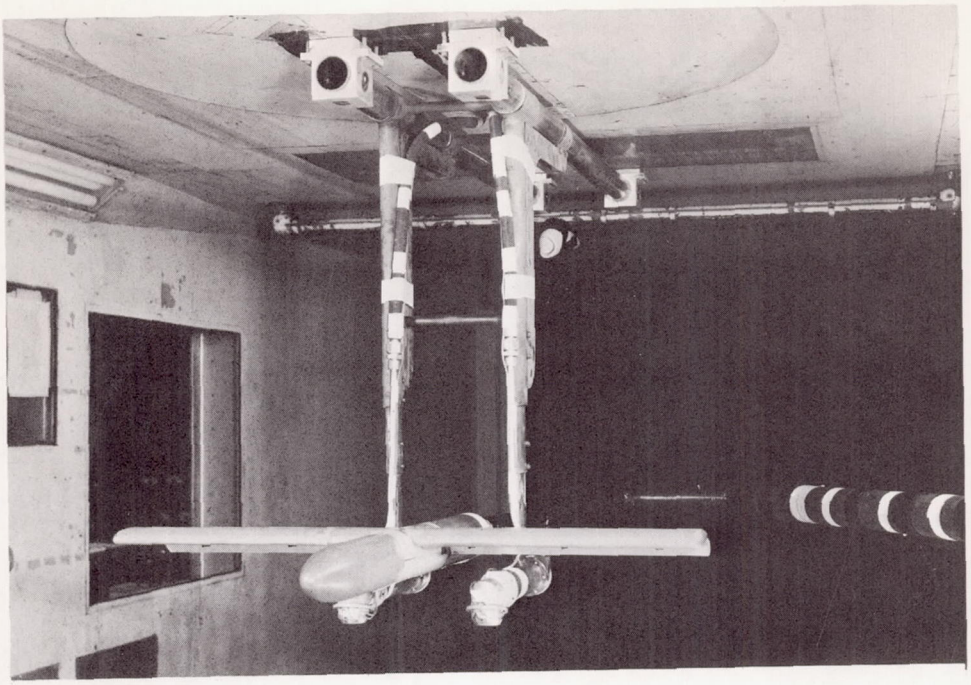

Front view

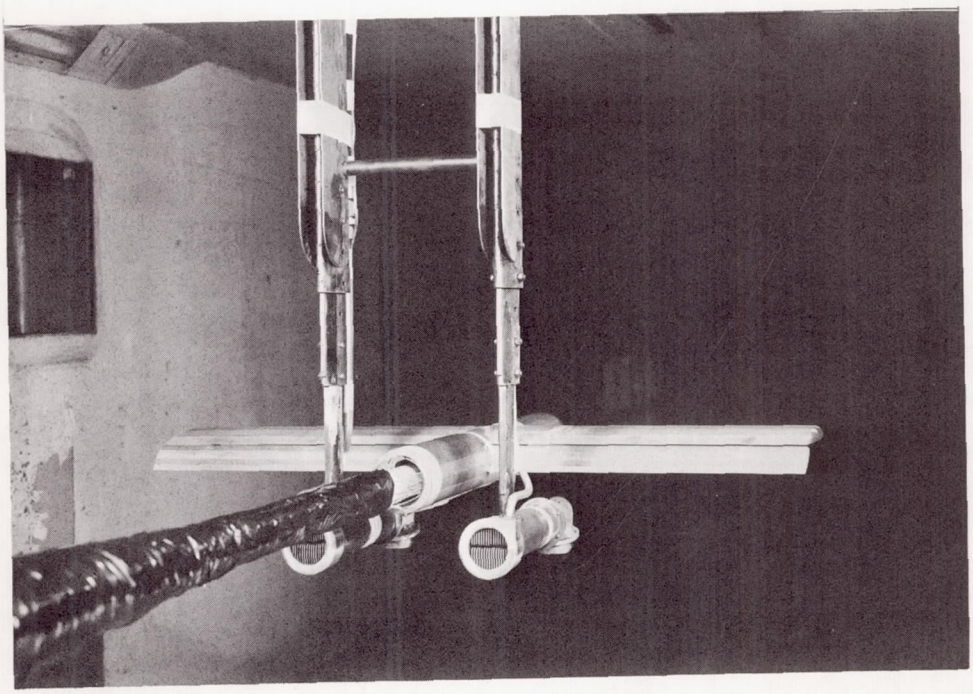

Rear view

L-69-1379

Figure 4.- Photographs of the model and ejectors in the Langley 300-MPH 7- by 10-foot tunnel..

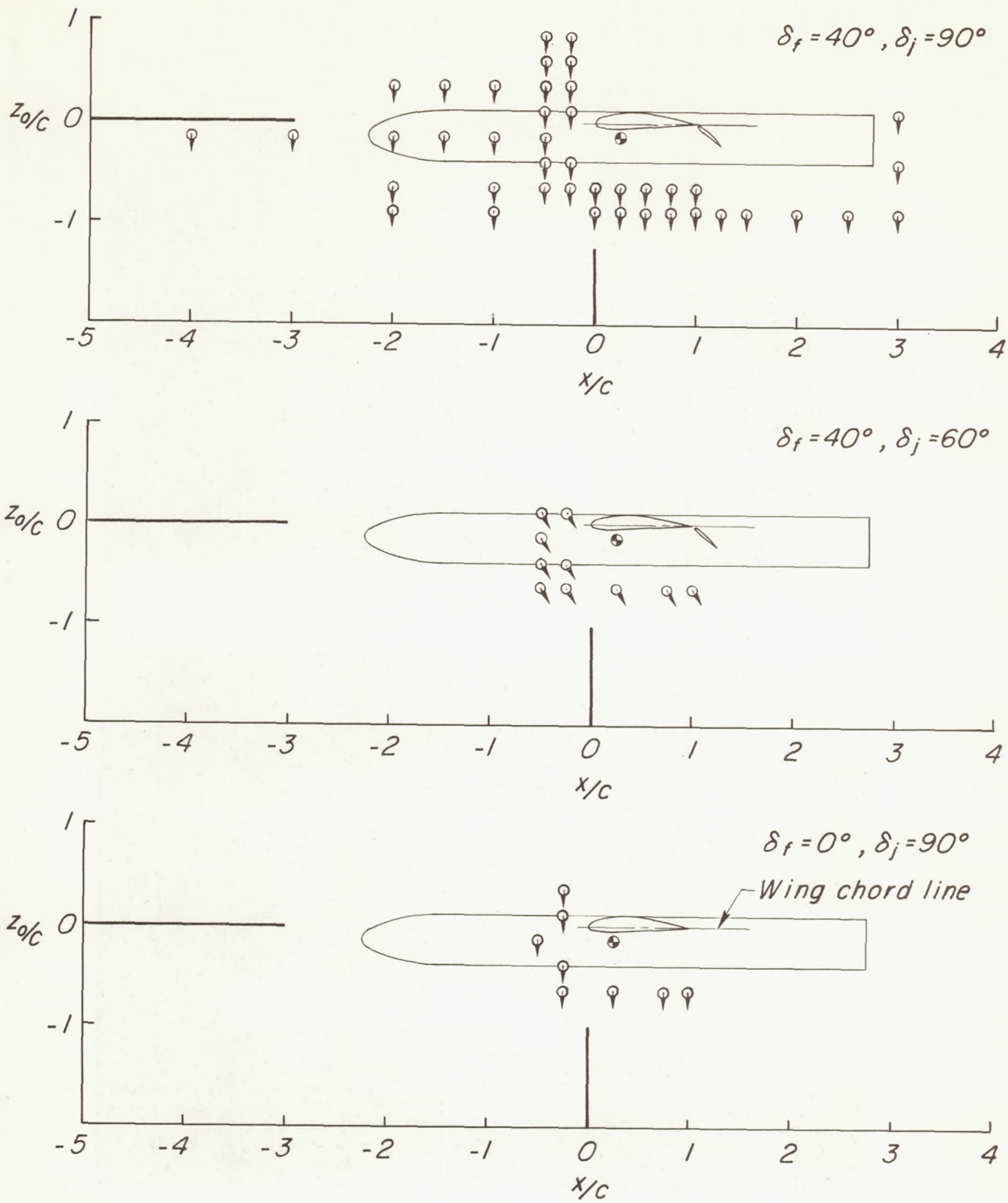

Figure 5.- Sketch of model indicating various locations of the jets for the investigation.

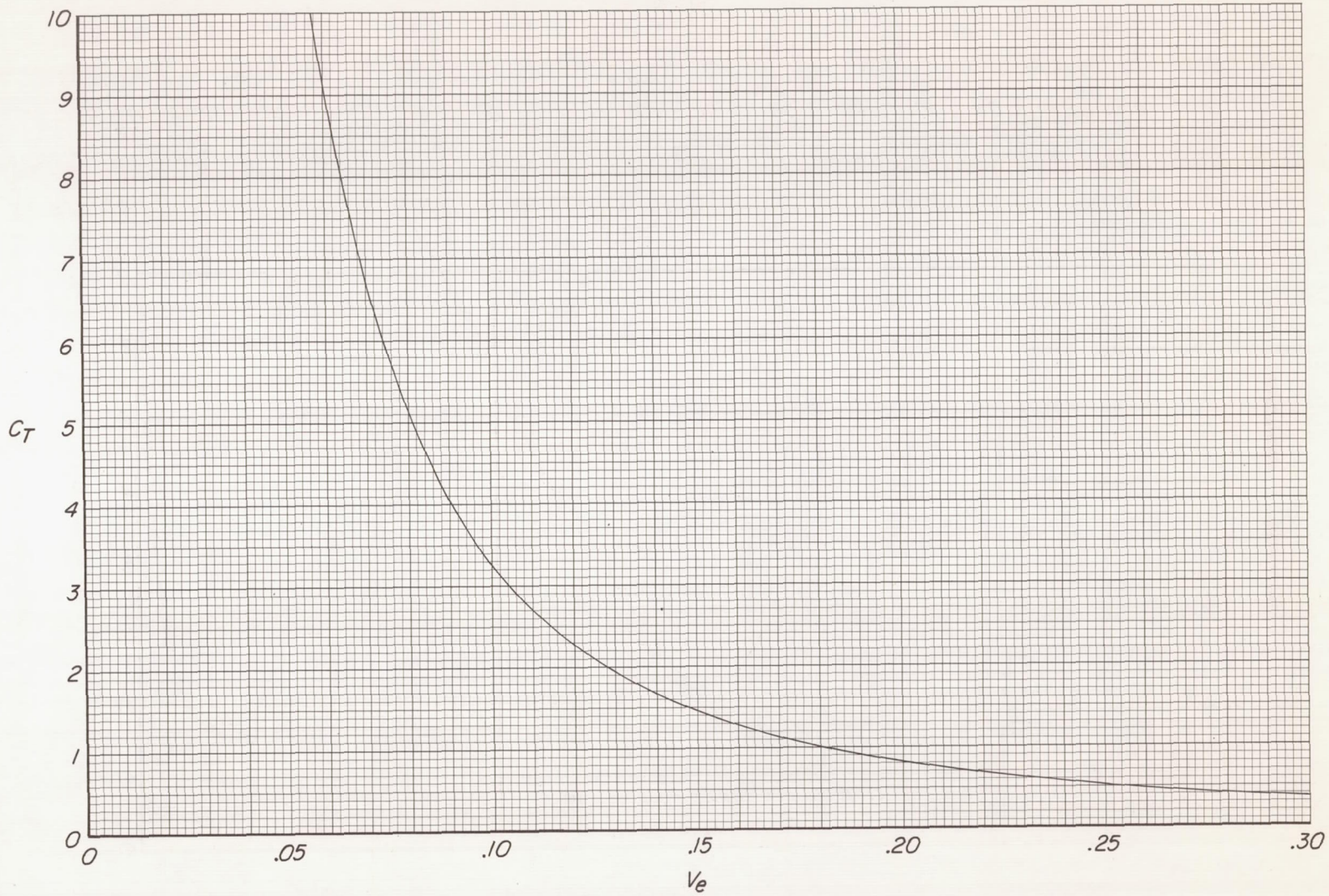

Figure 6.- Variation of thrust coefficient with effective velocity ratio for two jets.

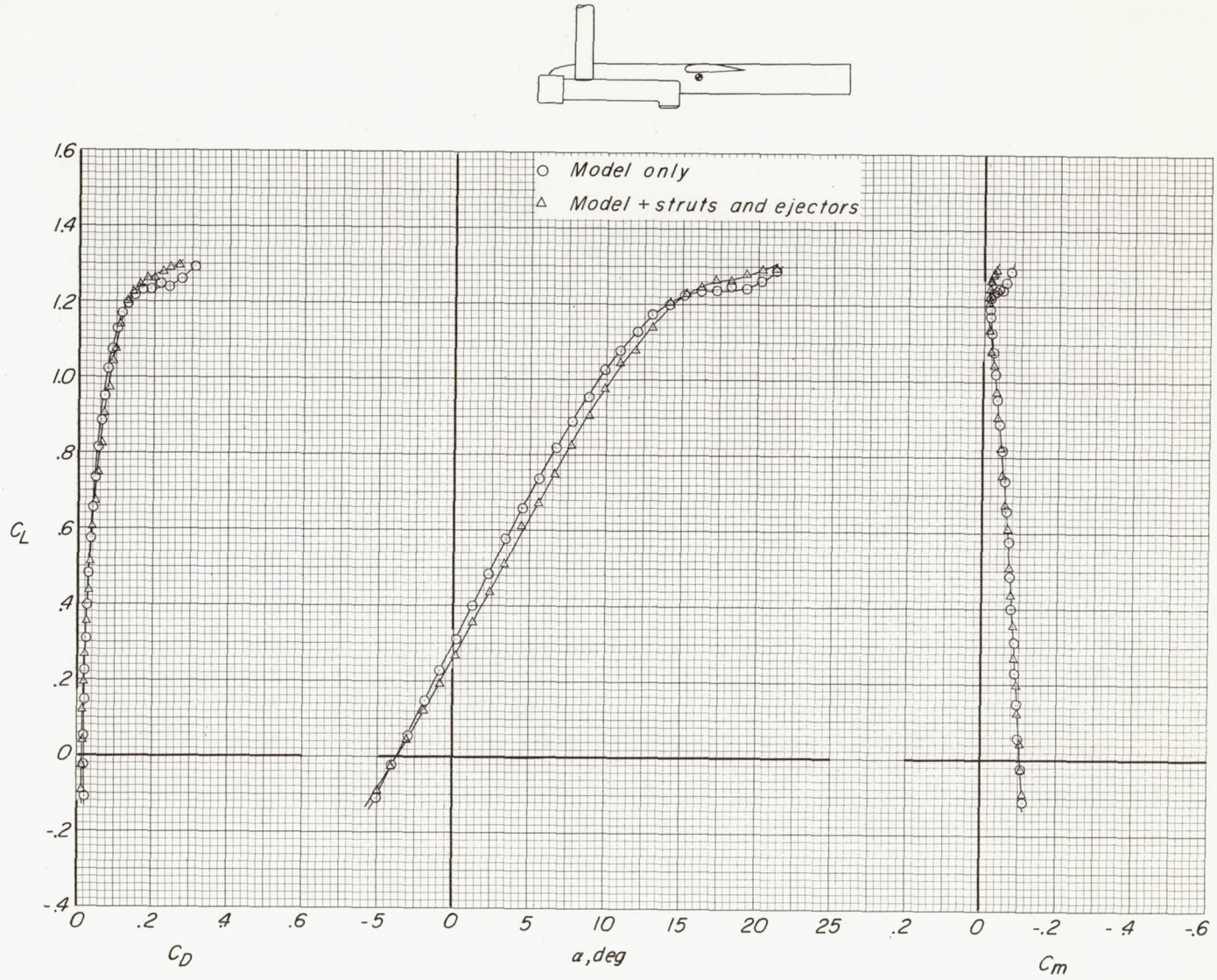

(a) $\delta_f = 0^0$.

Figure 7.- Effect of jet engines and supporting apparatus on the aerodynamic characteristics of the model. $C_T = 0$; $q_\infty = 60$ lbf/ft^2 (2870 newtons/meter^2). Nozzle exit location: $x/c = -0.25$, $z_0/c = -0.64$.

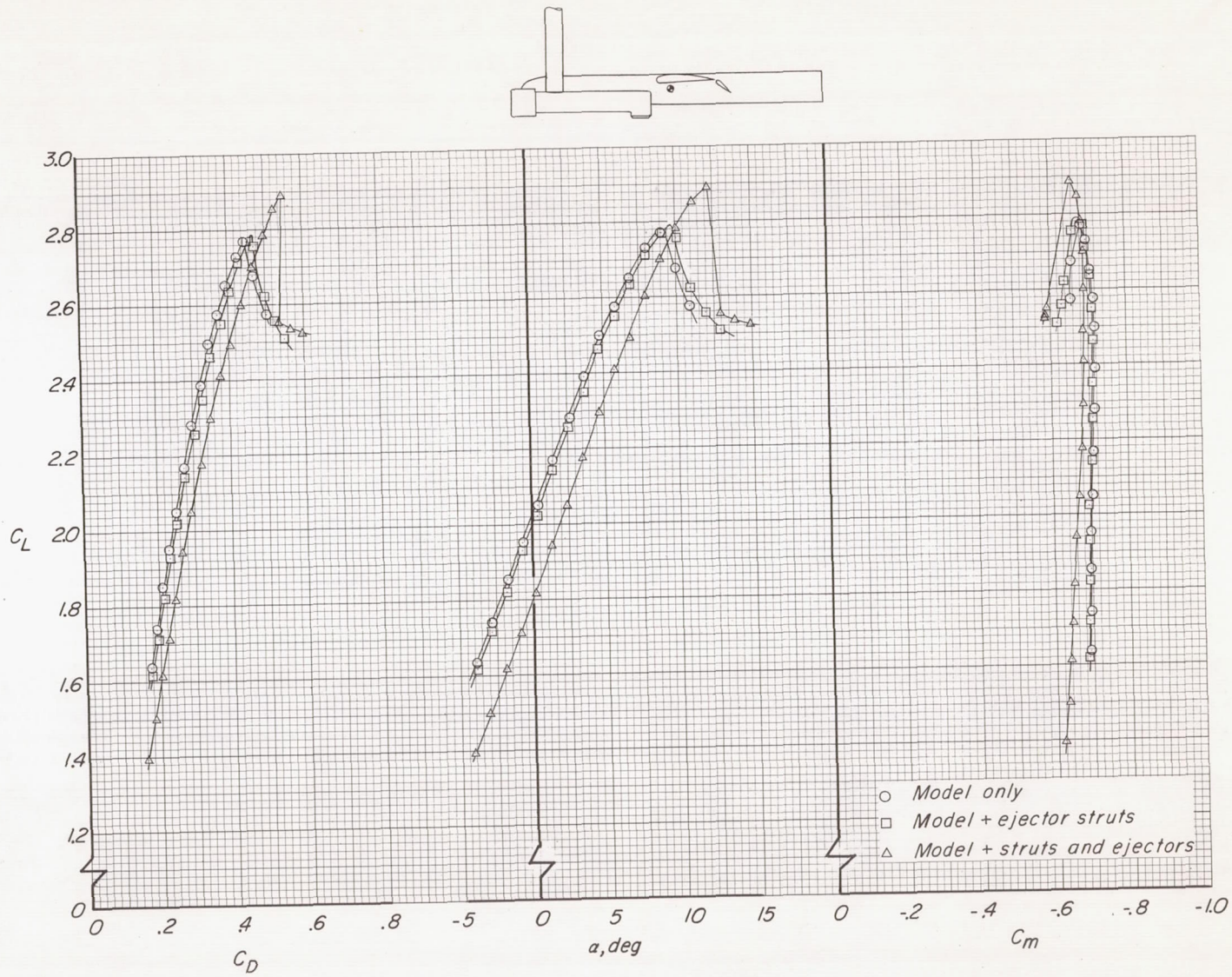

(b) $\delta_f = 40^0$.

Figure 7.- Concluded.

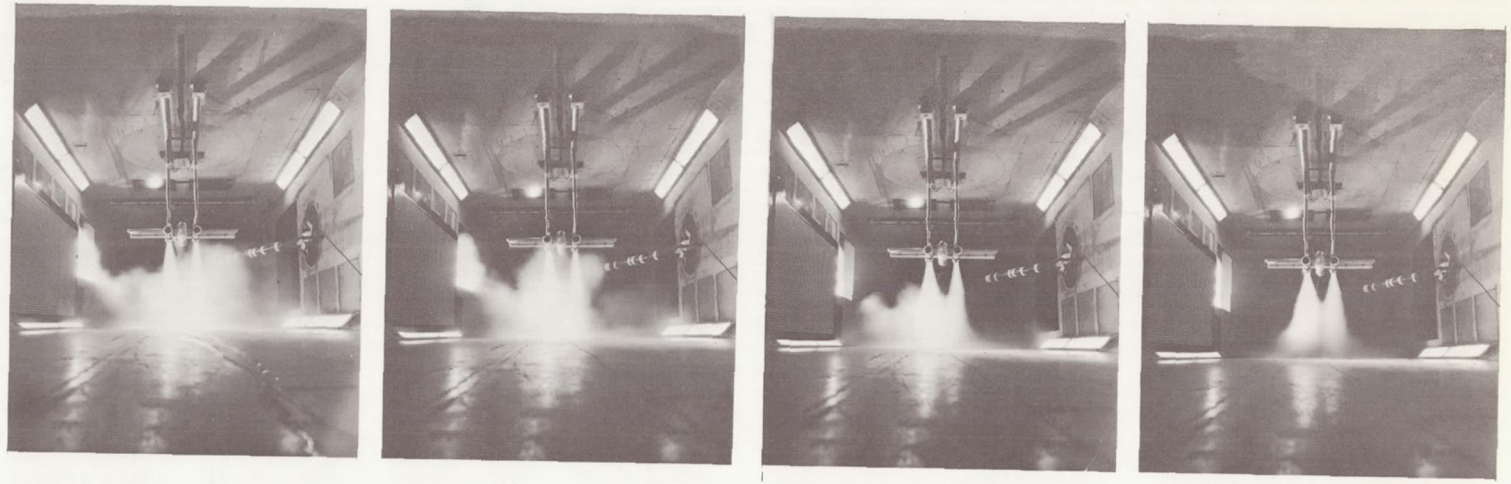

Front view

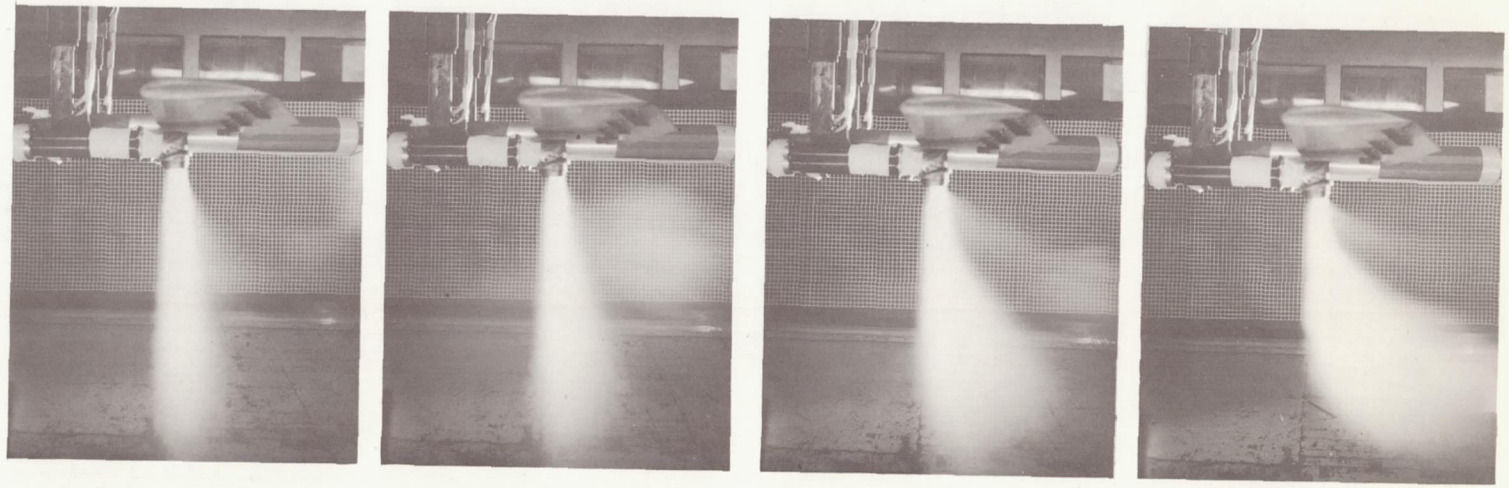

Side view

$V_e = 0.031$ $V_e = 0.046$ $V_e = 0.065$ $V_e = 0.096$

Figure 8.- Flow visualization of jet wake by means of water injection. $\delta_f = 40^0$; $\delta_j = 90^0$.

L-69-1380

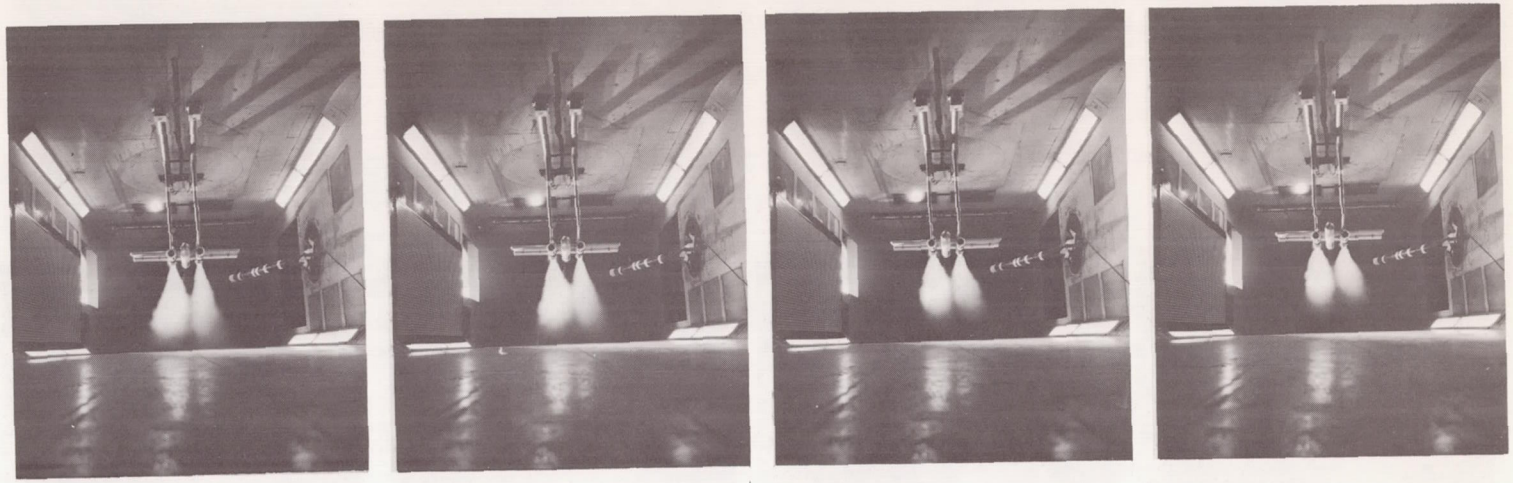

Front view

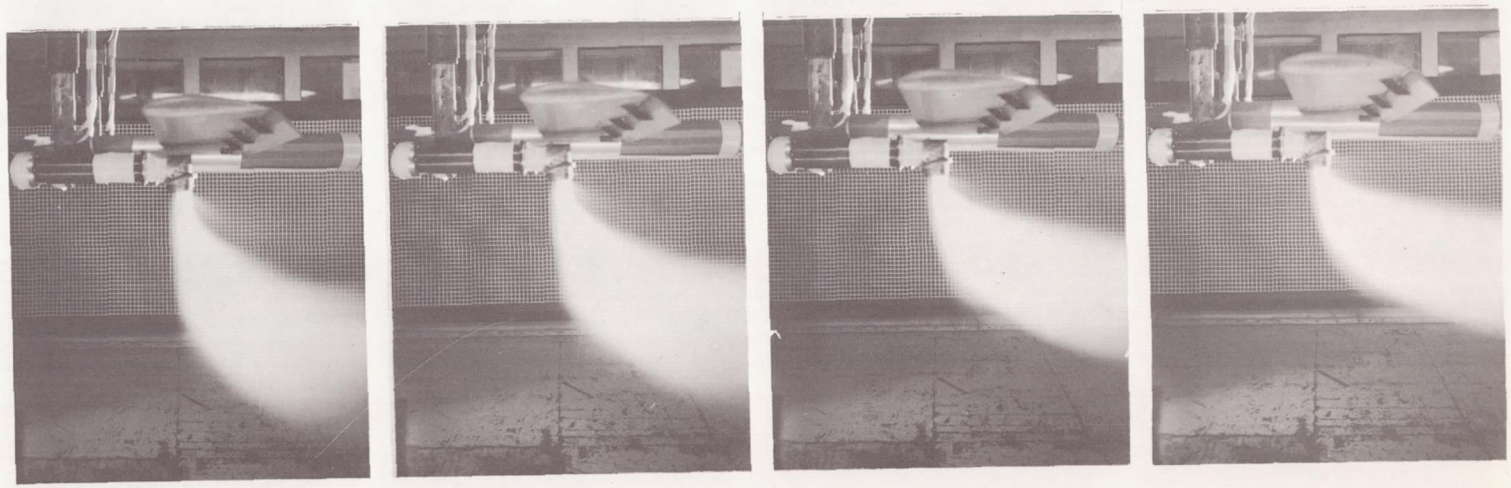

Side view

$V_e = 0.128$ $V_e = 0.150$ $V_e = 0.204$ $V_e = 0.247$

Figure 8.- Concluded.

L-69-1381

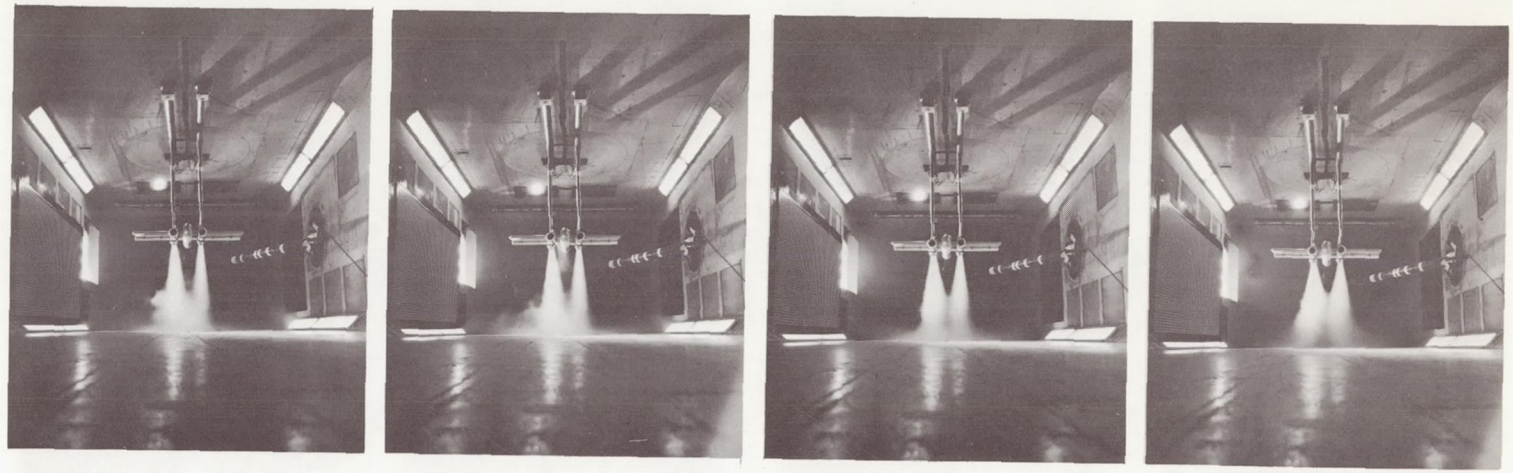

Front view

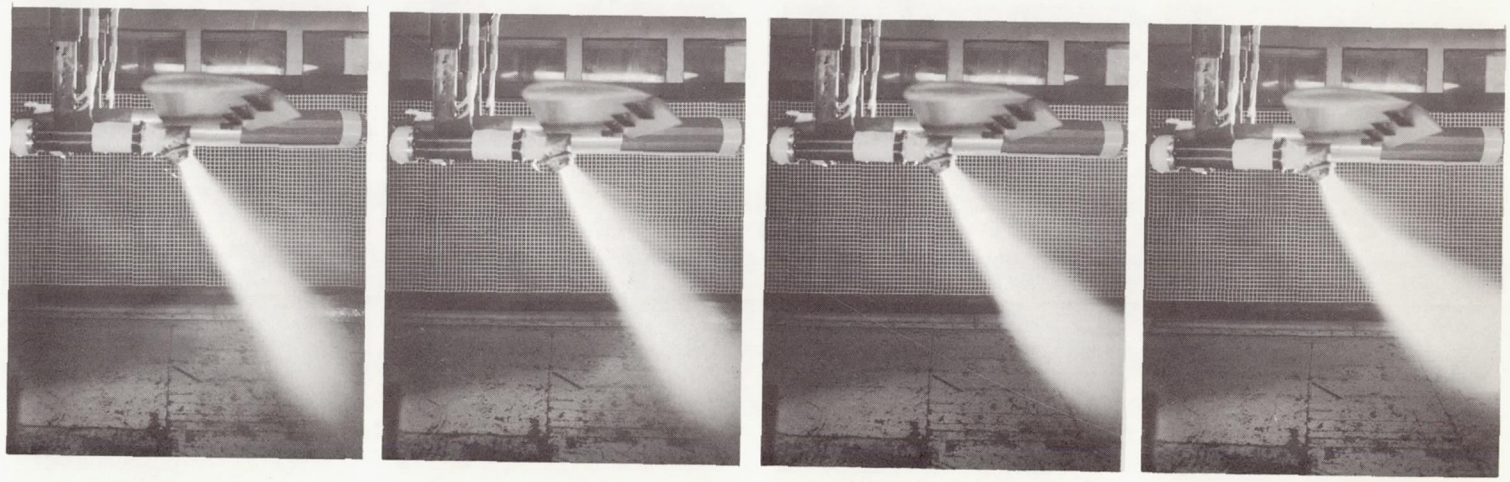

Side view

$V_e = 0.032$ $V_e = 0.039$ $V_e = 0.067$ $V_e = 0.098$

Figure 9.- Flow visualization of jet wake by means of water injection. $\delta_f = 40^0$; $\delta_j = 60^0$.

L-69-1382

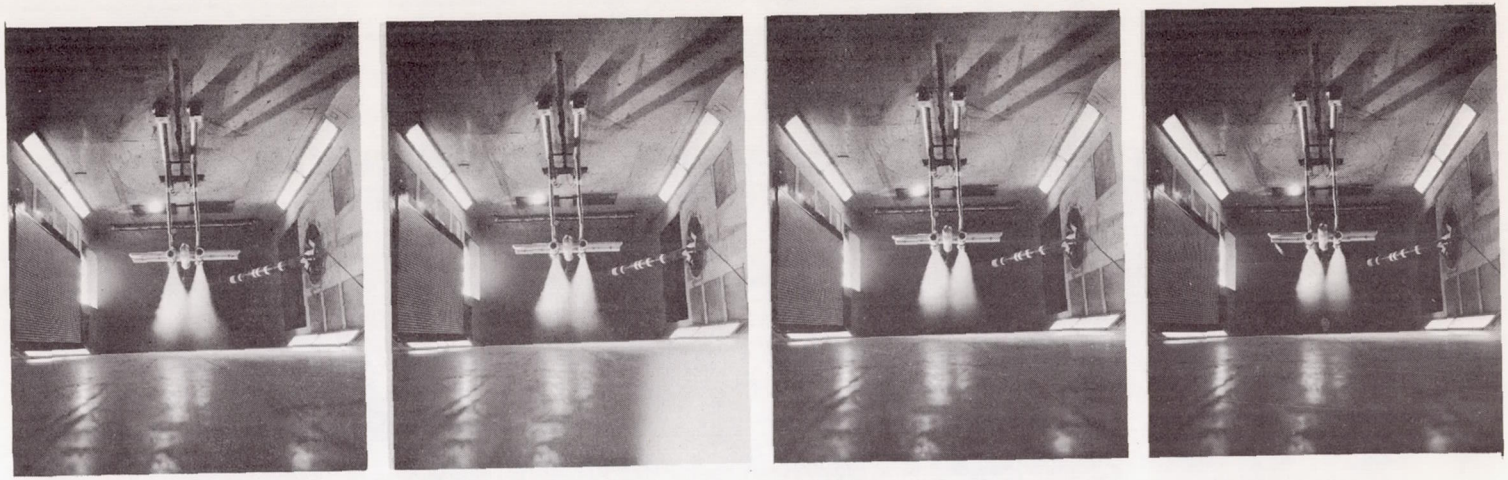

Front view

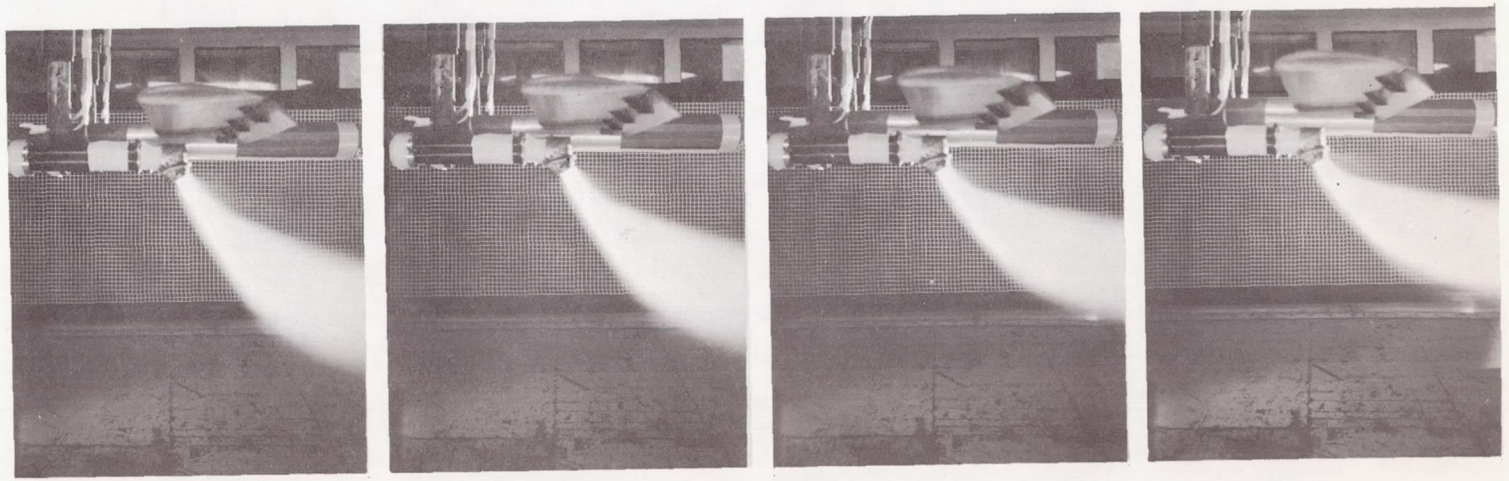

Side view

$V_e = 0.129$ $V_e = 0.152$ $V_e = 0.206$ $V_e = 0.248$

Figure 9.- Concluded.

L-69-1383

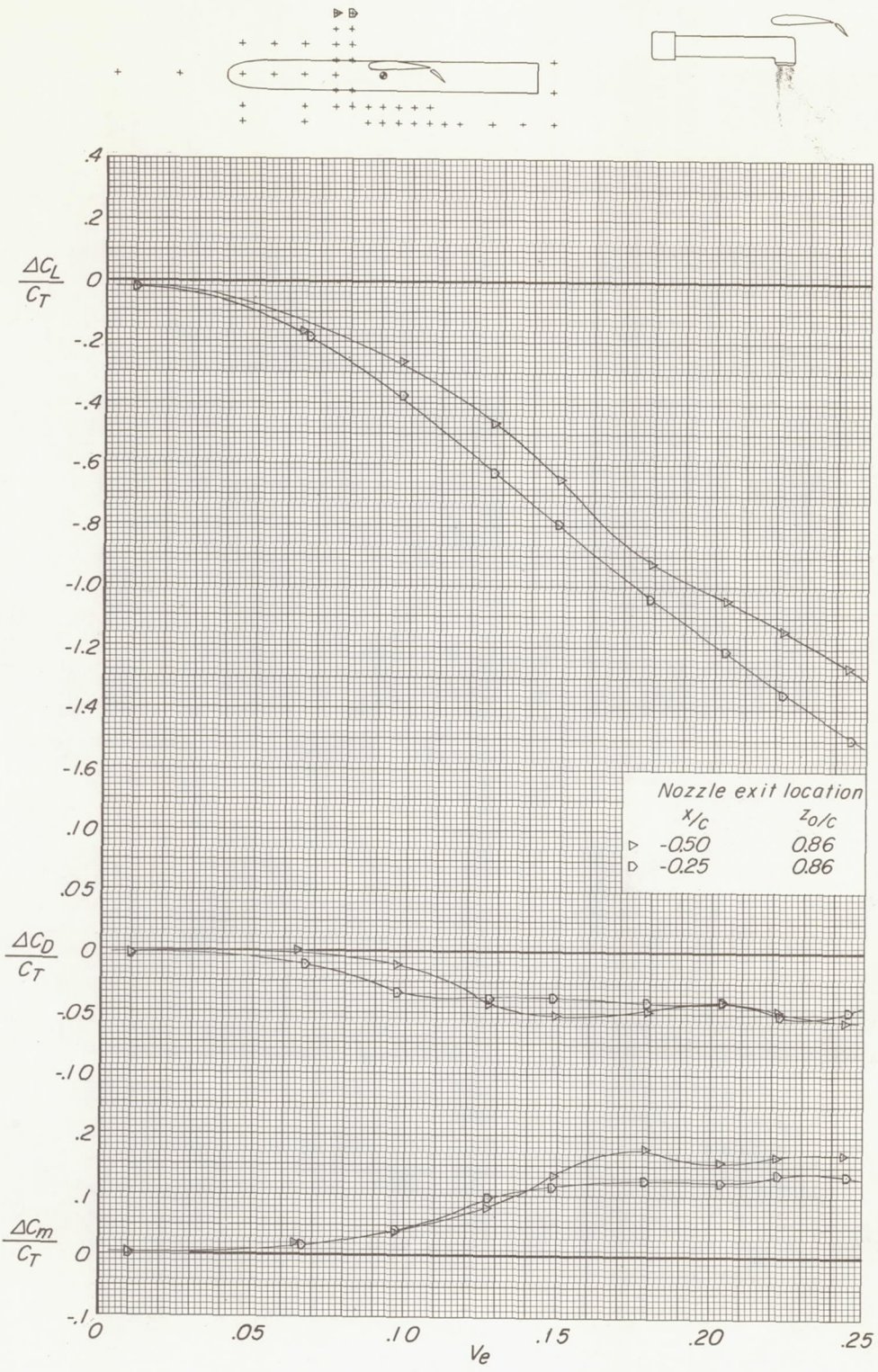

(a) $z_o/c = 0.86$.

Figure 10.- Variation of lift, drag, and pitching-moment increments due to power with effective velocity ratio. $\delta_f = 40^o$; $\delta_j = 90^o$.

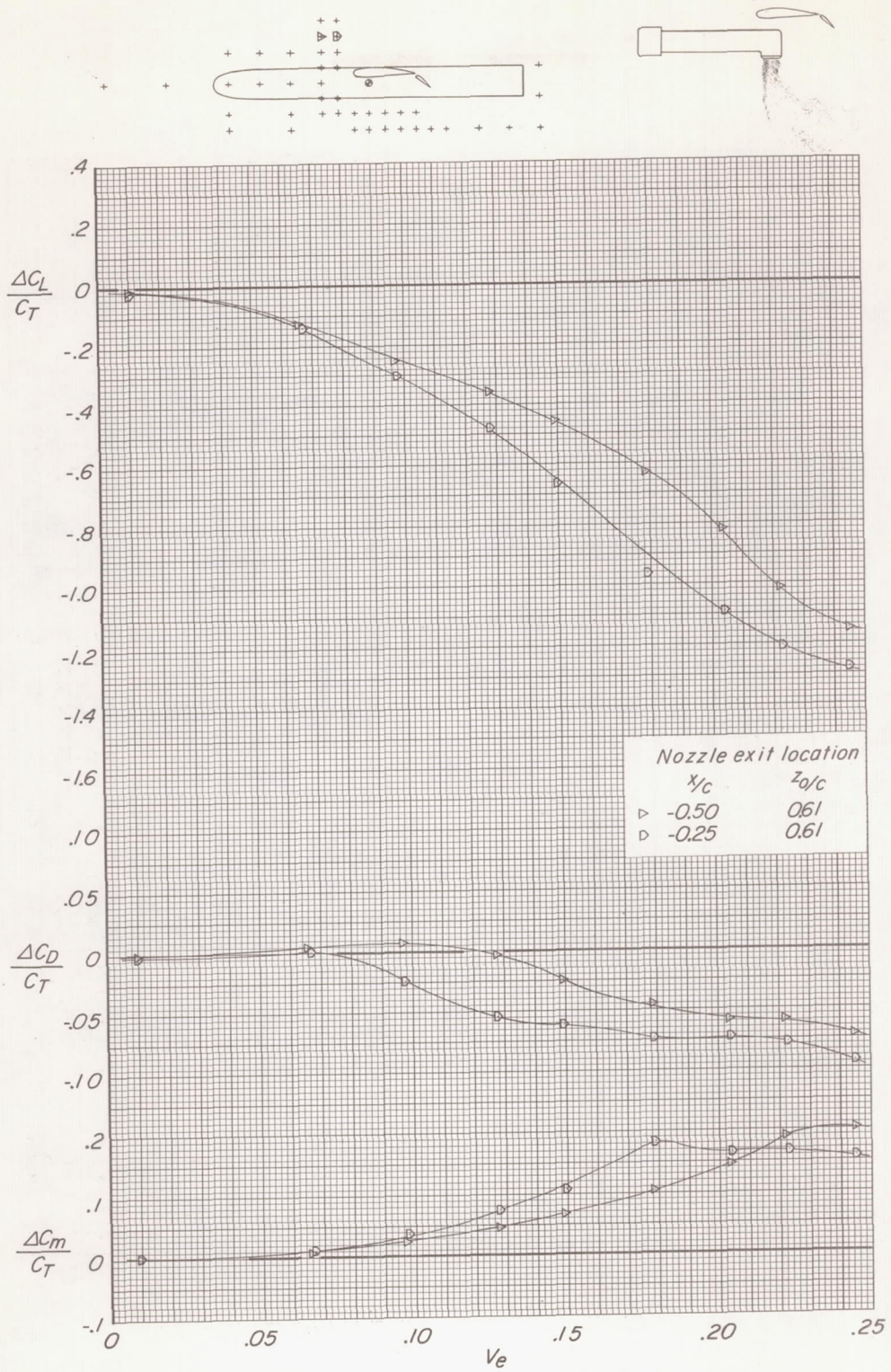

(b) $z_0/c = 0.61$.

Figure 10.- Continued.

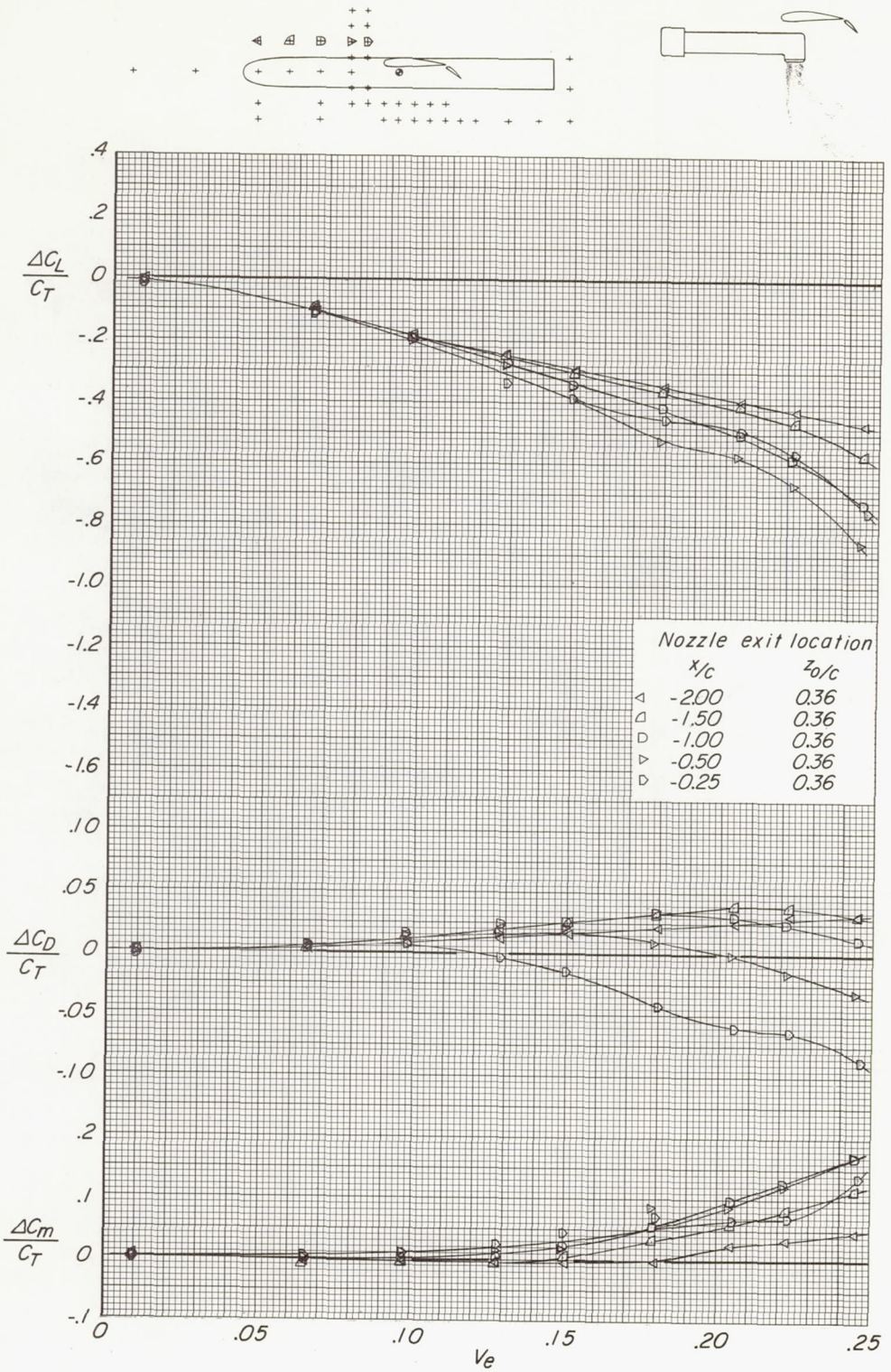

(c) $z_0/c = 0.36$.

Figure 10.- Continued.

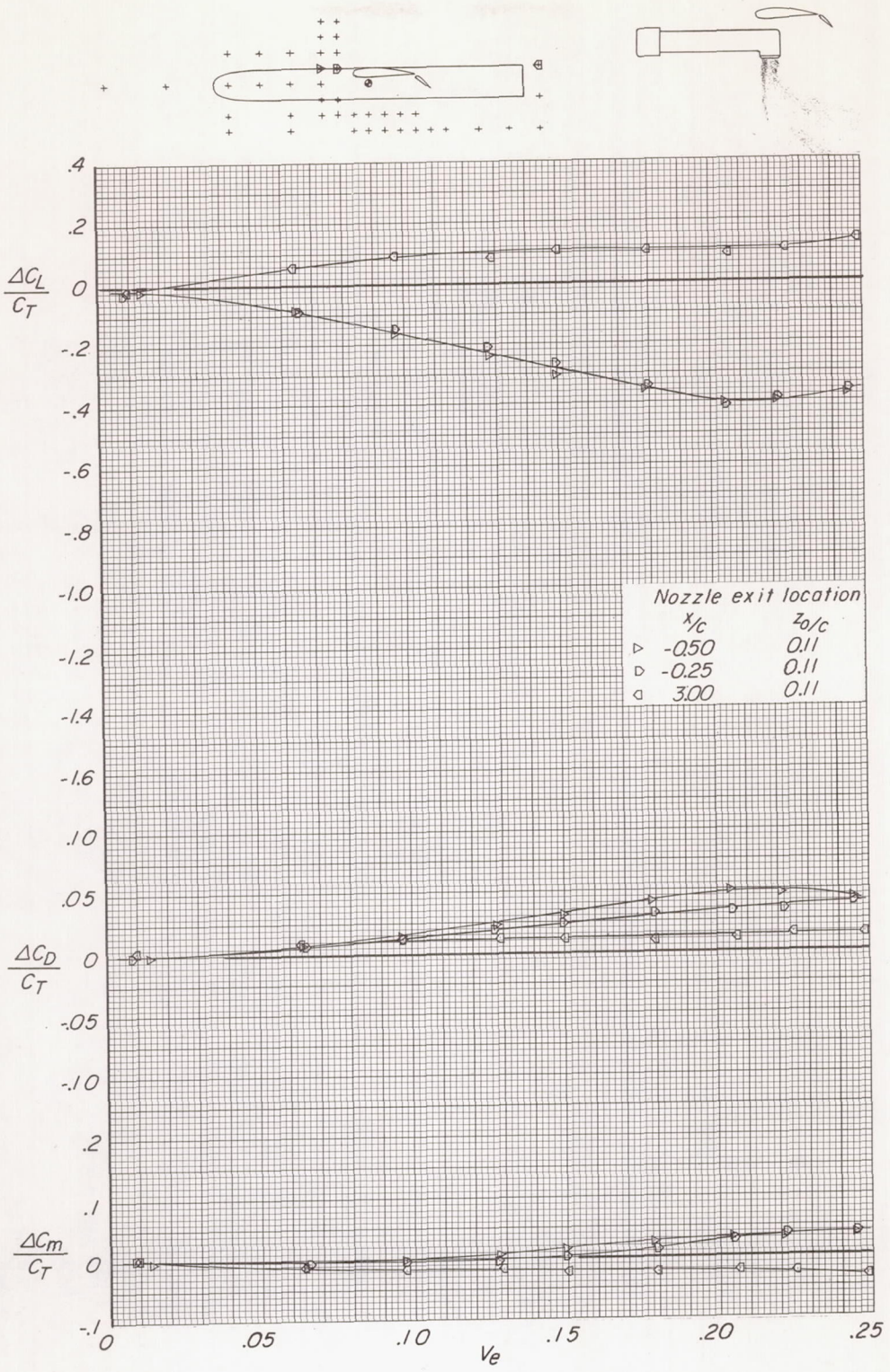

(d) $z_0/c = 0.11$.

Figure 10.- Continued.

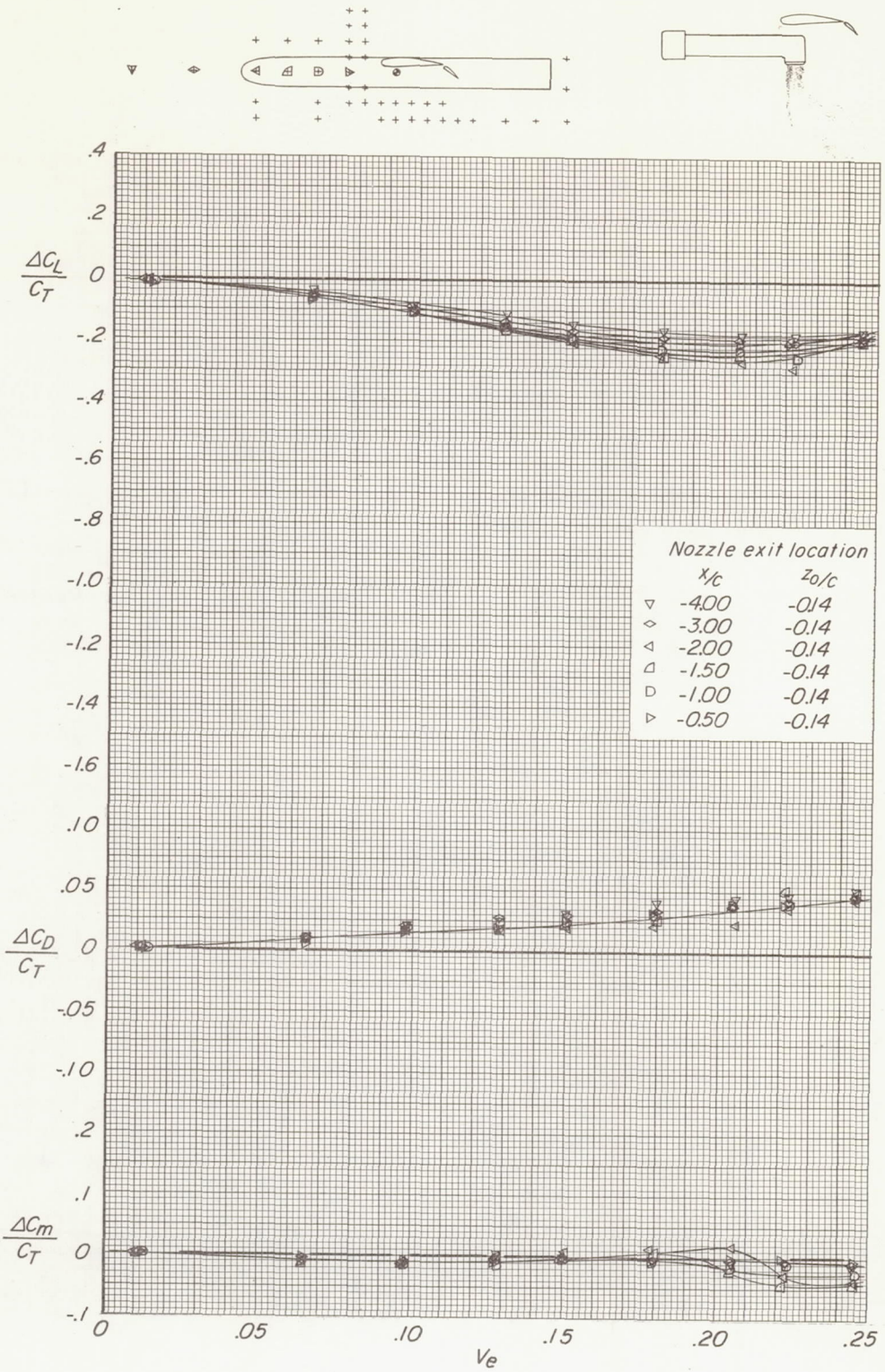

(e) $z_0/c = -0.14$.

Figure 10.- Continued.

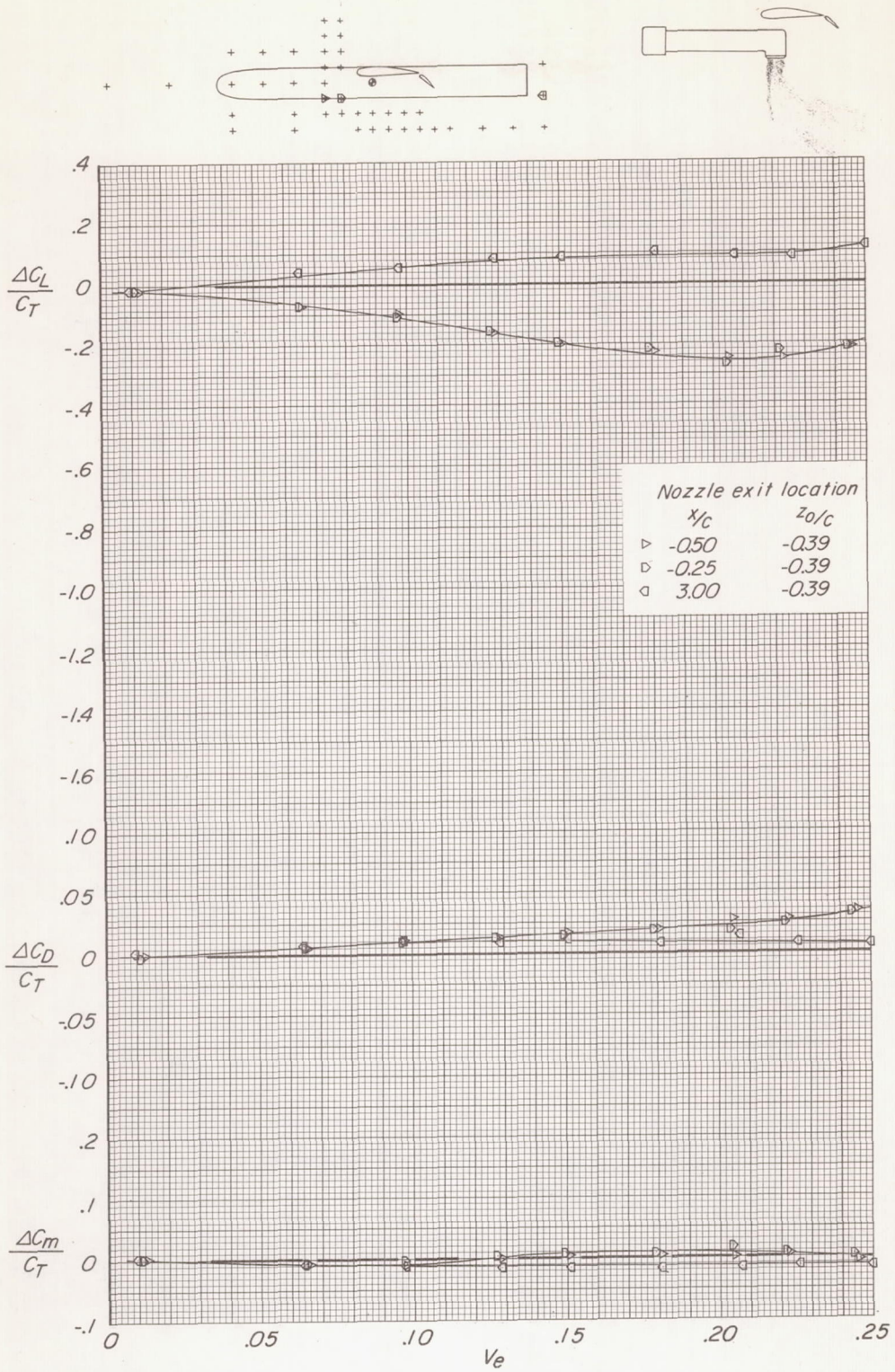

(f) $z_0/c = -0.39$.

Figure 10.- Continued.

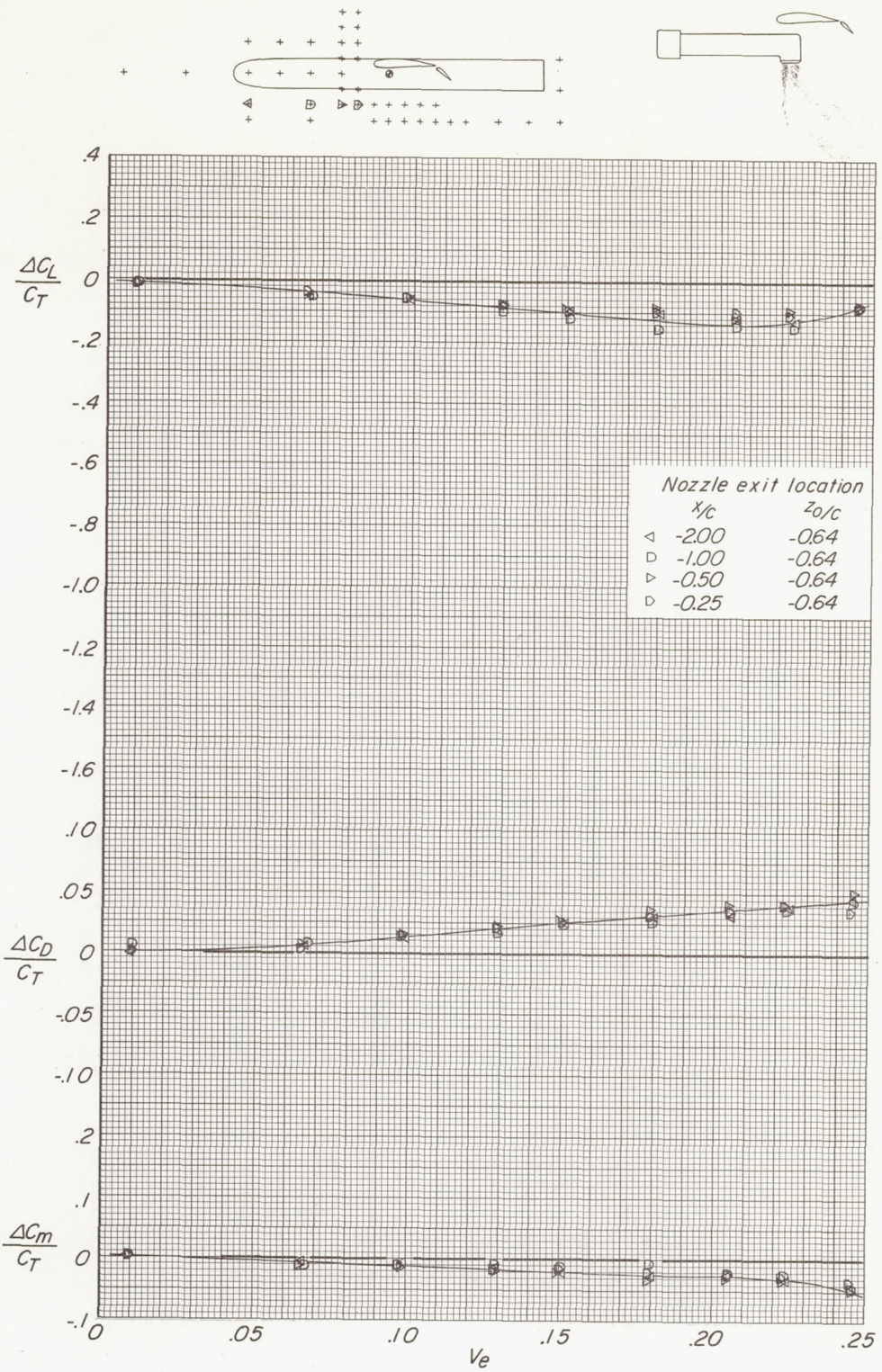

(g) $z_0/c = -0.64$.

Figure 10.- Continued.

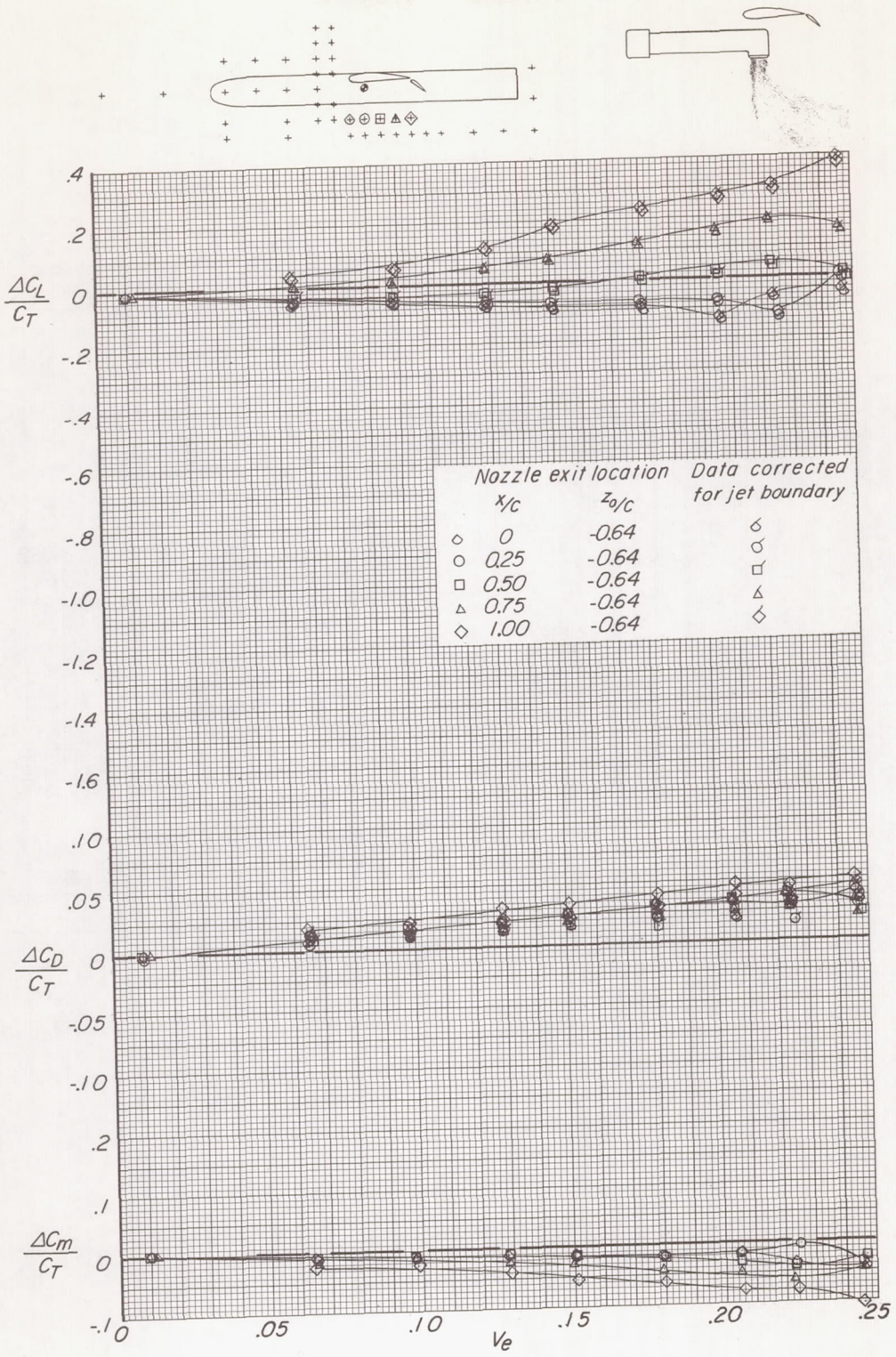

(g) Concluded.

Figure 10.- Continued.

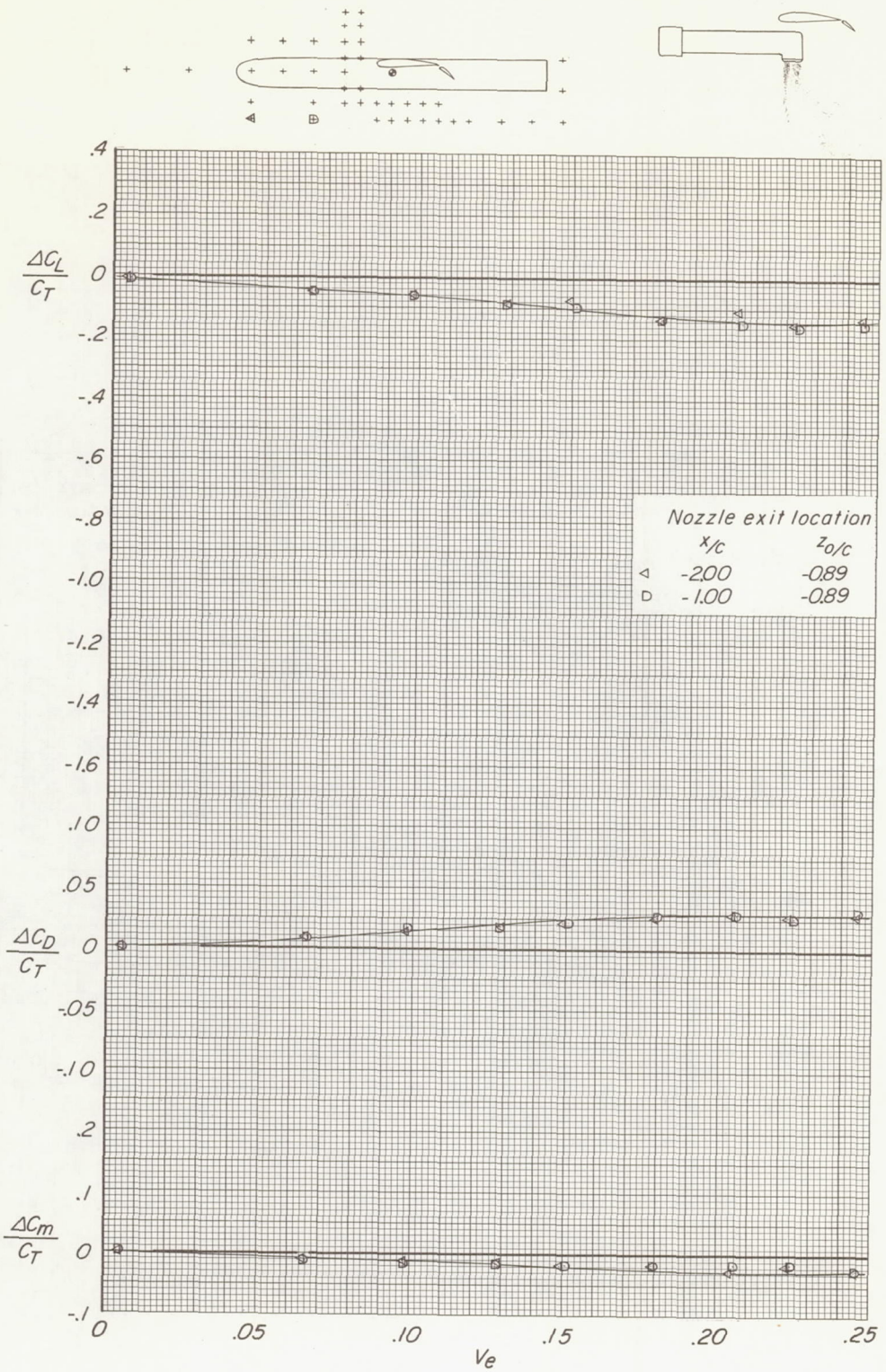

(h) $z_o/c = -0.89$.

Figure 10.- Continued.

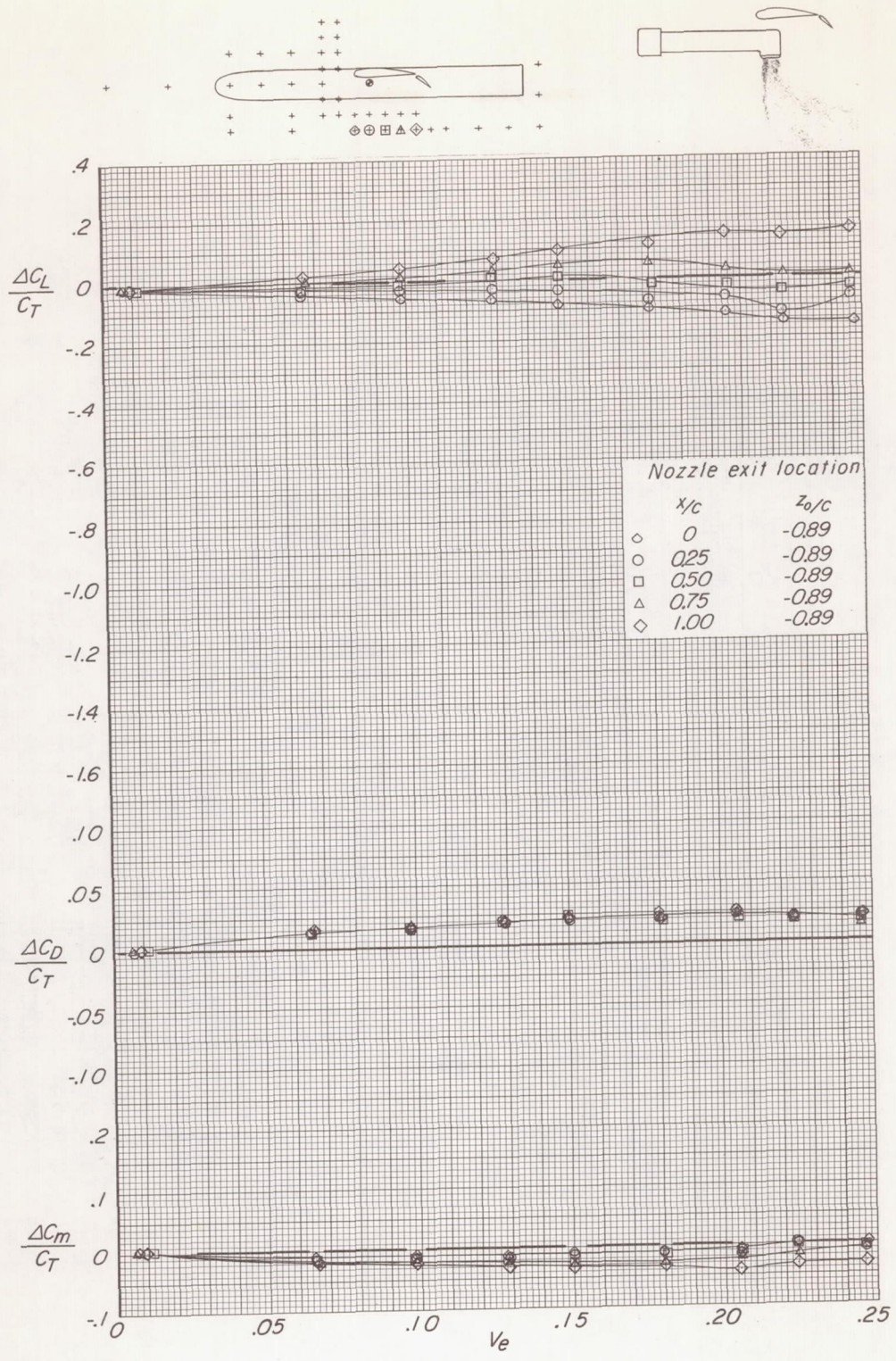

(h) Continued.

Figure 10.- Continued.

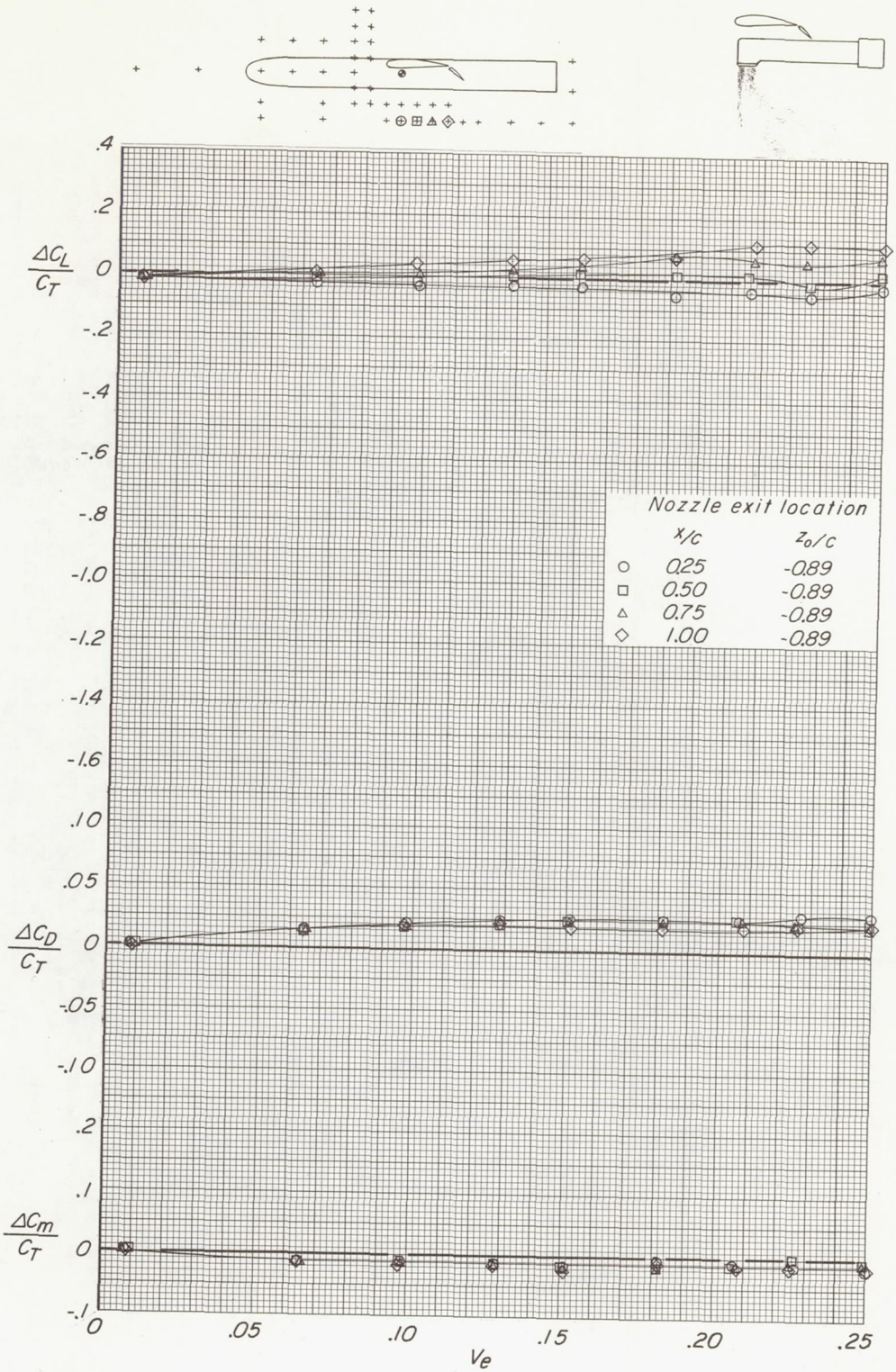

(h) Continued.

Figure 10.- Continued.

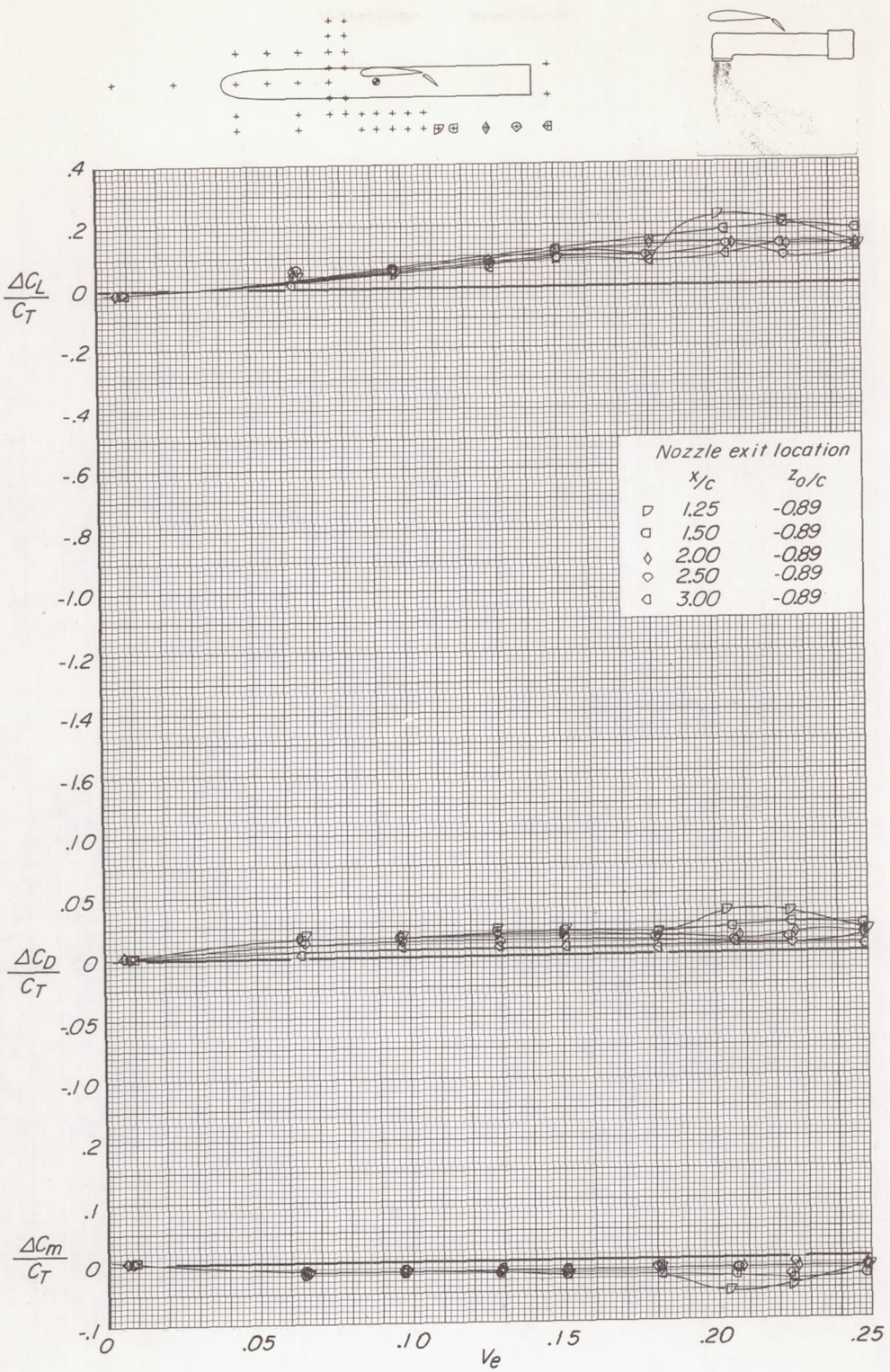

(h) Concluded.

Figure 10.- Concluded.

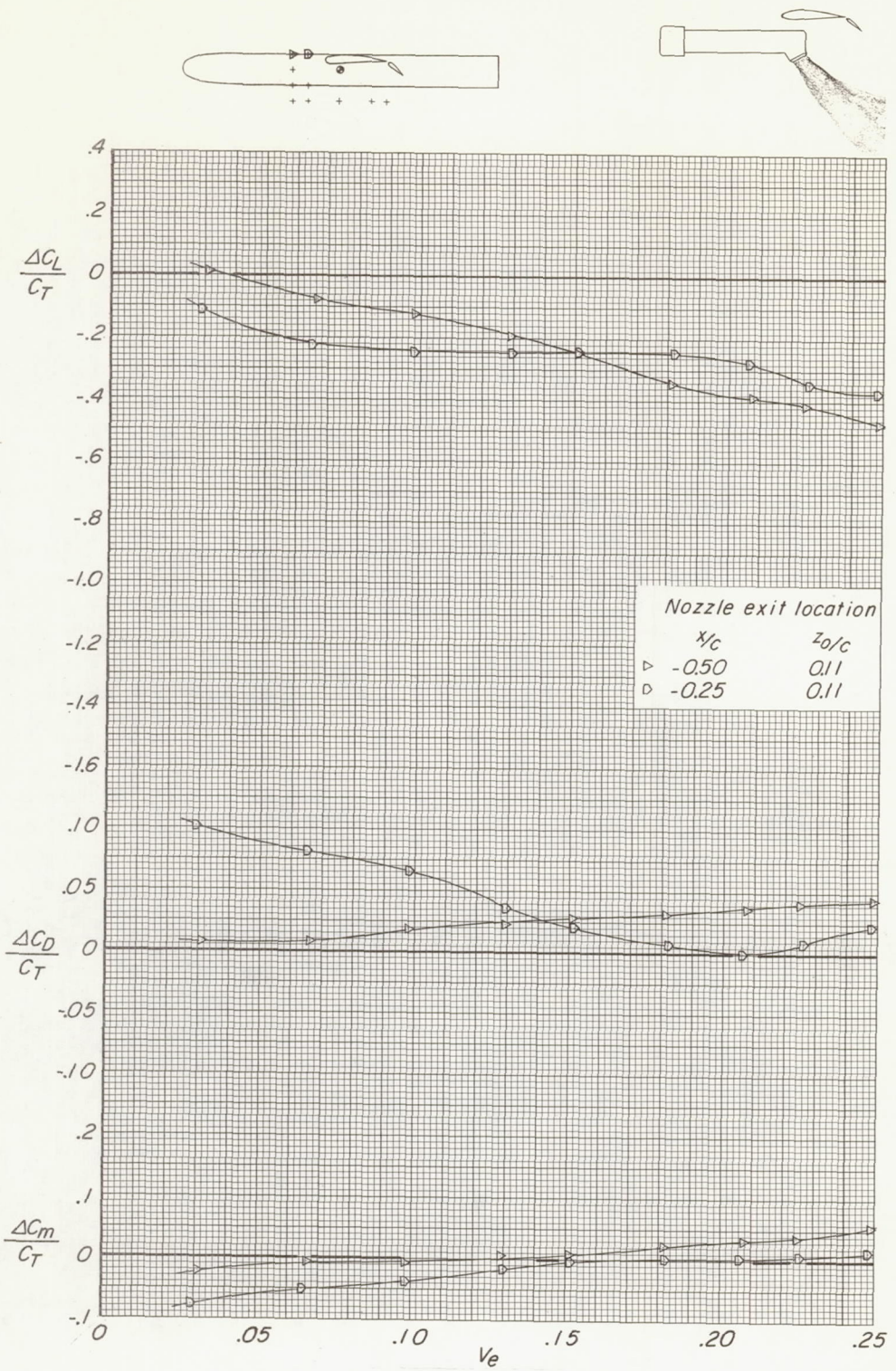

(a) $z_o/c = 0.11$.

Figure 11.- Variation of lift, drag, and pitching-moment increments due to power with effective velocity ratio. $\delta_f = 40^o$; $\delta_j = 60^o$.

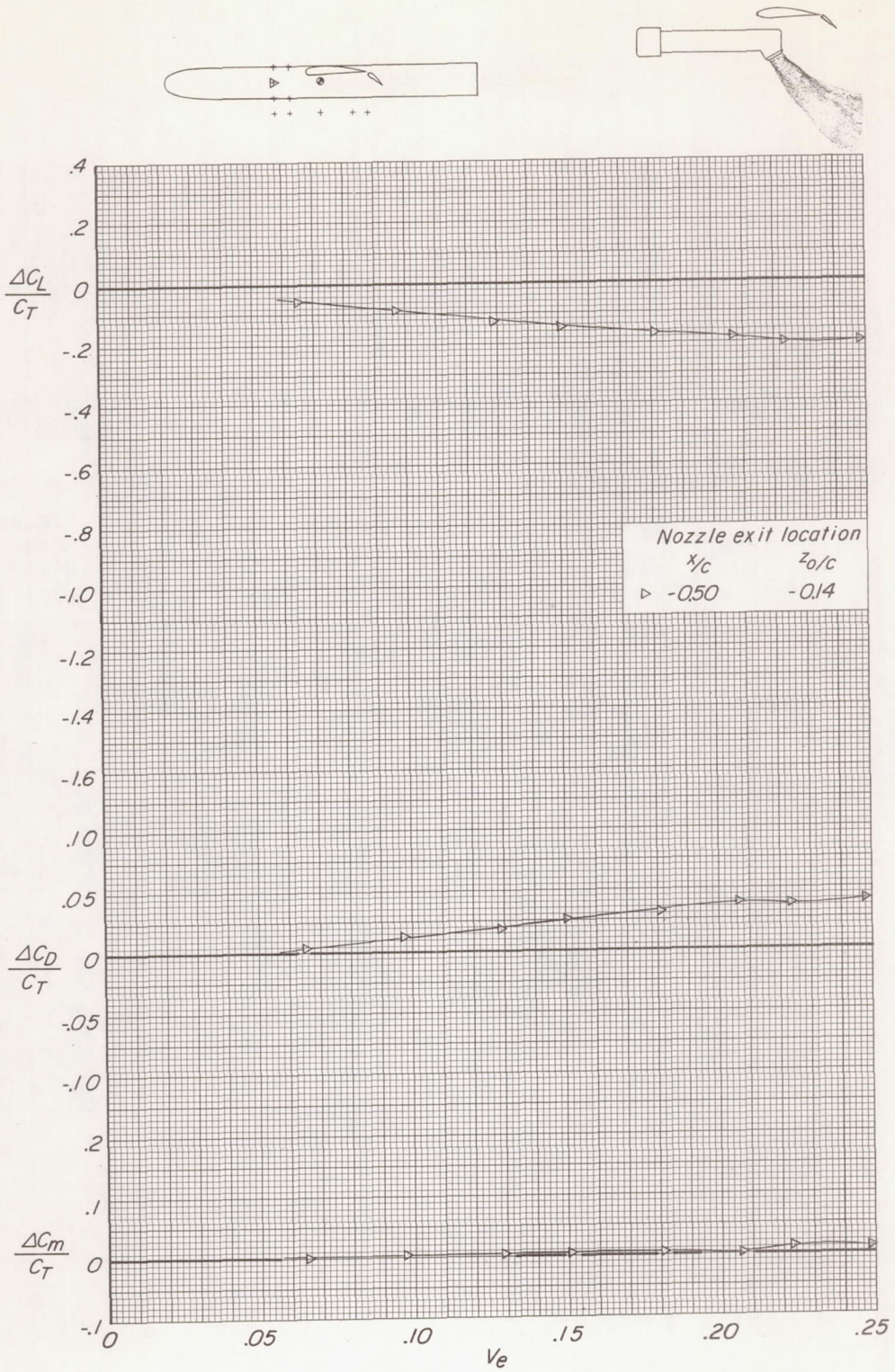

(b) $z_0/c = -0.14$.

Figure 11.- Continued.

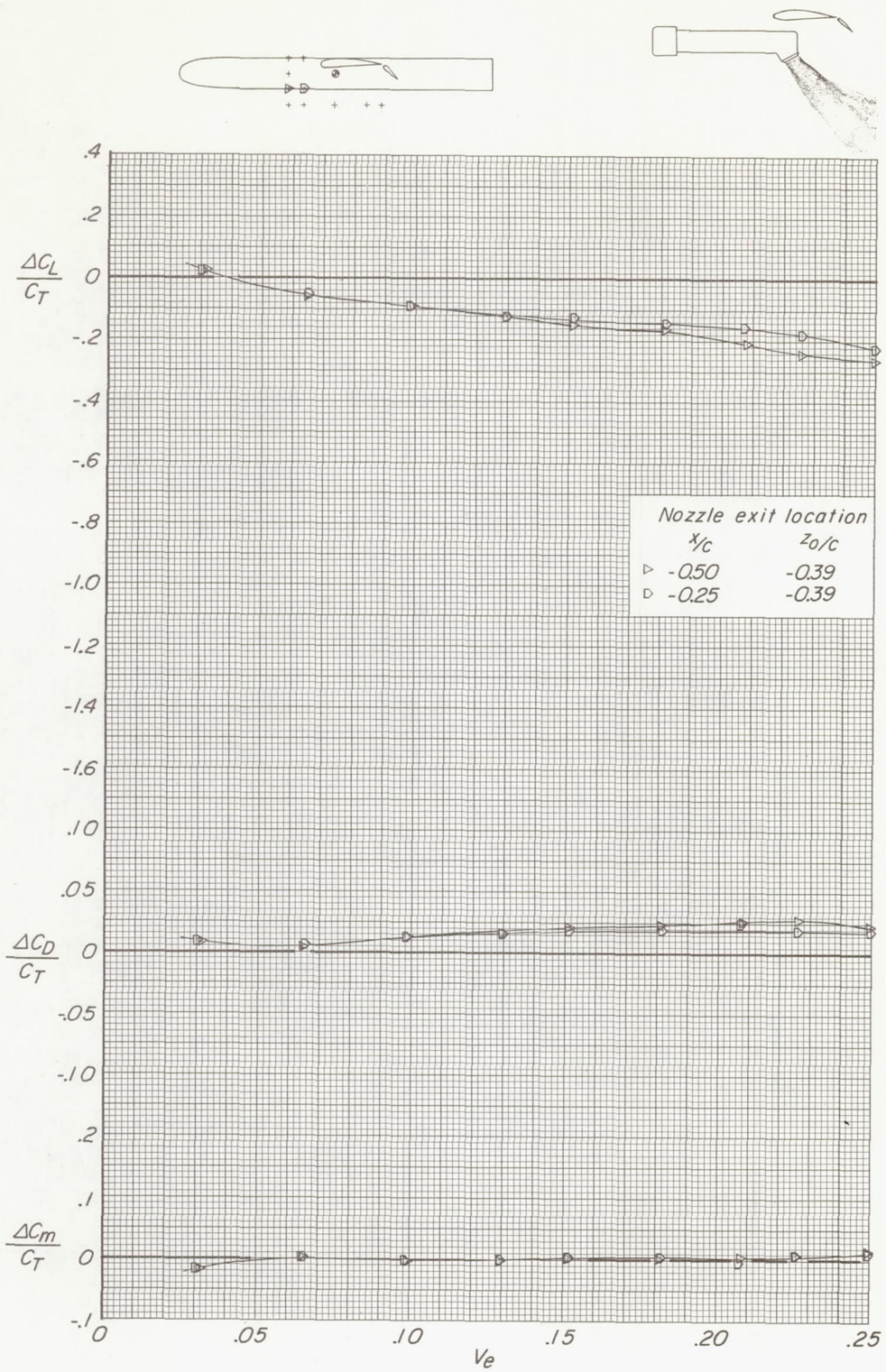

(c) $z_0/c = -0.39$.

Figure 11.- Continued.

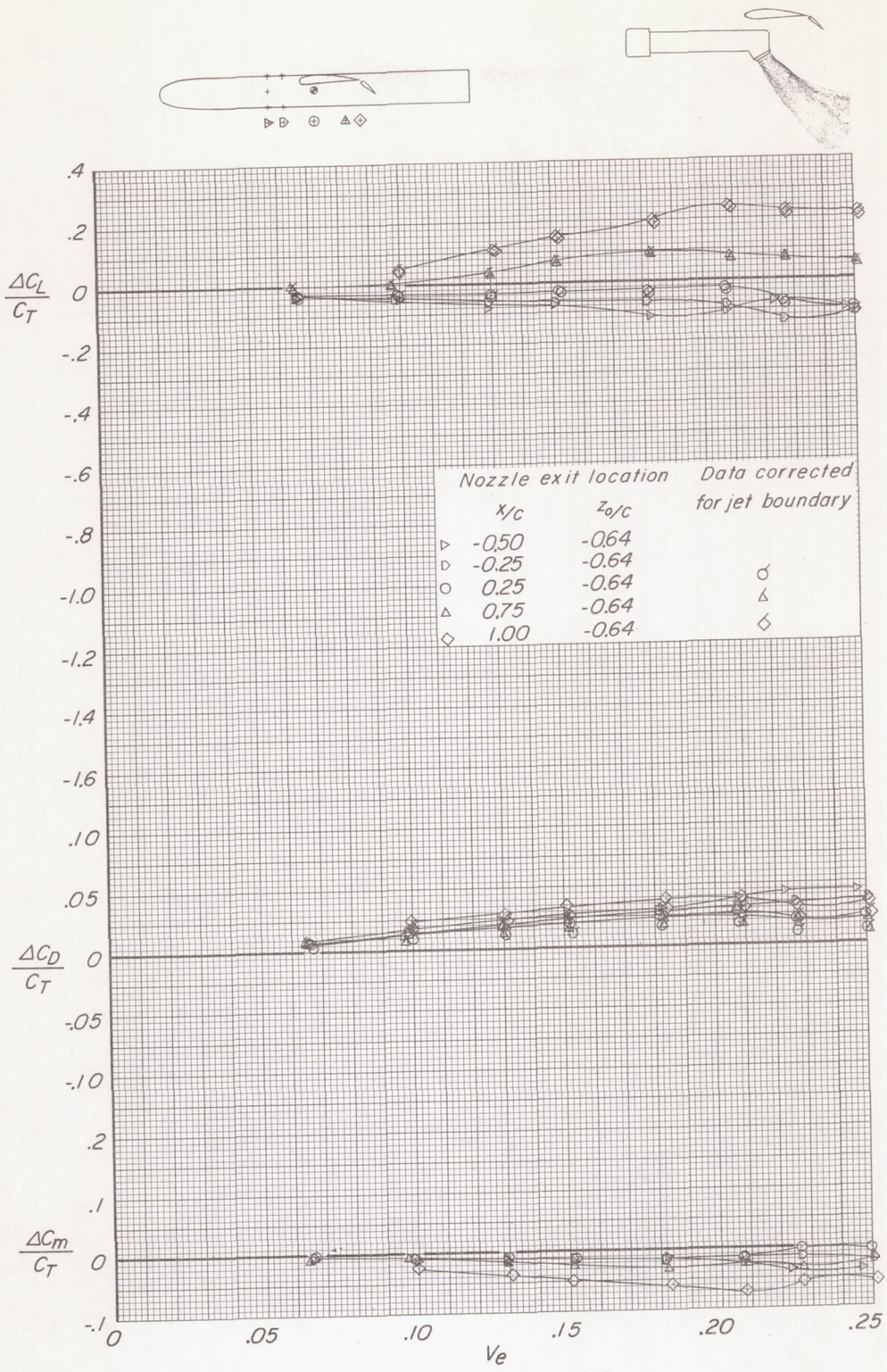

(d) $z_o/c = -0.64$.

Figure 11.- Concluded.

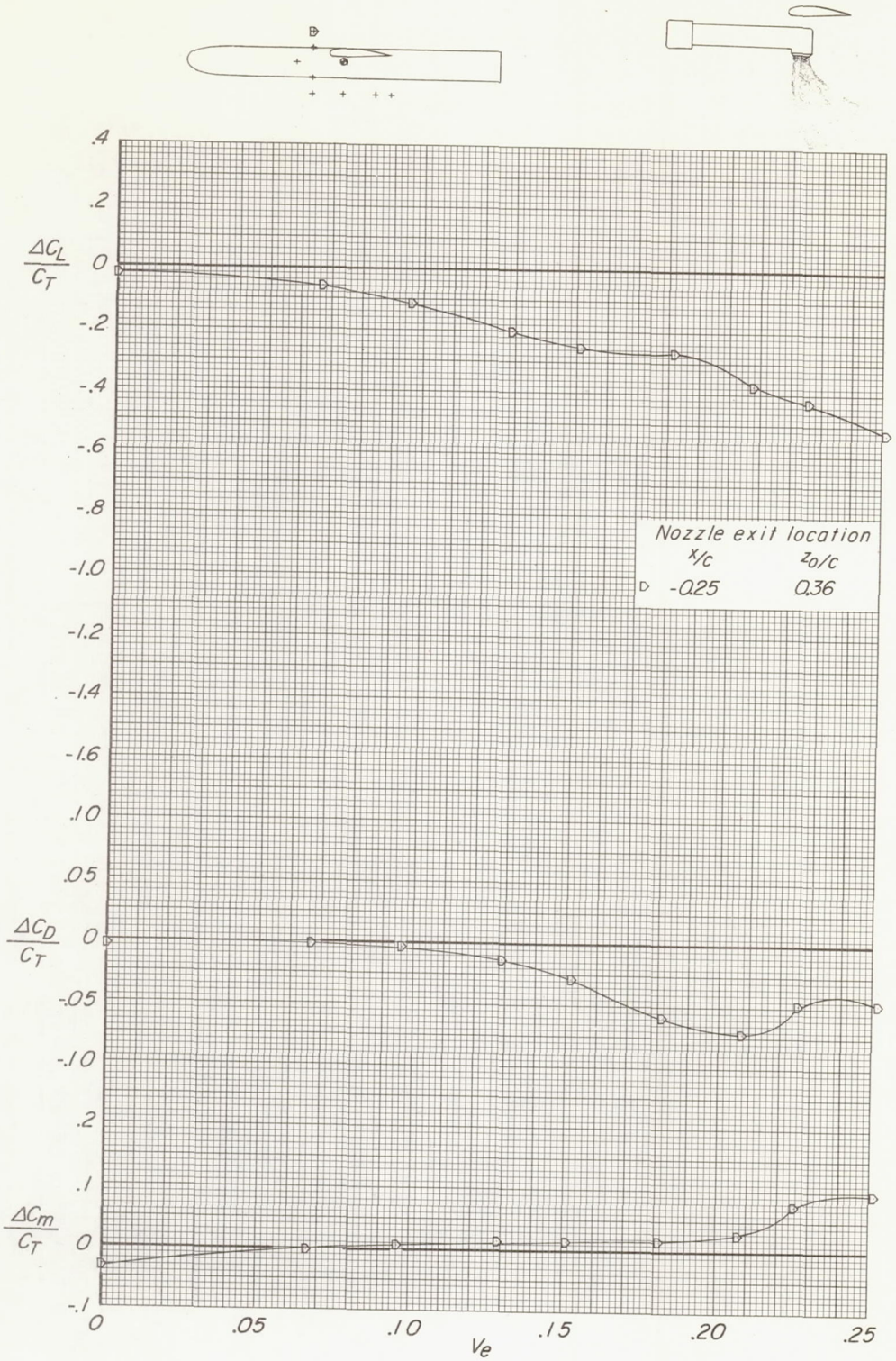

(a) $z_o/c = 0.36$.

Figure 12.- Variation of lift, drag, and pitching-moment increments due to power with effective velocity ratio. $\delta_f = 0^0$; $\delta_j = 90^0$.

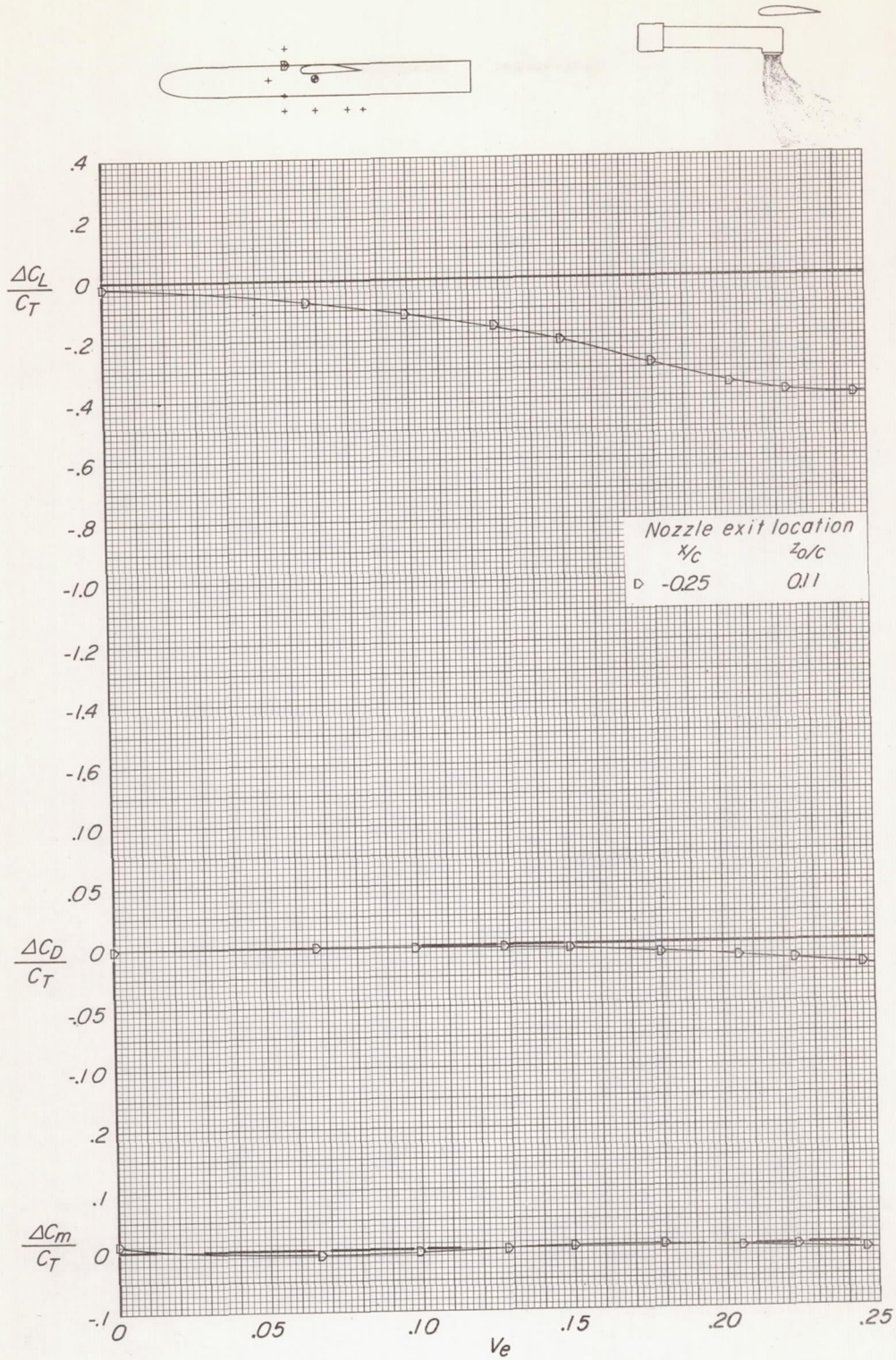

(b) $z_0/c = 0.11$.

Figure 12.- Continued.

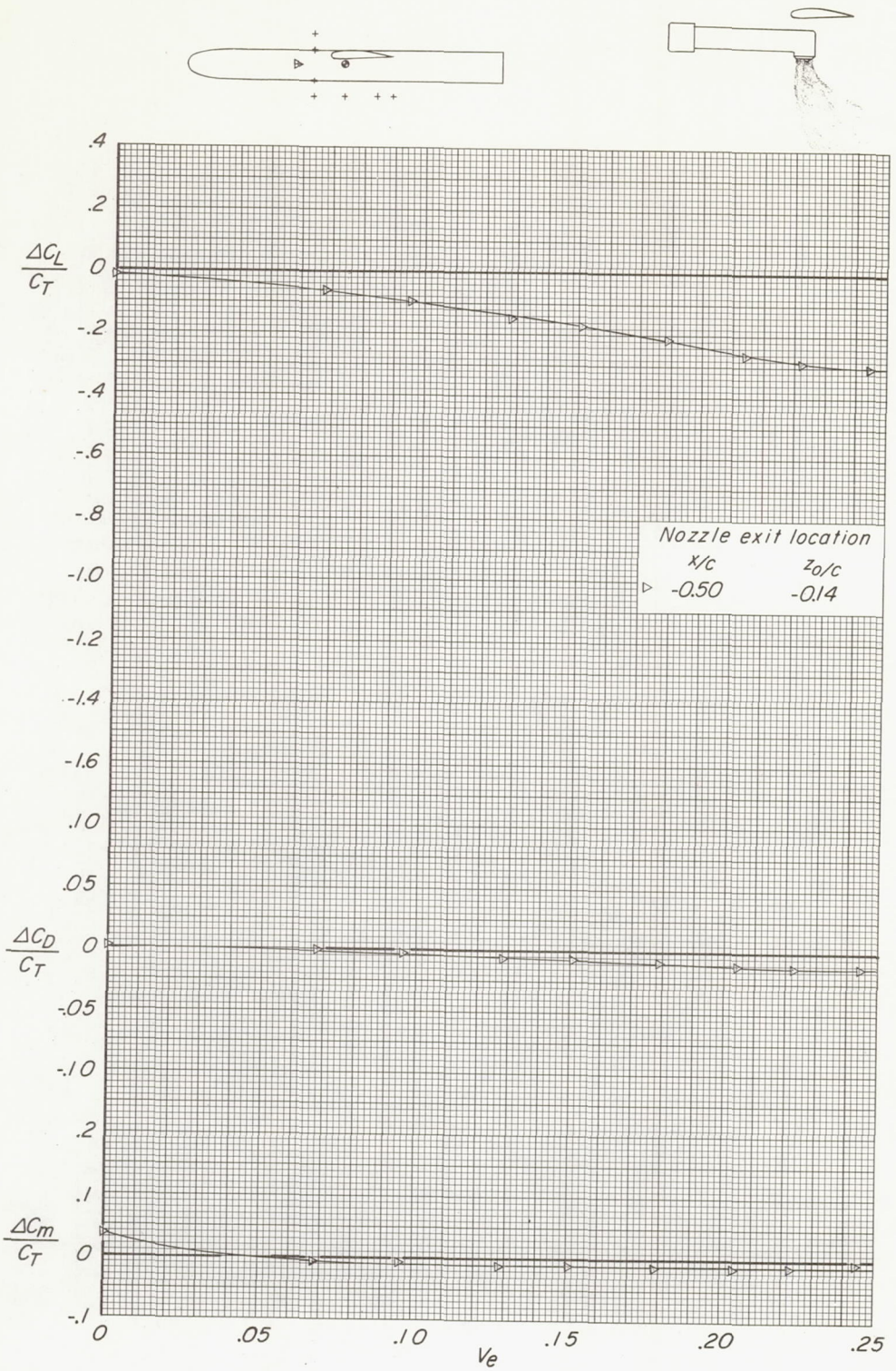

(c) $z_o/c = -0.14$.

Figure 12.- Continued.

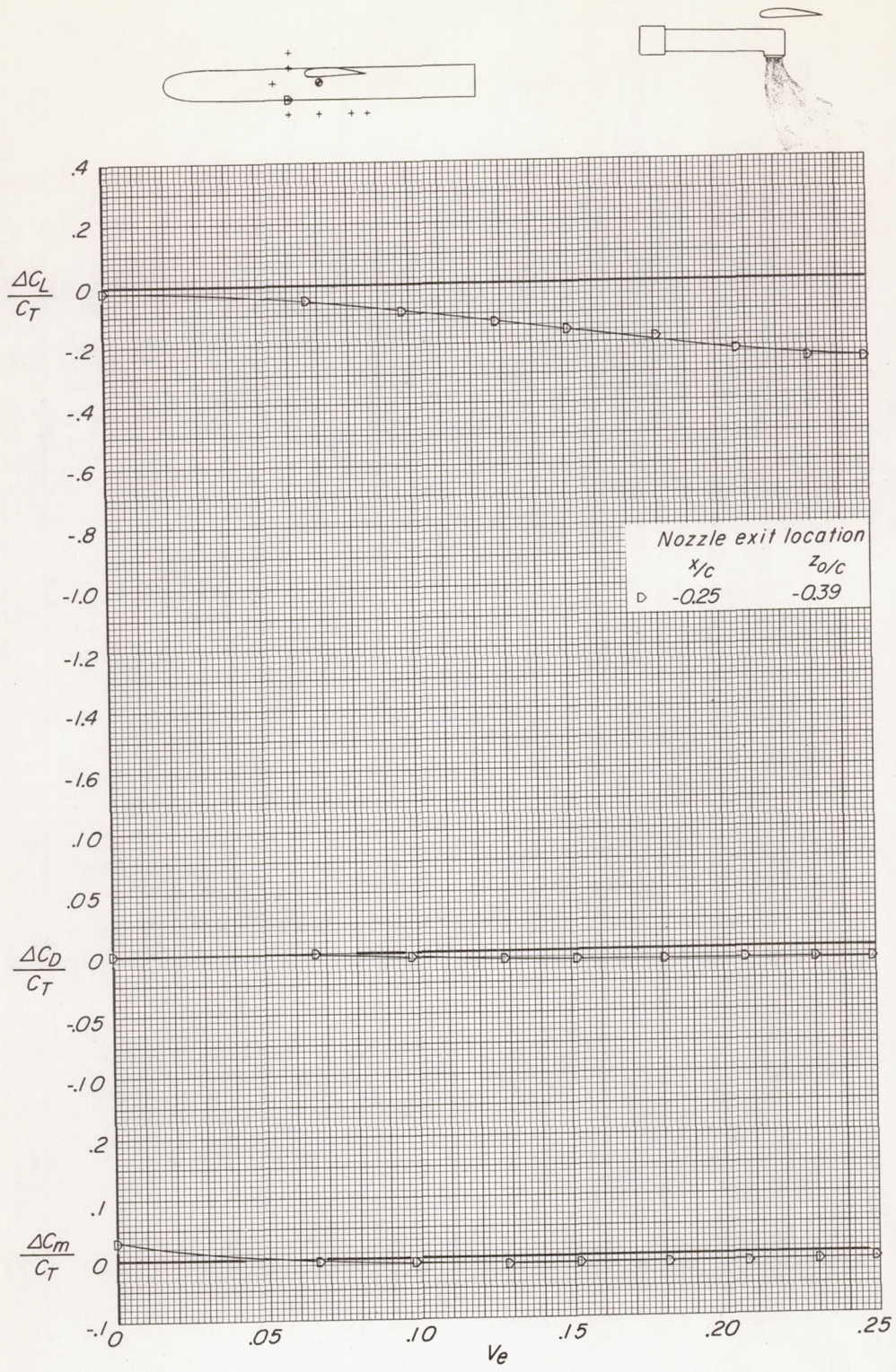

(d) $z_0/c = -0.39$.

Figure 12.- Continued.

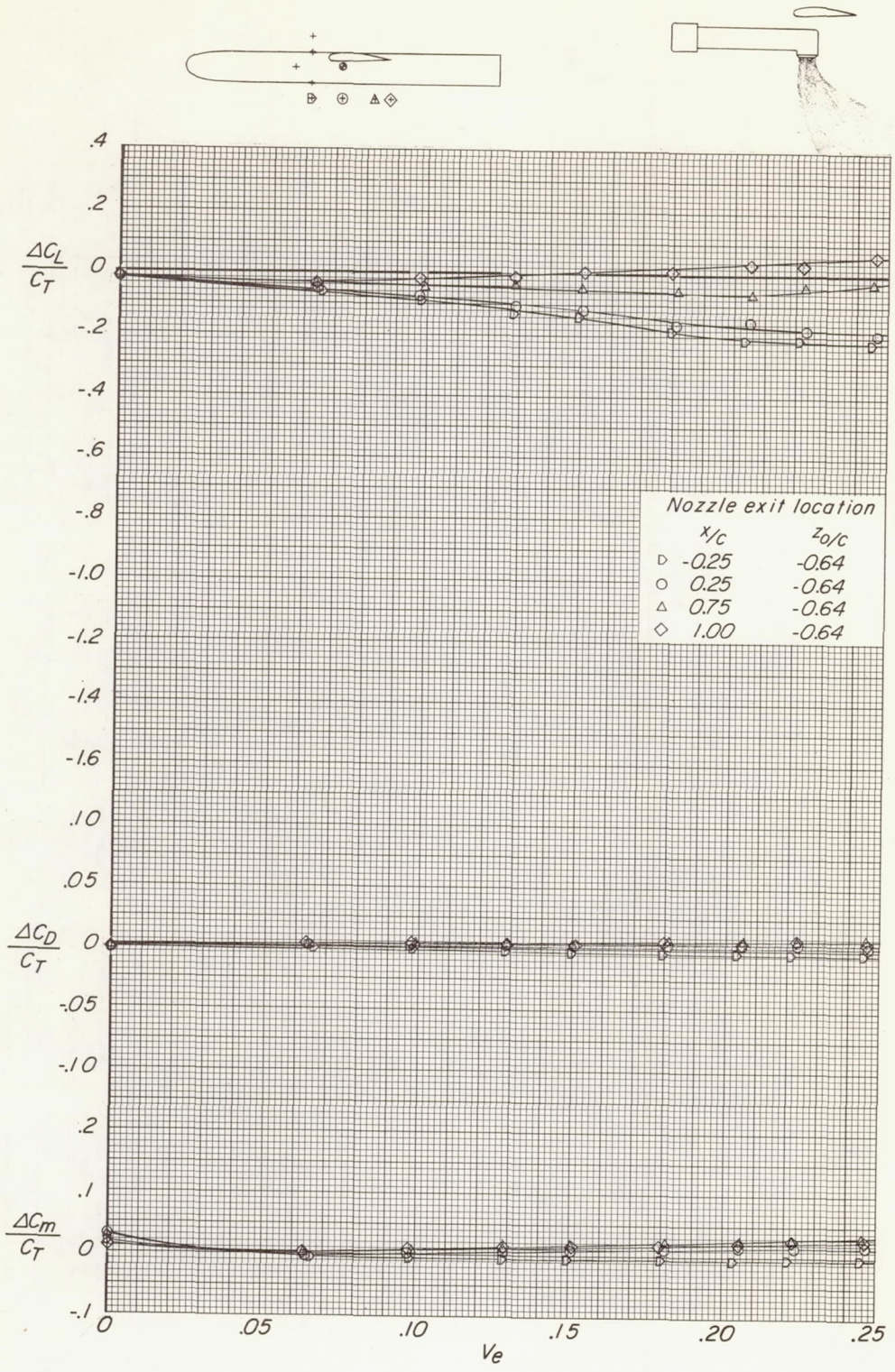

(e) $z_0/c = -0.64$.

Figure 12.- Concluded.

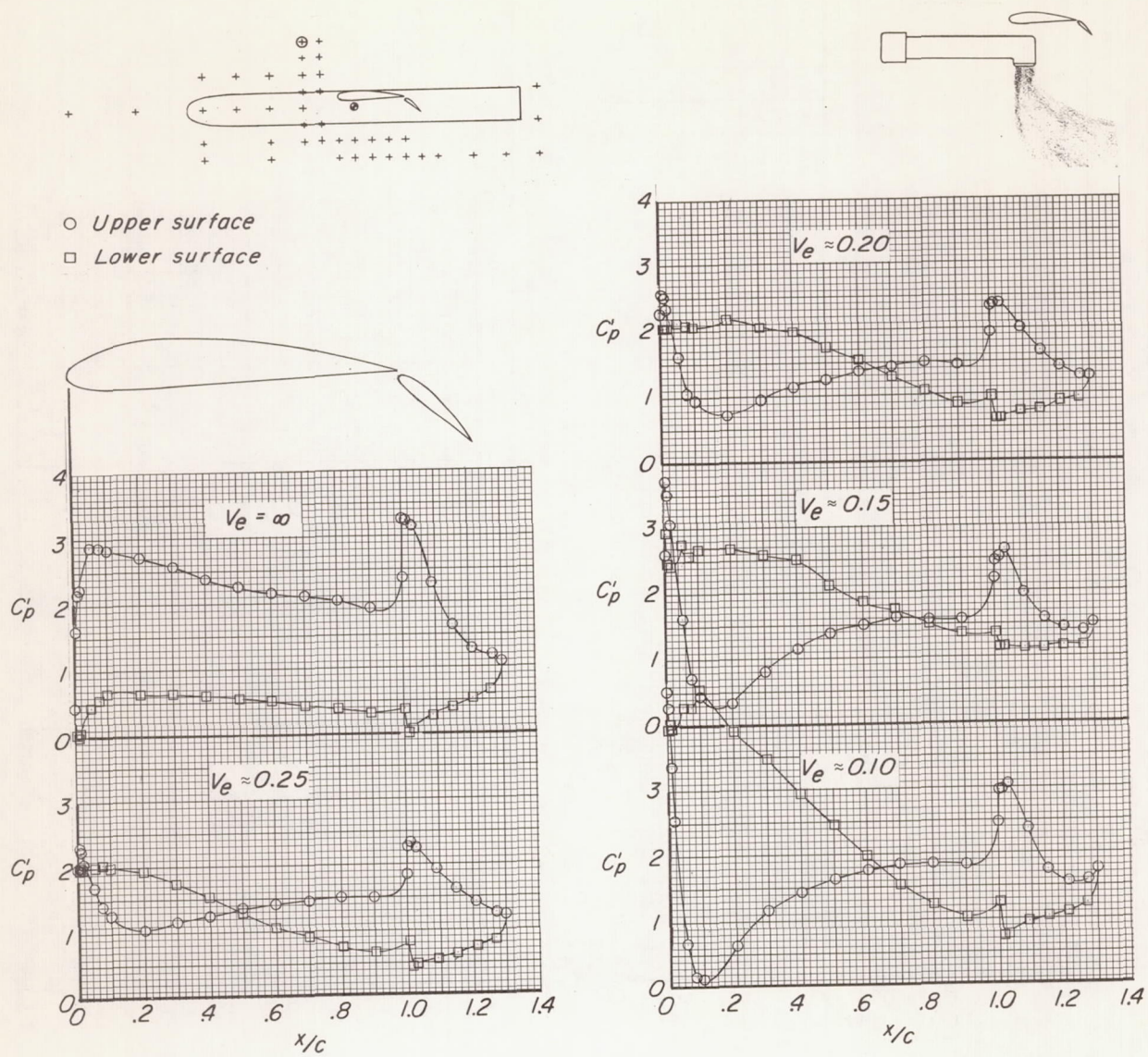

(a) Nozzle exit location: $x/c = -0.50$, $z_0/c = 0.86$.

Figure 13.- Basic pressure distributions on wing and flap of the model at typical locations of the jets. $\delta_f = 40^0$; $\delta_j = 90^0$.

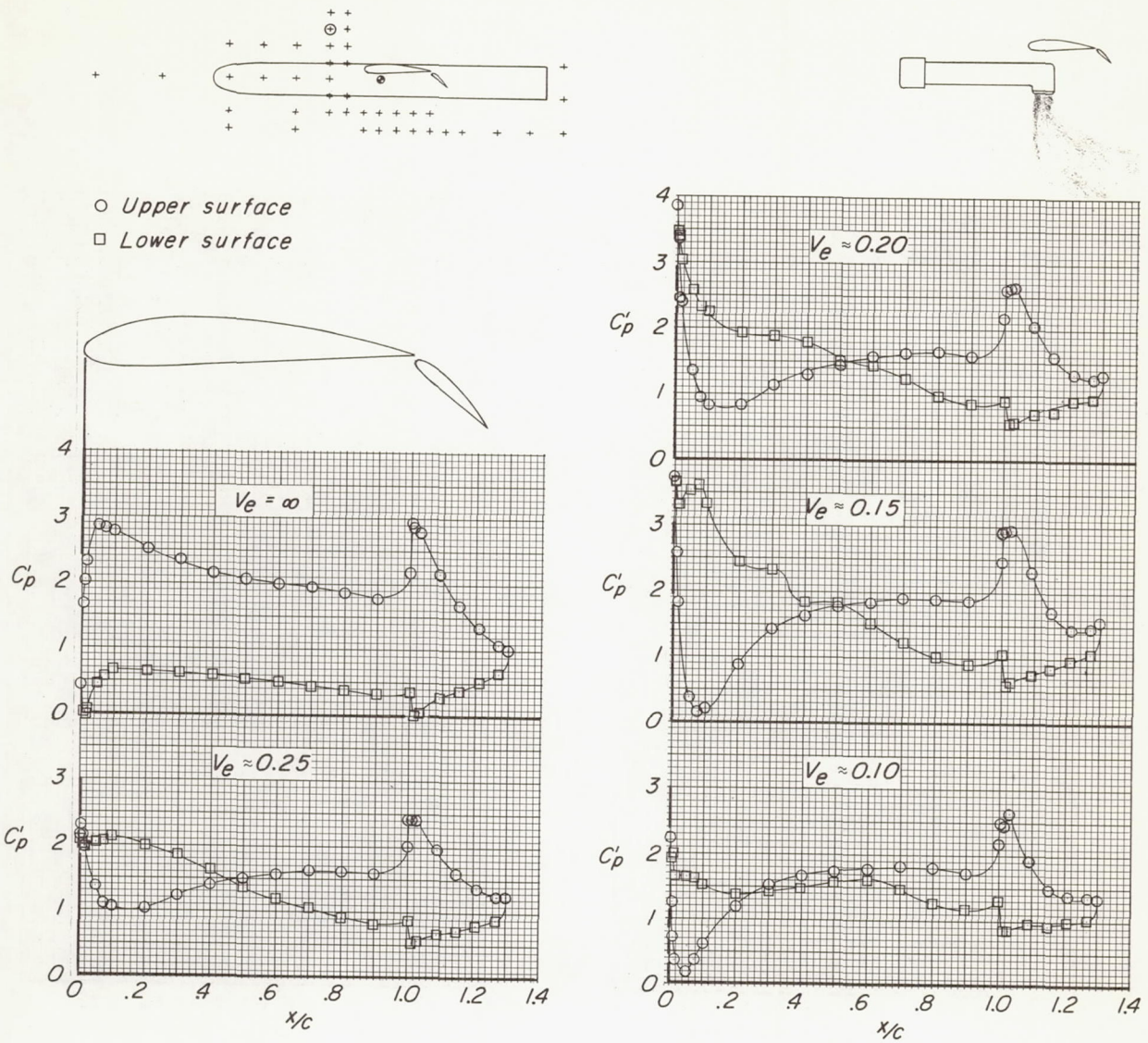

(b) Nozzle exit location: $x/c = -0.50$, $z_0/c = 0.61$.

Figure 13.- Continued.

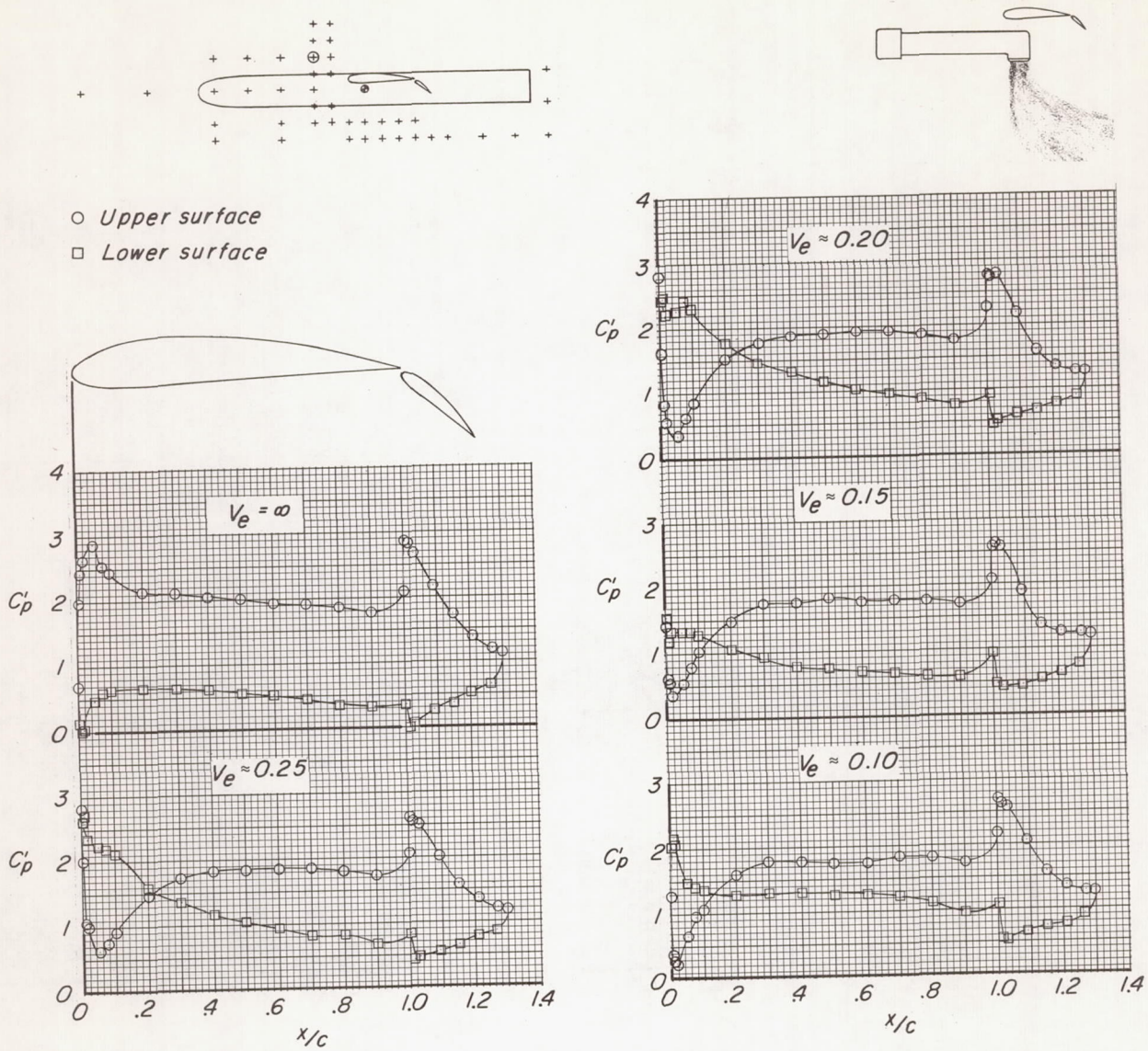

(c) Nozzle exit location: $x/c = -0.50$, $z_0/c = 0.36$.

Figure 13.- Continued.

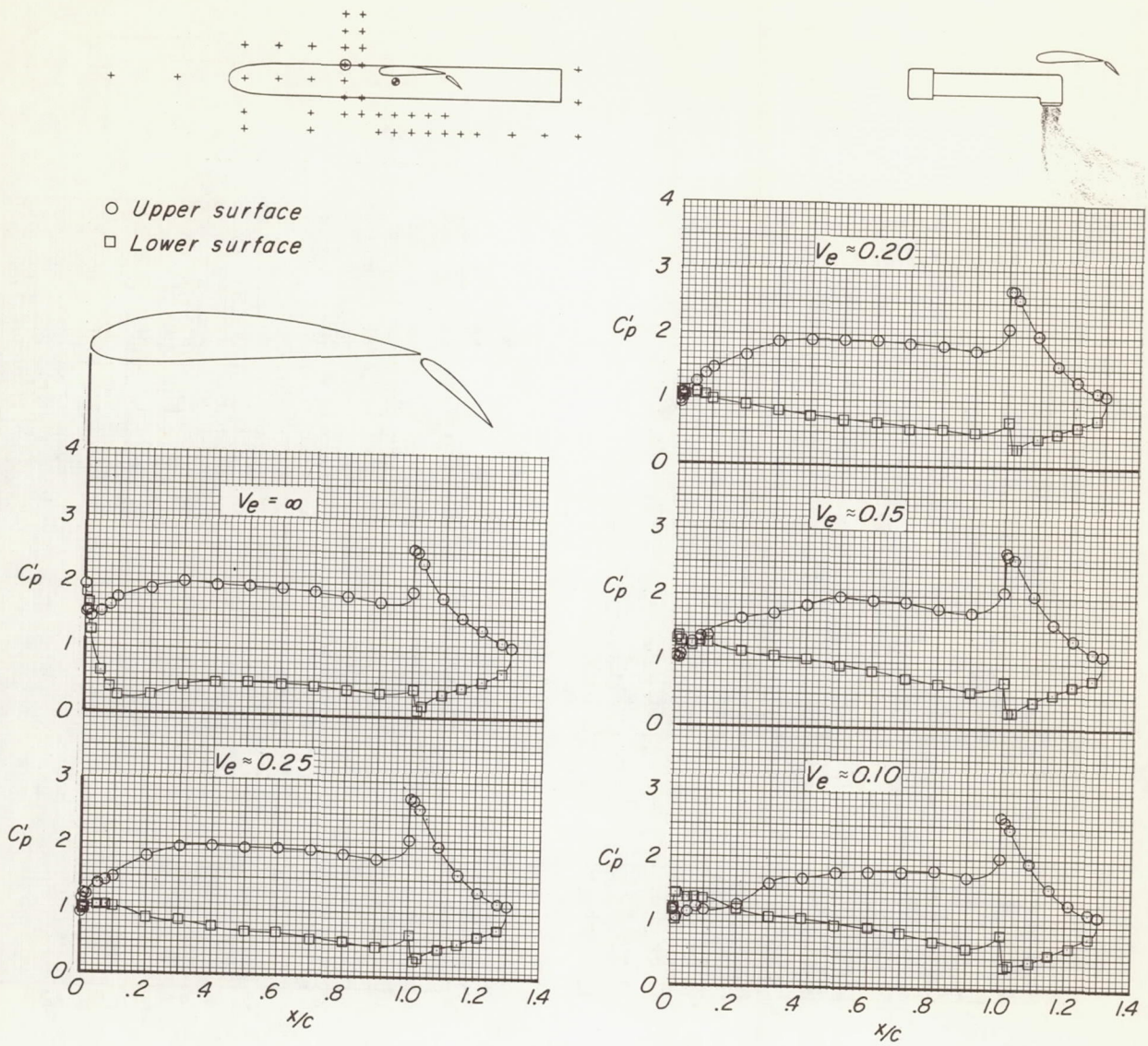

(d) Nozzle exit location: $x/c = -0.50$, $z_0/c = 0.11$.

Figure 13.- Continued.

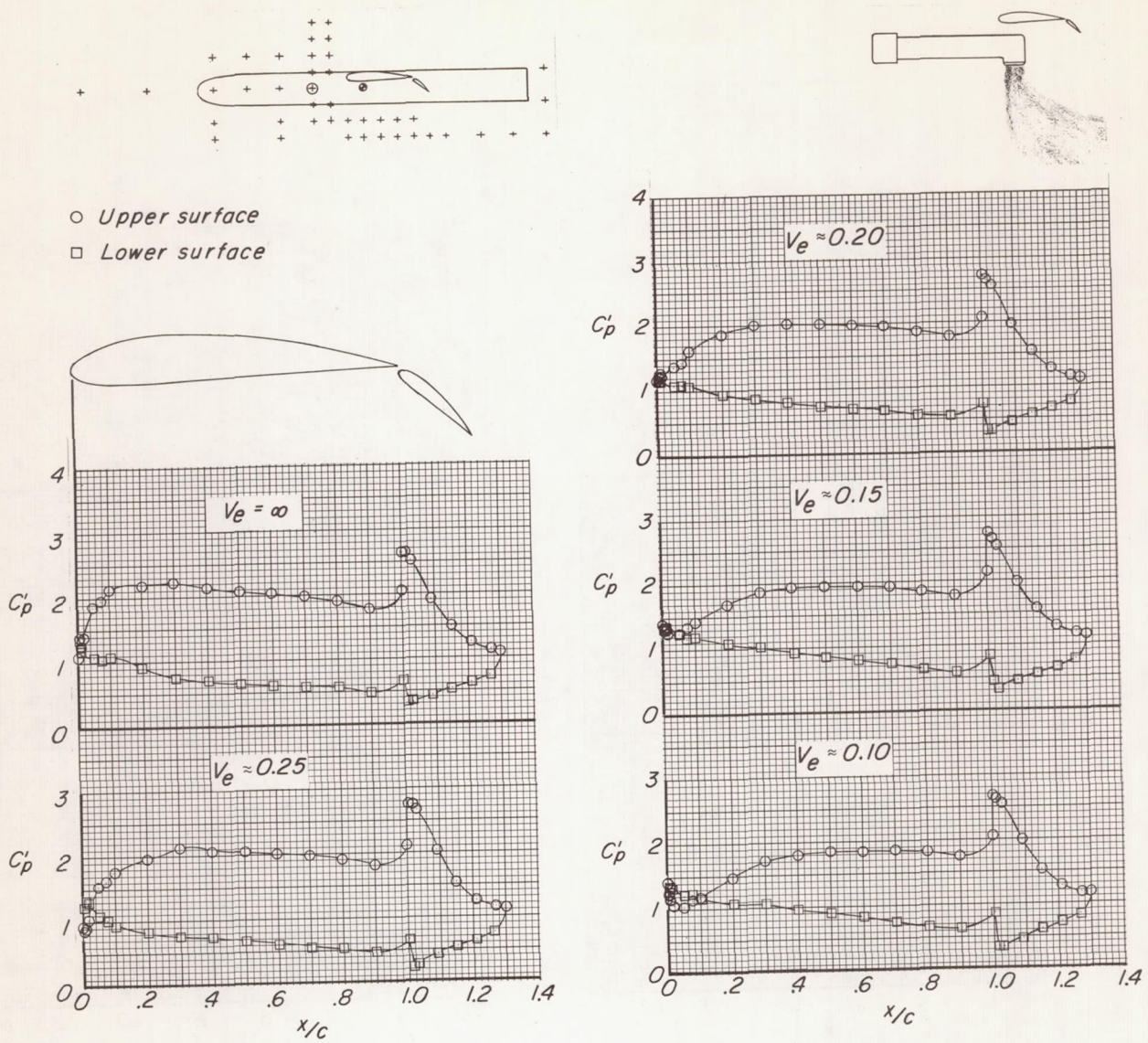

(e) Nozzle exit location: $x/c = -0.50$, $z_0/c = -0.14$.

Figure 13.- Continued.

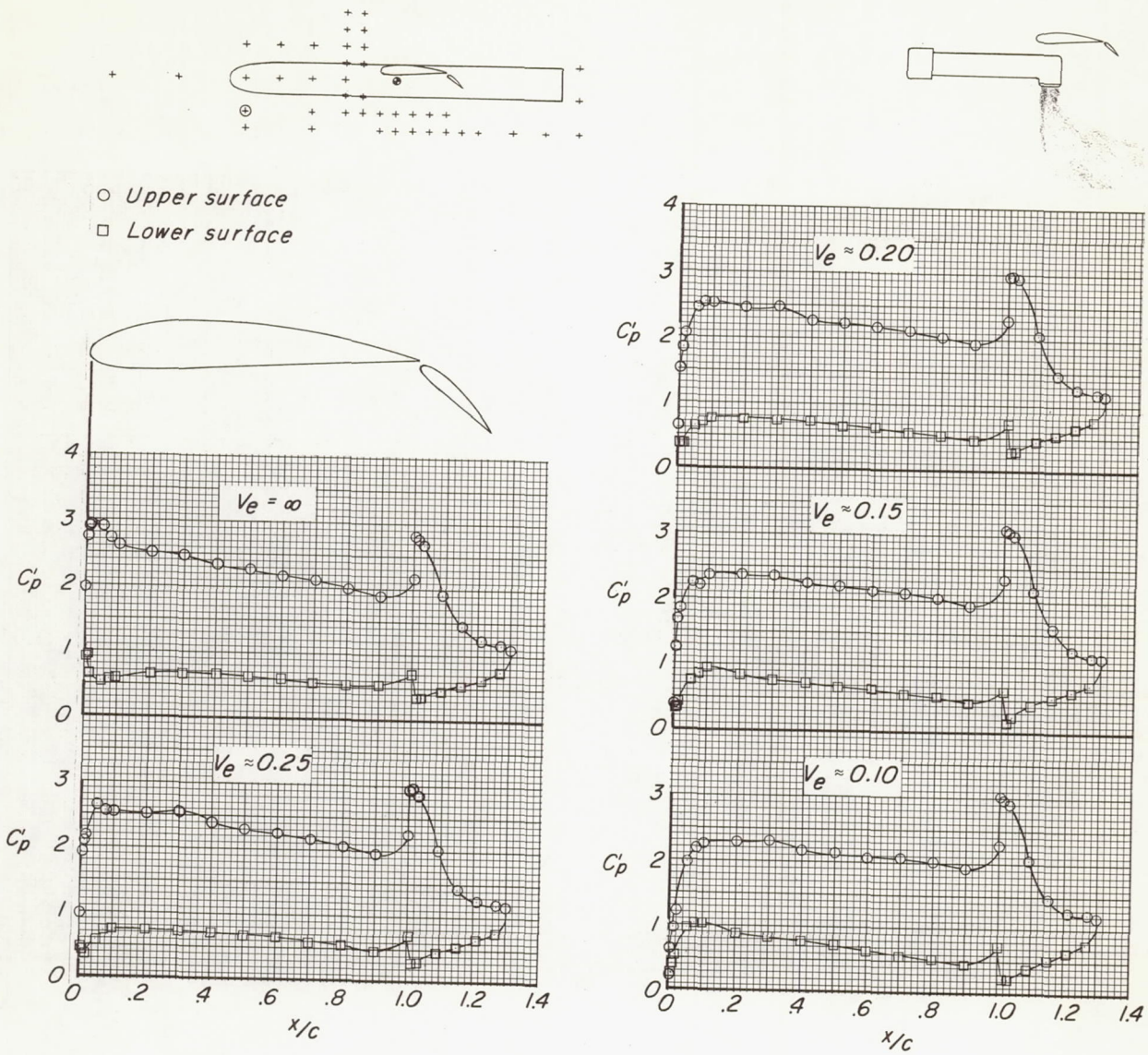

(f) Nozzle exit location: $x/c = -2.00$, $z_0/c = -0.64$.

Figure 13.- Continued.

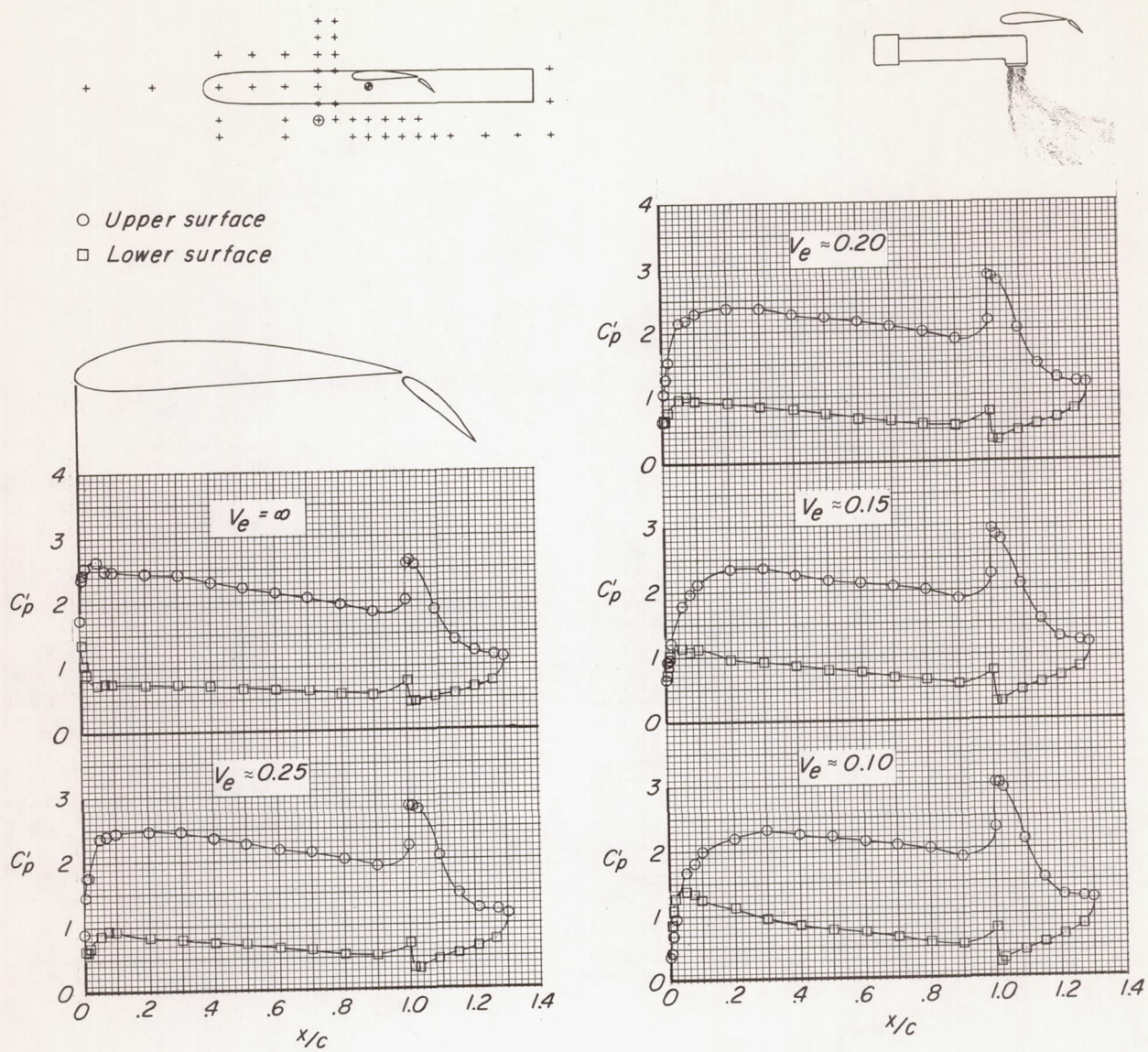

(g) Nozzle exit location: $x/c = -0.50$, $z_0/c = -0.64$.

Figure 13.- Continued.

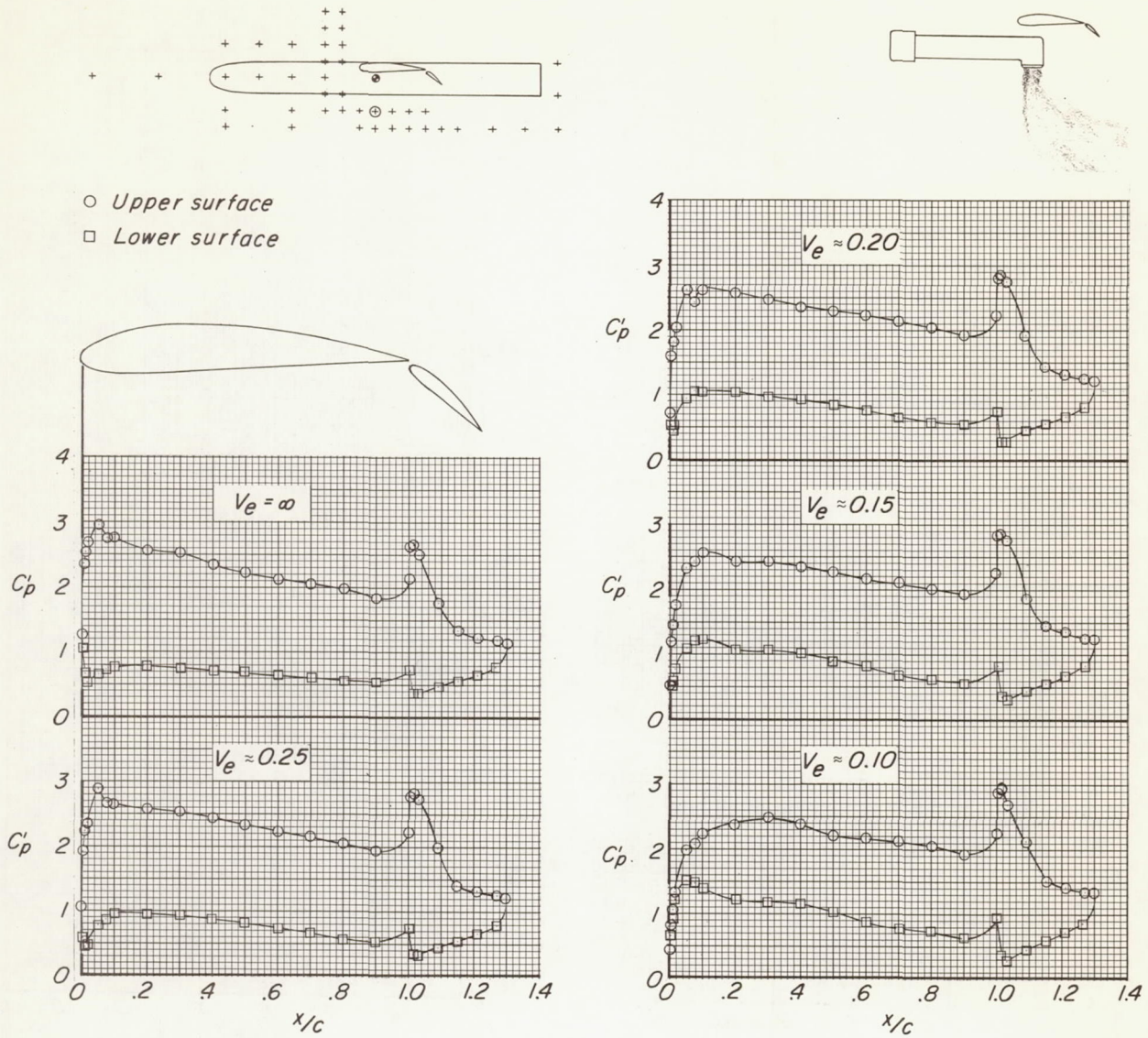

(h) Nozzle exit location: $x/c = 0.25$, $z_0/c = -0.64$.

Figure 13.- Continued.

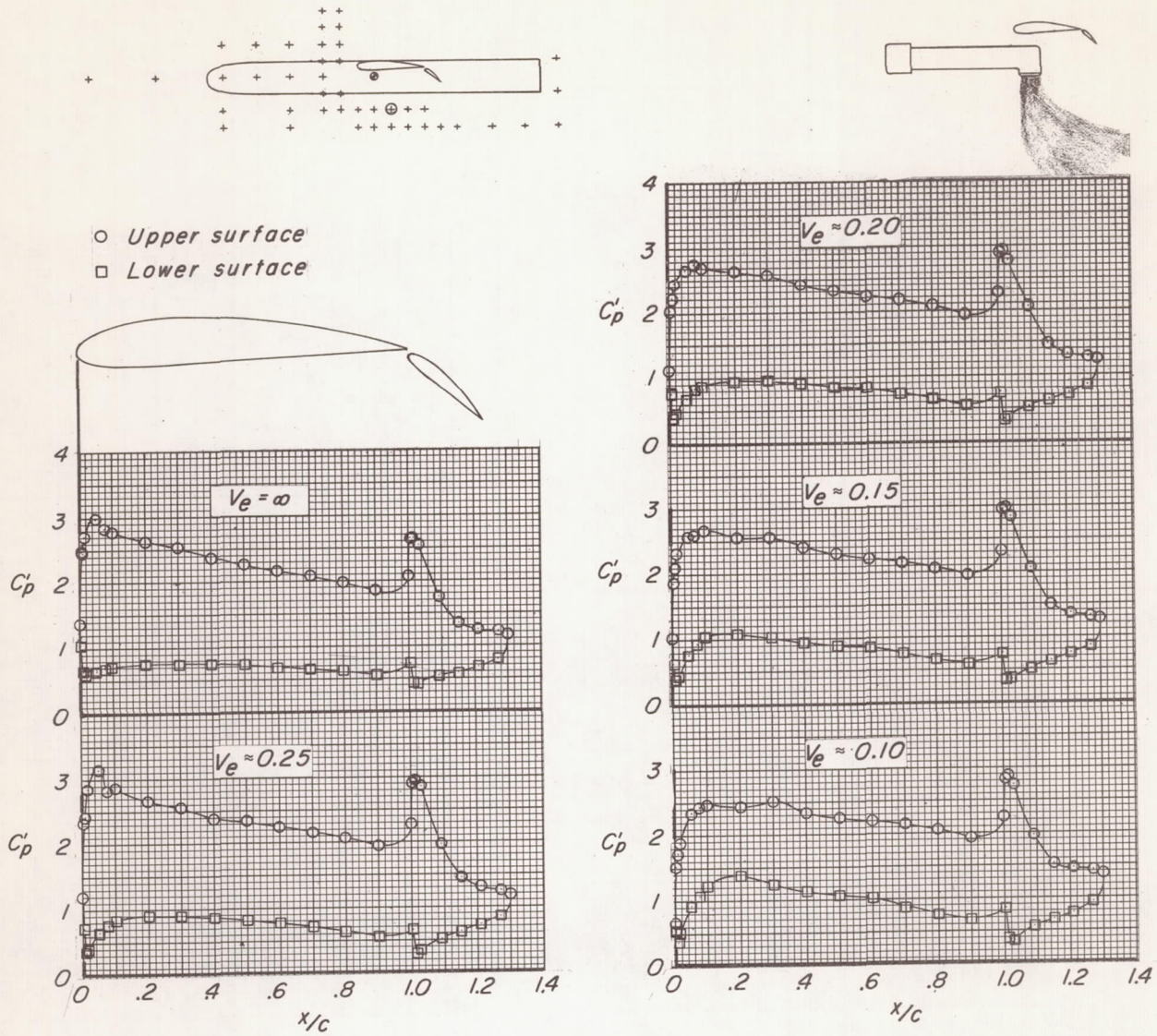

(i) Nozzle exit location: $x/c = 0.50$, $z_0/c = -0.64$.

Figure 13.- Continued.

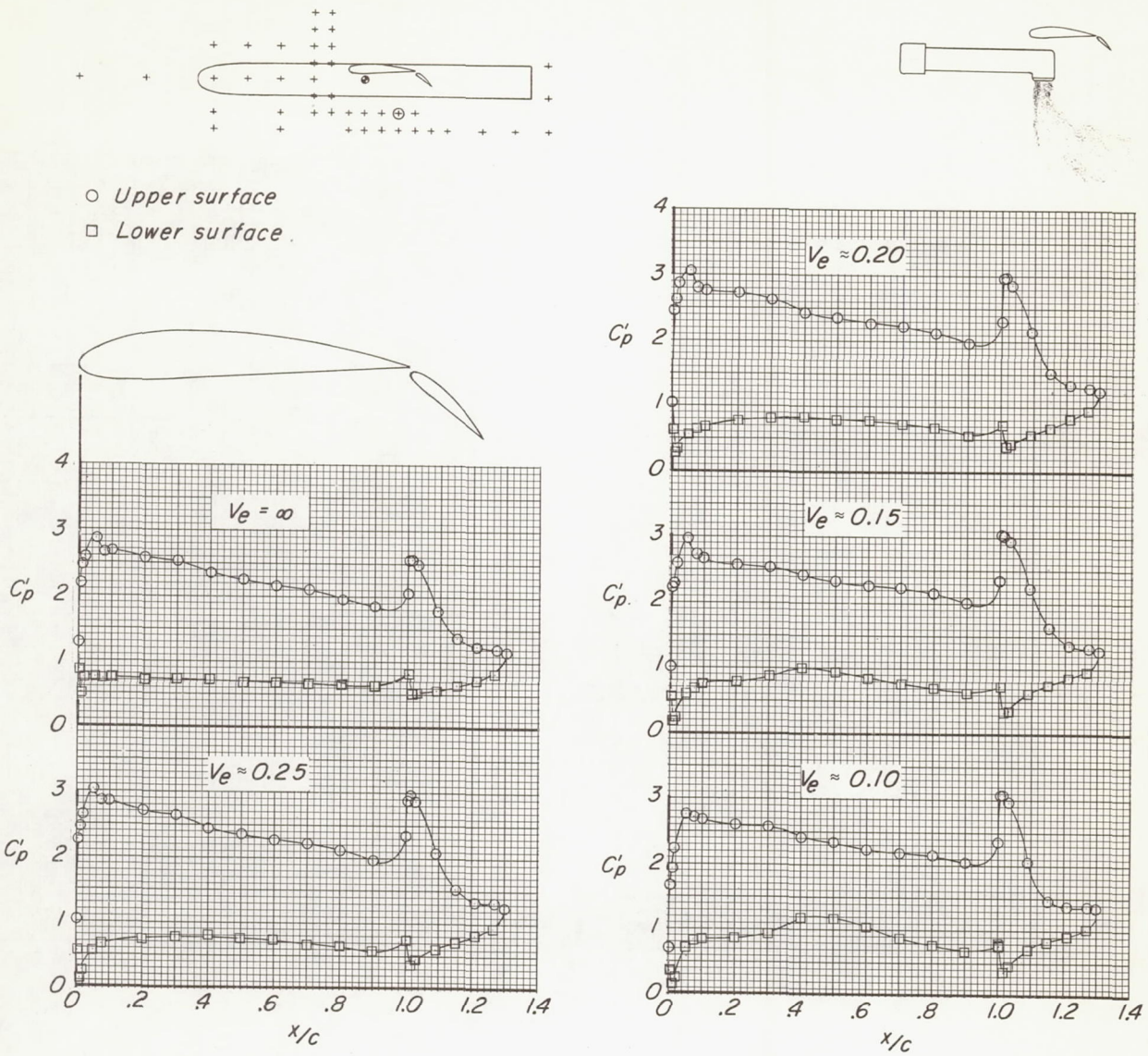

(j) Nozzle exit location: $x/c = 0.75$, $z_0/c = -0.64$.

Figure 13.- Continued.

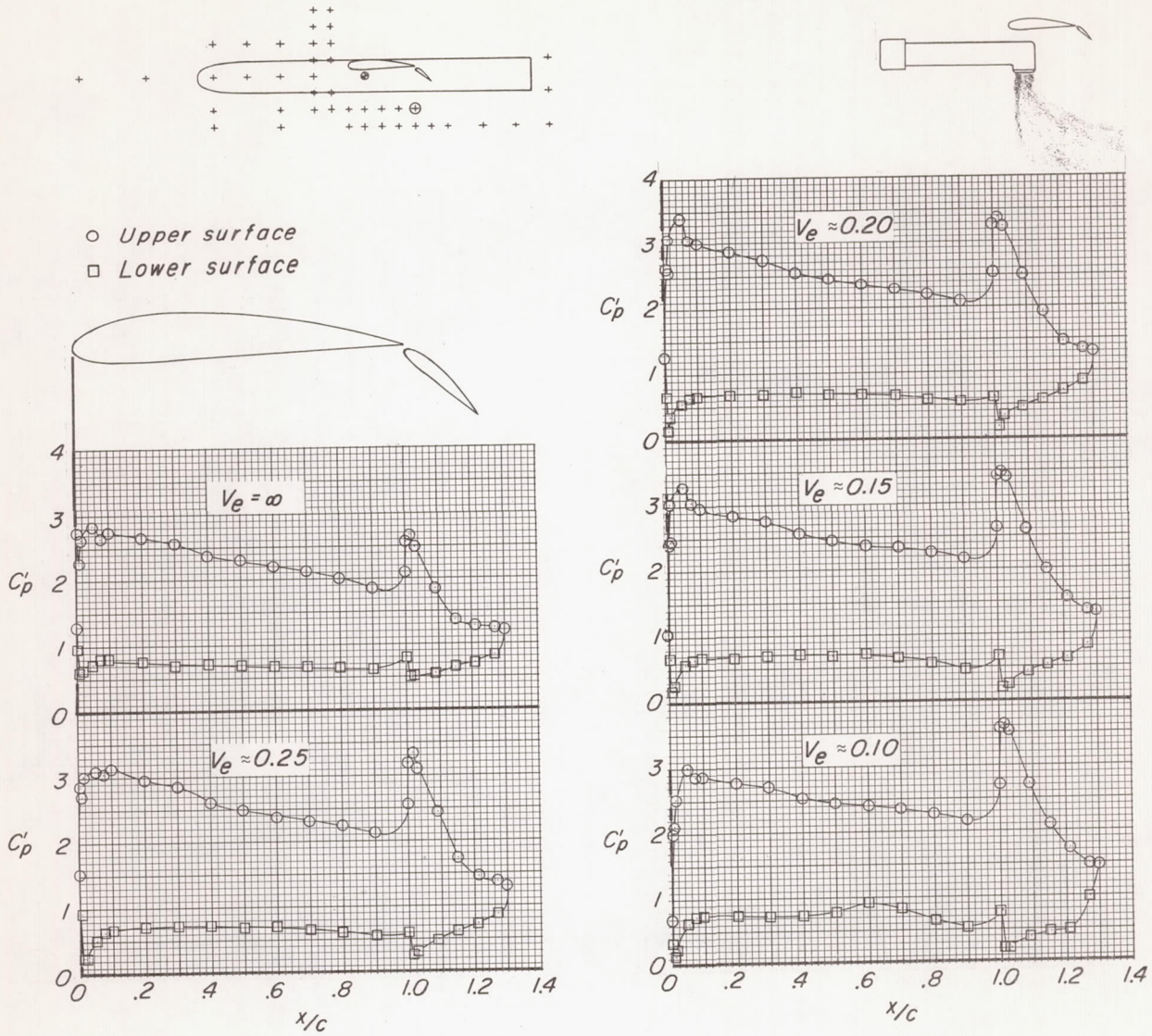

(k) Nozzle exit location: $x/c = 1.00$, $z_0/c = -0.64$.

Figure 13.- Continued.

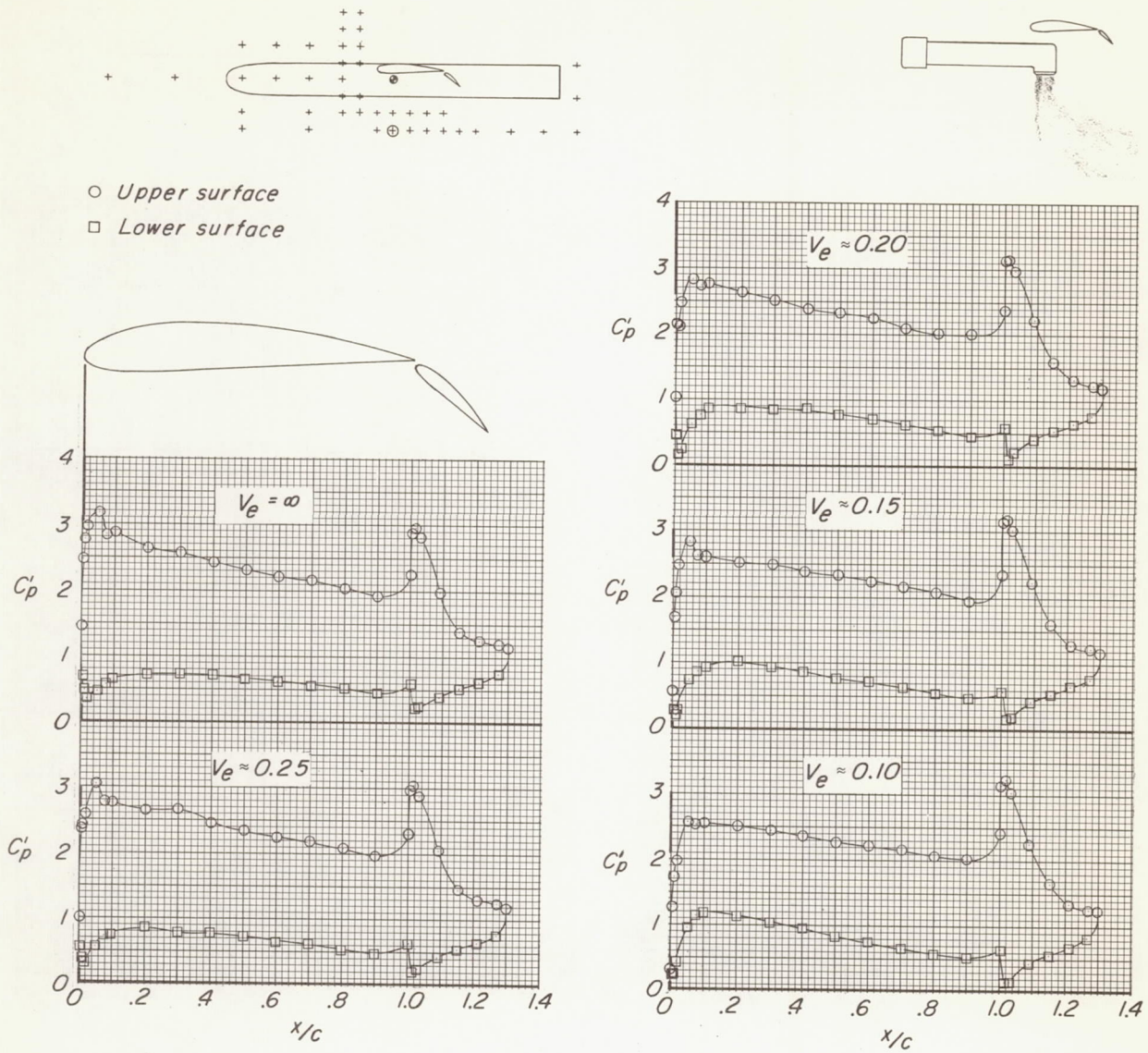

(l) Nozzle exit location: $x/c = 0.25$, $z_0/c = -0.89$.

Figure 13.- Continued.

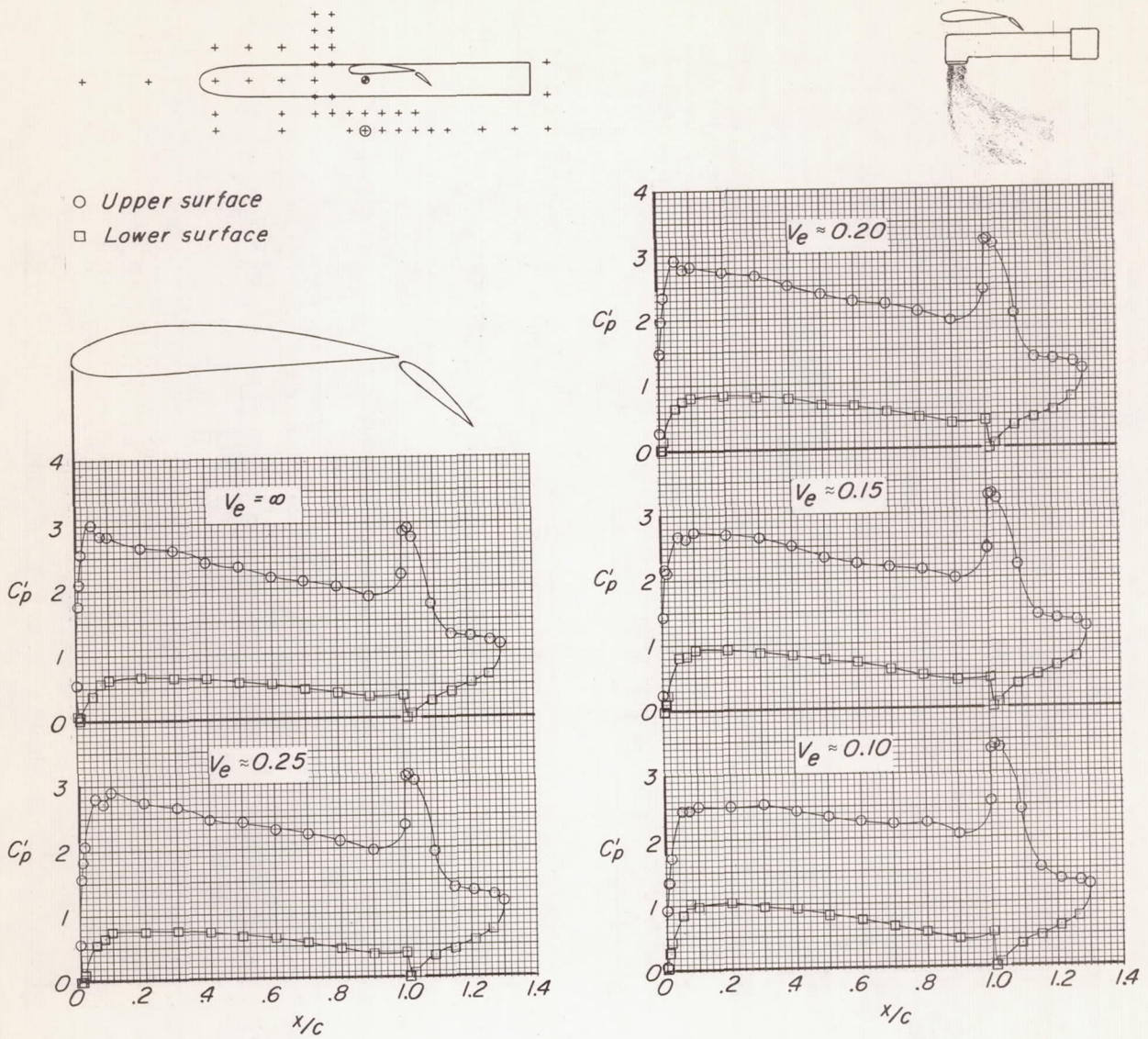

(m) Nozzle exit location: $x/c = 0.25$, $z_0/c = -0.89$. Jet support apparatus behind wing.

Figure 13.- Continued.

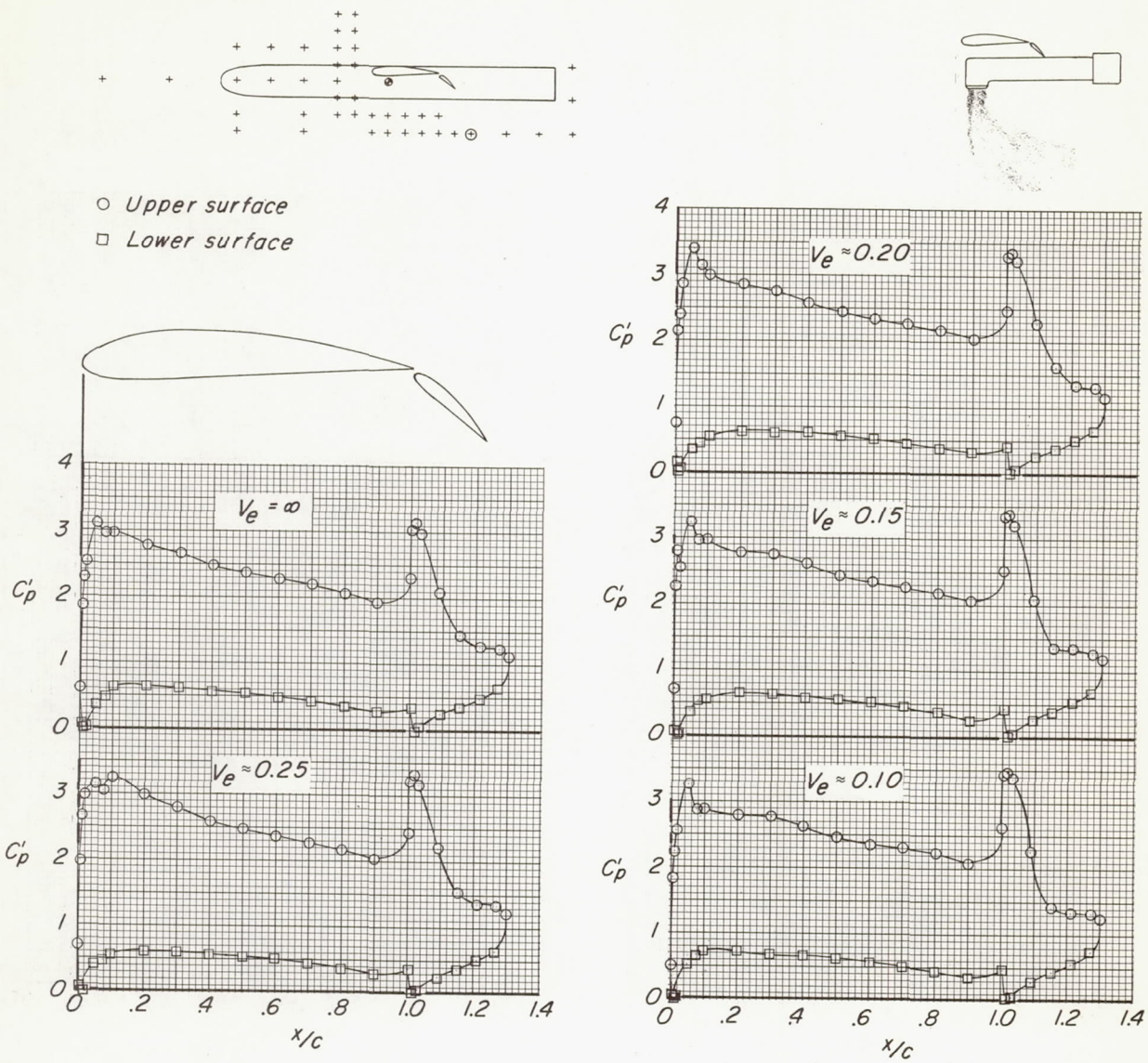

(n) Nozzle exit location: $x/c = 1.50$, $z_0/c = -0.89$. Jet support apparatus behind wing.

Figure 13.- Continued.

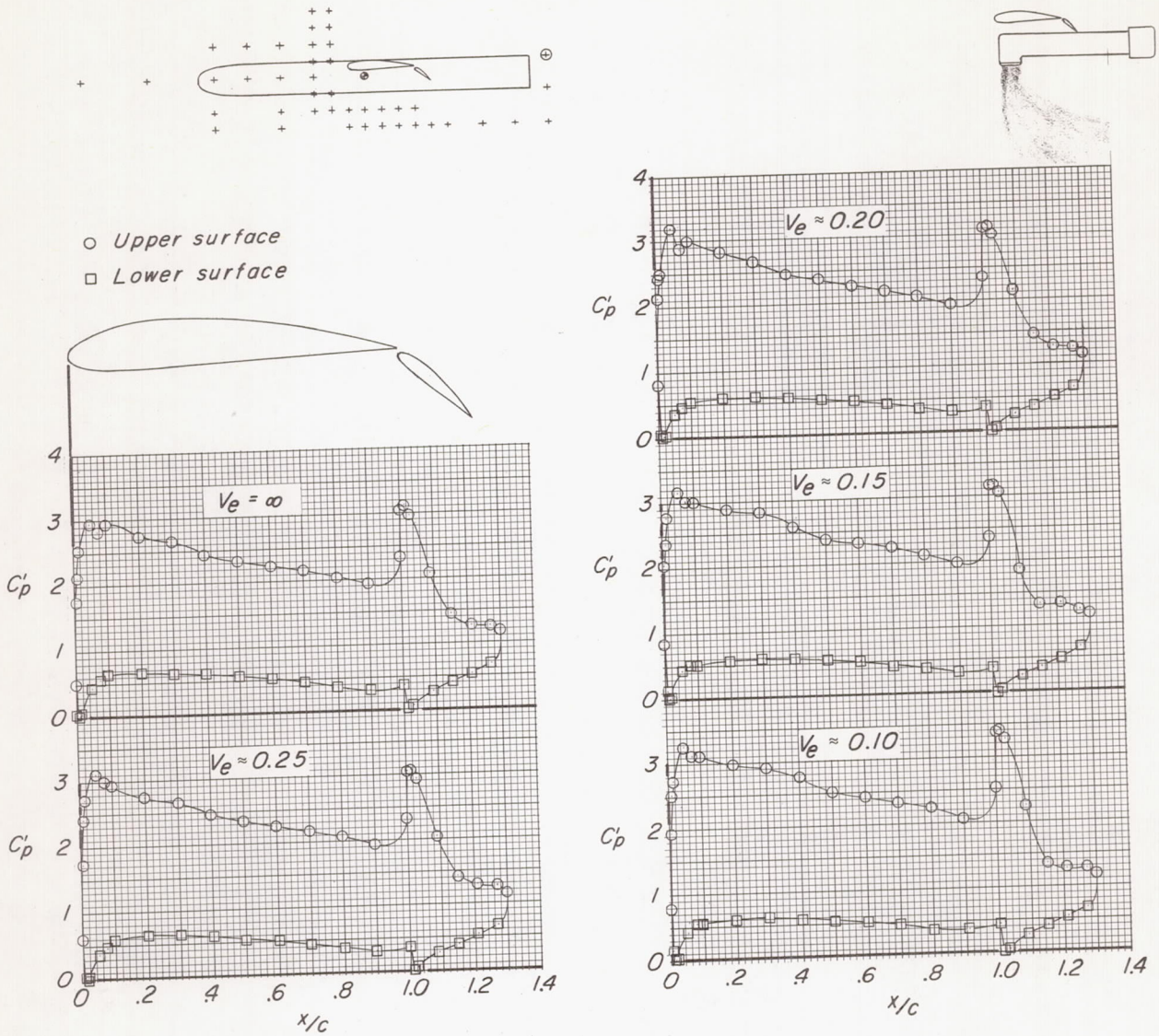

(o) Nozzle exit location: $x/c = 3.00$, $z_0/c = 0.11$. Jet support apparatus behind wing.

Figure 13.- Continued.

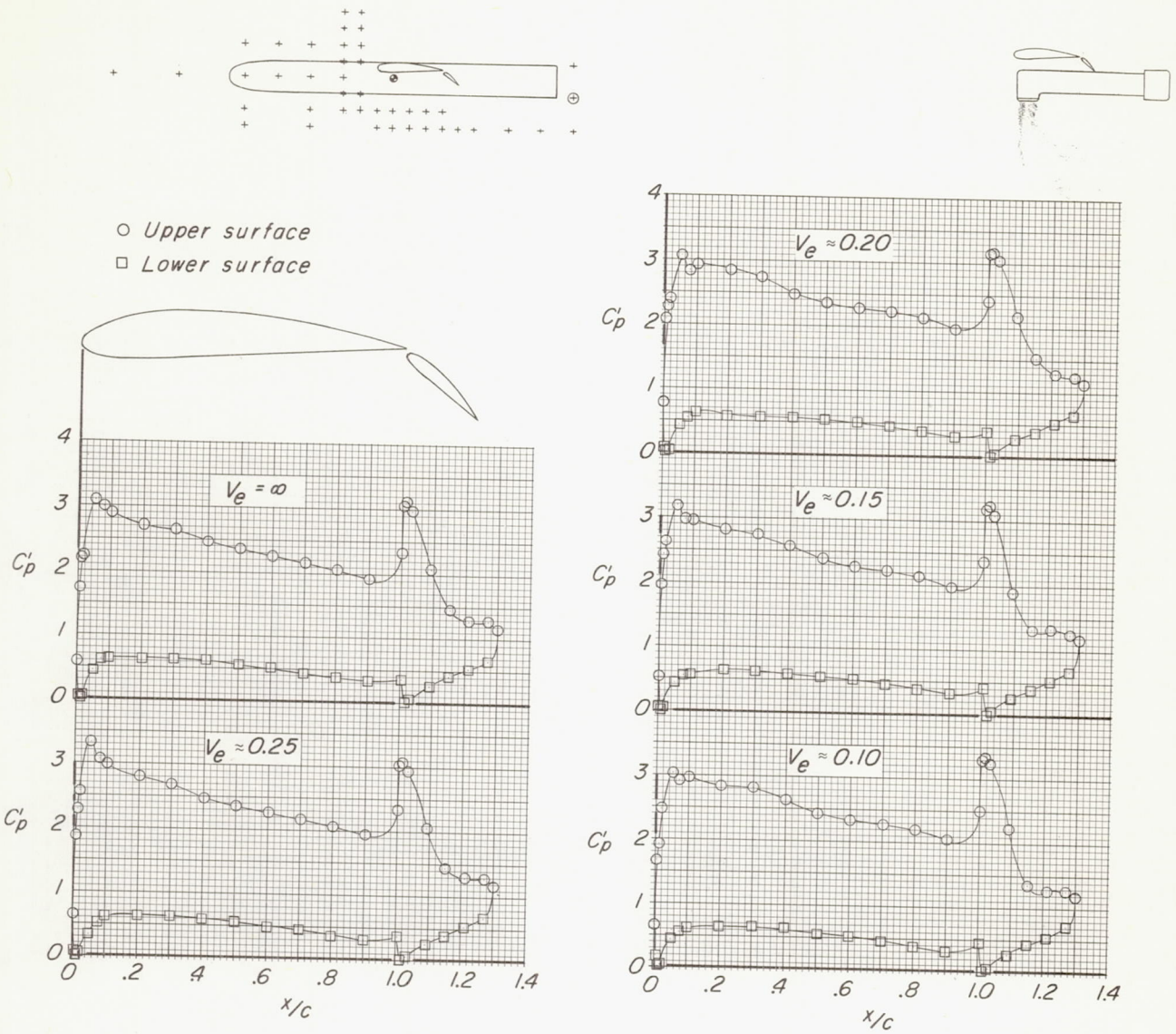

(p) Nozzle exit location: $x/c = 3.00$, $z_0/c = -0.39$. Jet support apparatus behind wing.

Figure 13.- Continued.

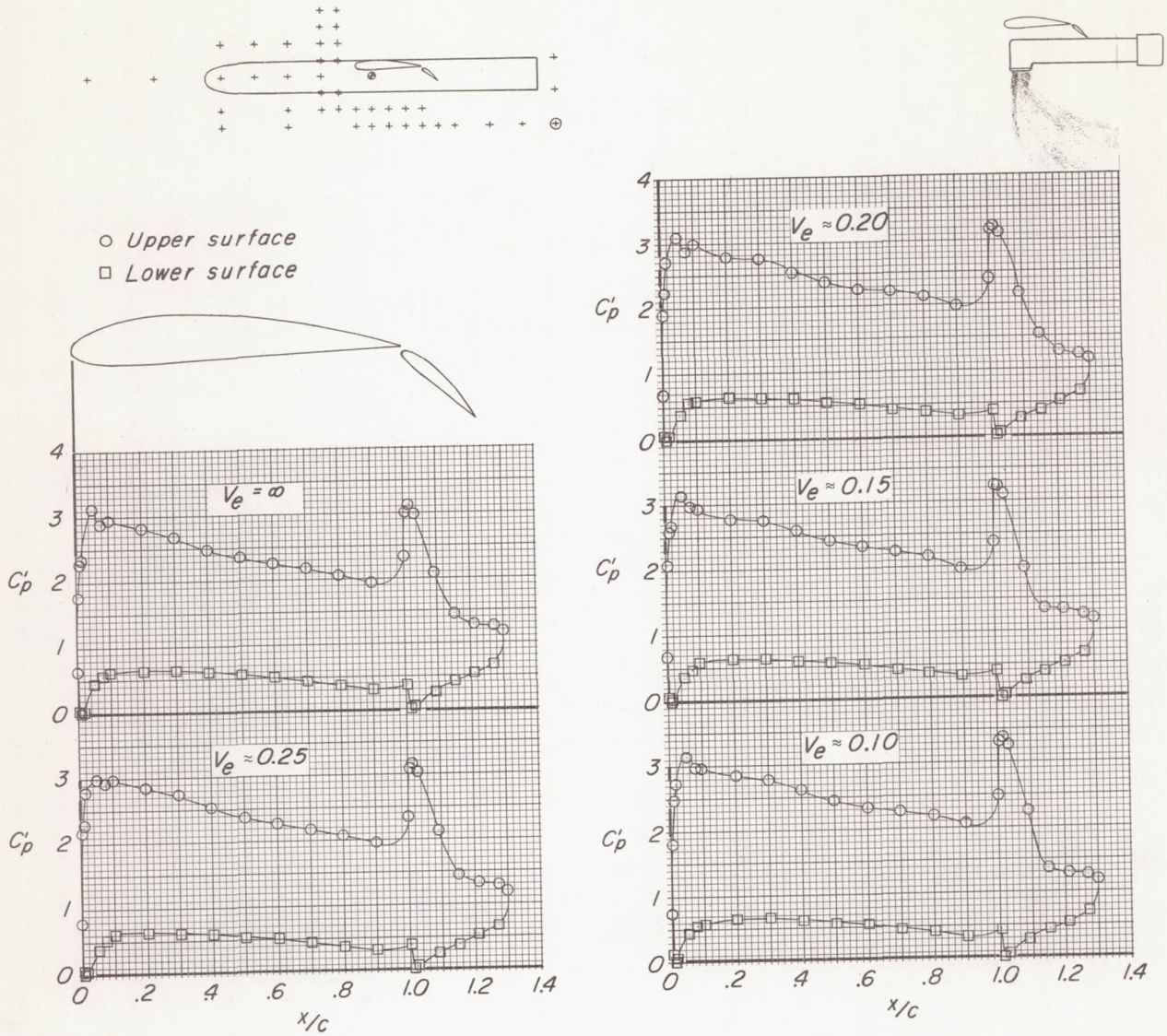

(q) Nozzle exit location: $x/c = 3.00$, $z_0/c = -0.89$. Jet support apparatus behind wing.

Figure 13.- Concluded.

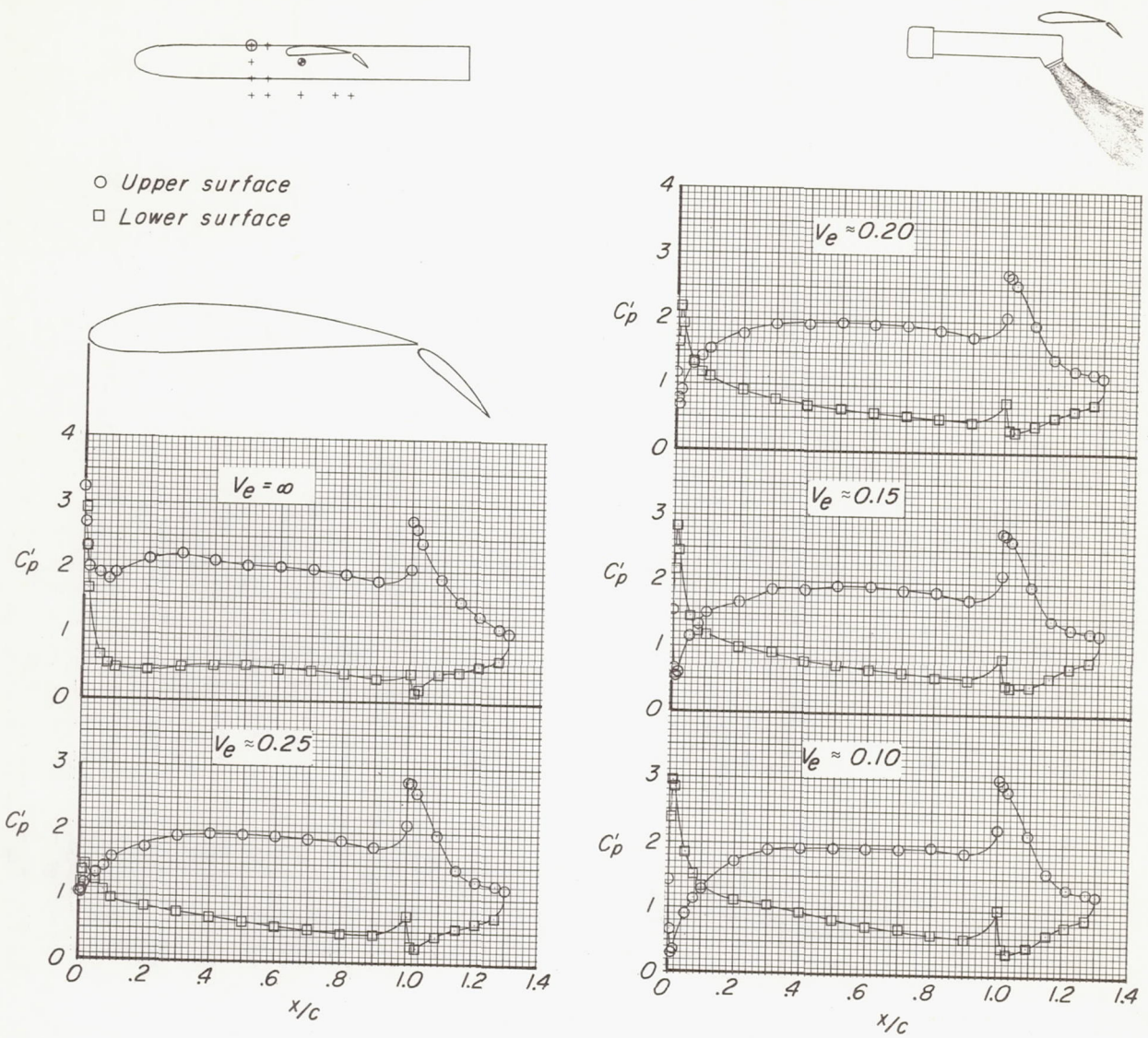

(a) Nozzle exit location: $x/c = -0.50$, $z_0/c = 0.11$.

Figure 14.- Basic pressure distributions on wing and flap of the model at typical locations of the jets. $\delta_f = 40^0$; $\delta_j = 60^0$.

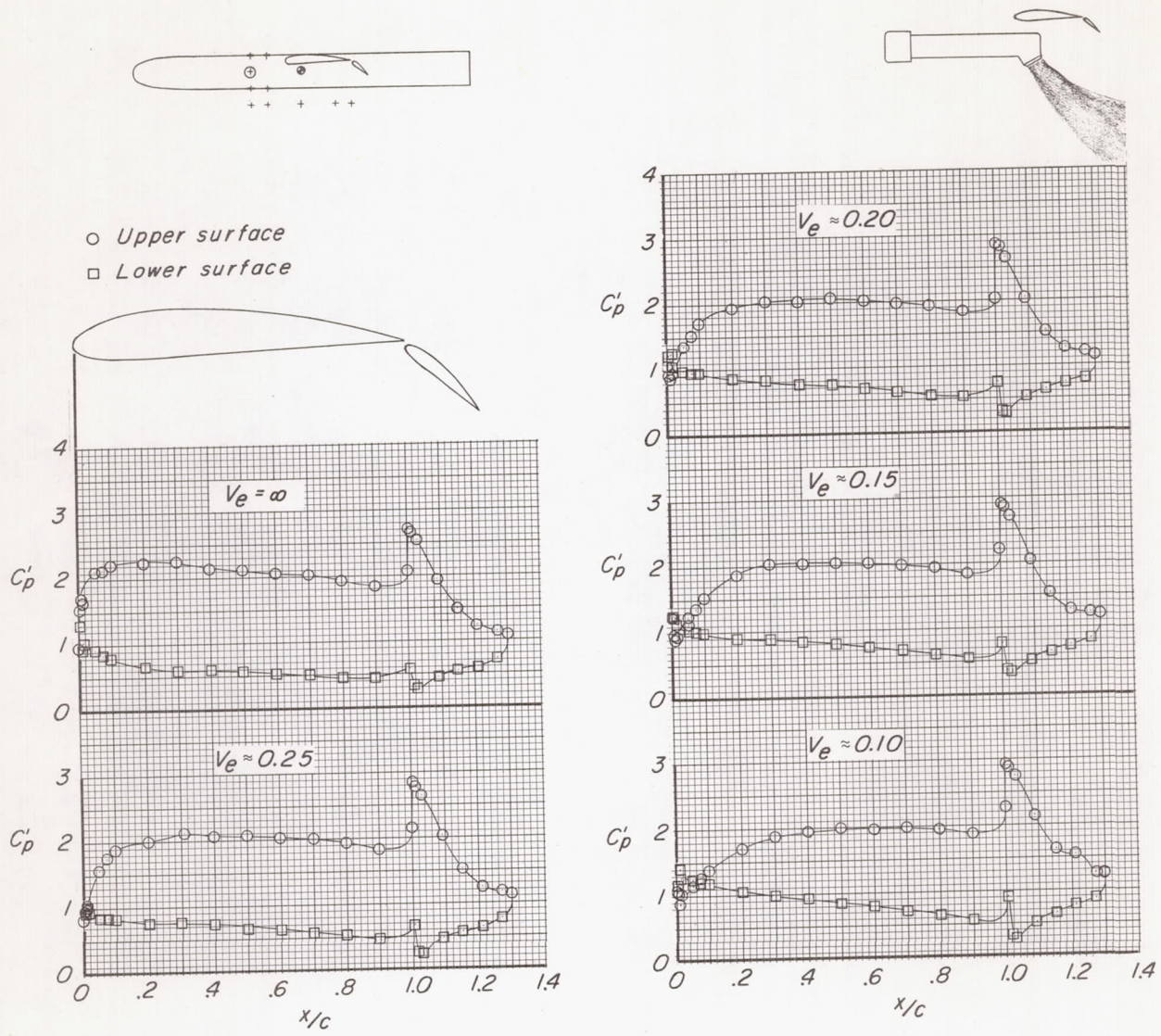

(b) Nozzle exit location: $x/c = -0.50$, $z_0/c = -0.14$.

Figure 14.- Continued.

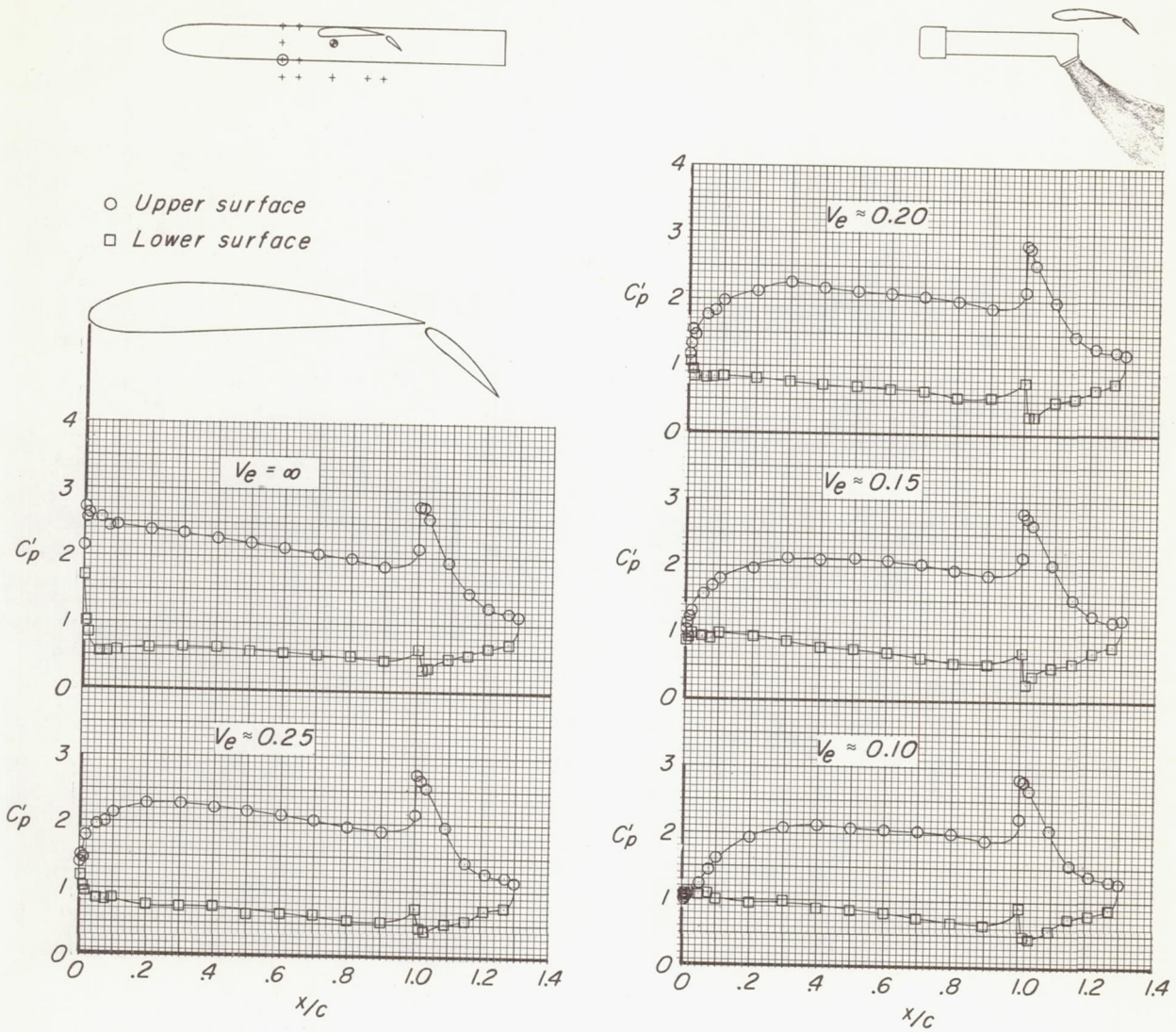

(c) Nozzle exit location: $x/c = -0.50$, $z_0/c = -0.39$.

Figure 14.- Continued.

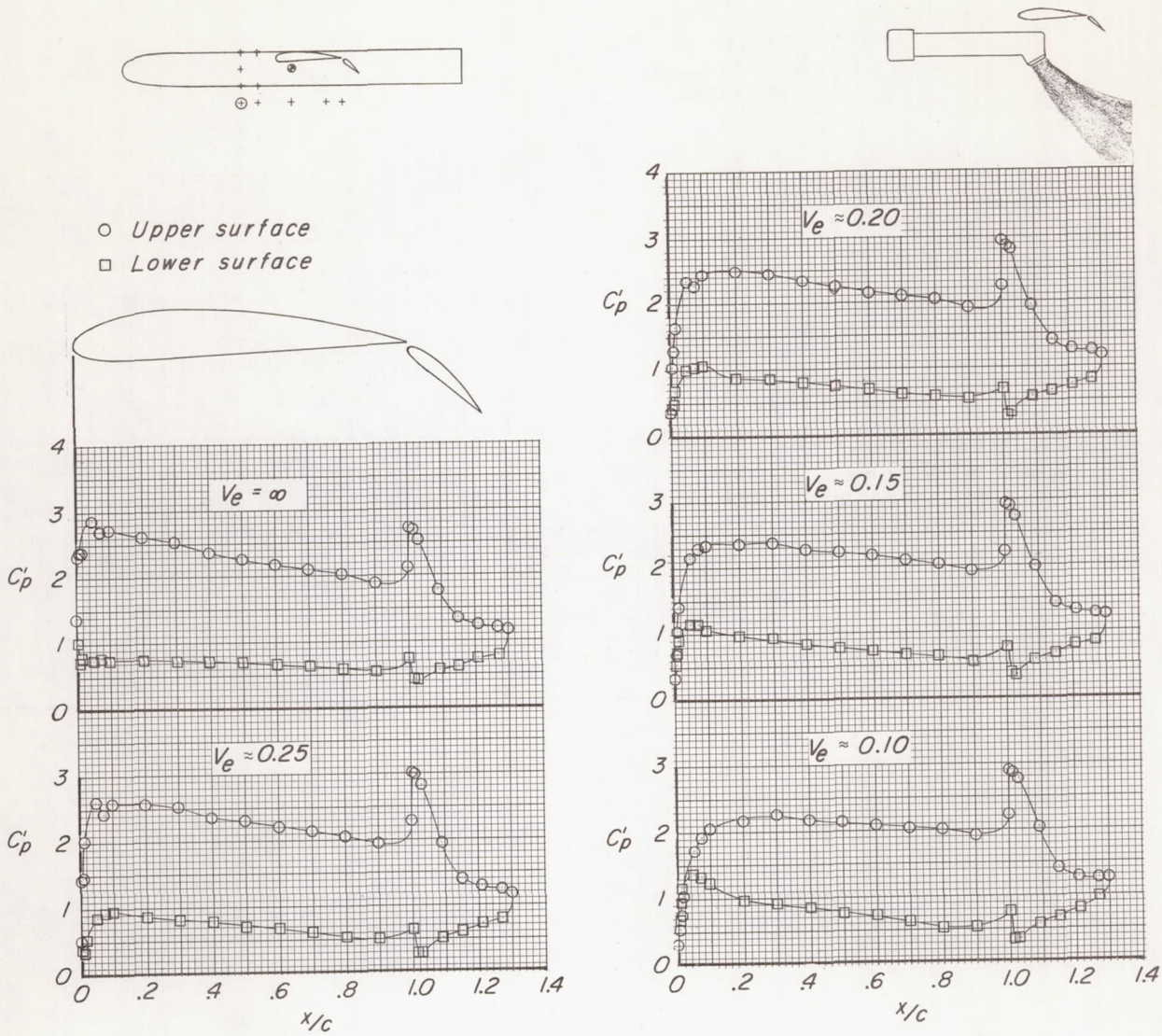

(d) Nozzle exit location: $x/c = -0.50$, $z_0/c = -0.64$.

Figure 14.- Continued.

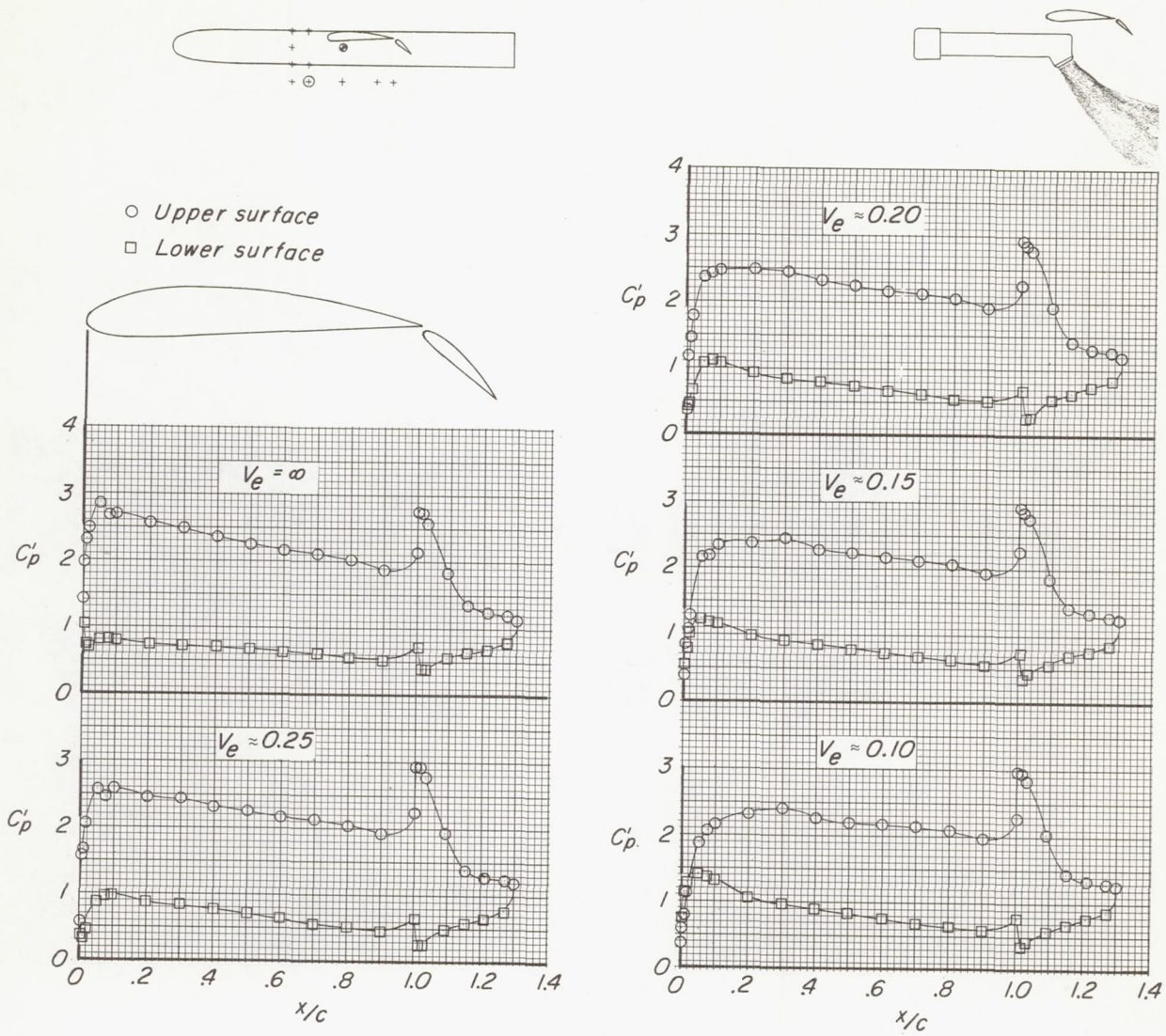

(e) Nozzle exit location: $x/c = -0.25$, $z_0/c = -0.64$.

Figure 14.- Continued.

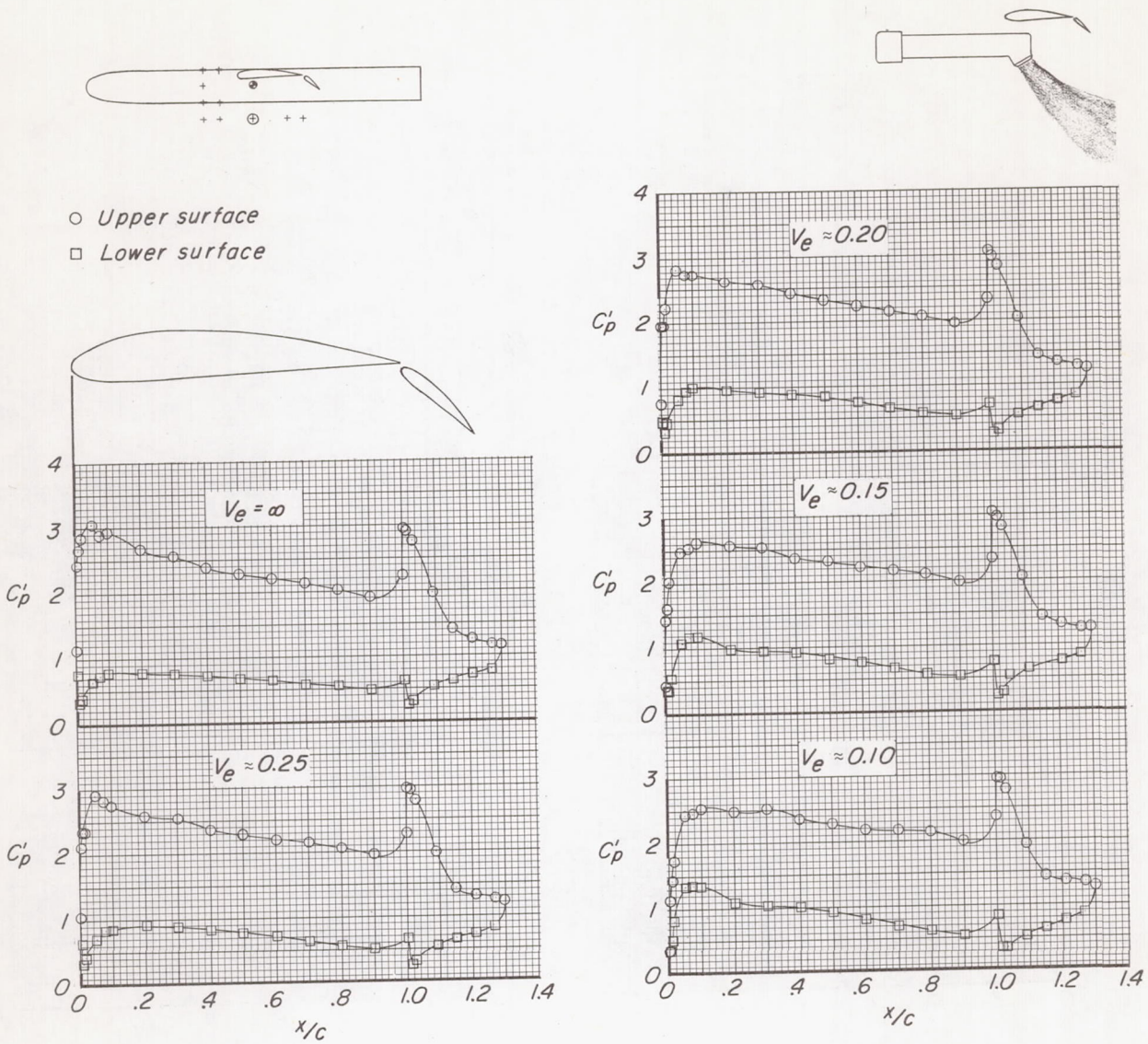

(f) Nozzle exit location: $x/c = 0.25$, $z_0/c = -0.64$.

Figure 14.- Continued.

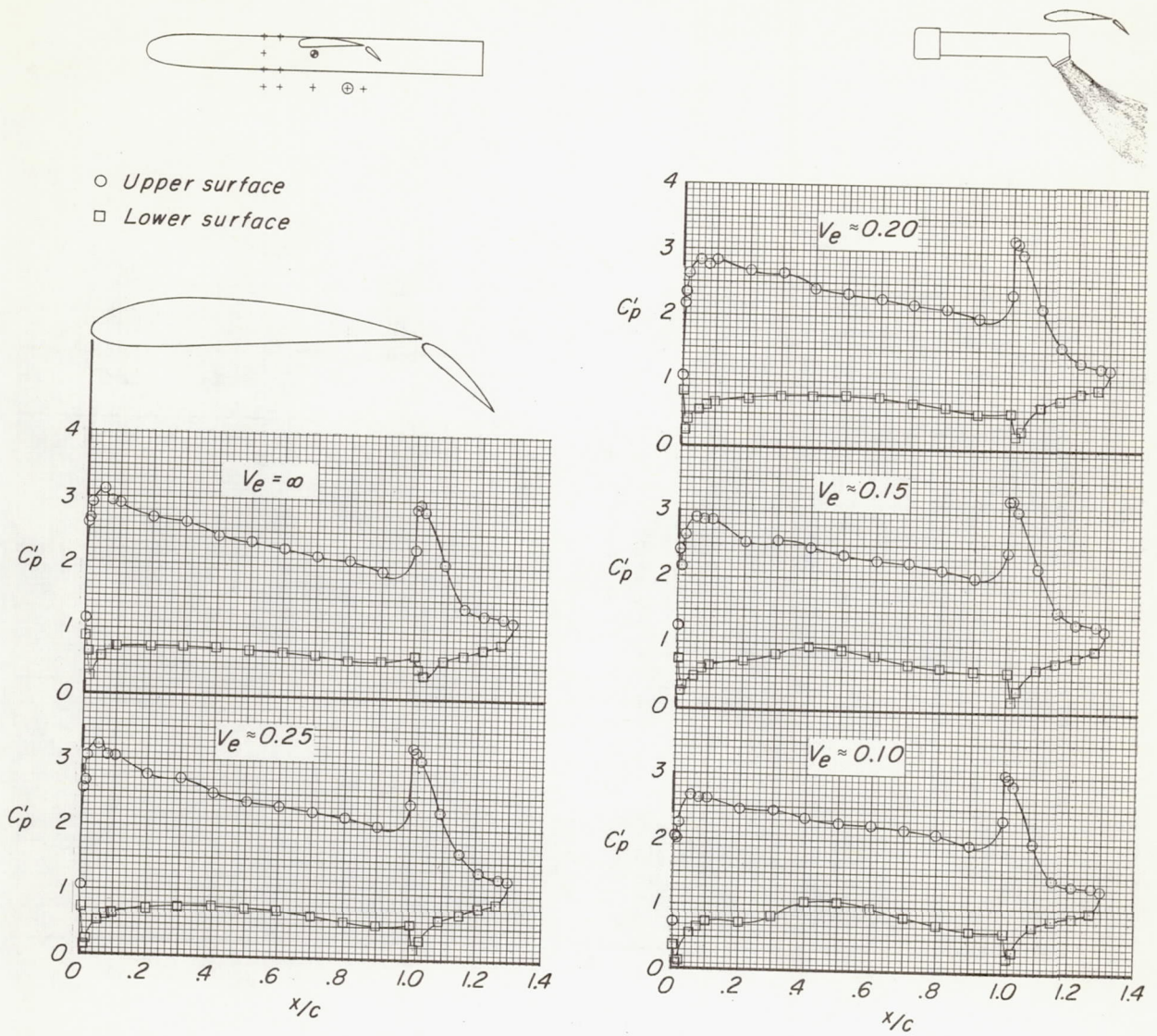

(g) Nozzle exit location: $x/c = 0.75$, $z_0/c = -0.64$.

Figure 14.- Continued.

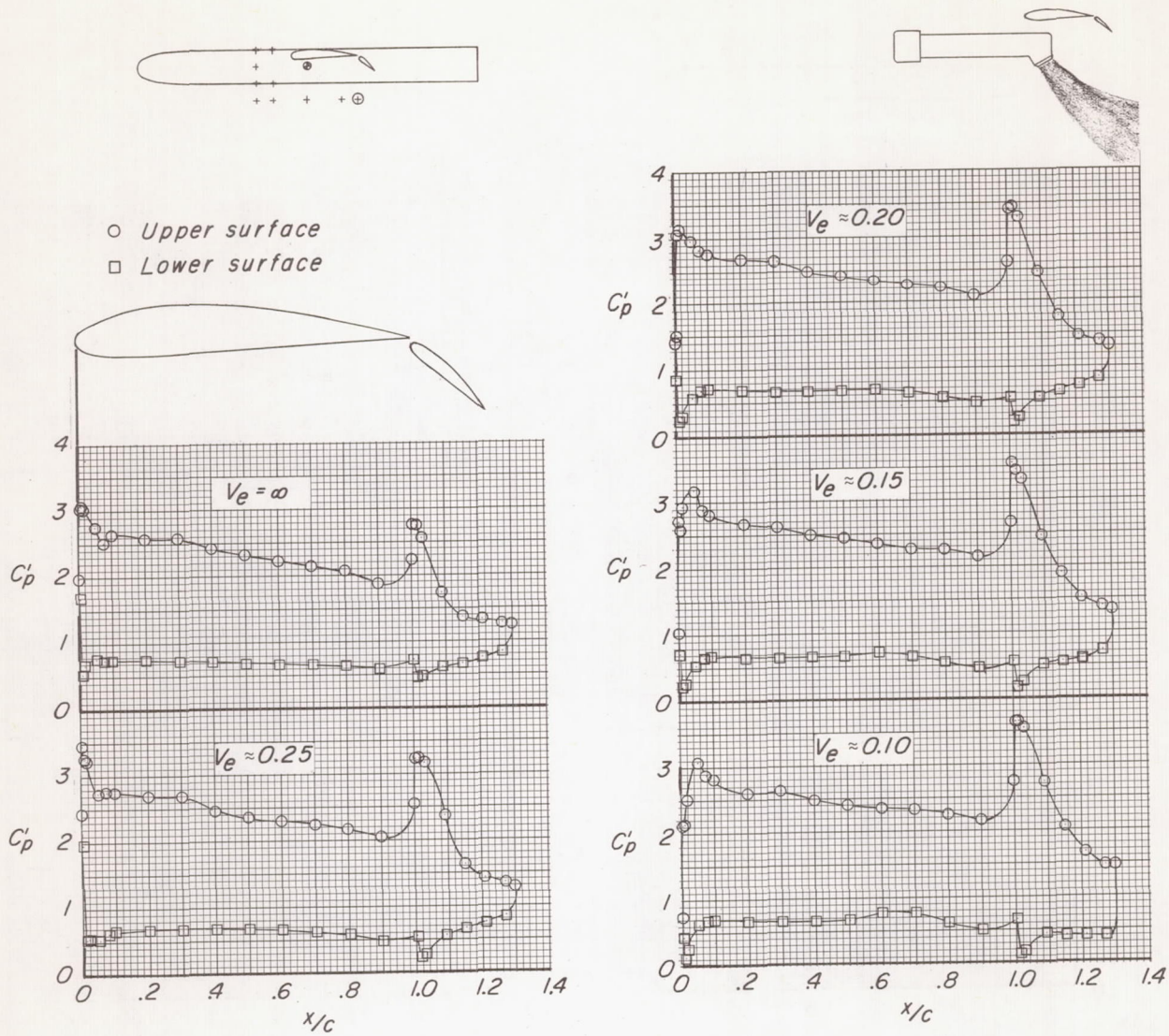

(h) Nozzle exit location: $x/c = 1.00$, $z_0/c = -0.64$.

Figure 14.- Concluded.

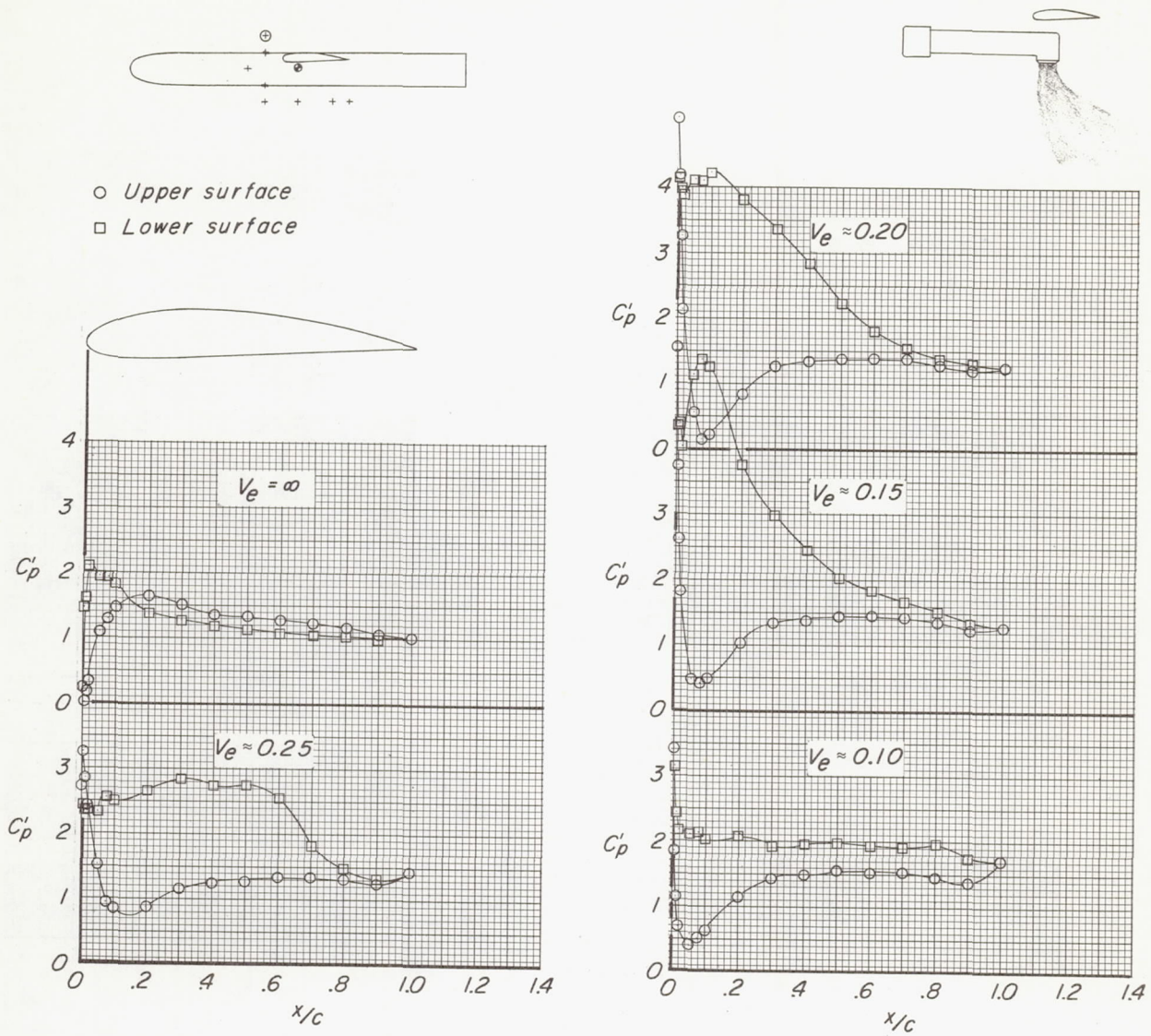

(a) Nozzle exit location: $x/c = -0.25$, $z_0/c = 0.36$.

Figure 15.- Basic pressure distributions on wing of the model at typical locations of the jets. $\delta_f = 0^0$; $\delta_j = 90^0$.

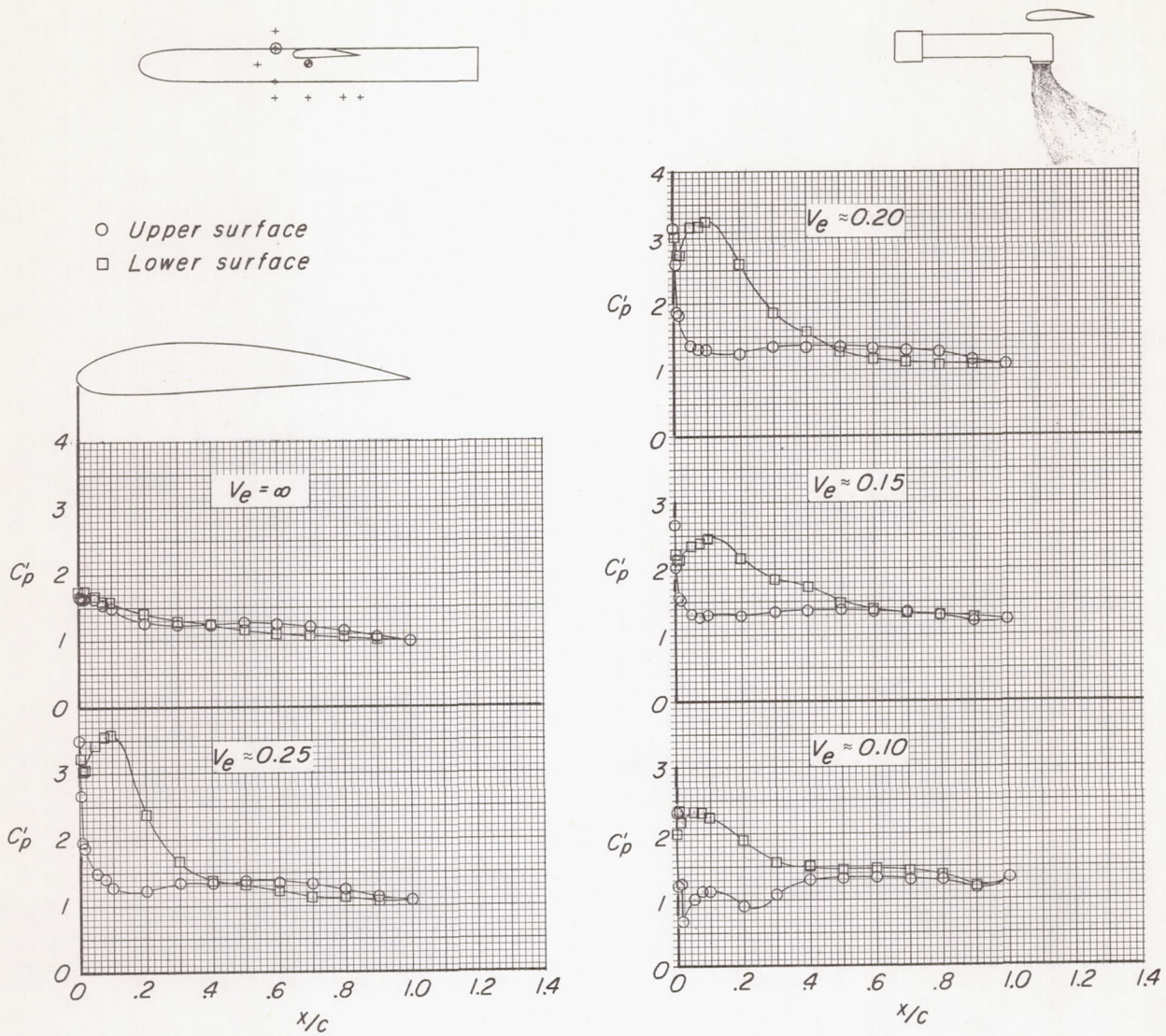

(b) Nozzle exit location: $x/c = -0.25$, $z_0/c = 0.11$.

Figure 15.- Continued.

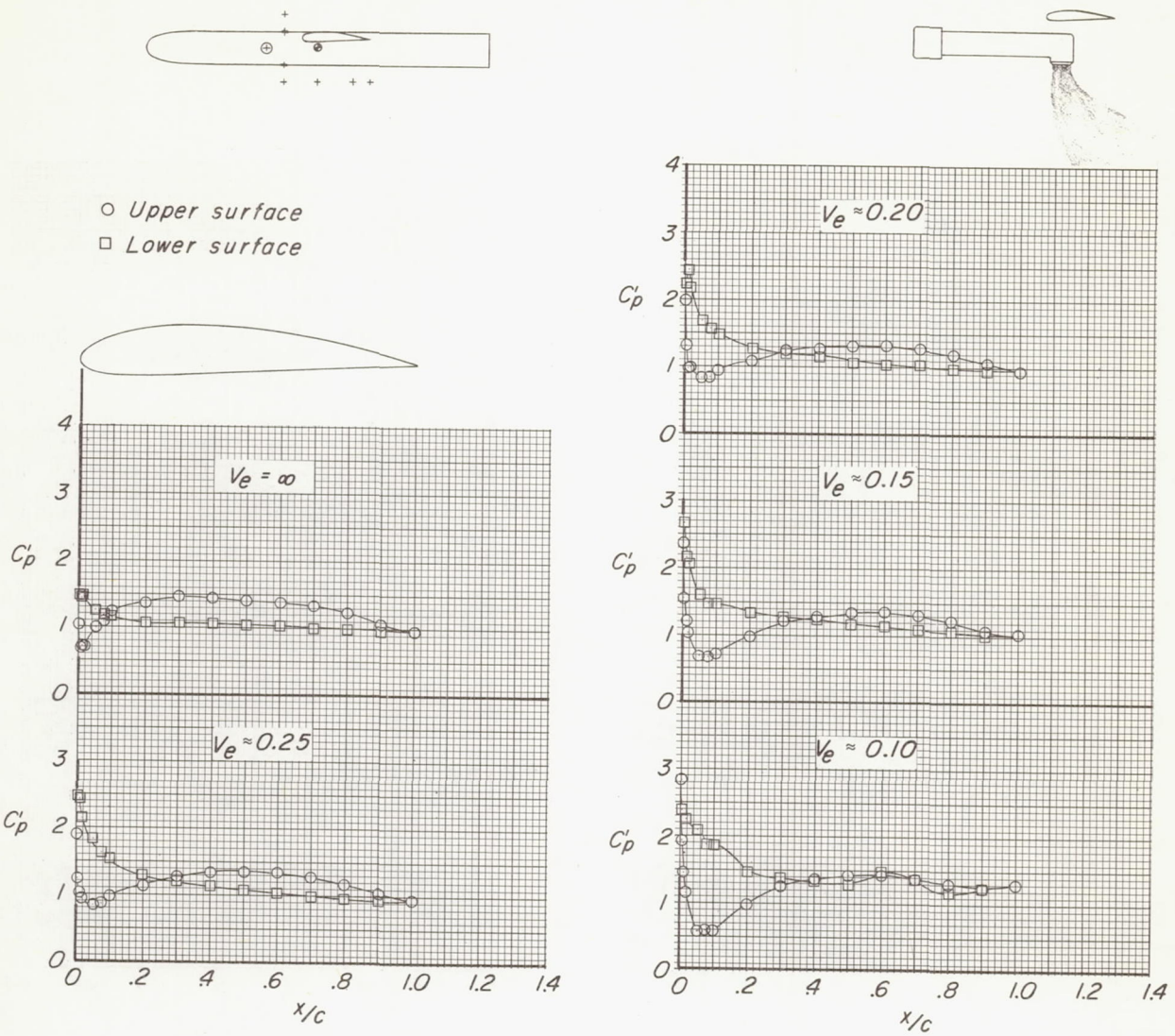

(c) Nozzle exit location: $x/c = -0.50$, $z_0/c = -0.14$.

Figure 15.- Continued.

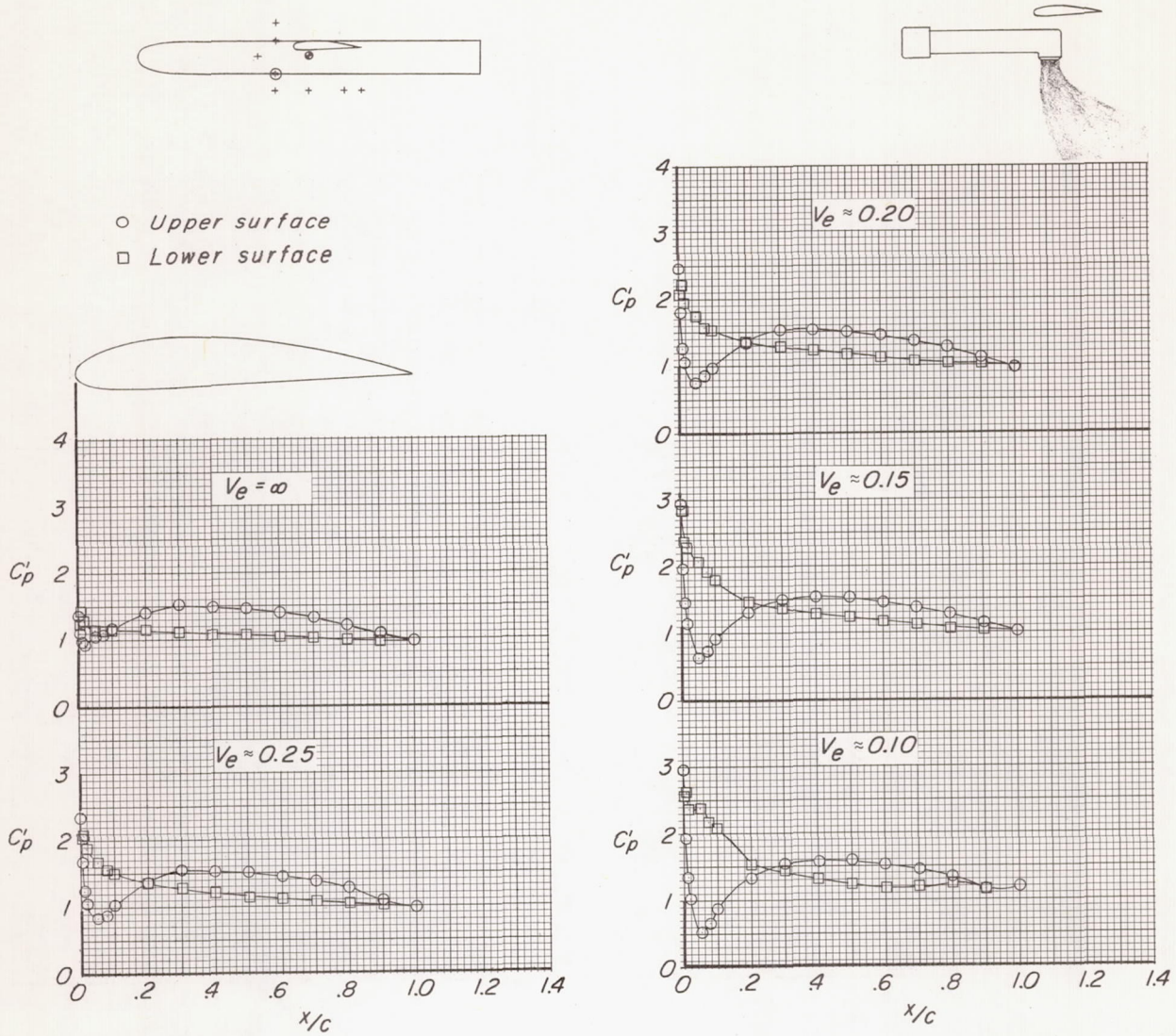

(d) Nozzle exit location: $x/c = -0.25$, $z_0/c = -0.39$.

Figure 15.- Continued.

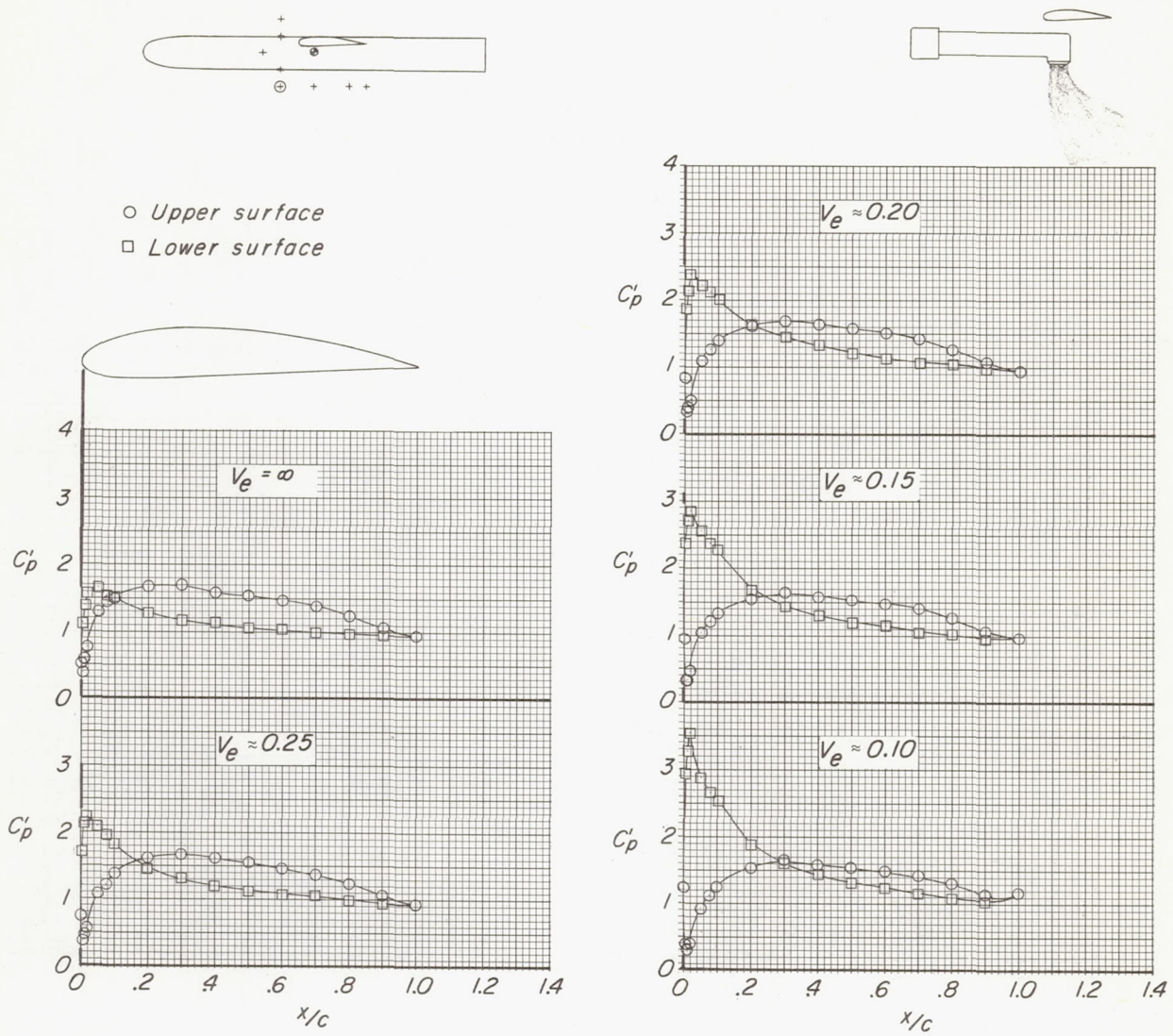

(e) Nozzle exit location: $x/c = -0.25$, $z_0/c = -0.64$.

Figure 15.- Continued.

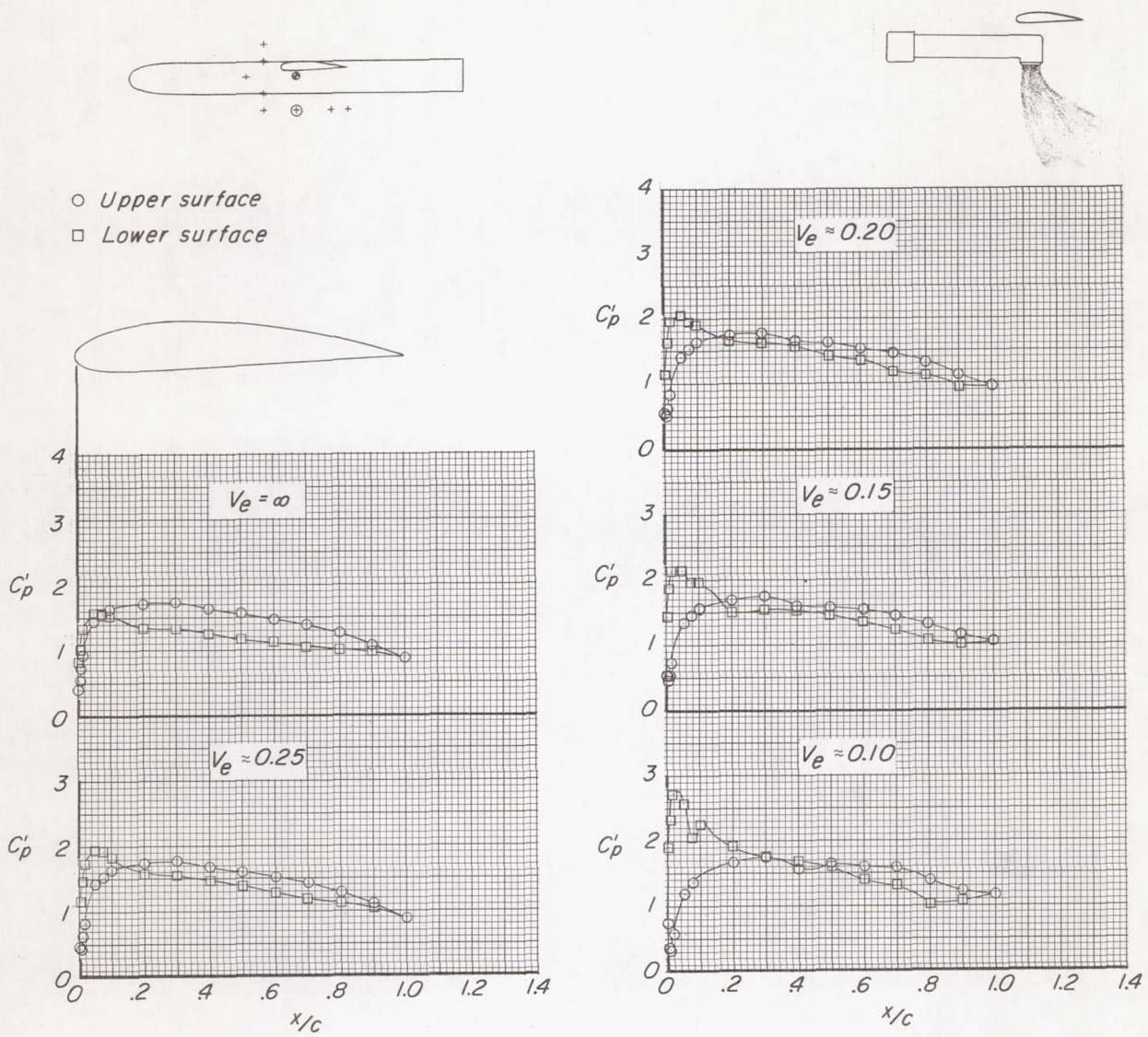

(f) Nozzle exit location: $x/c = 0.25$, $z_0/c = -0.64$.

Figure 15.- Continued.

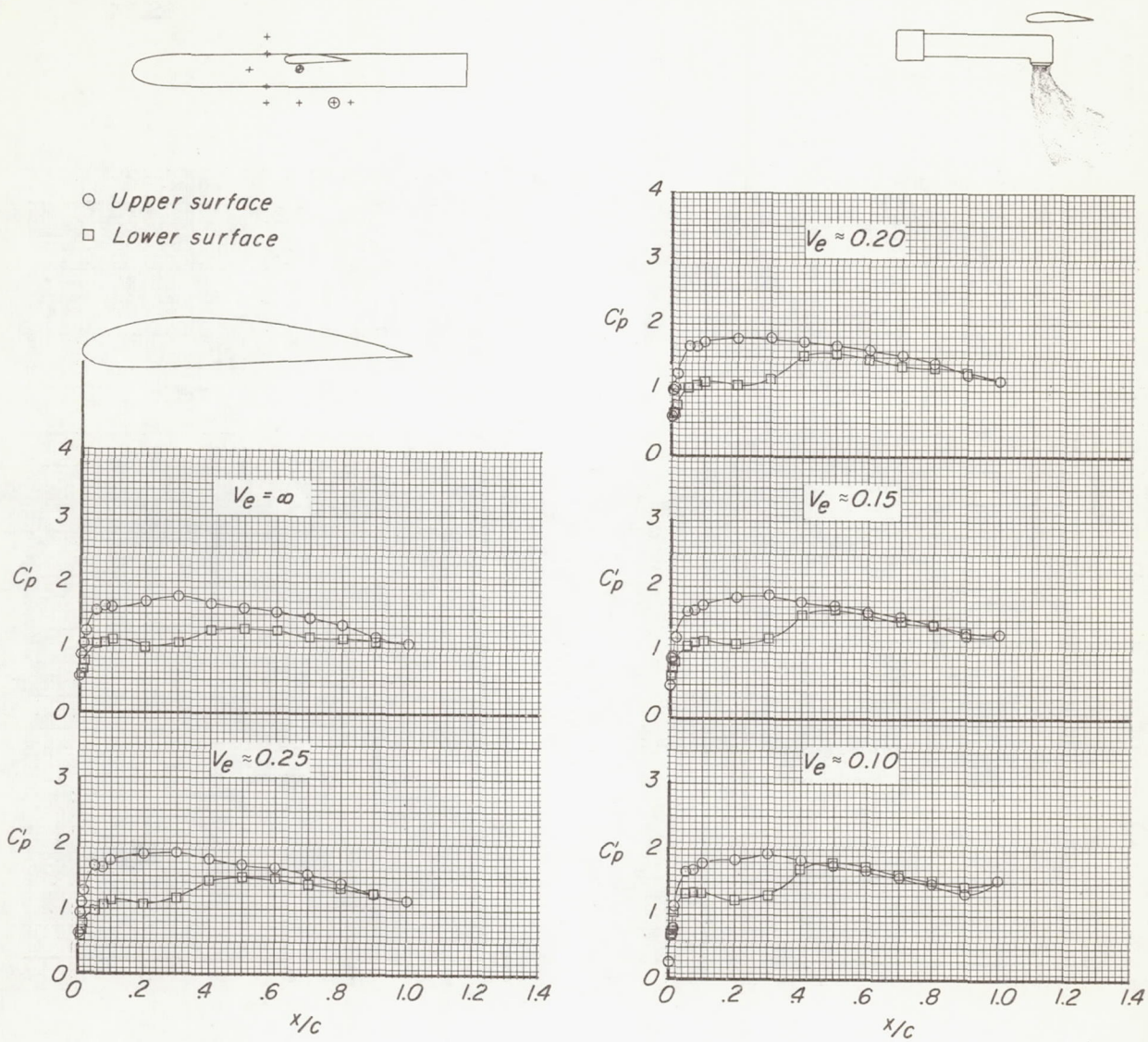

(g) Nozzle exit location: $x/c = 0.75$, $z_0/c = -0.64$.

Figure 15.- Continued.

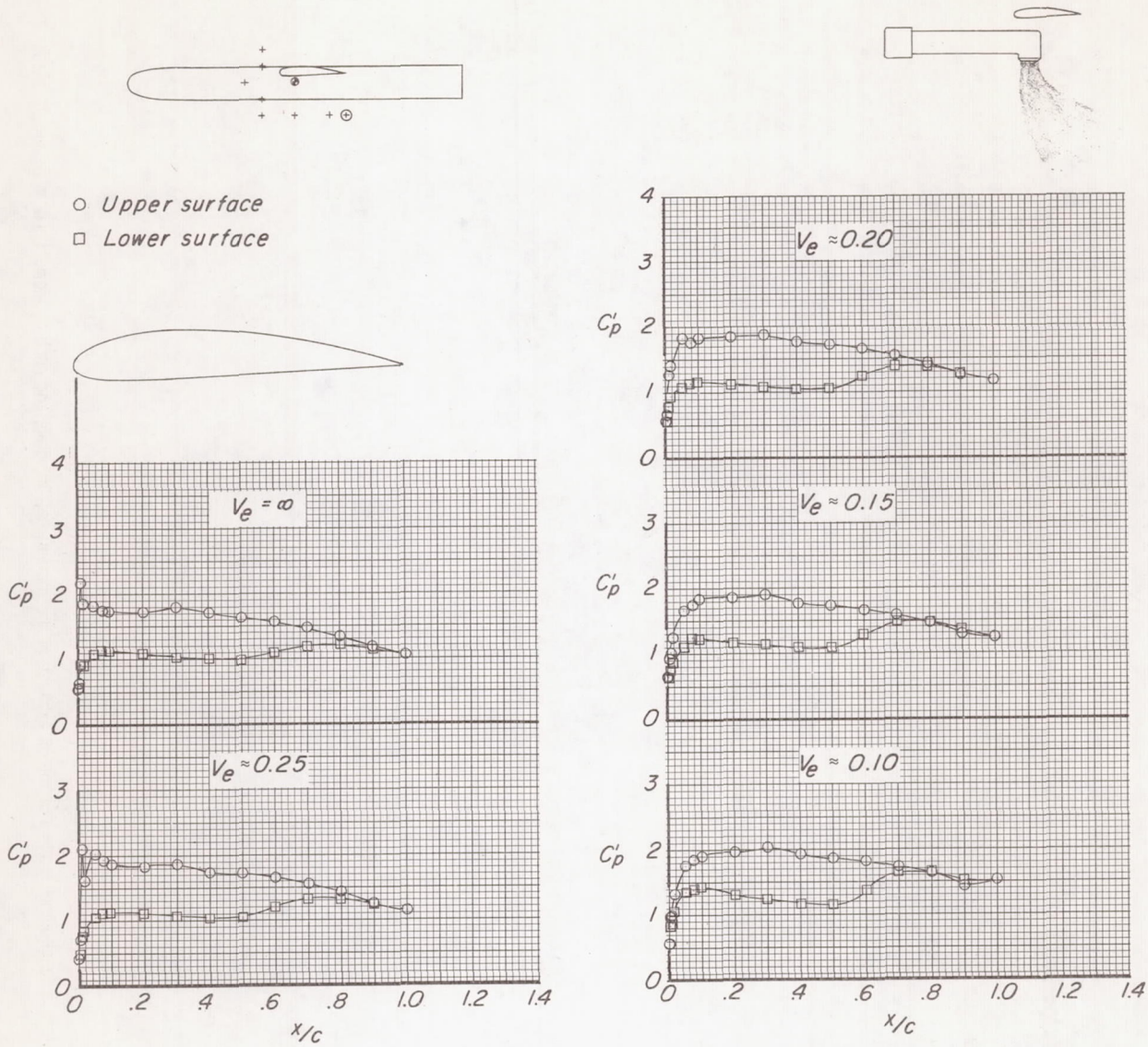

(h) Nozzle exit location: $x/c = 1.00$, $z_0/c = -0.64$.

Figure 15.- Concluded.

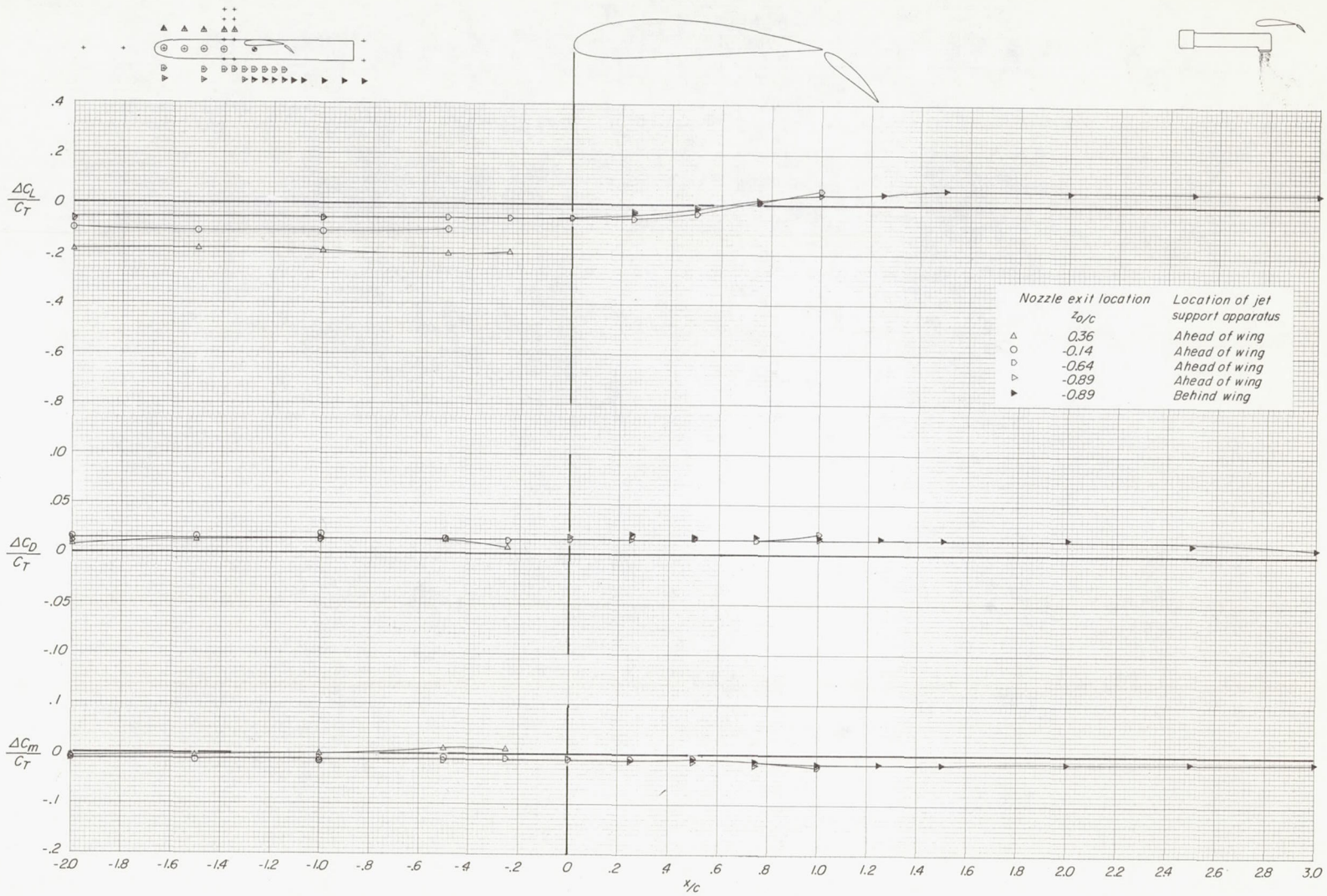

(a) $V_e \approx 0.10$.

Figure 16.- Effect of longitudinal location of the jet exhaust on the incremental lift, drag, and pitching moment due to power. $\delta_f = 40^o$; $\delta_j = 90^o$.

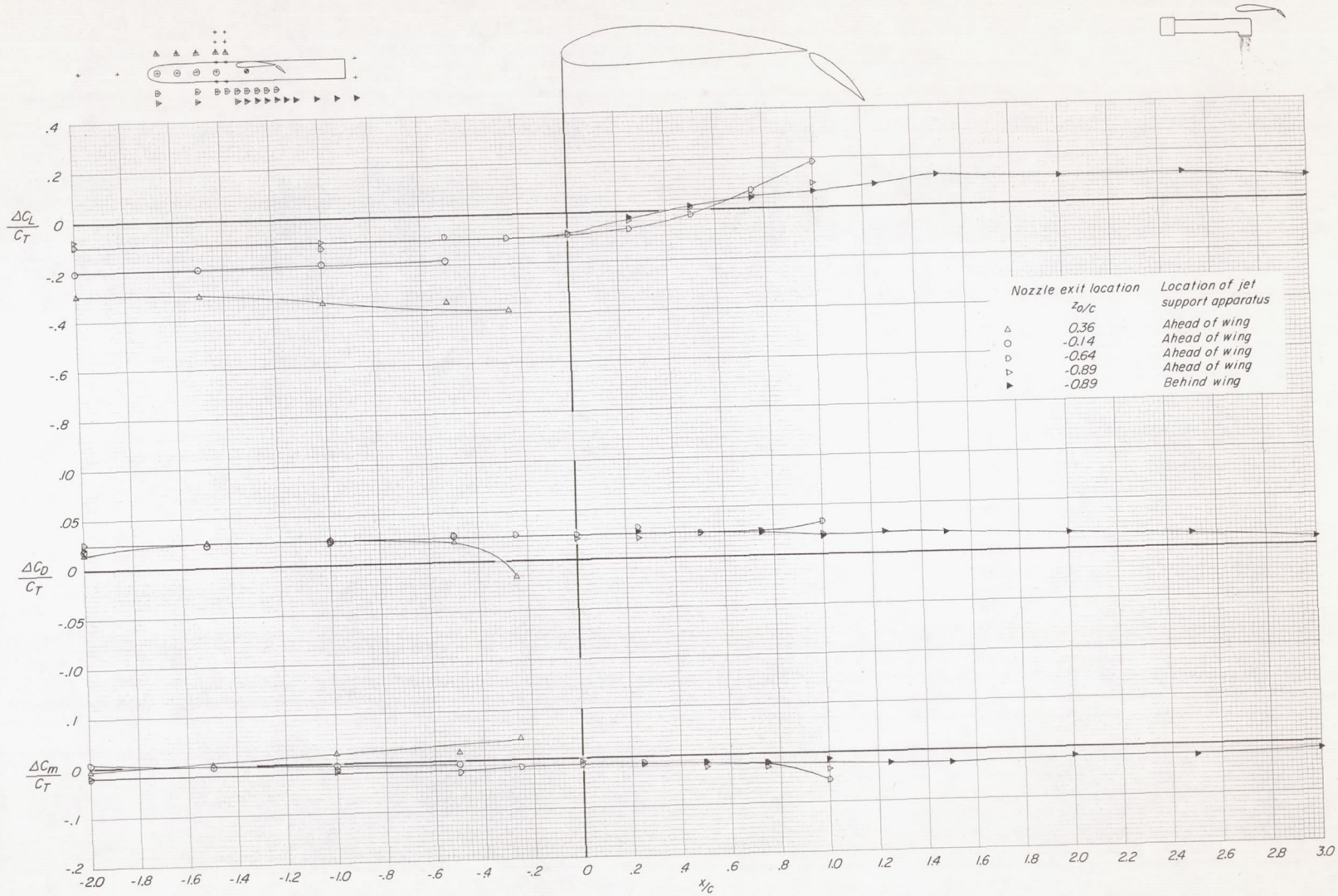

(b) $V_e \approx 0.15$.

Figure 16.- Continued.

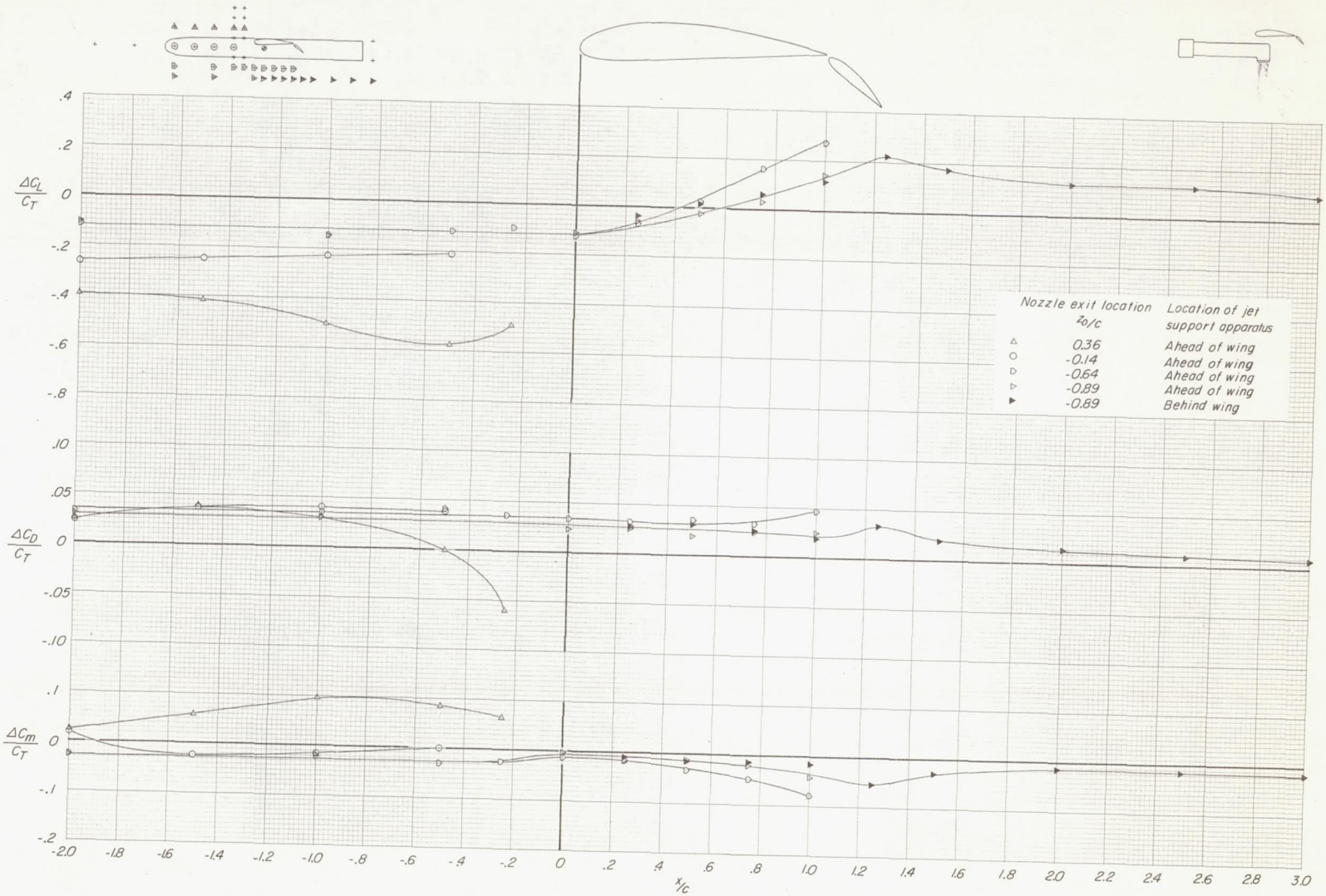

(c) $V_e \approx 0.20$.

Figure 16.- Continued.

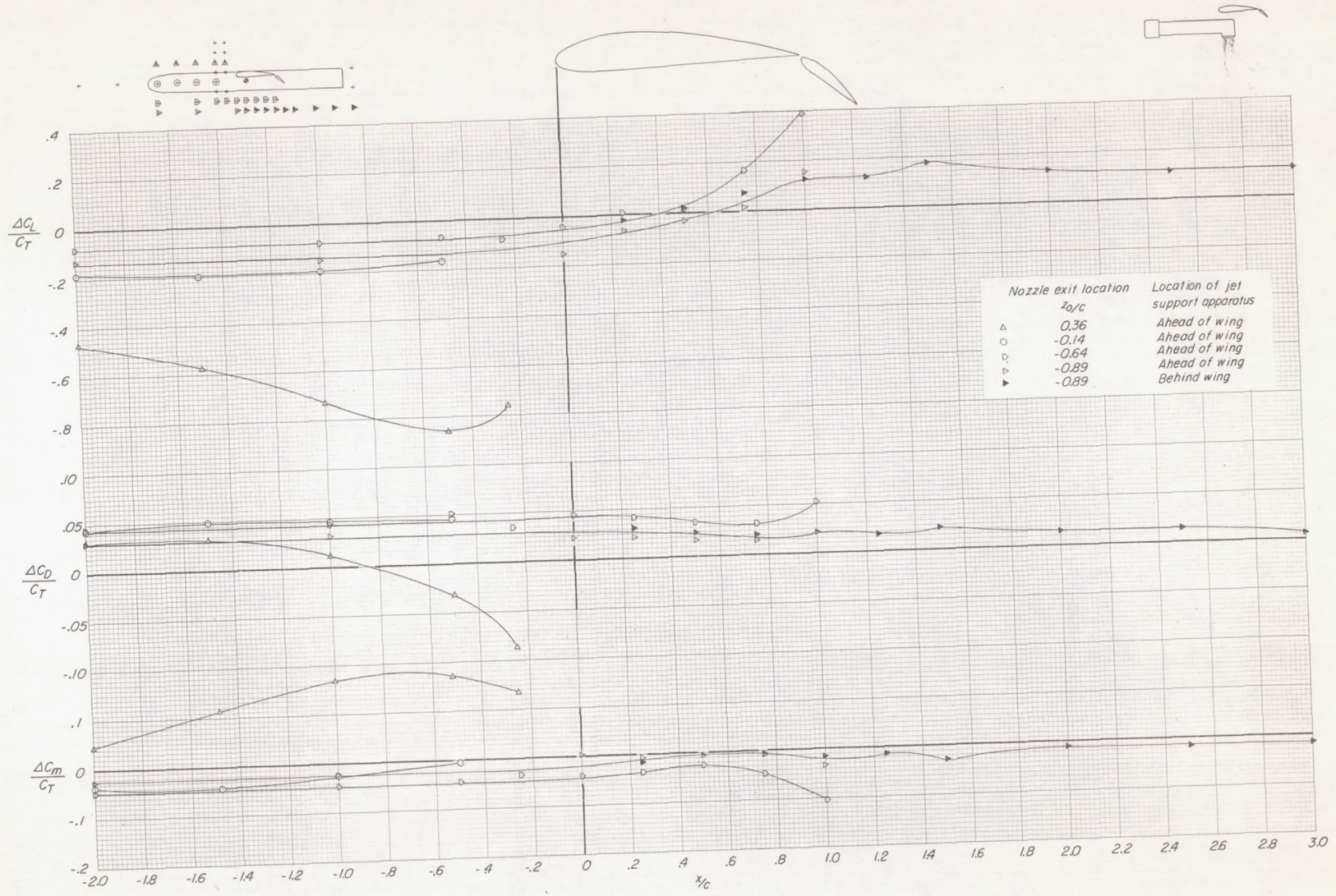

(d) $V_e \approx 0.25$.

Figure 16.- Concluded.

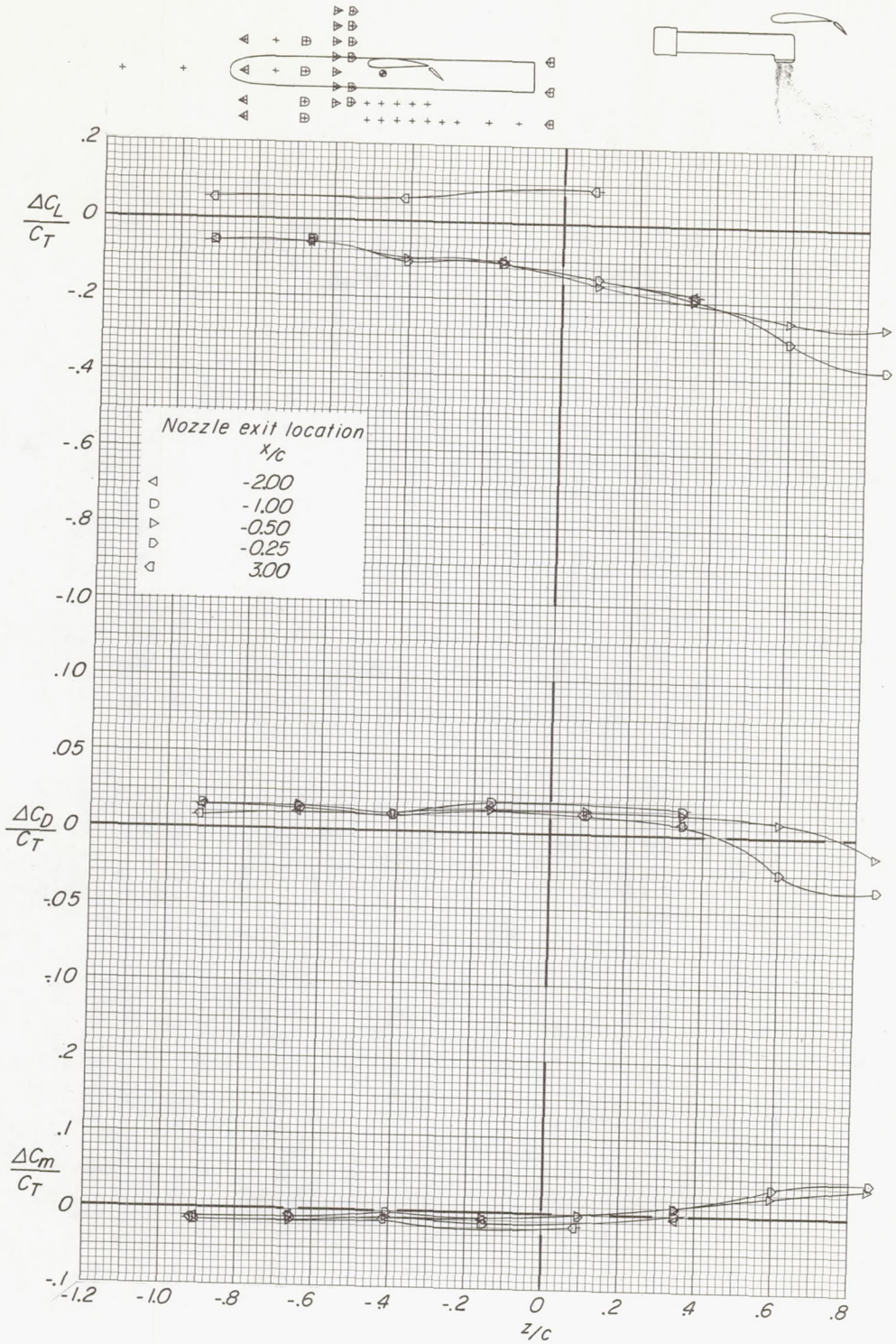

(a) $V_e \approx 0.10$.

Figure 17.- Effect of vertical location of the jet exhaust on the incremental lift, drag, and pitching moment due to power. $\delta_f = 40^o$; $\delta_j = 90^o$.

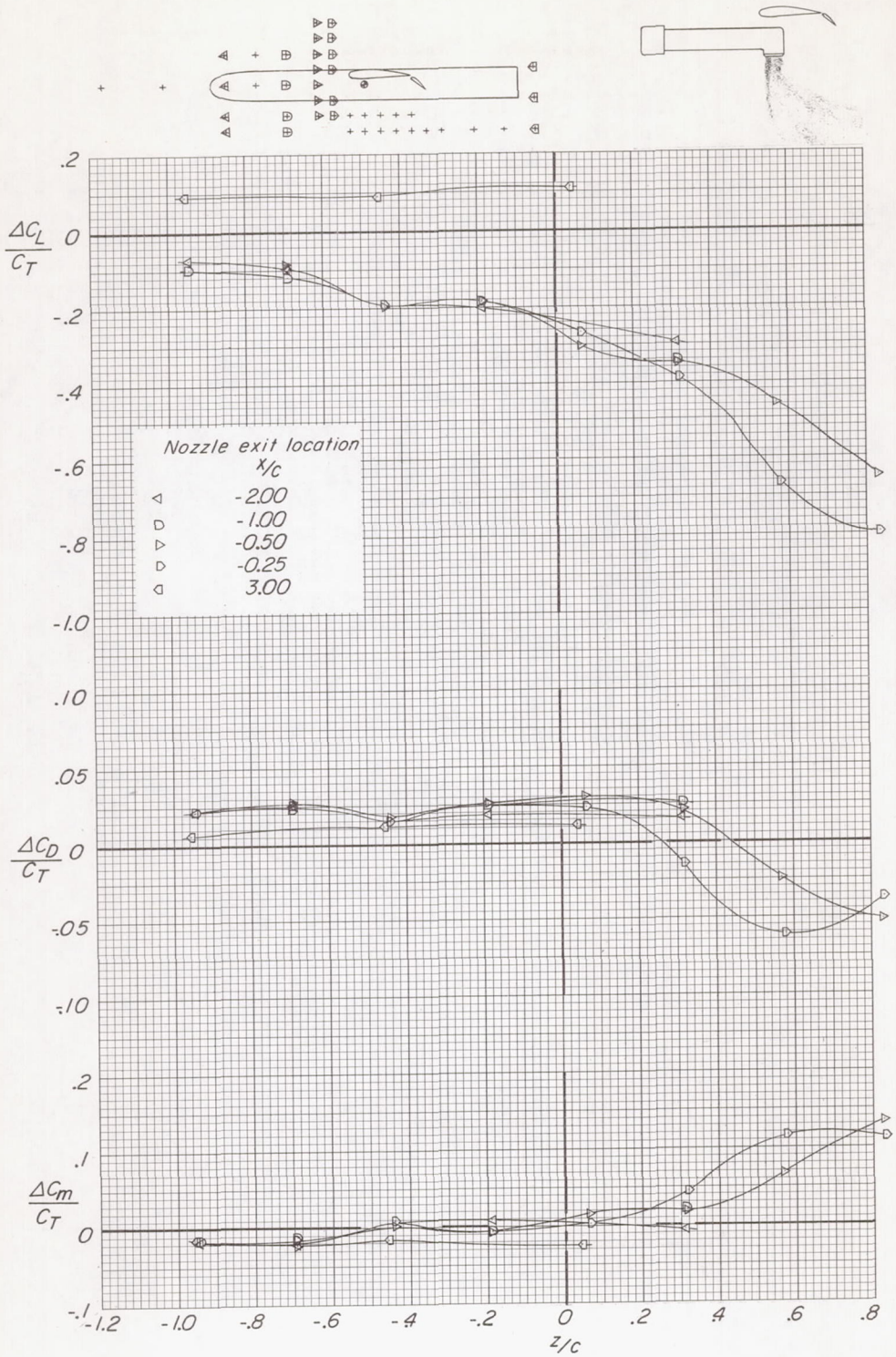

(b) $V_e \approx 0.15$.

Figure 17.- Continued.

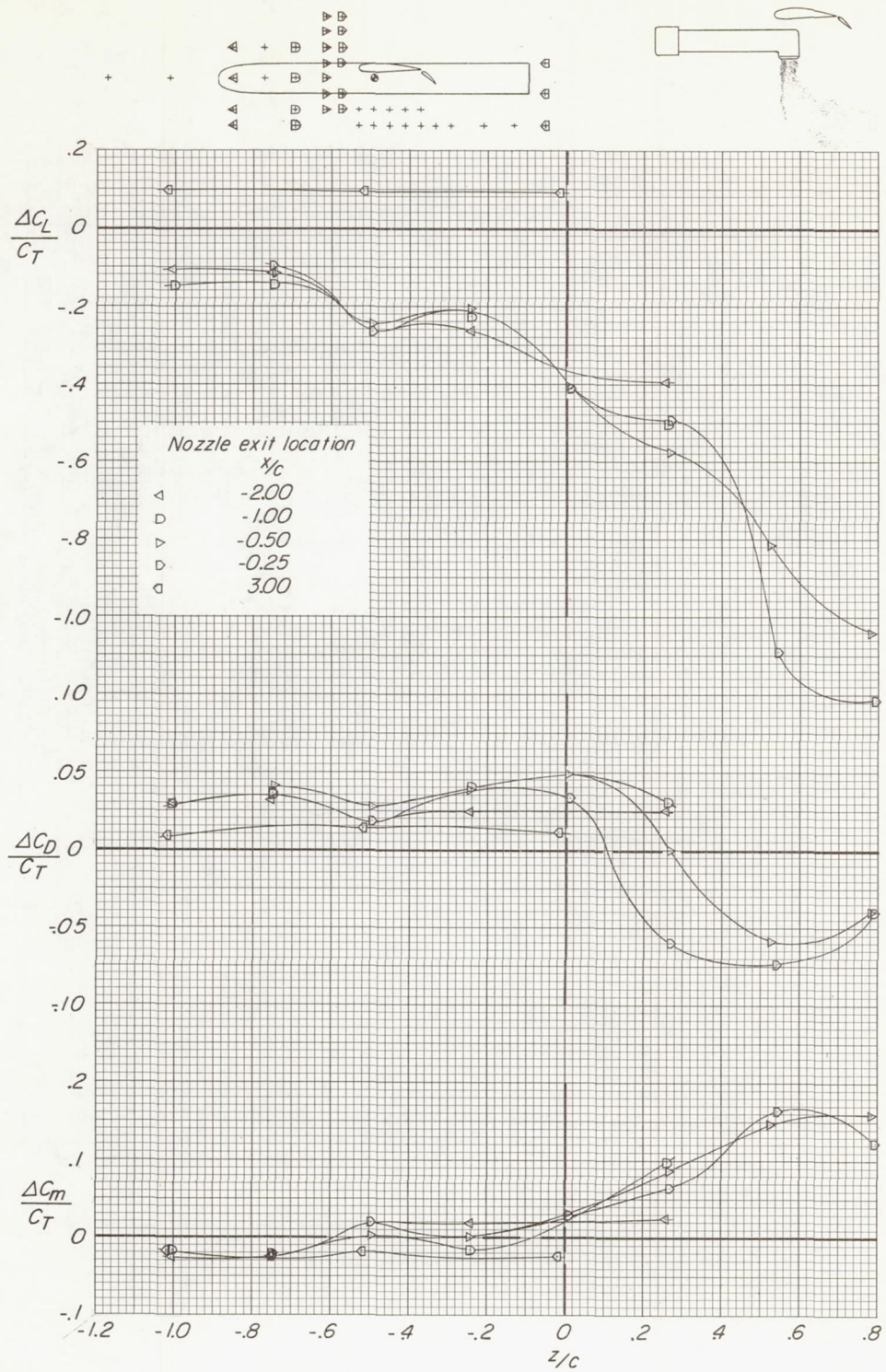

(c) $V_e \approx 0.20$.

Figure 17.- Continued.

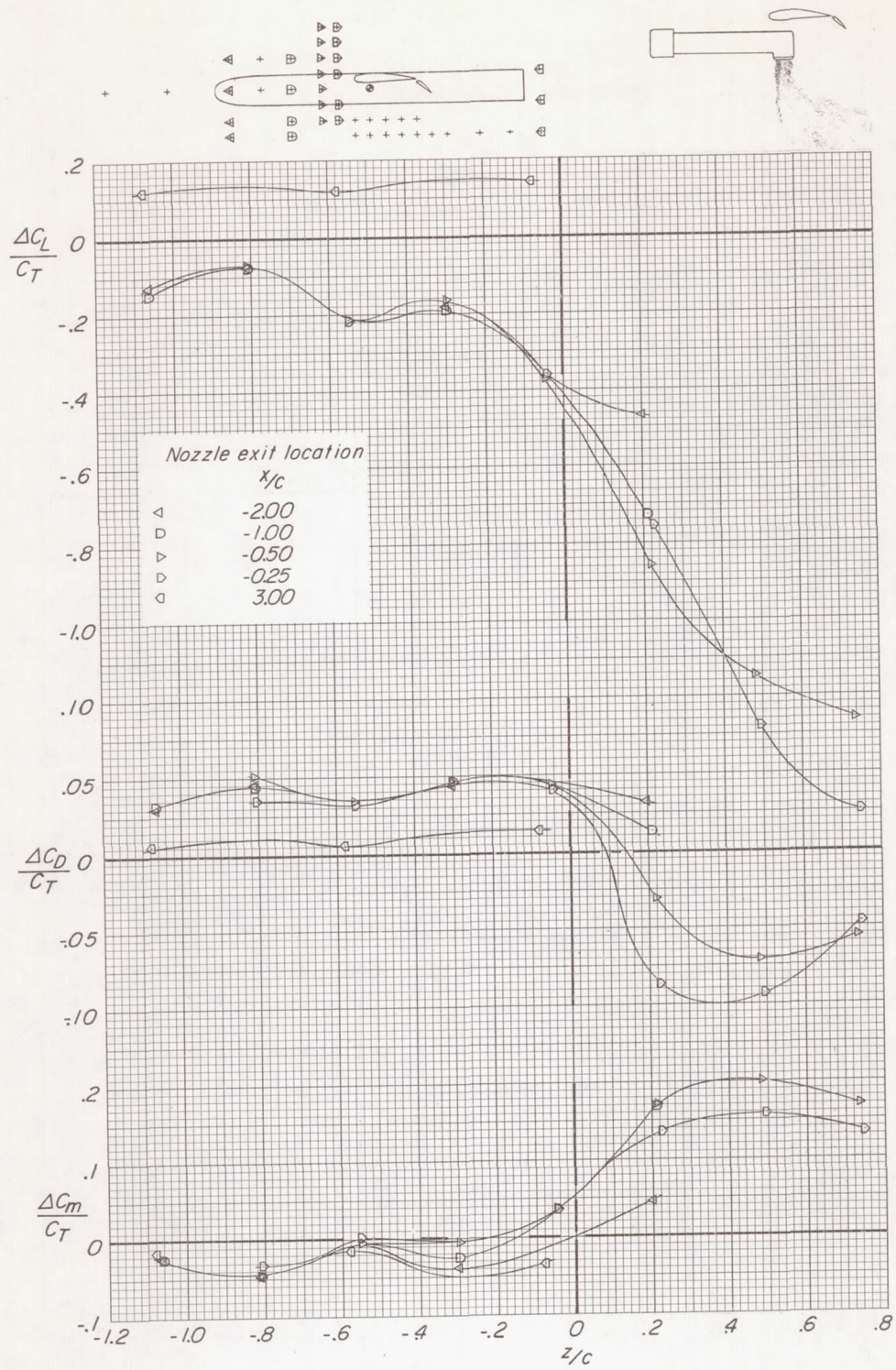

(d) $V_e \approx 0.25$.

Figure 17.- Concluded.

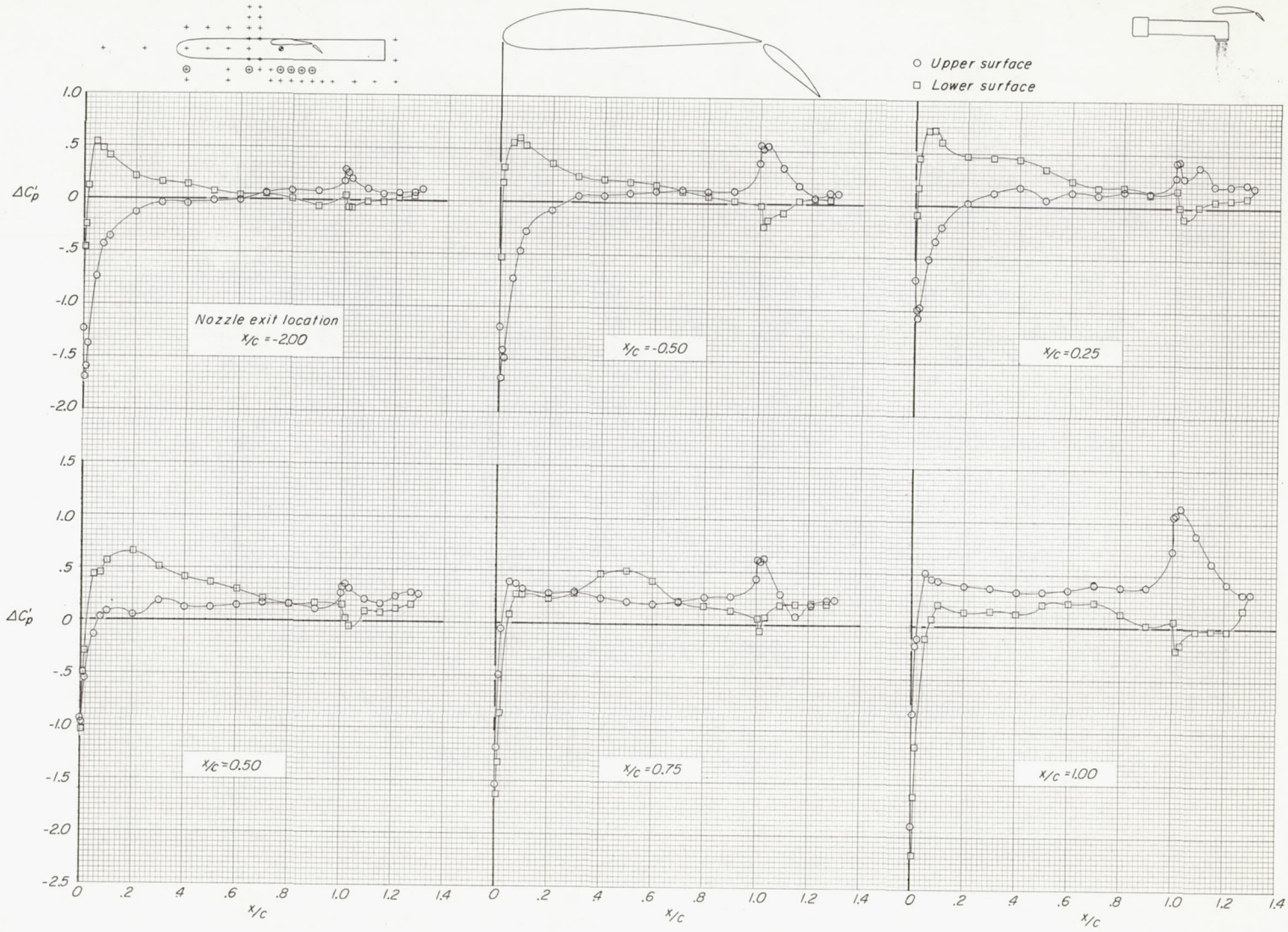

(a) $V_e \approx 0.10$.

Figure 18.- Effect of longitudinal location of the jet exhaust on the incremental upper- and lower-surface pressure distributions due to power. $\delta_f = 40^0$; $\delta_j = 90^0$; $z_0/c = -0.64$.

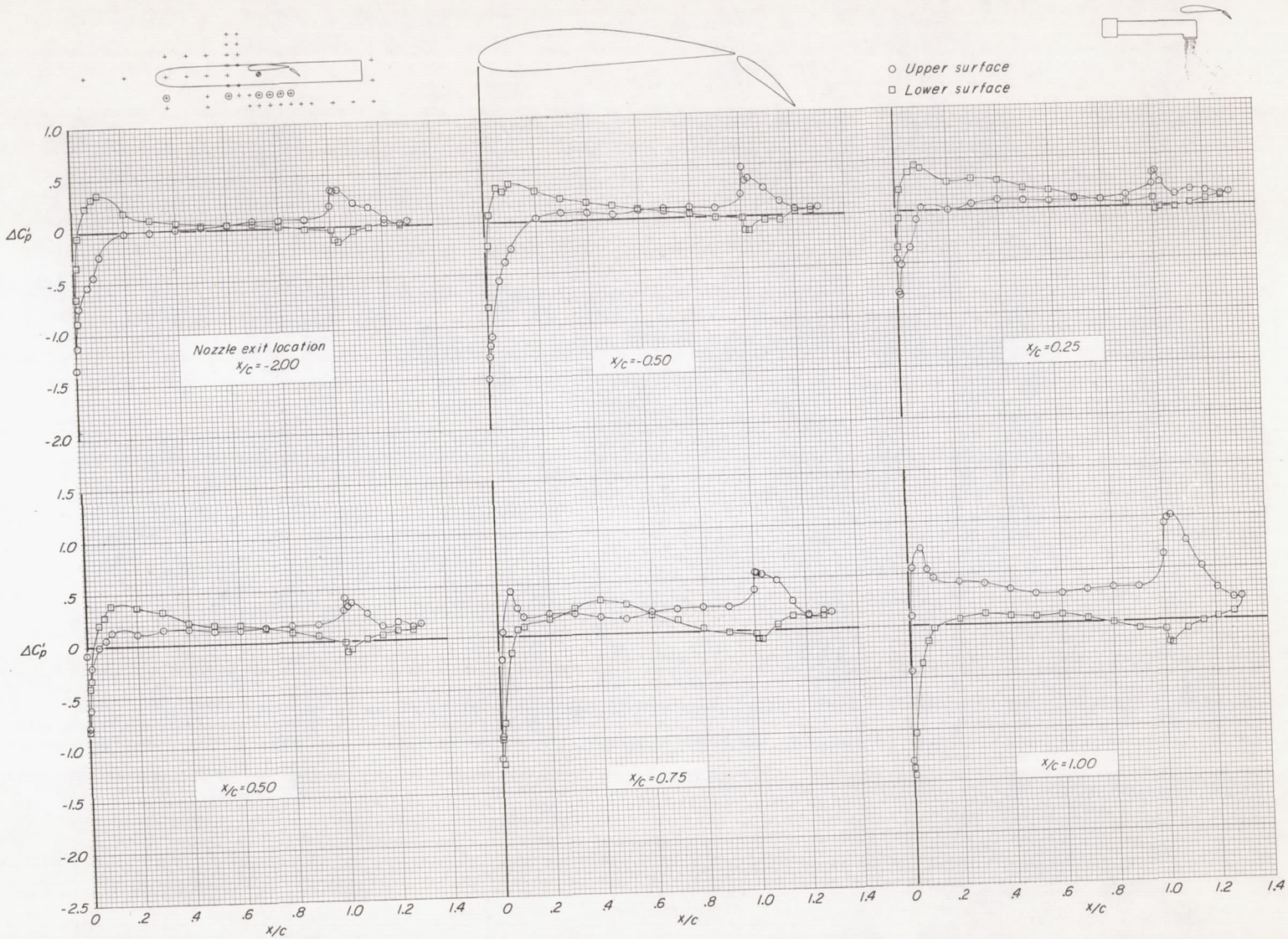

(b) $V_e \approx 0.15$.

Figure 18.- Continued.

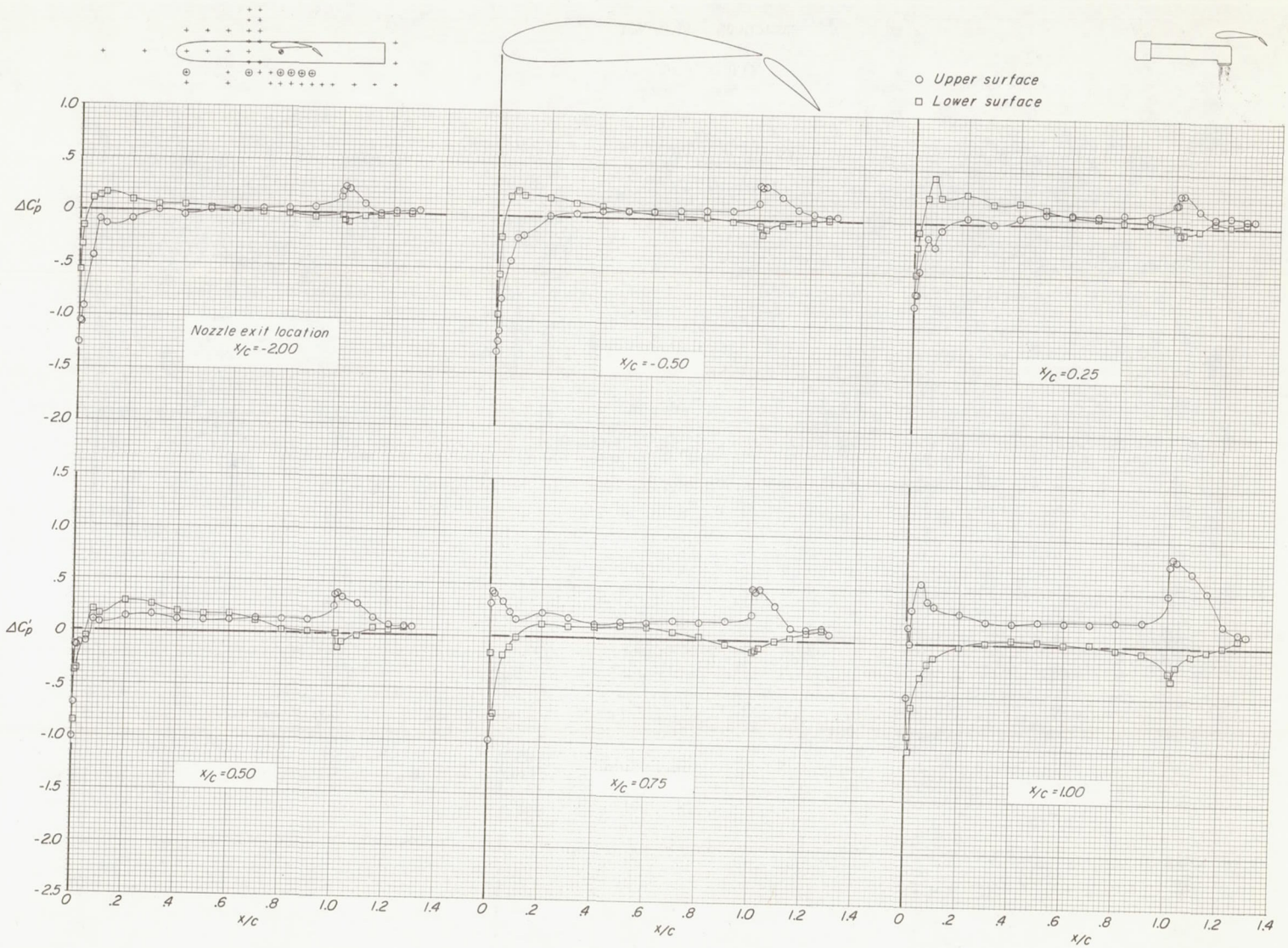

(c) $V_e \approx 0.20$.

Figure 18.- Continued.

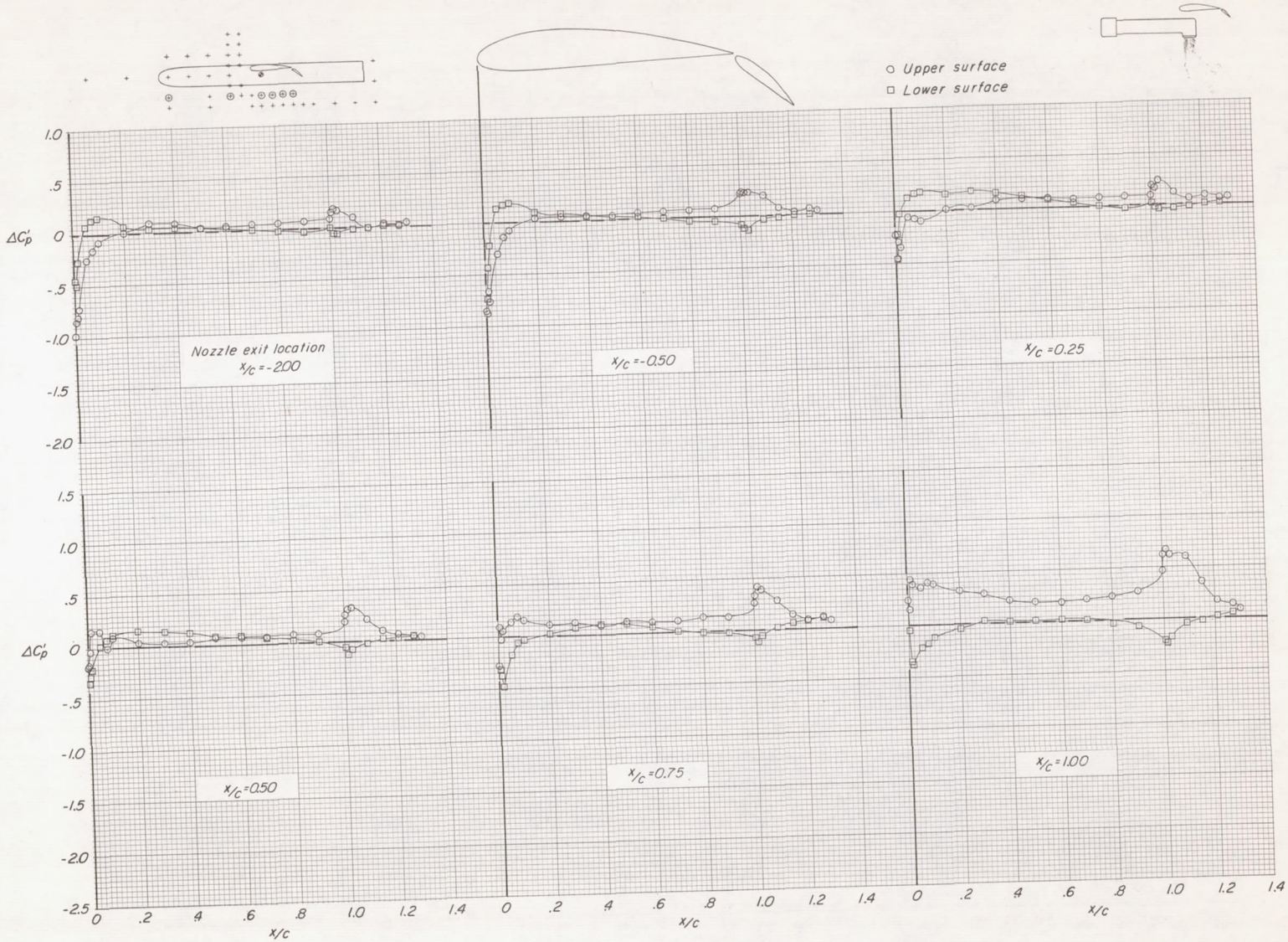

(d) $V_e \approx 0.25$.

Figure 18.- Concluded.

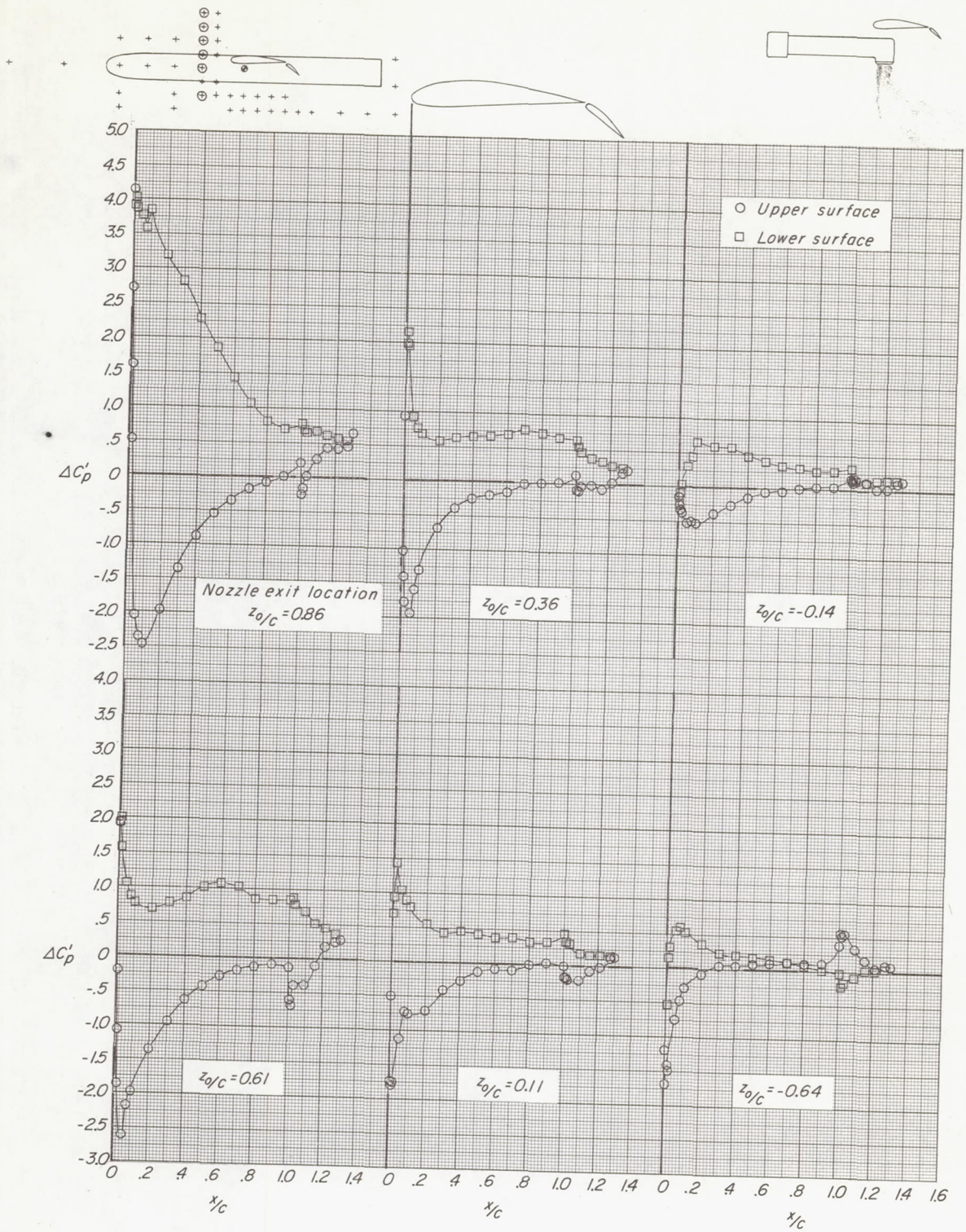

(a) $V_e \approx 0.10$.

Figure 19.- Effect of vertical location of the jet exhaust on the incremental upper- and lower-surface pressure distributions due to power. $\delta_f = 40^0$; $\delta_j = 90^0$; $x/c = -0.50$.

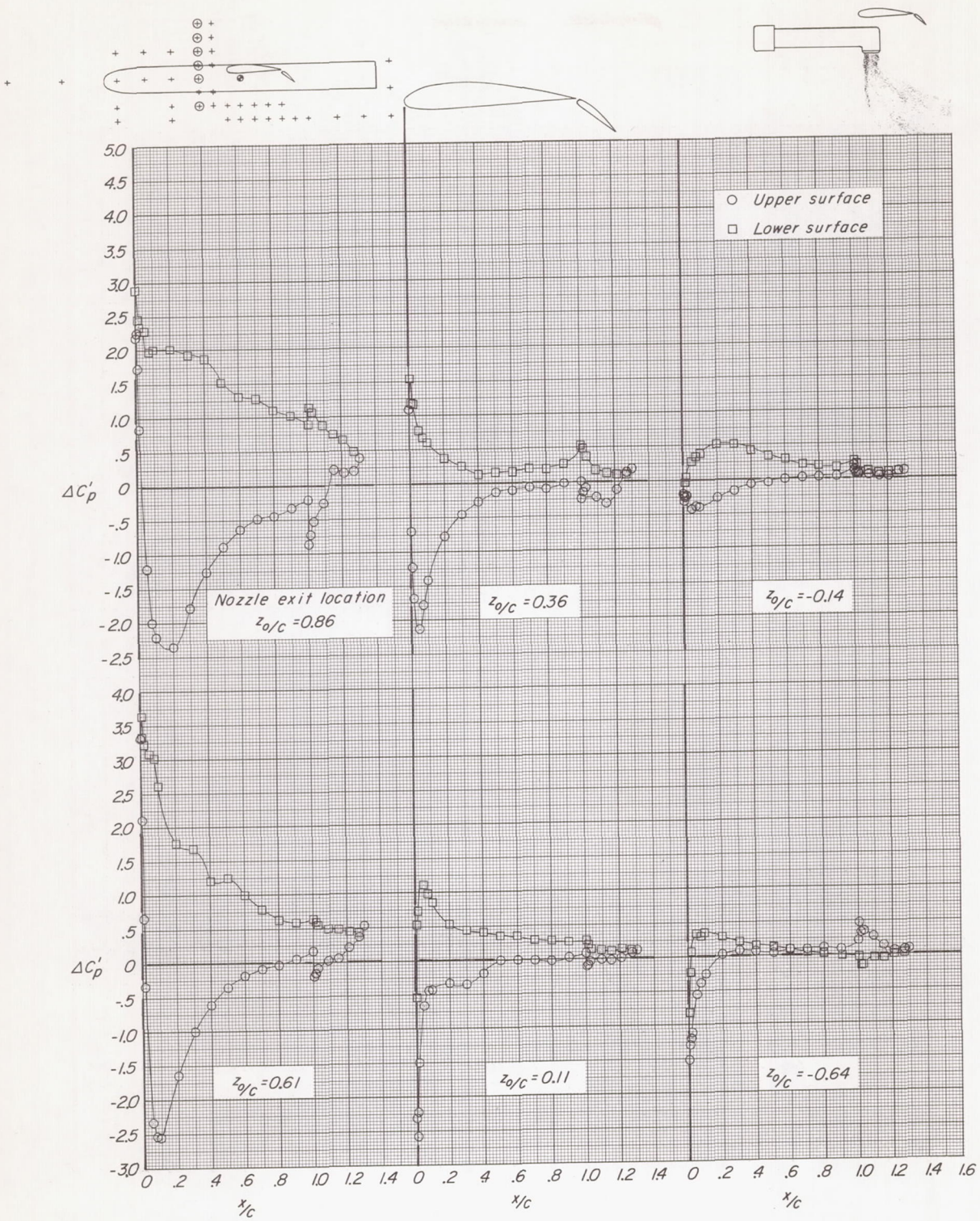

(b) $V_e \approx 0.15$.

Figure 19.- Continued.

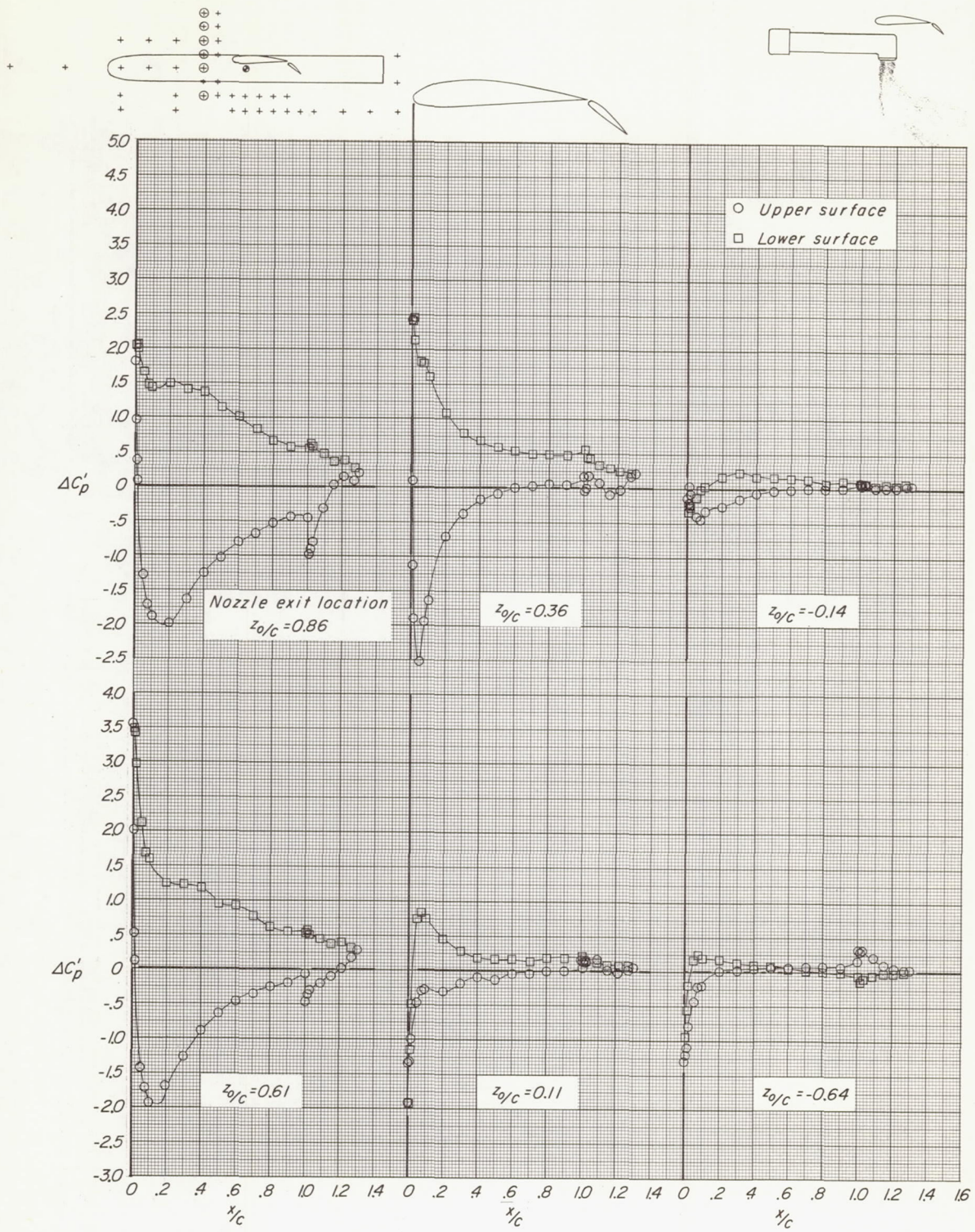

(c) $V_e \approx 0.20$.

Figure 19.- Continued.

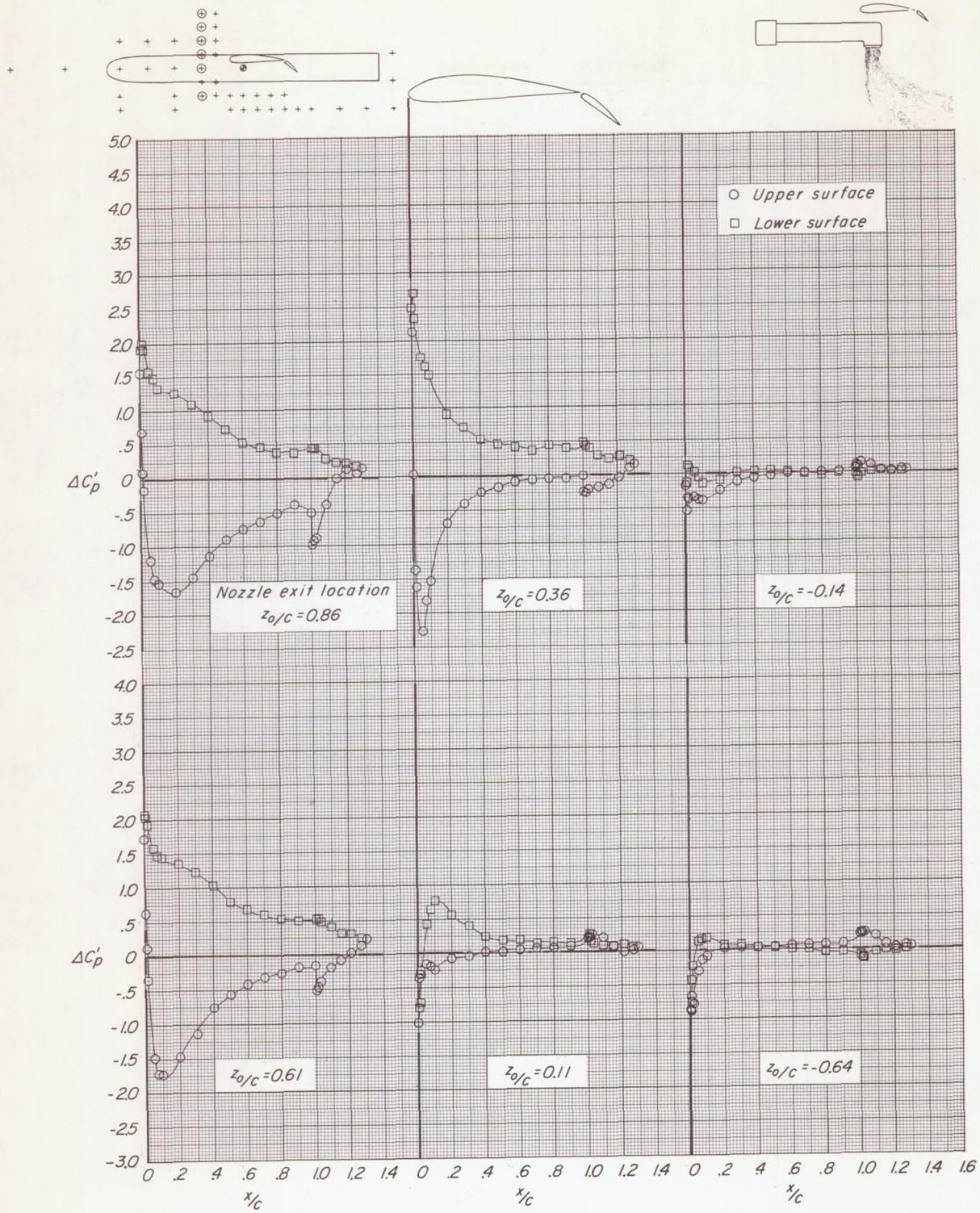

(d) $V_e \approx 0.25$.

Figure 19.- Concluded.

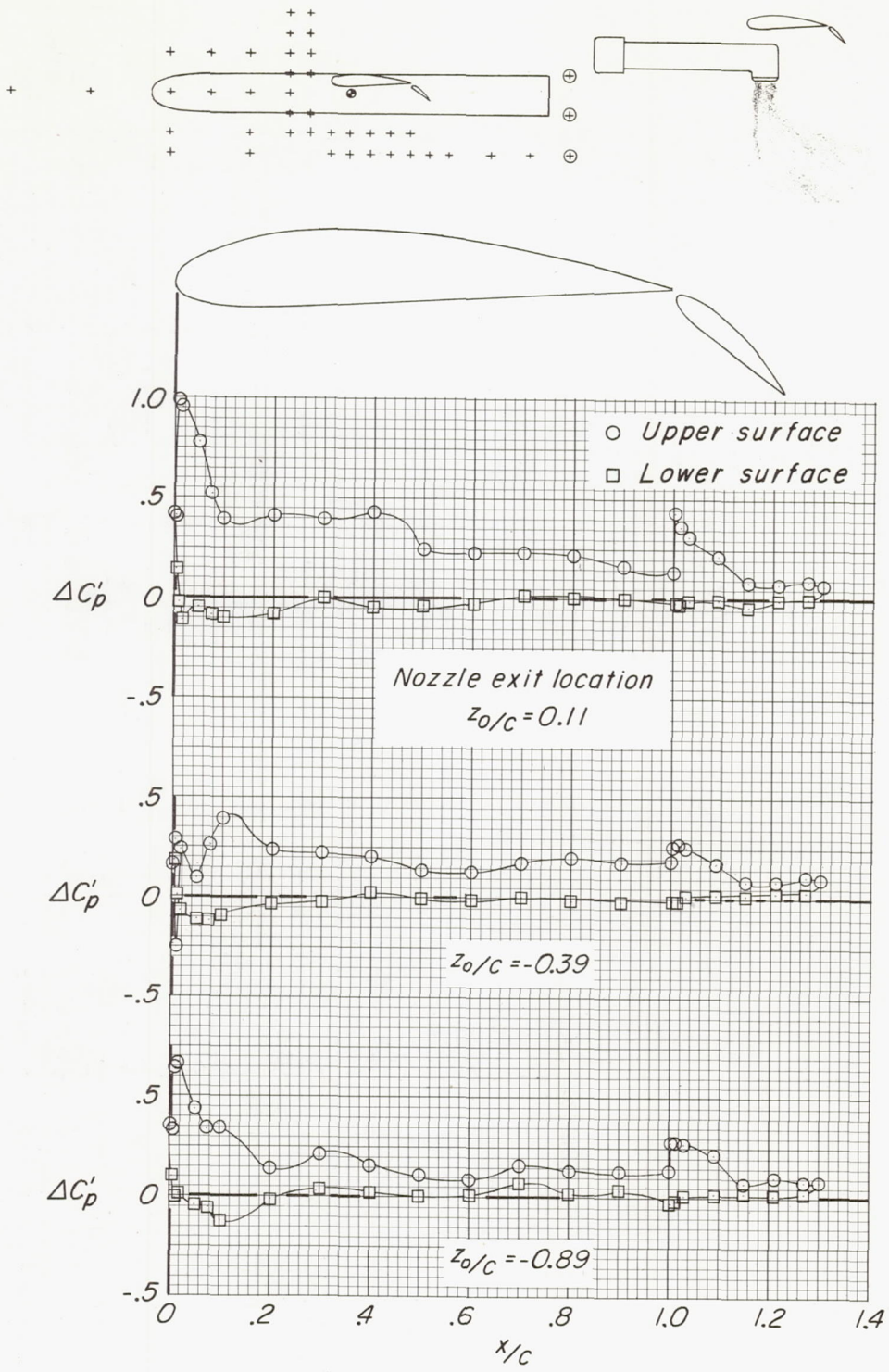

(a) $V_e \approx 0.10$.

Figure 20.- Effect of vertical location of the jet exhaust on the incremental upper- and lower-surface pressure distributions due to power. $\delta_f = 40^o$; $\delta_j = 90^o$; $x/c = 3.00$.

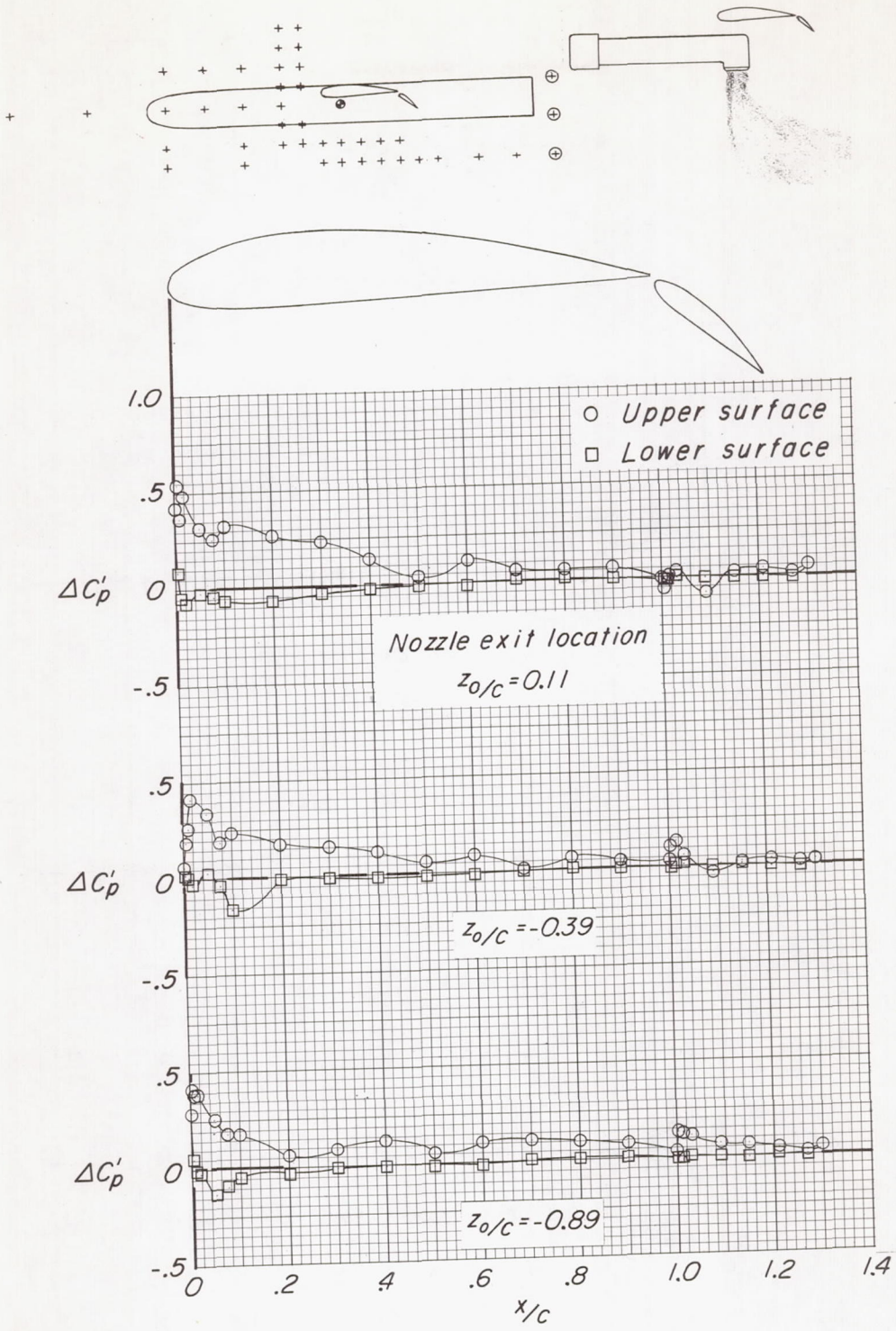

(b) $V_e \approx 0.15$.

Figure 20.- Continued.

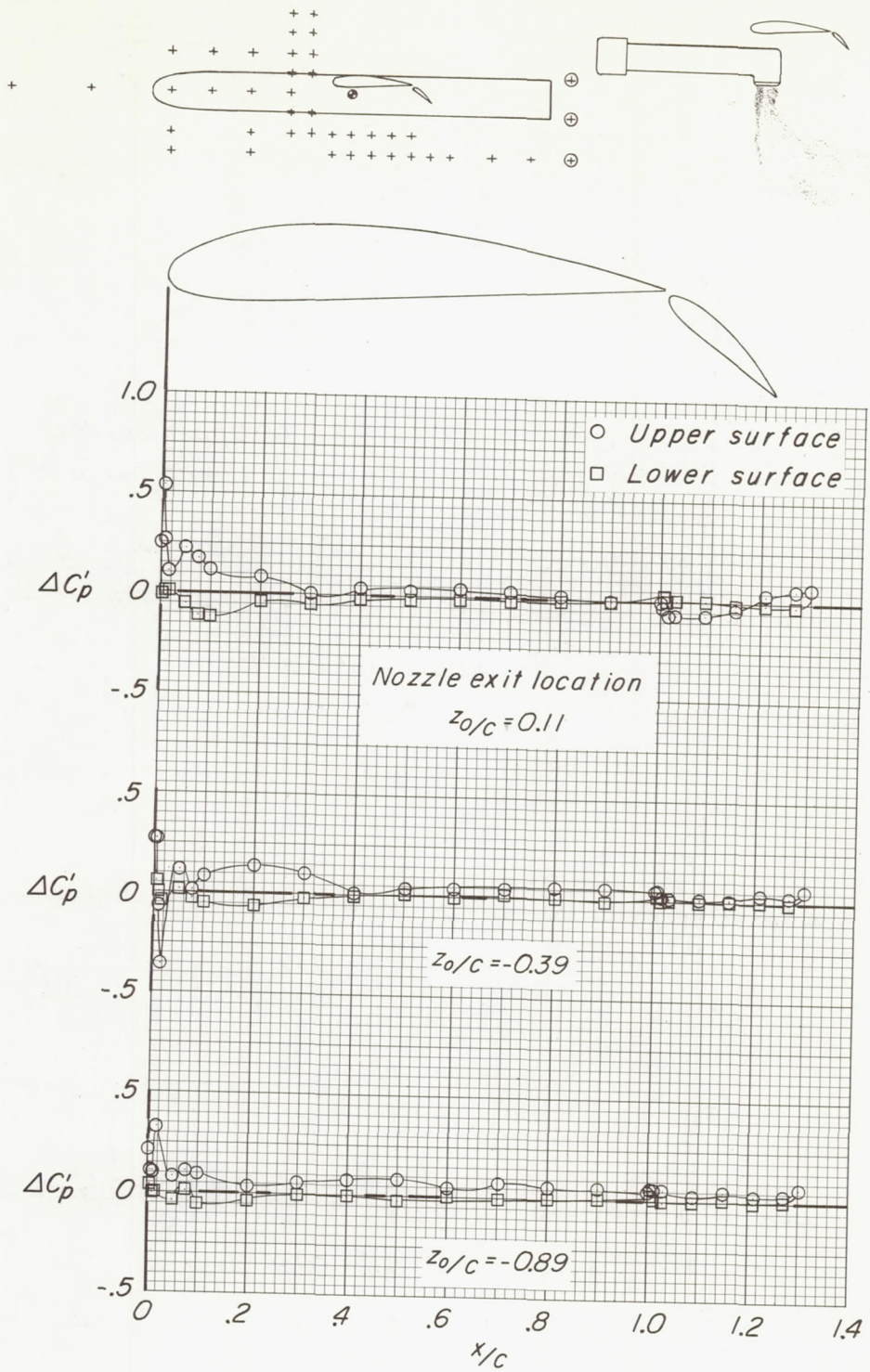

(c) $V_e \approx 0.20$.

Figure 20.- Continued.

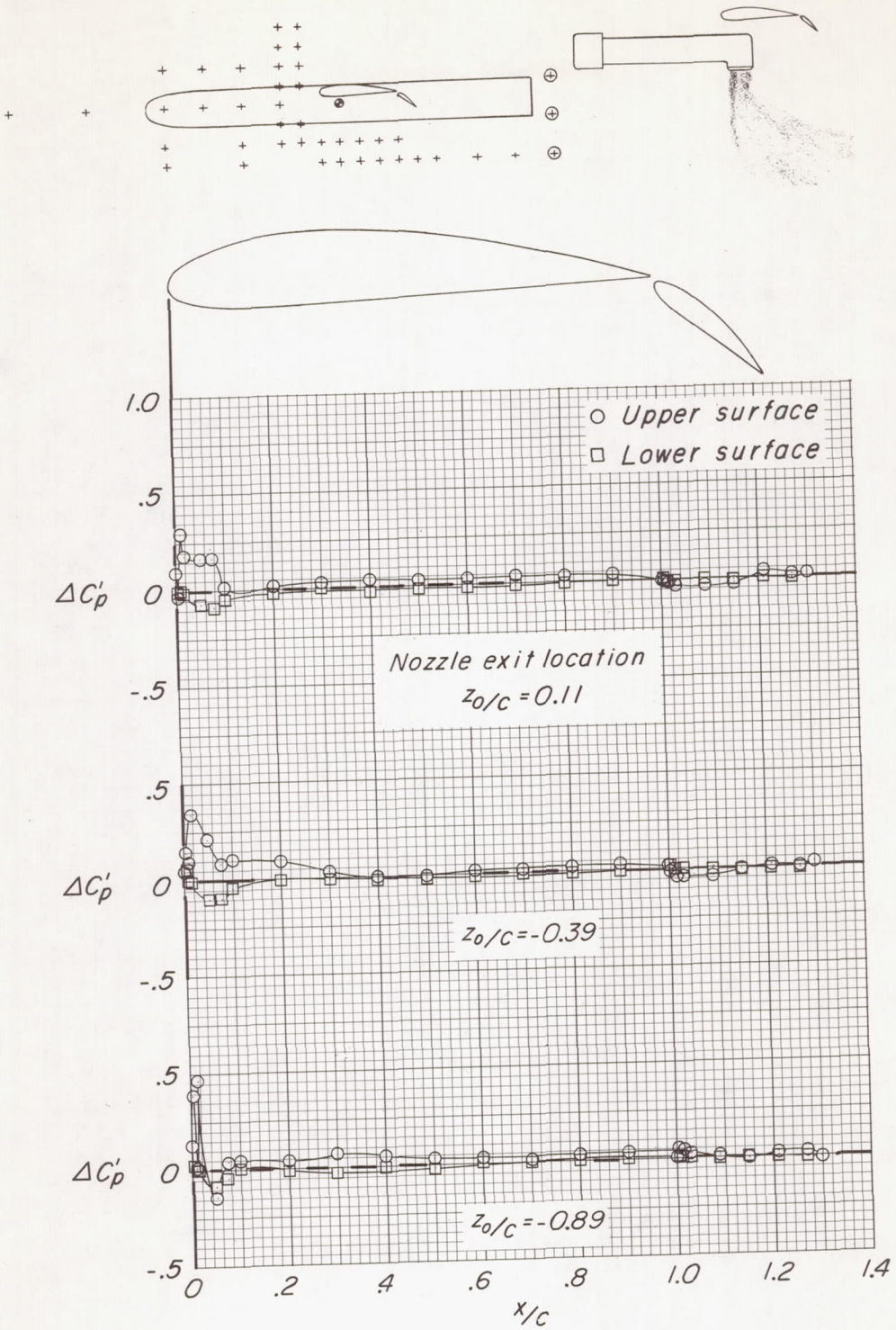

(d) $V_e \approx 0.25$.

Figure 20.- Concluded.

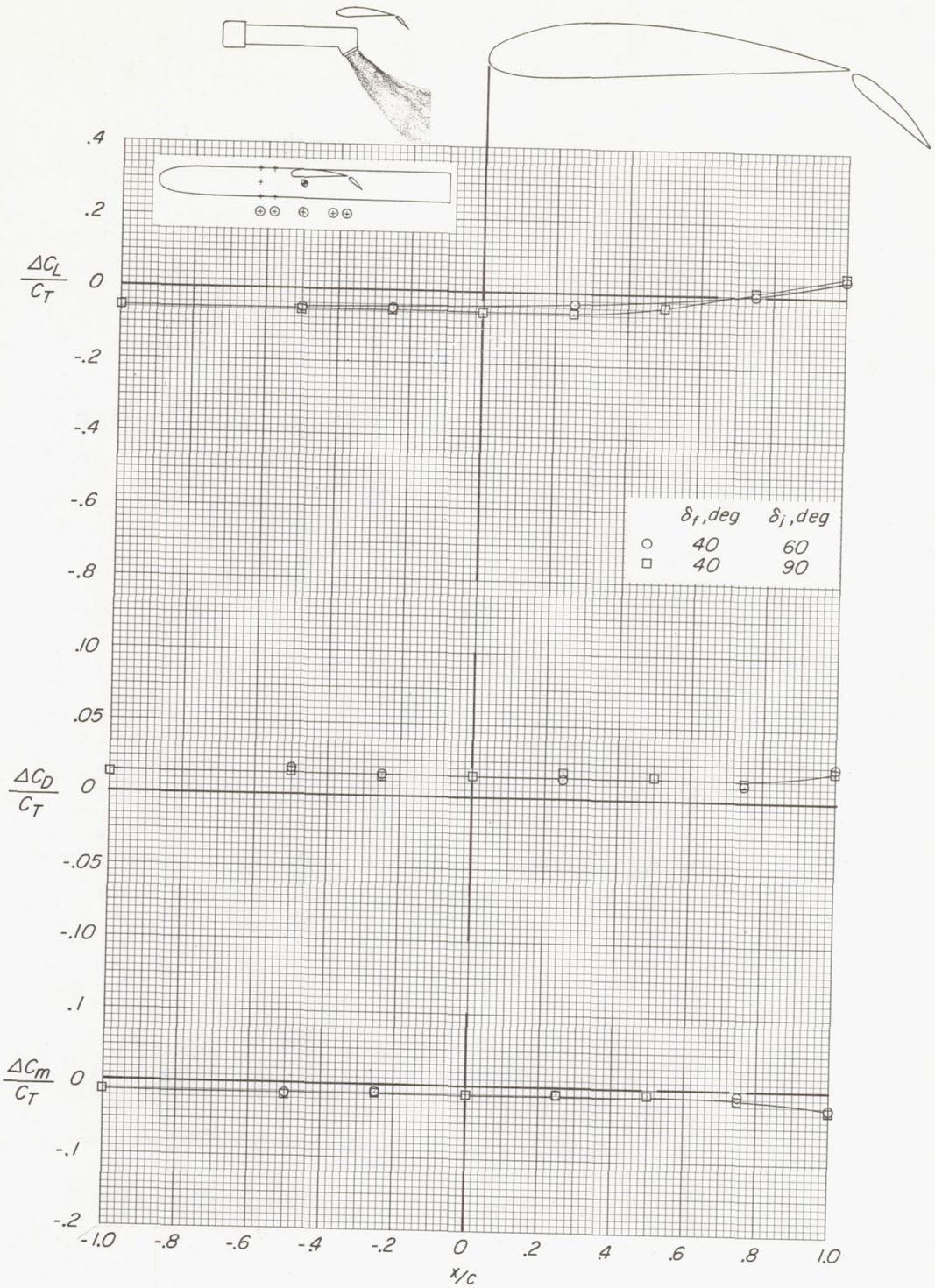

(a) $V_e \approx 0.10$.

Figure 21.- Effect of deflection of jet exhaust on the incremental lift, drag, and pitching moment due to power at several longitudinal locations of the jets. $z_0/c = -0.64$.

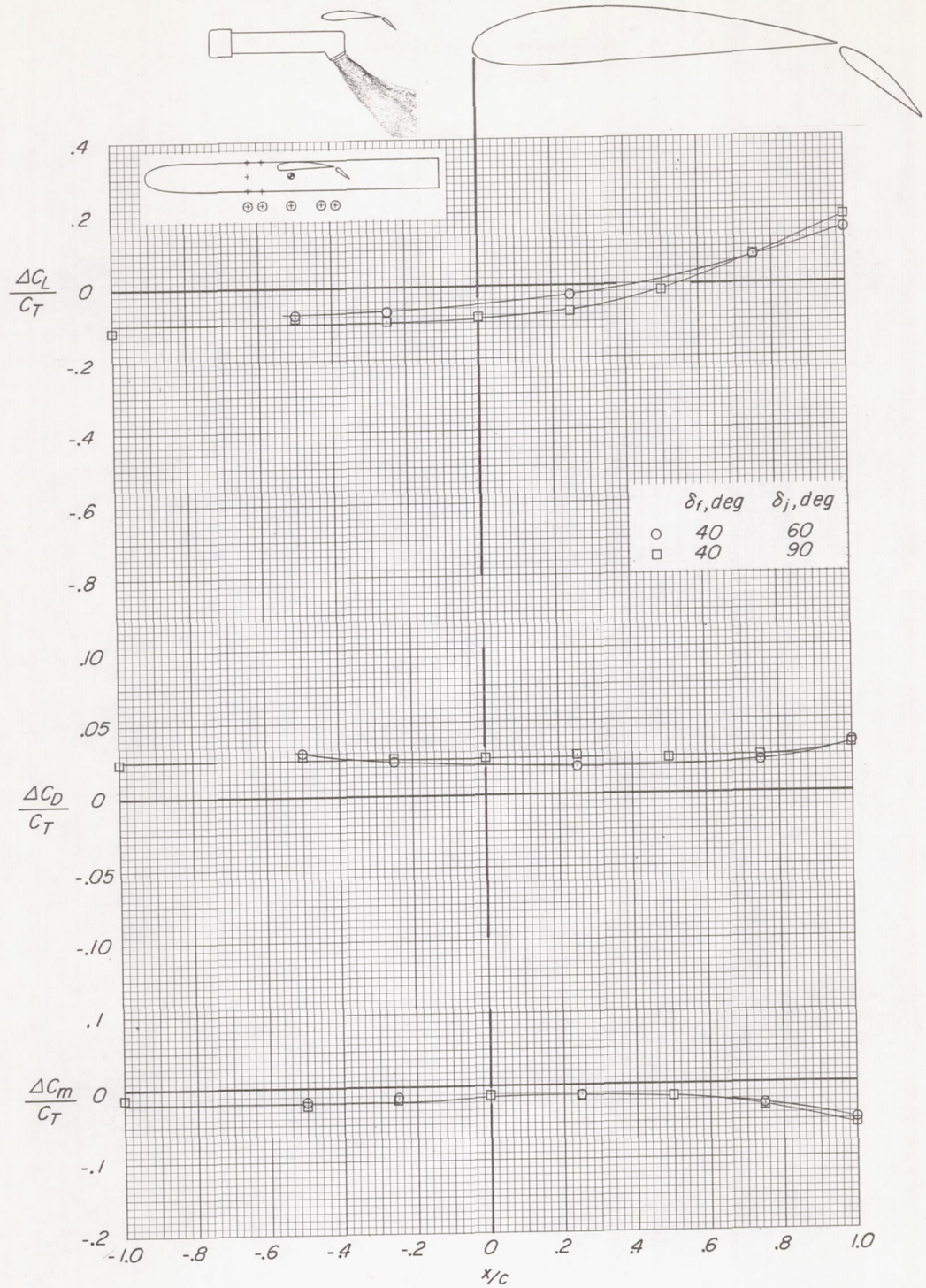

(b) $V_e \approx 0.15$.

Figure 21.- Continued.

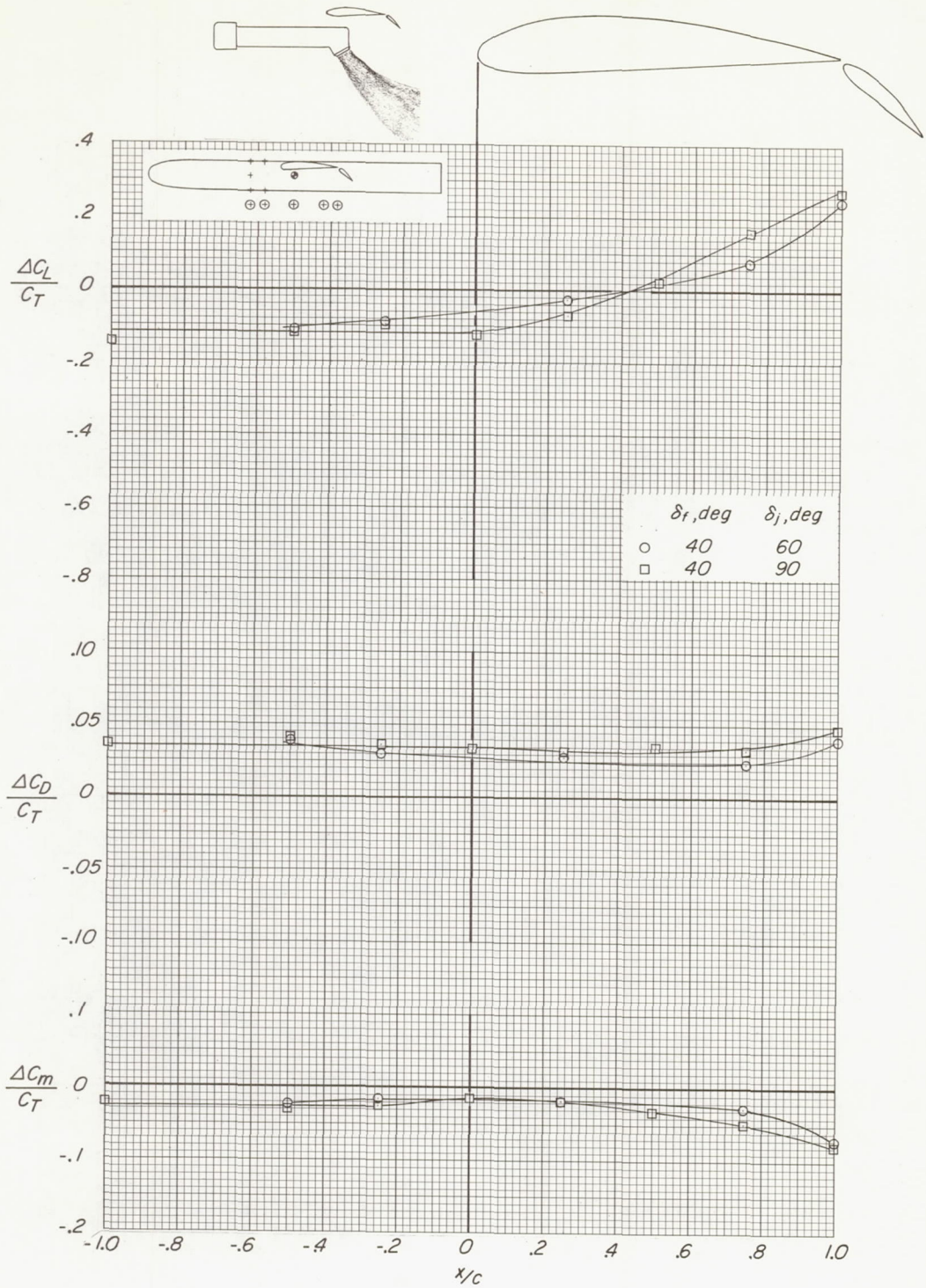

(c) $V_e \approx 0.20$.

Figure 21.- Continued.

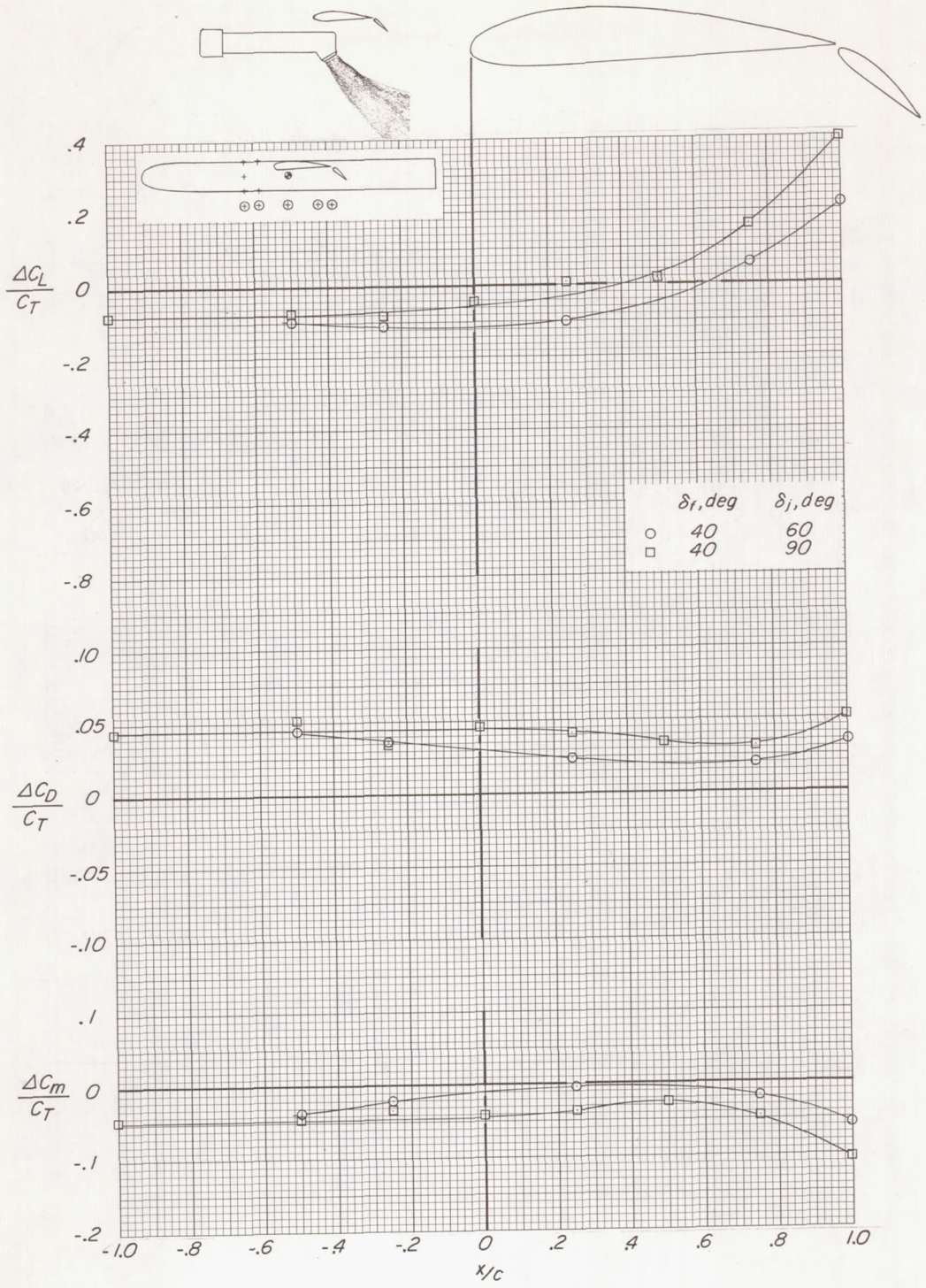

(d) $V_e \approx 0.25$.

Figure 21.- Concluded.

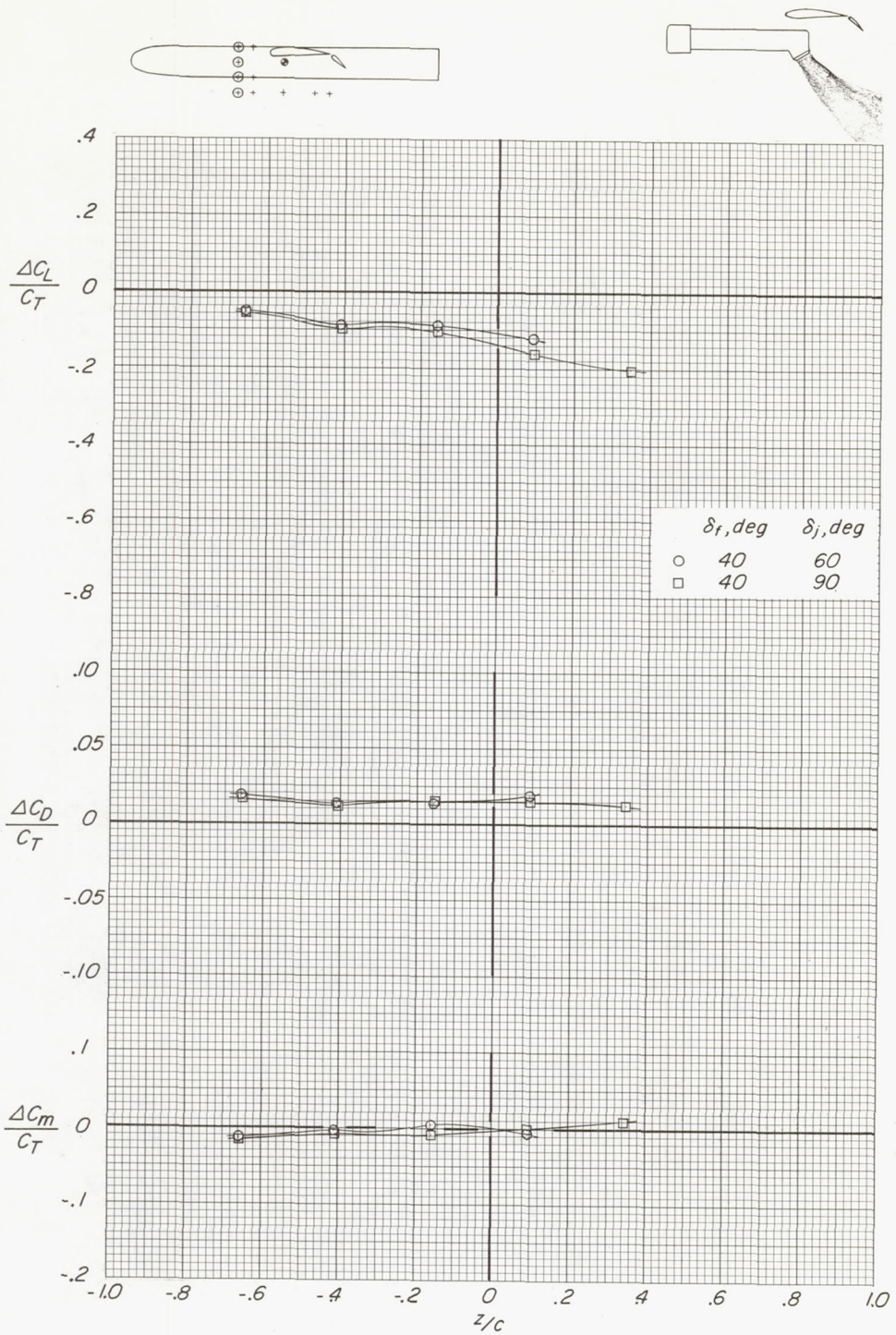

(a) $V_e \approx 0.10$.

Figure 22.- Effect of deflection of jet exhaust on the incremental lift, drag, and pitching moment due to power at several vertical locations of the jets. x/c = -0.50.

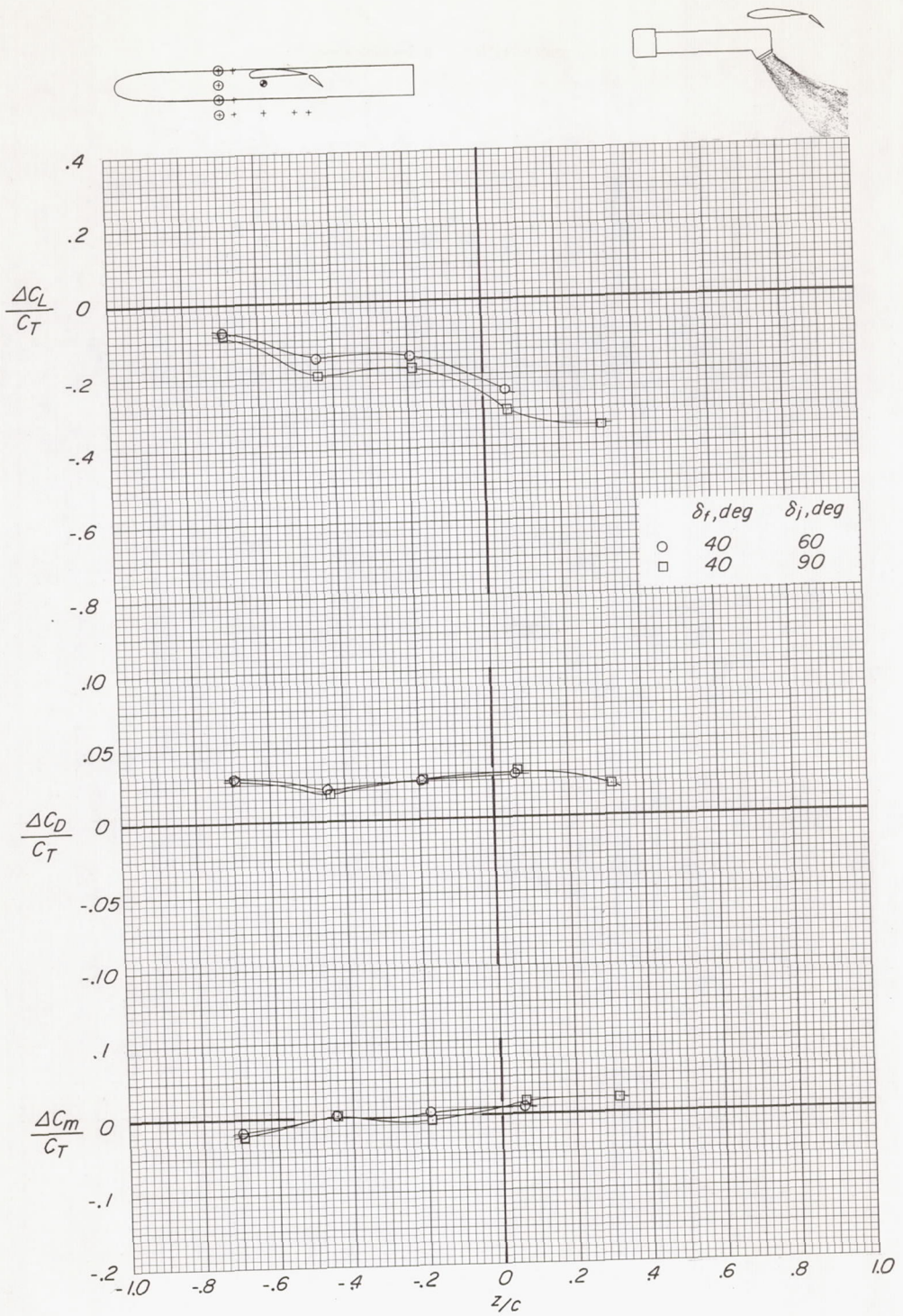

(b) $V_e \approx 0.15$.

Figure 22.- Continued.

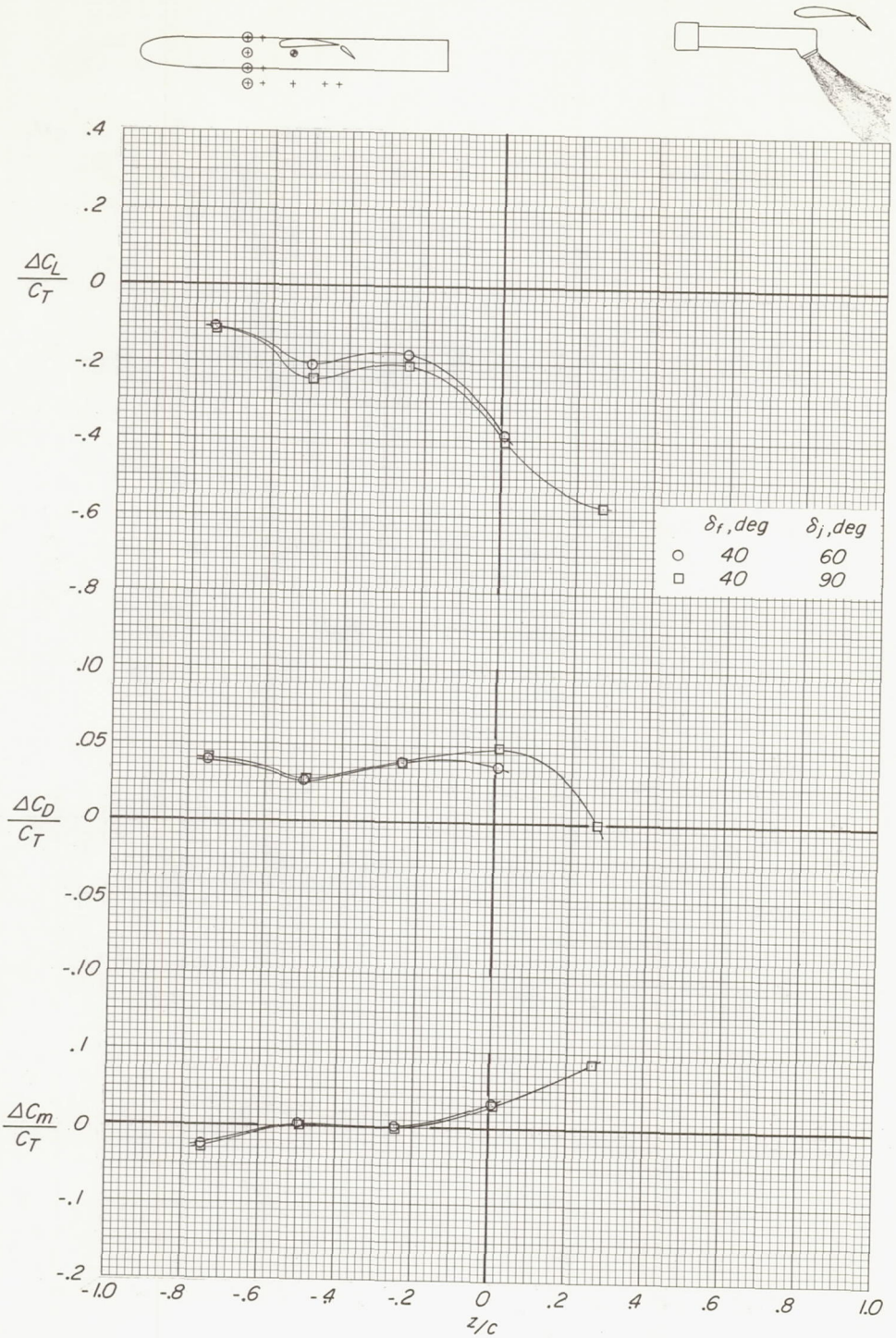

(c) $V_e \approx 0.20$.

Figure 22.- Continued.

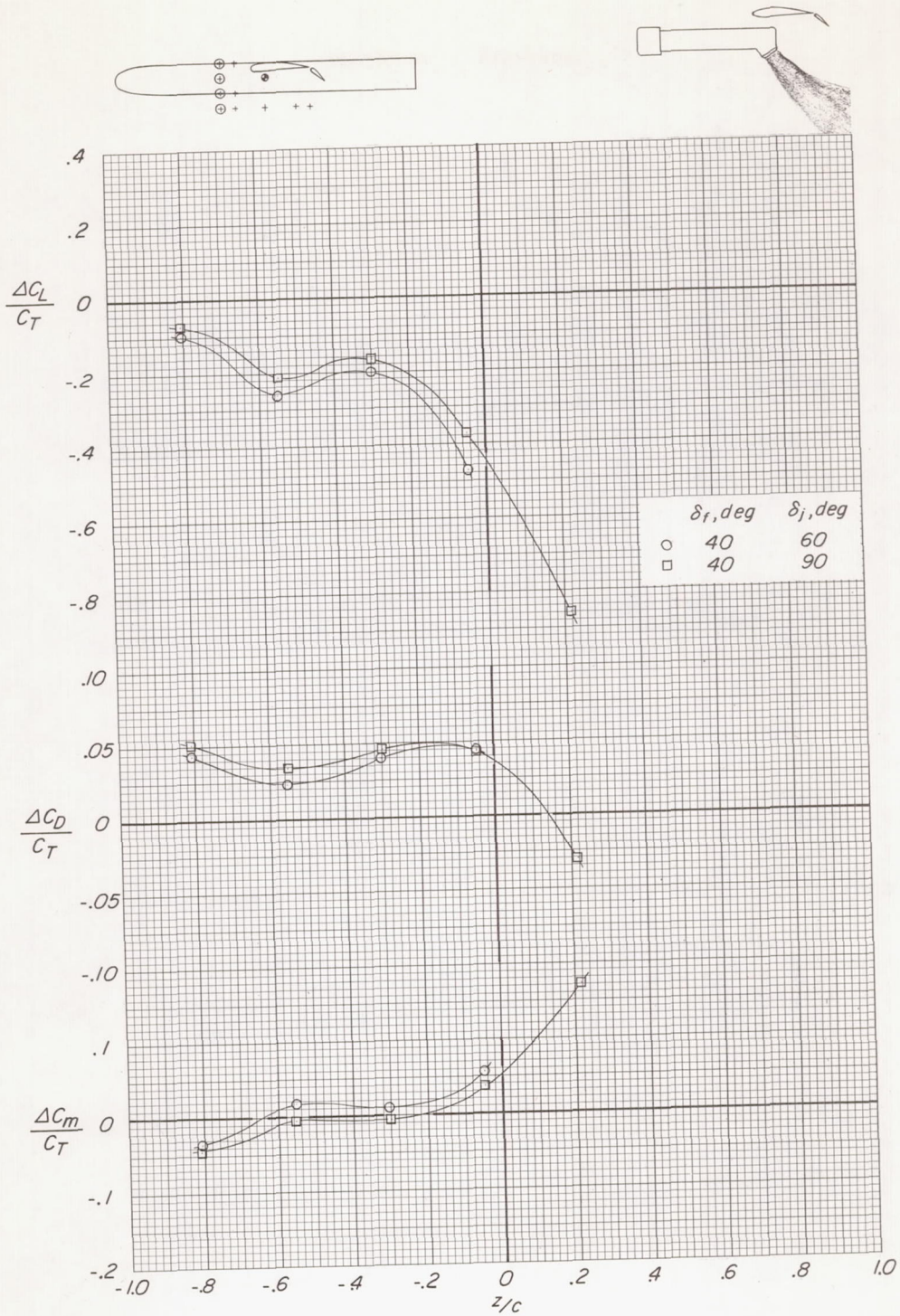

(d) $V_e \approx 0.25$.

Figure 22.- Concluded.

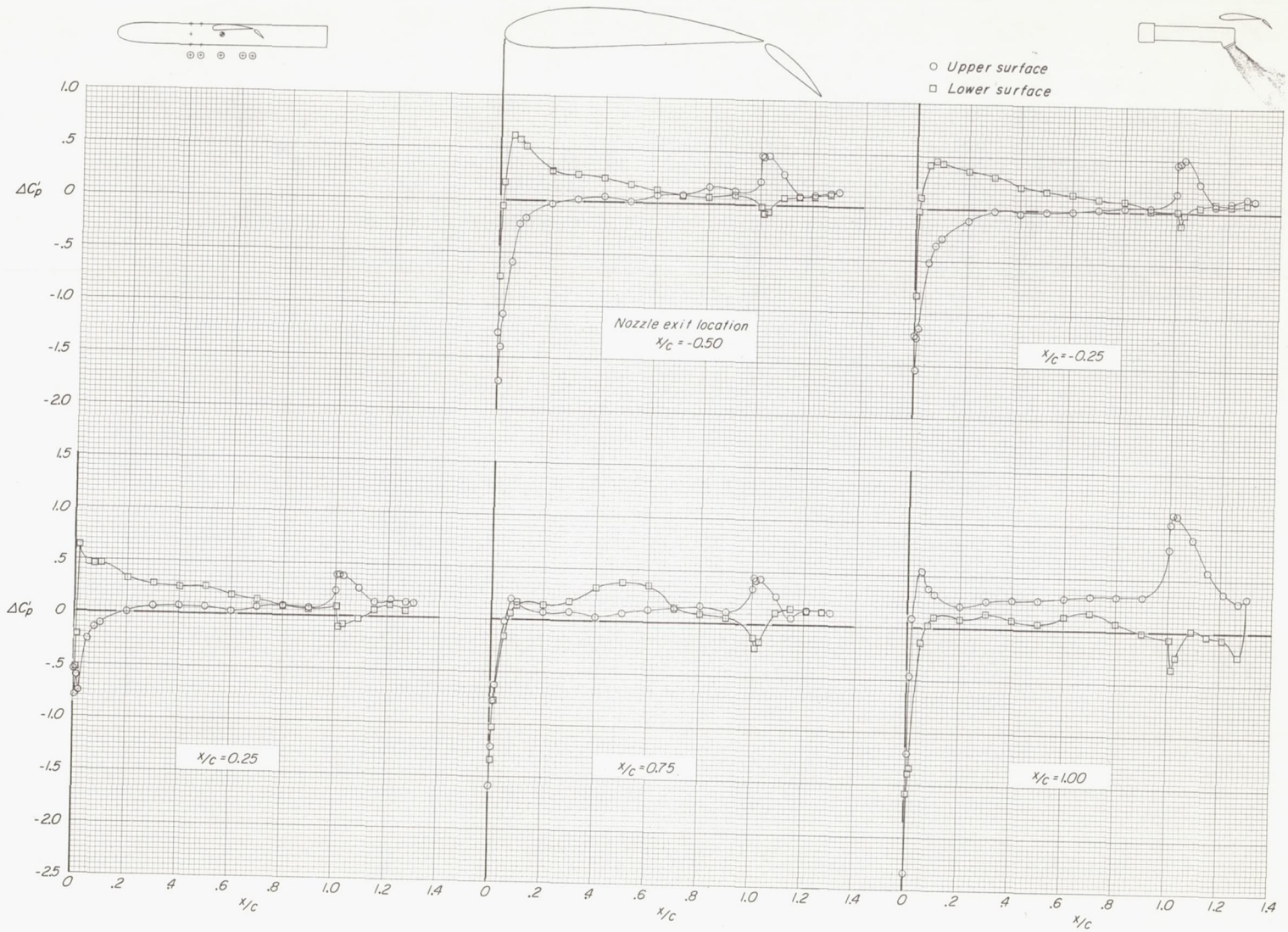

(a) $V_e \approx 0.10$.

Figure 23.- Effect of longitudinal location of the jet exhaust on the incremental upper- and lower-surface pressure distributions due to power. $\delta_f = 40^0$; $\delta_j = 60^0$; $z_0/c = -0.64$.

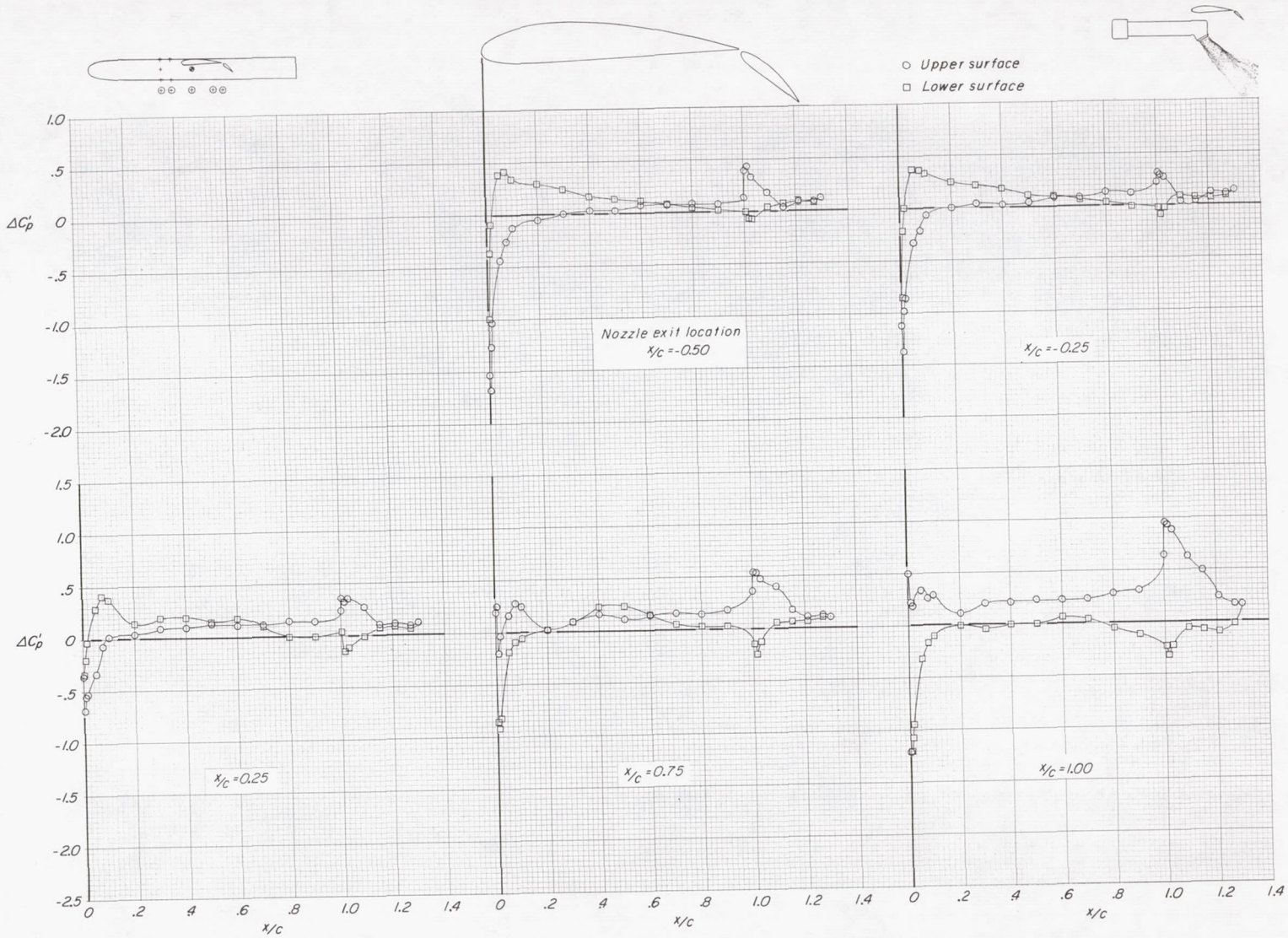

(b) $V_e \approx 0.15$.

Figure 23.- Continued.

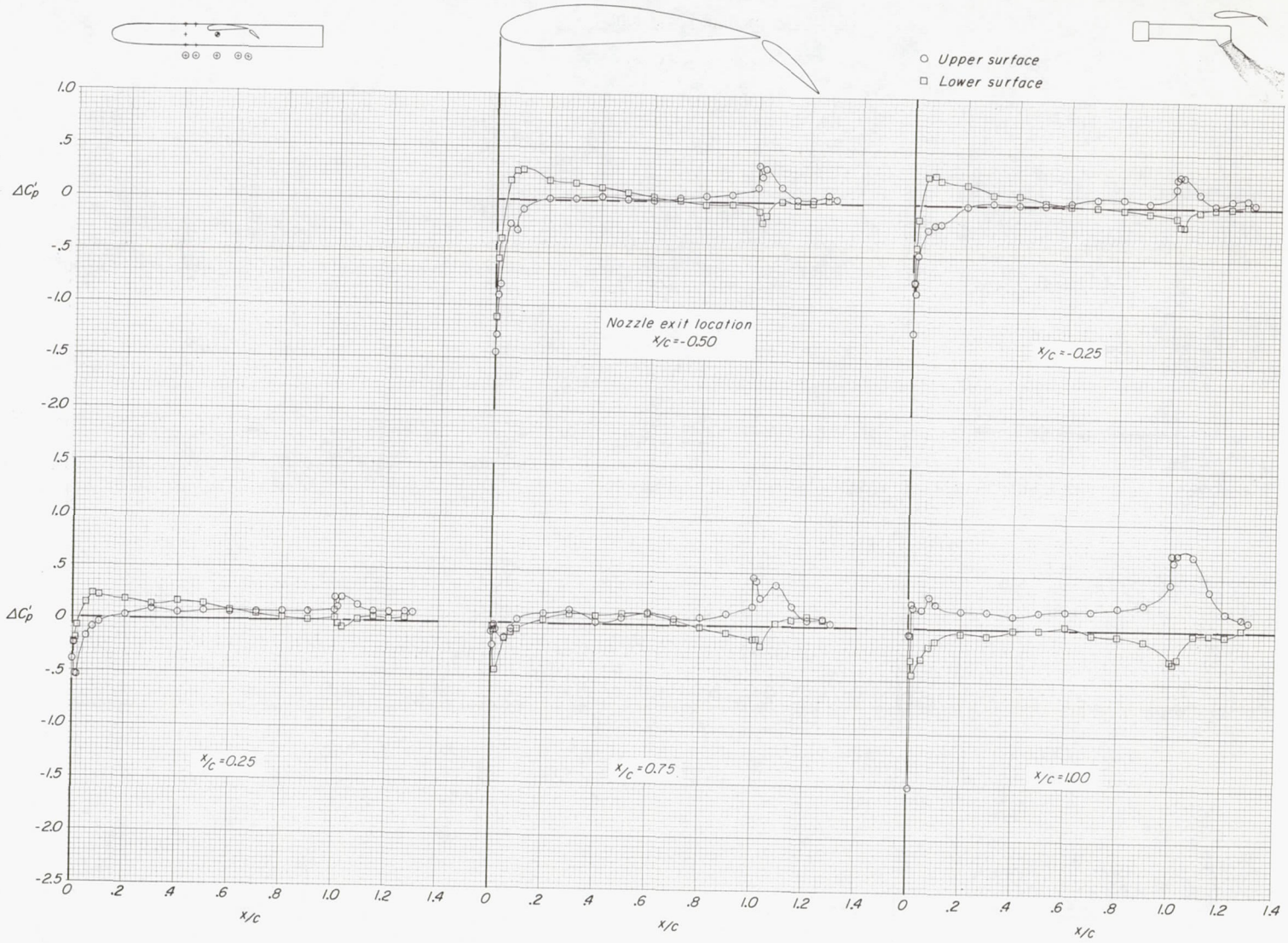

(c) $V_e \approx 0.20$.

Figure 23.- Continued.

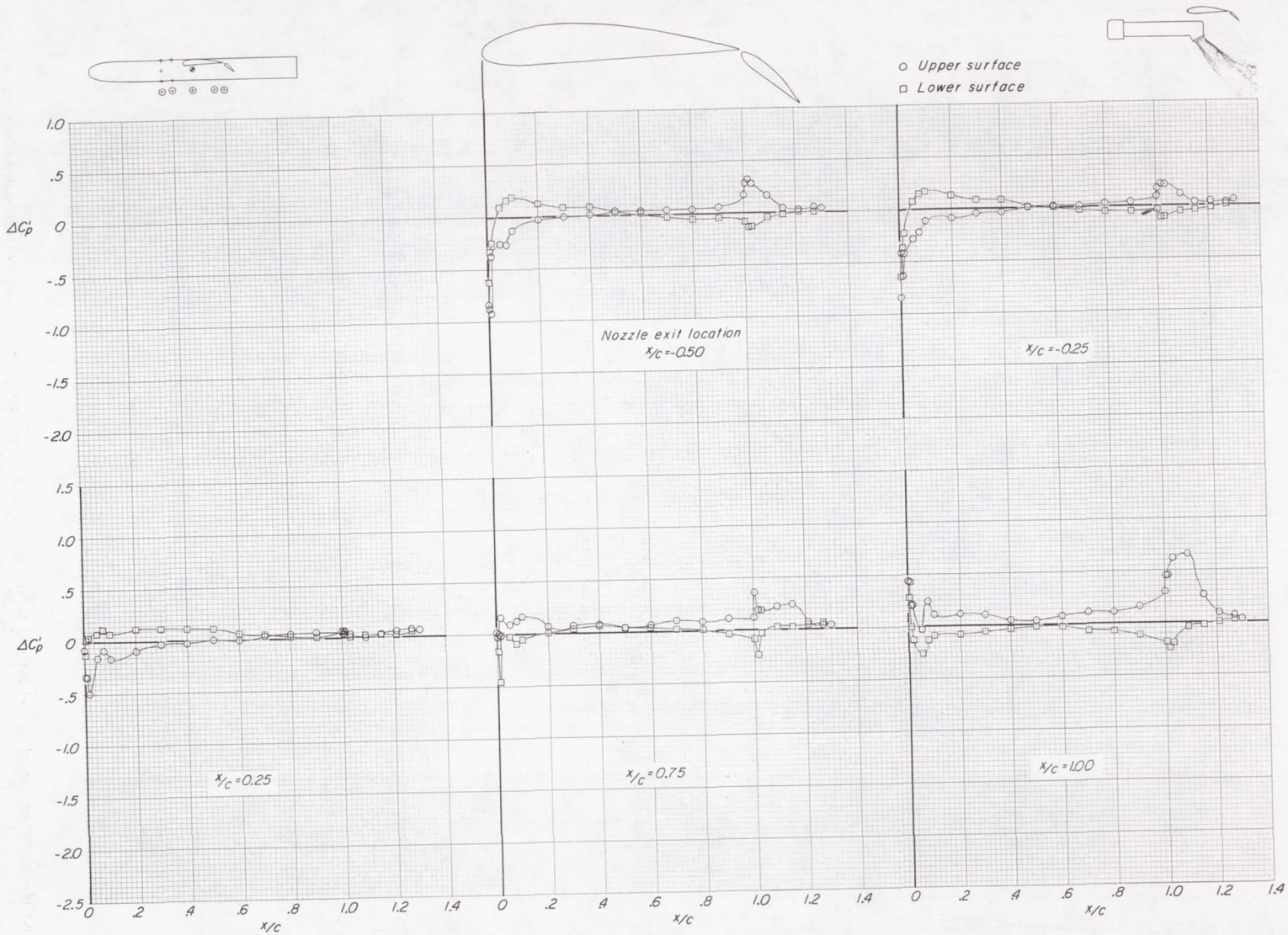

(d) $V_e \approx 0.25$.

Figure 23.- Concluded.

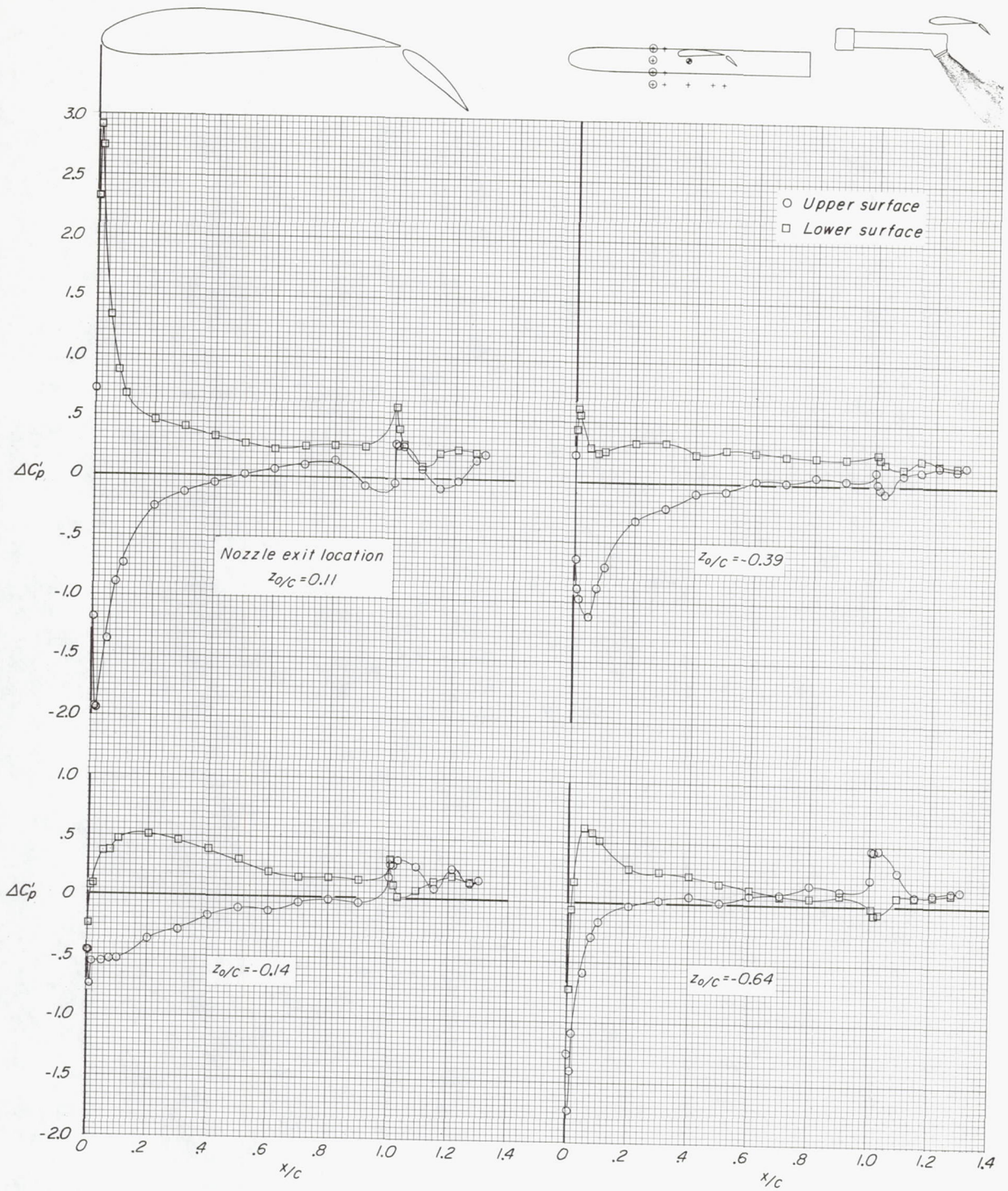

(a) $V_e \approx 0.10$.

Figure 24.- Effect of vertical location of the jet exhaust on the incremental upper- and lower-surface pressure distributions due to power. $\delta_f = 40^o$; $\delta_j = 60^o$; $x/c = -0.50$.

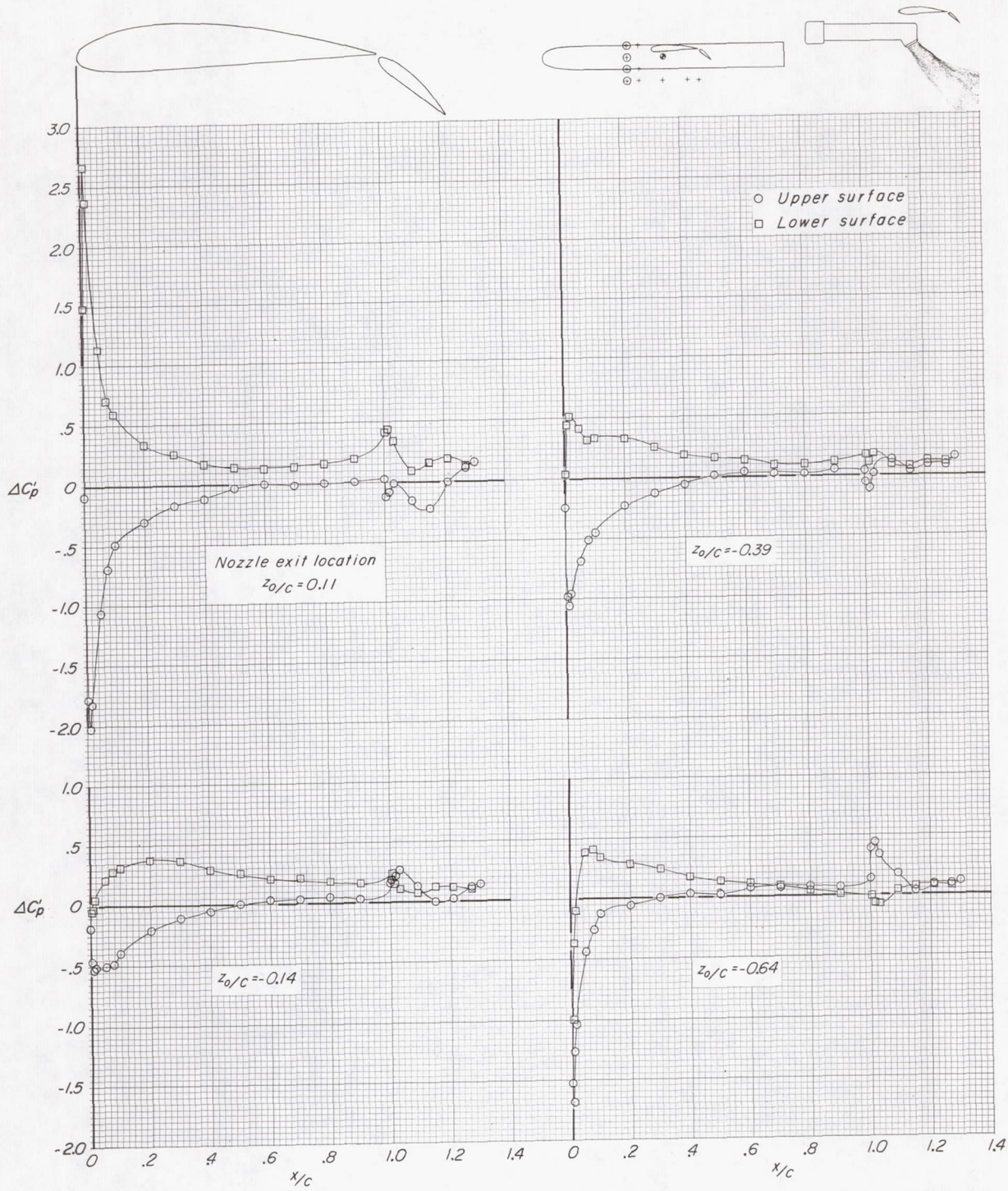

(b) $V_e \approx 0.15$.

Figure 24.- Continued.

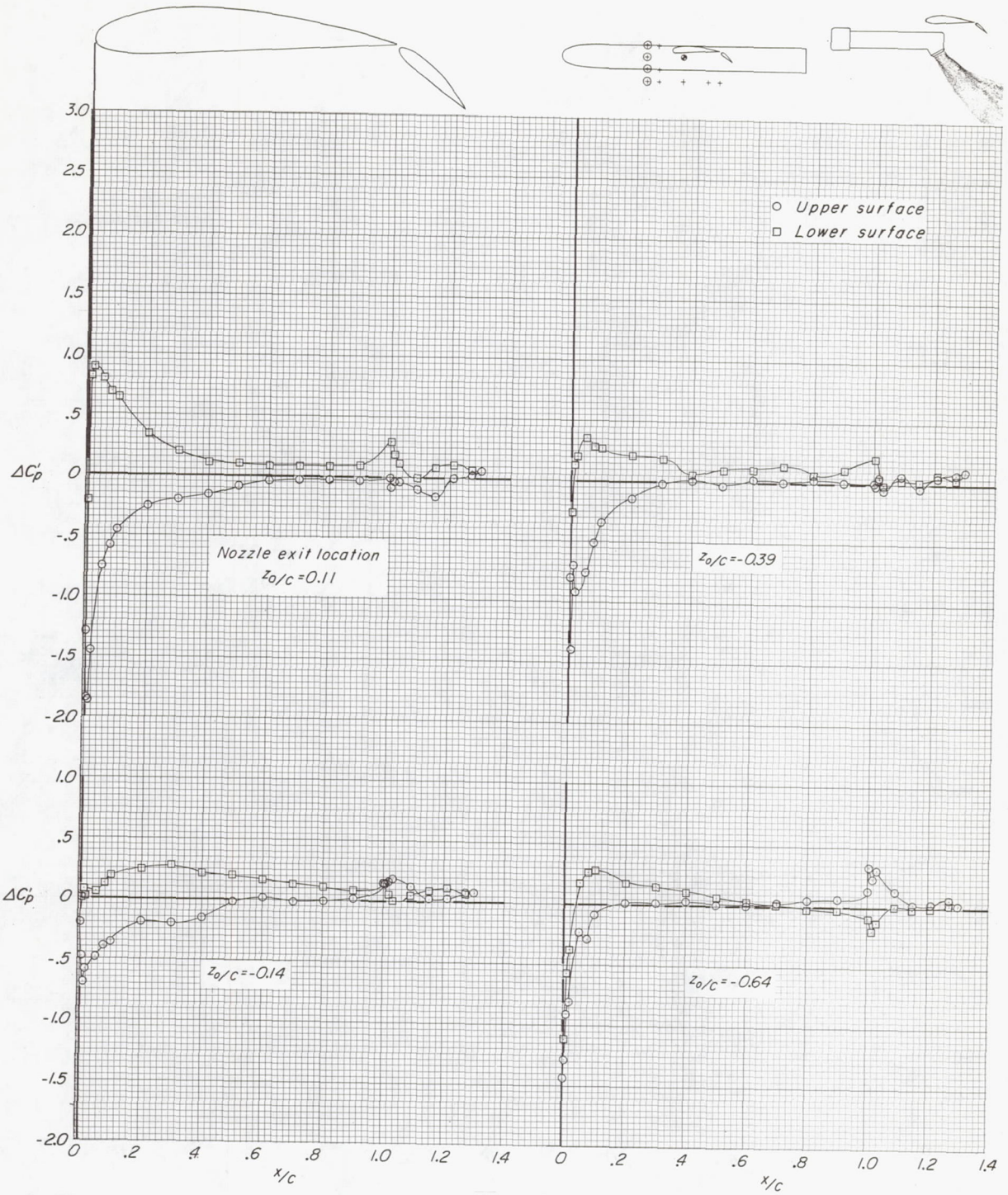

(c) $V_e \approx 0.20$.

Figure 24.- Continued.

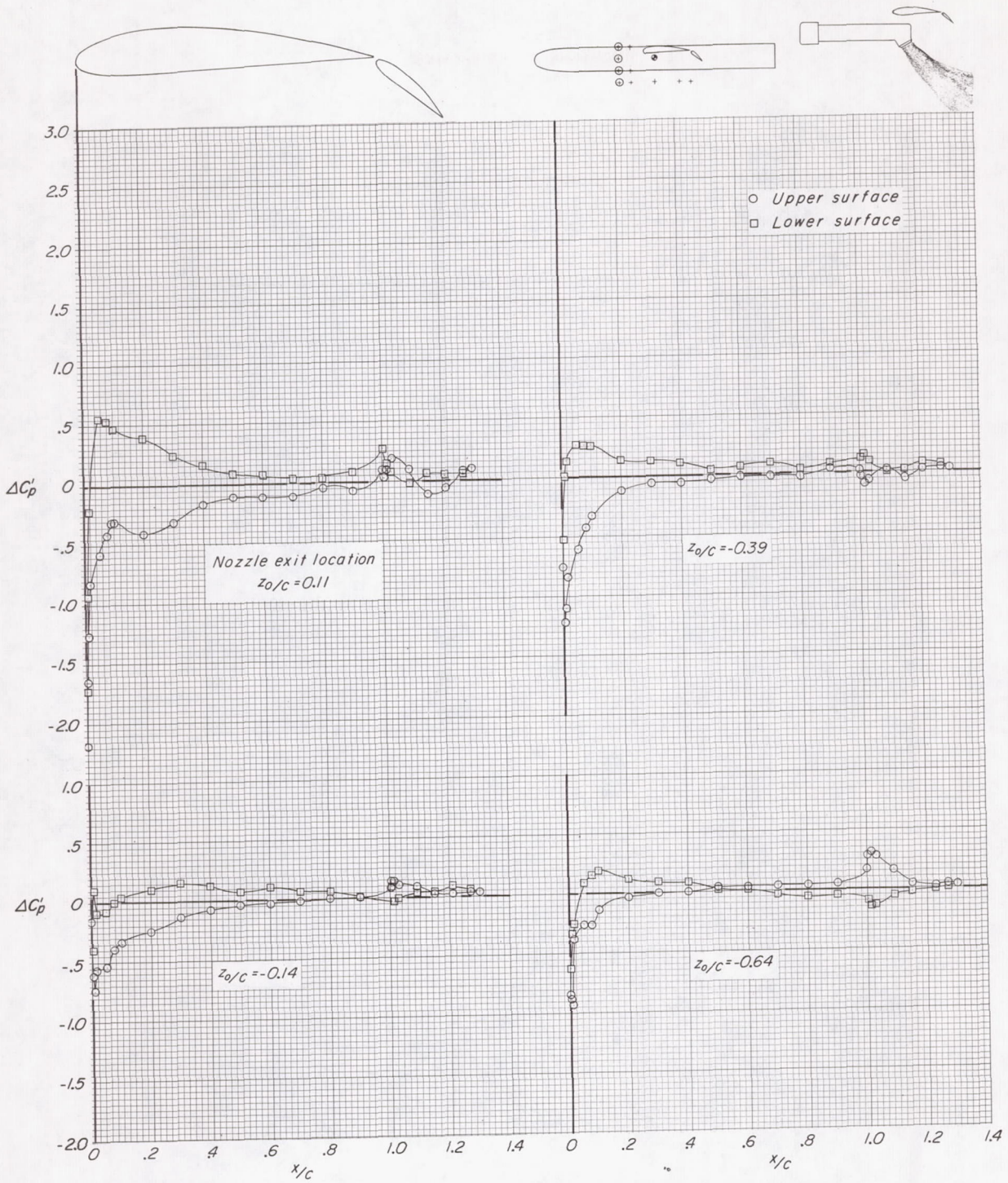

(d) $V_e \approx 0.25$.

Figure 24.- Concluded.

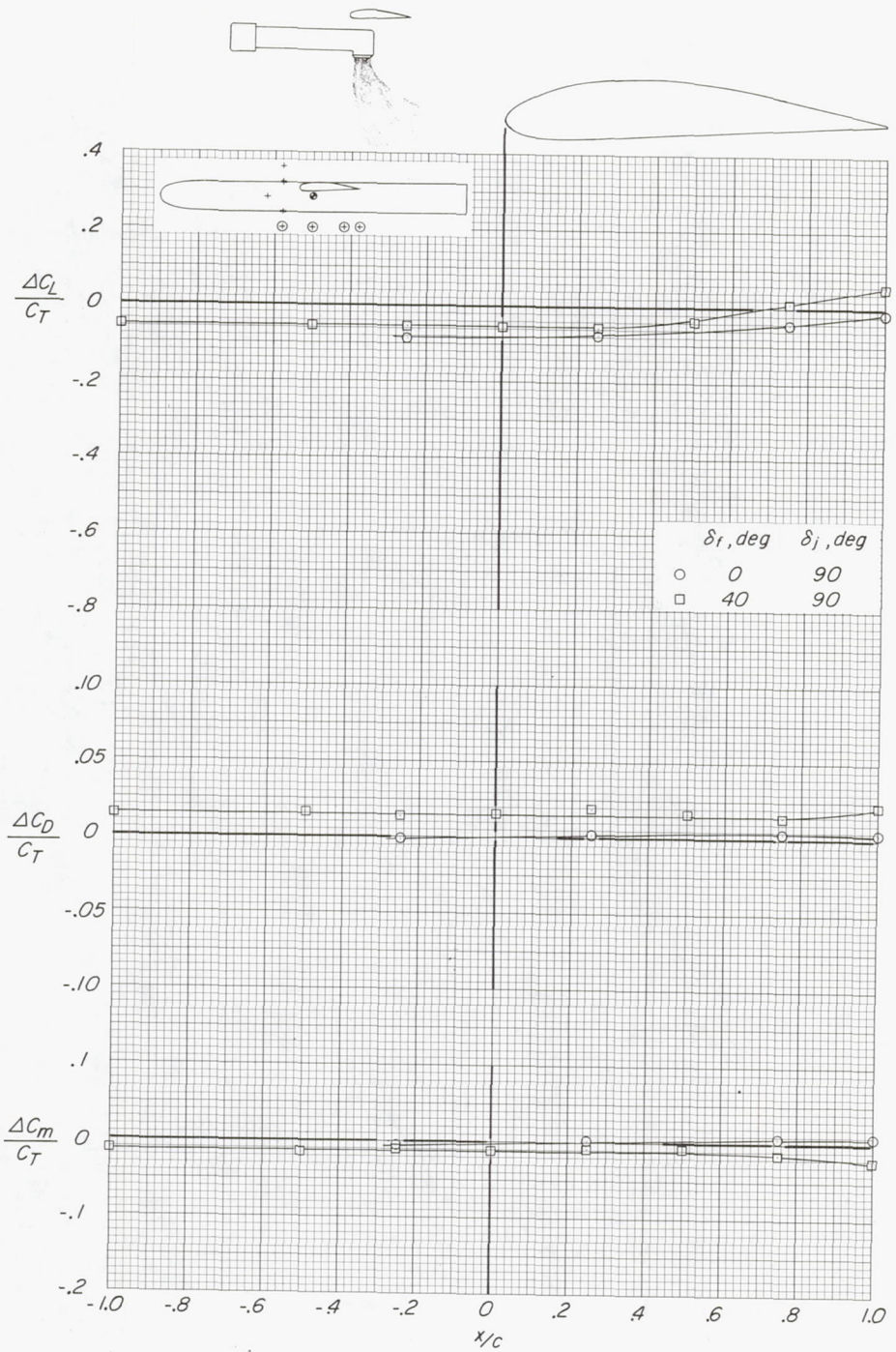

(a) $V_e \approx 0.10$.

Figure 25.- Effect of deflection of wing flaps on the incremental lift, drag, and pitching moment due to power at several longitudinal locations of the jets. $z_0/c = -0.64$.

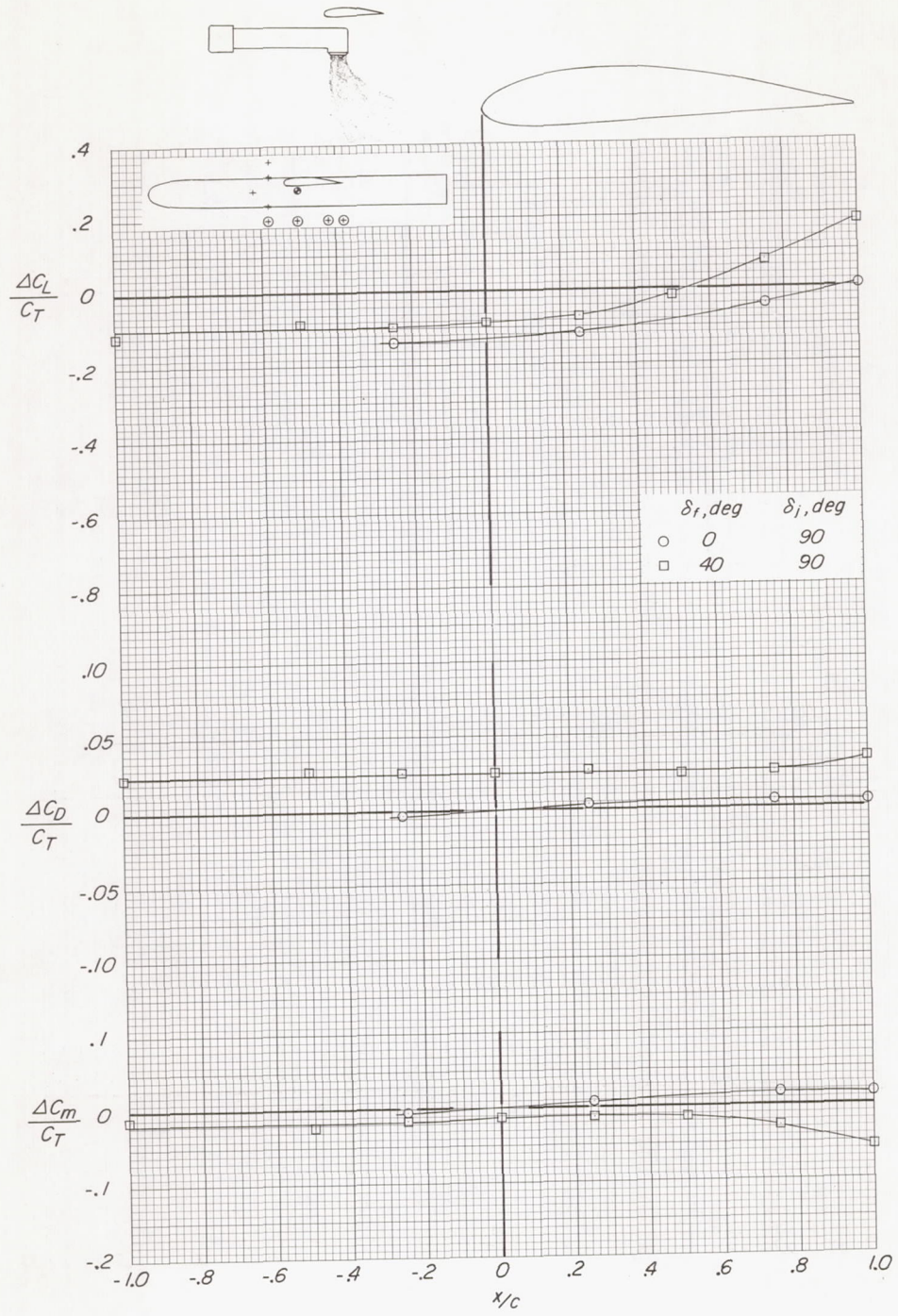

(b) $V_e \approx 0.15$.

Figure 25.- Continued.

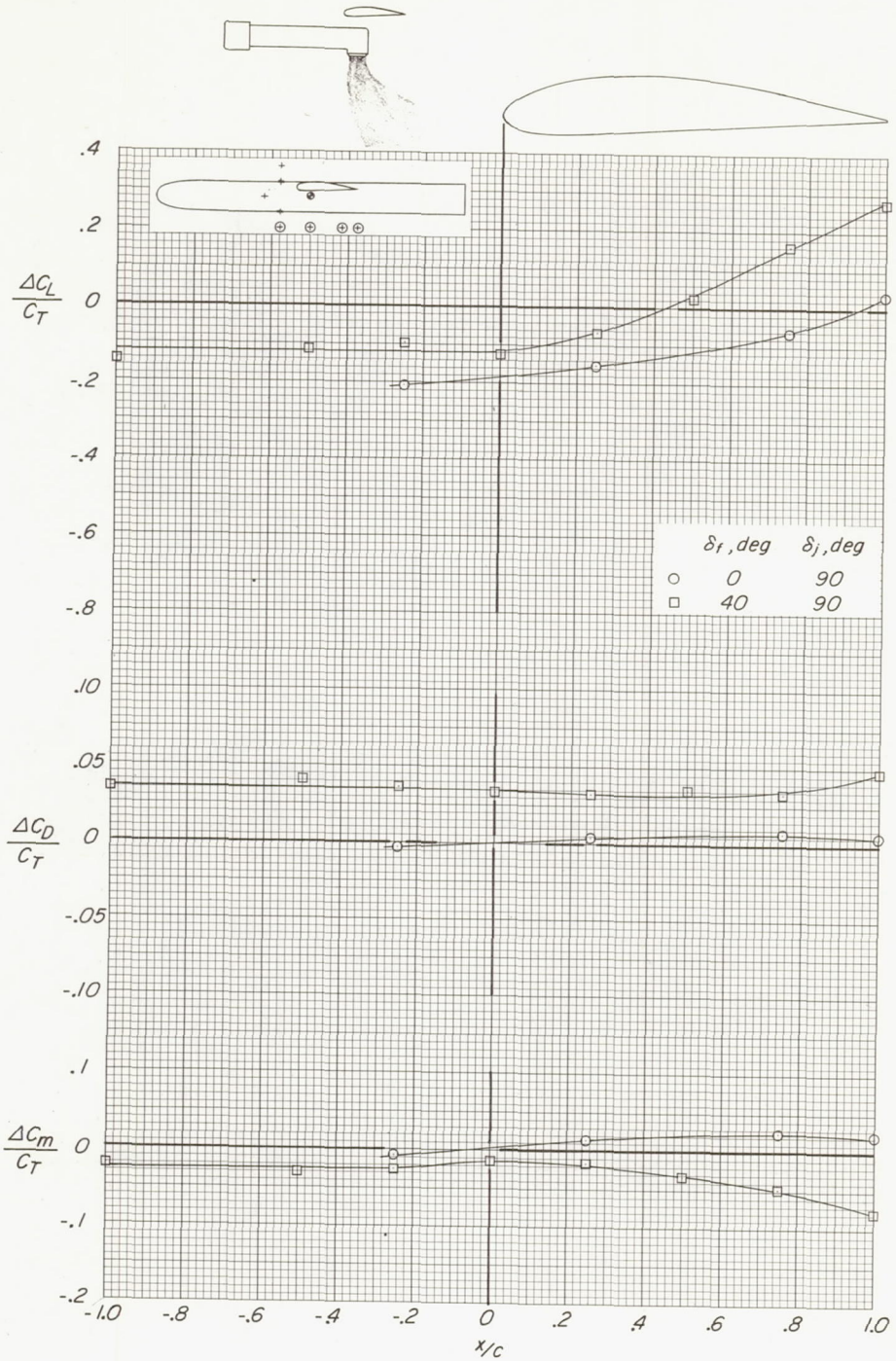

(c) $V_e \approx 0.20$.

Figure 25.- Continued.

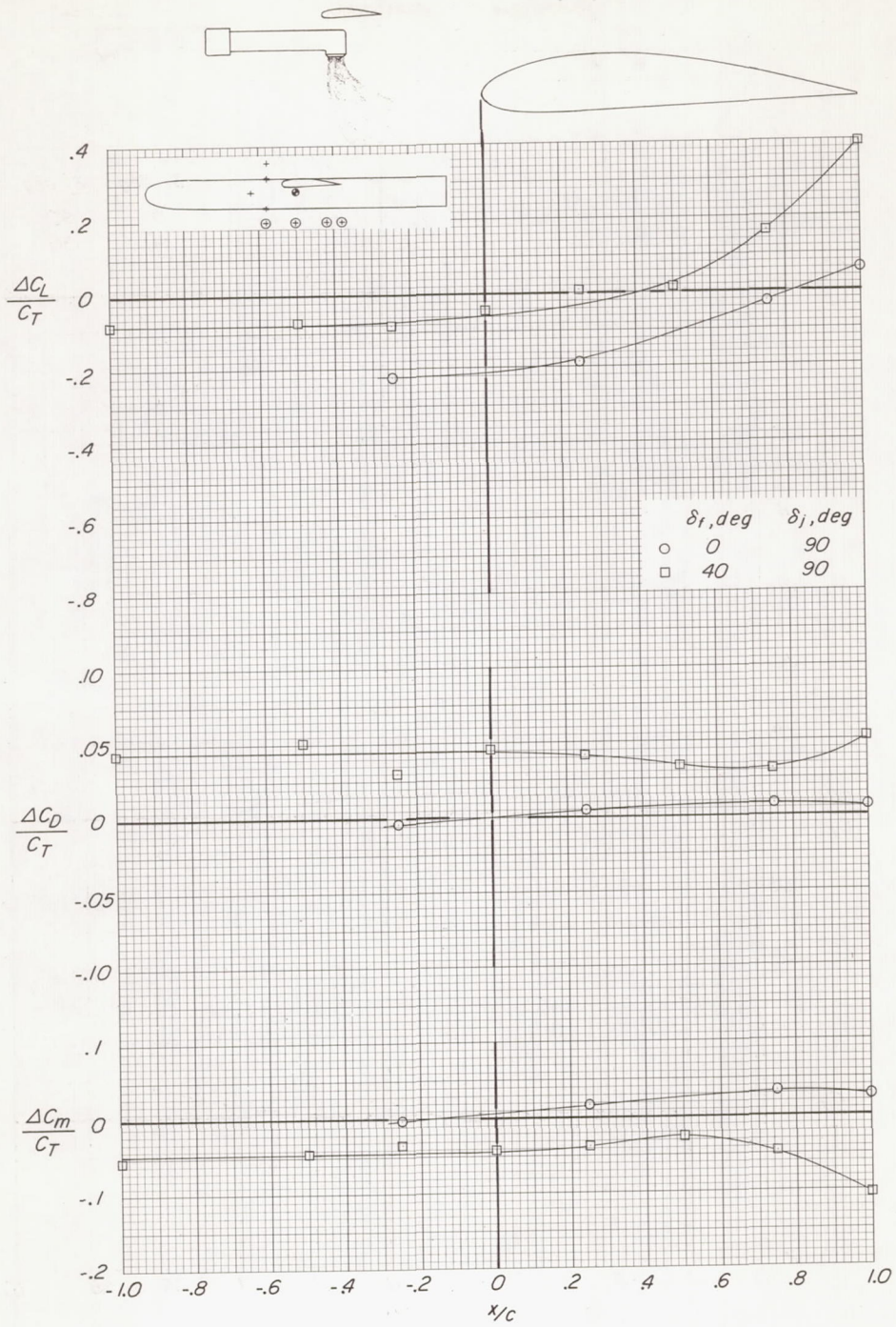

(d) $V_e \approx 0.25$.

Figure 25.- Concluded.

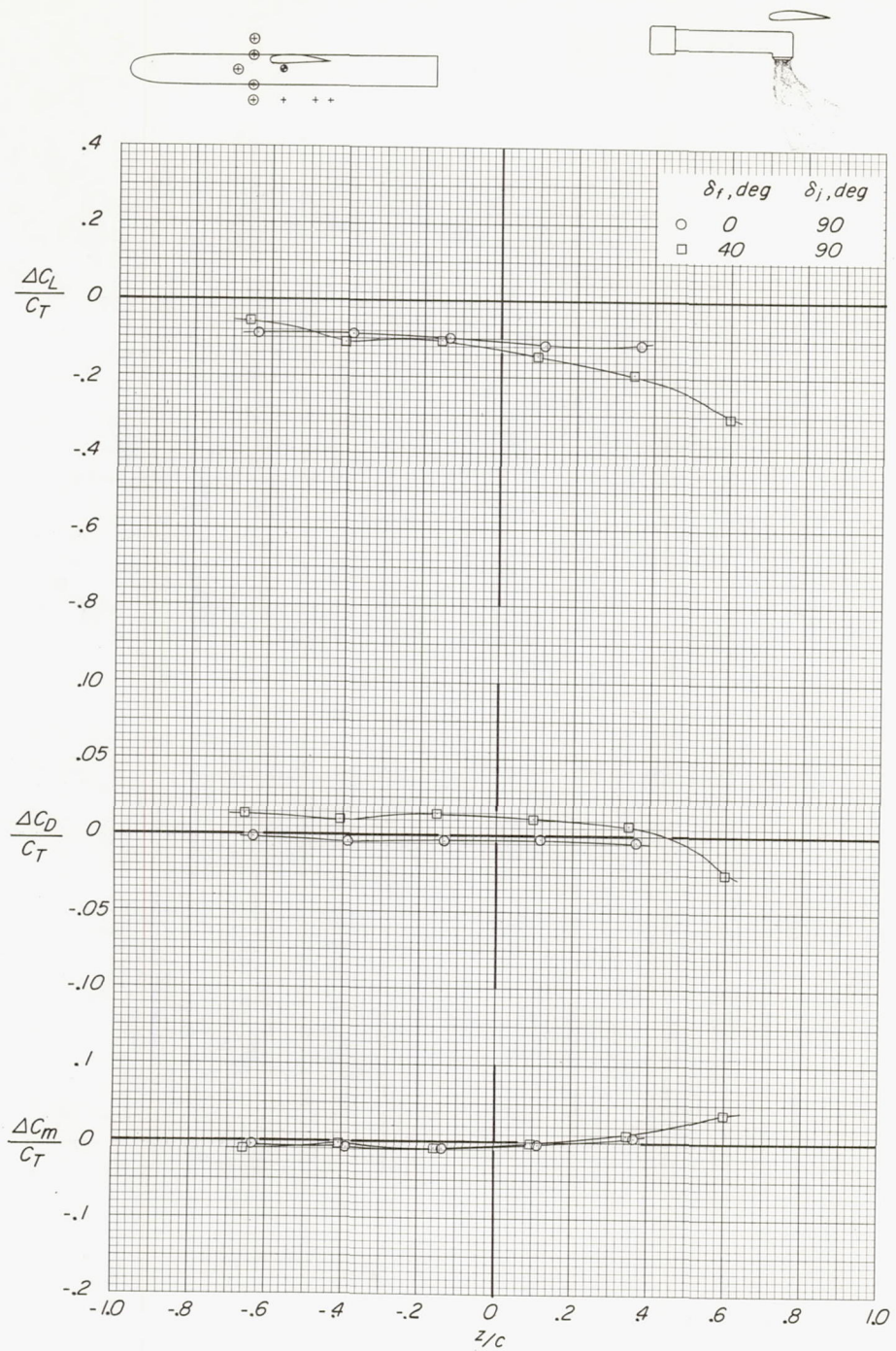

(a) $V_e \approx 0.10$.

Figure 26.- Effect of deflection of wing flaps on the incremental lift, drag, and pitching moment due to power at several vertical locations of the jets. x/c = -0.25.

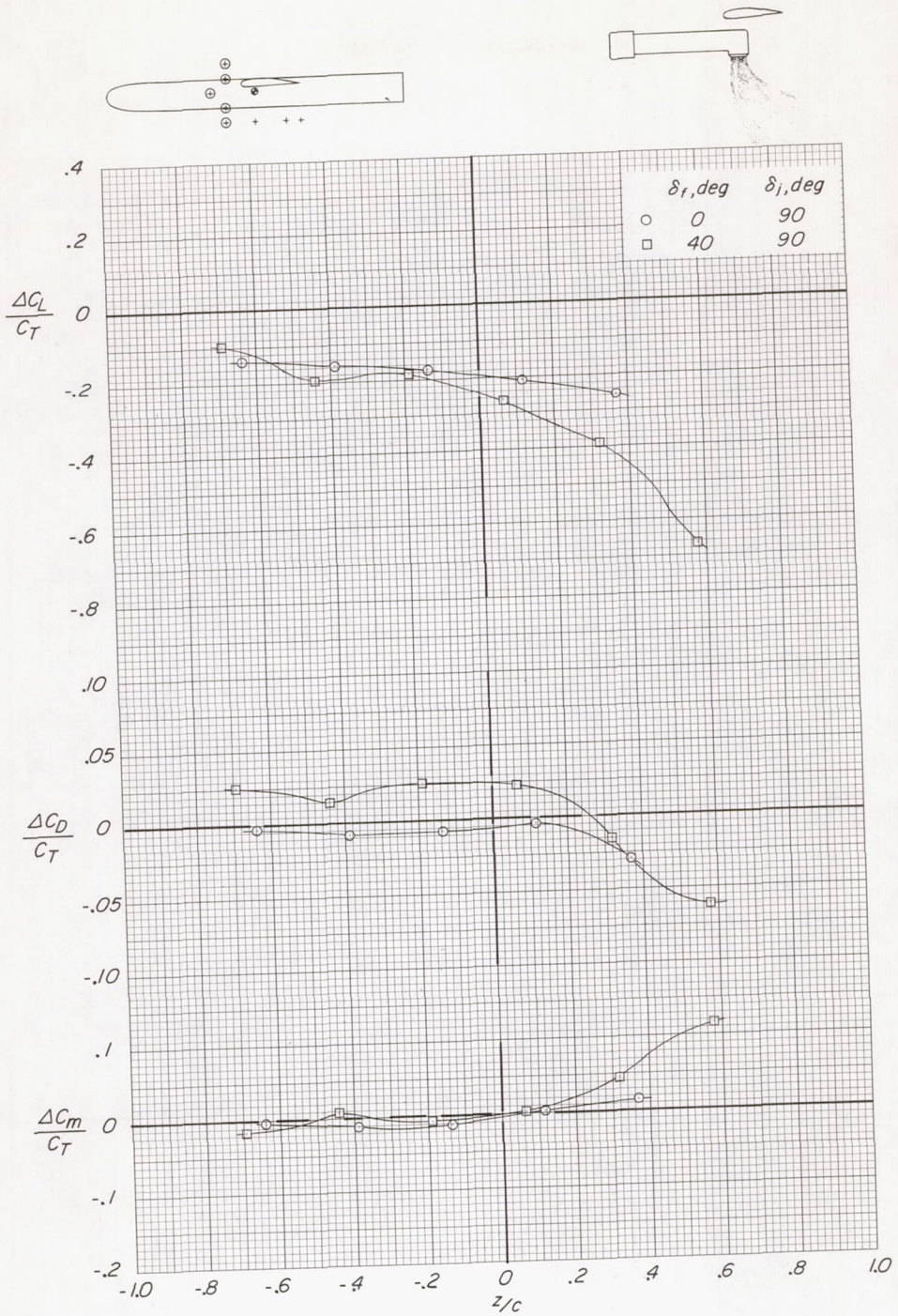

(b) $V_e \approx 0.15$.

Figure 26.- Continued.

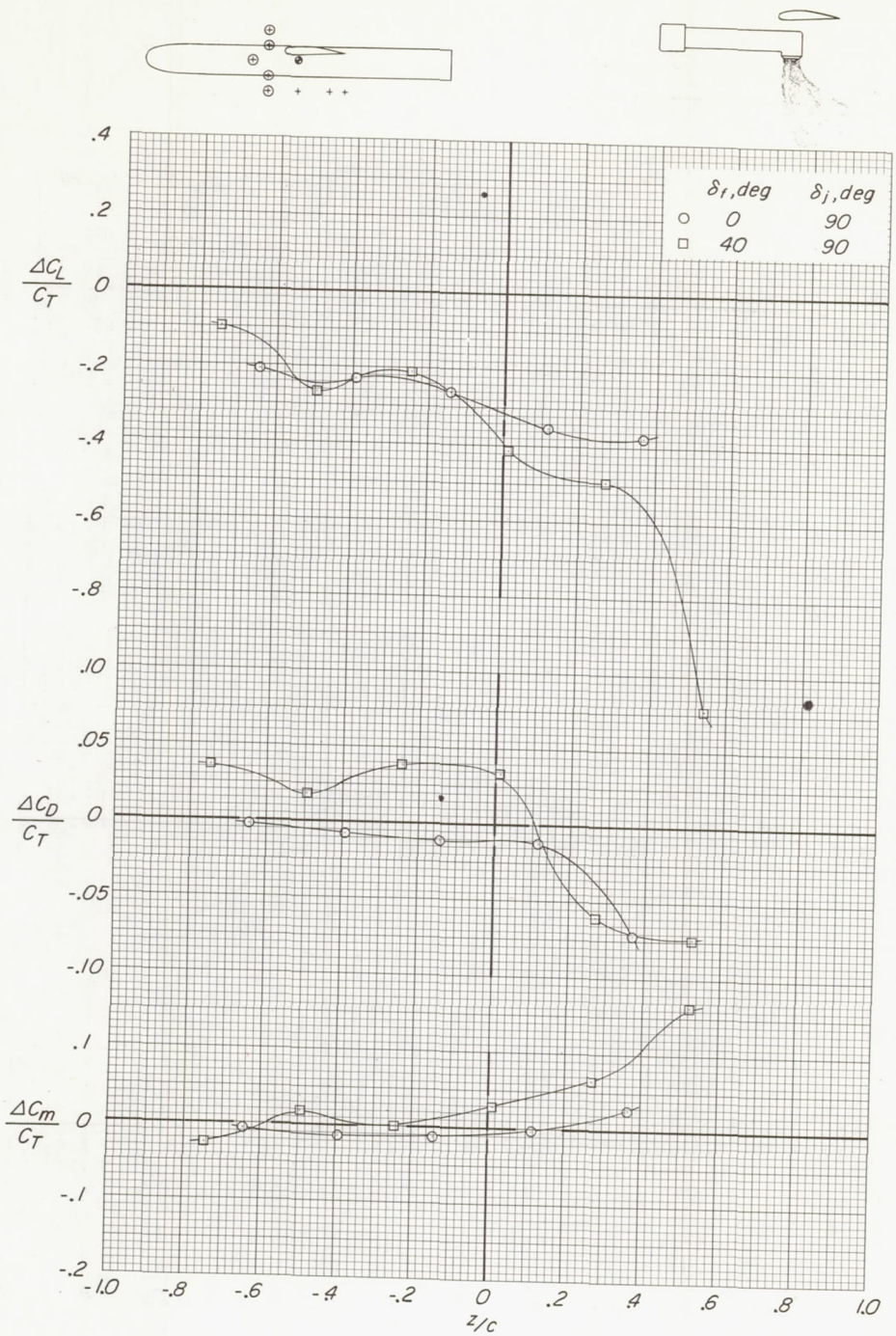

(c) $V_e \approx 0.20$.

Figure 26.- Continued.

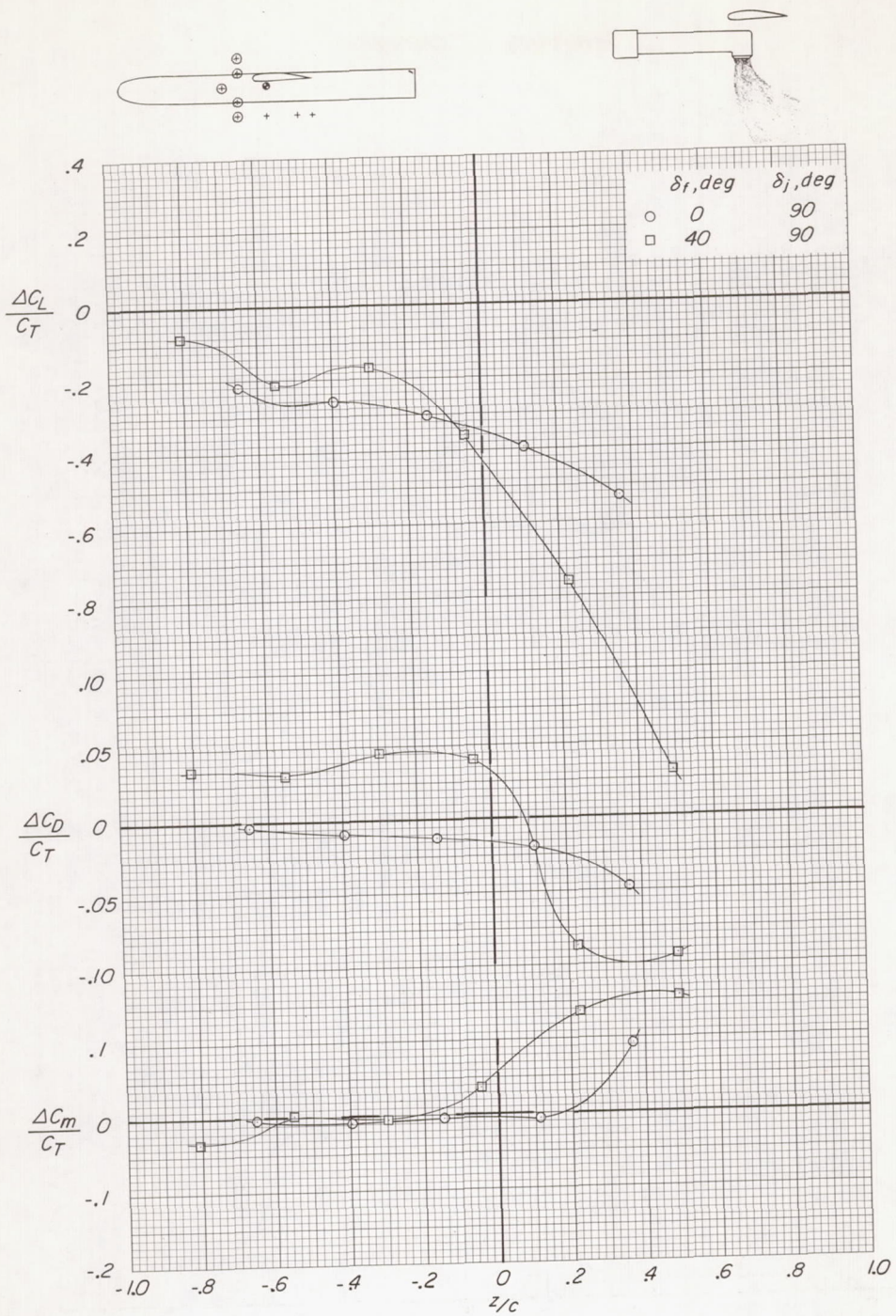

(d) $V_e \approx 0.25$.

Figure 26.- Concluded.

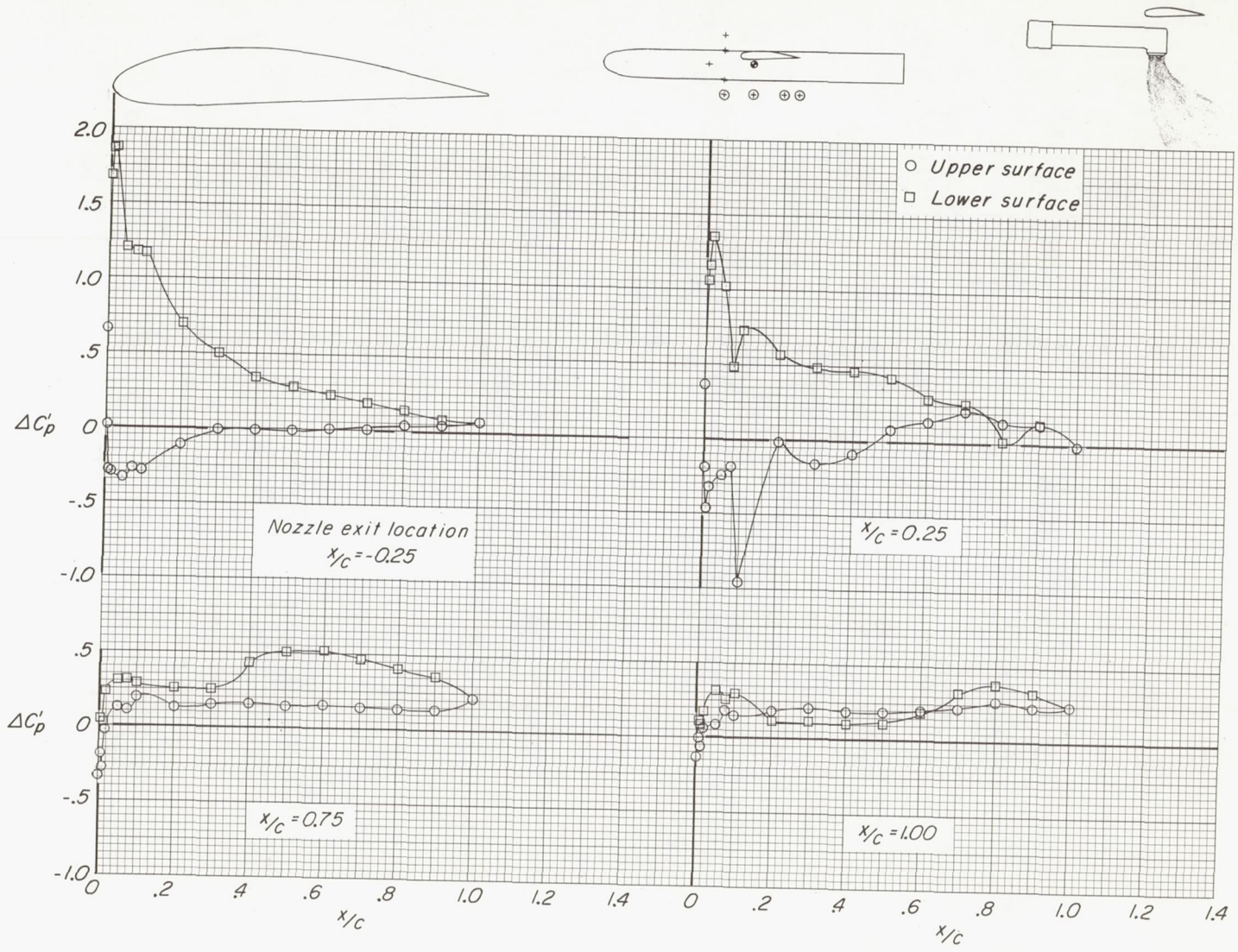

(a) $V_e \approx 0.10$.

Figure 27.- Effect of longitudinal location of the jet exhaust on the incremental upper- and lower-surface pressure distributions due to power. $\delta_f = 0^0$; $\delta_j = 90^0$; $z_0/c = -0.64$.

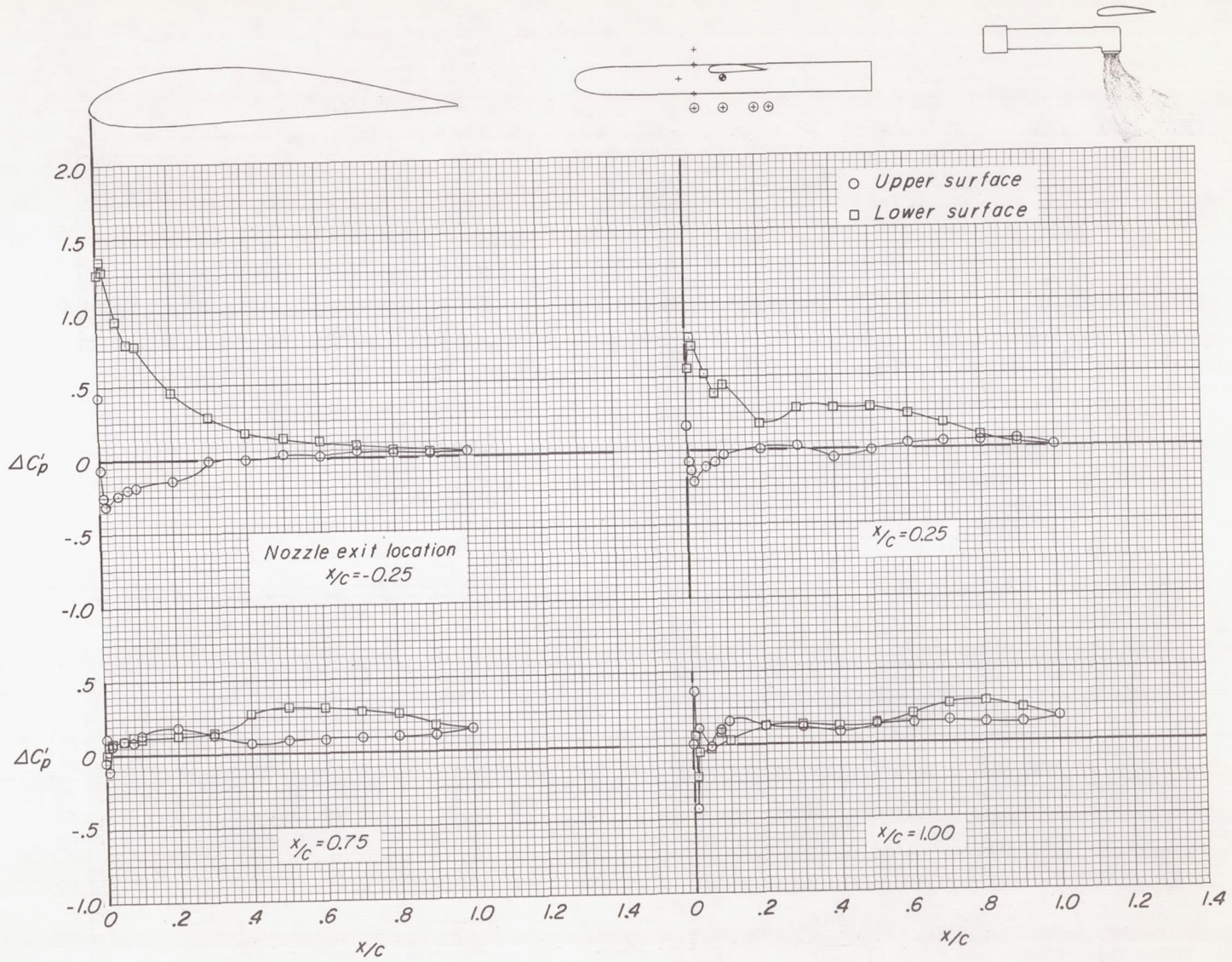

(b) $V_e \approx 0.15$.

Figure 27.- Continued.

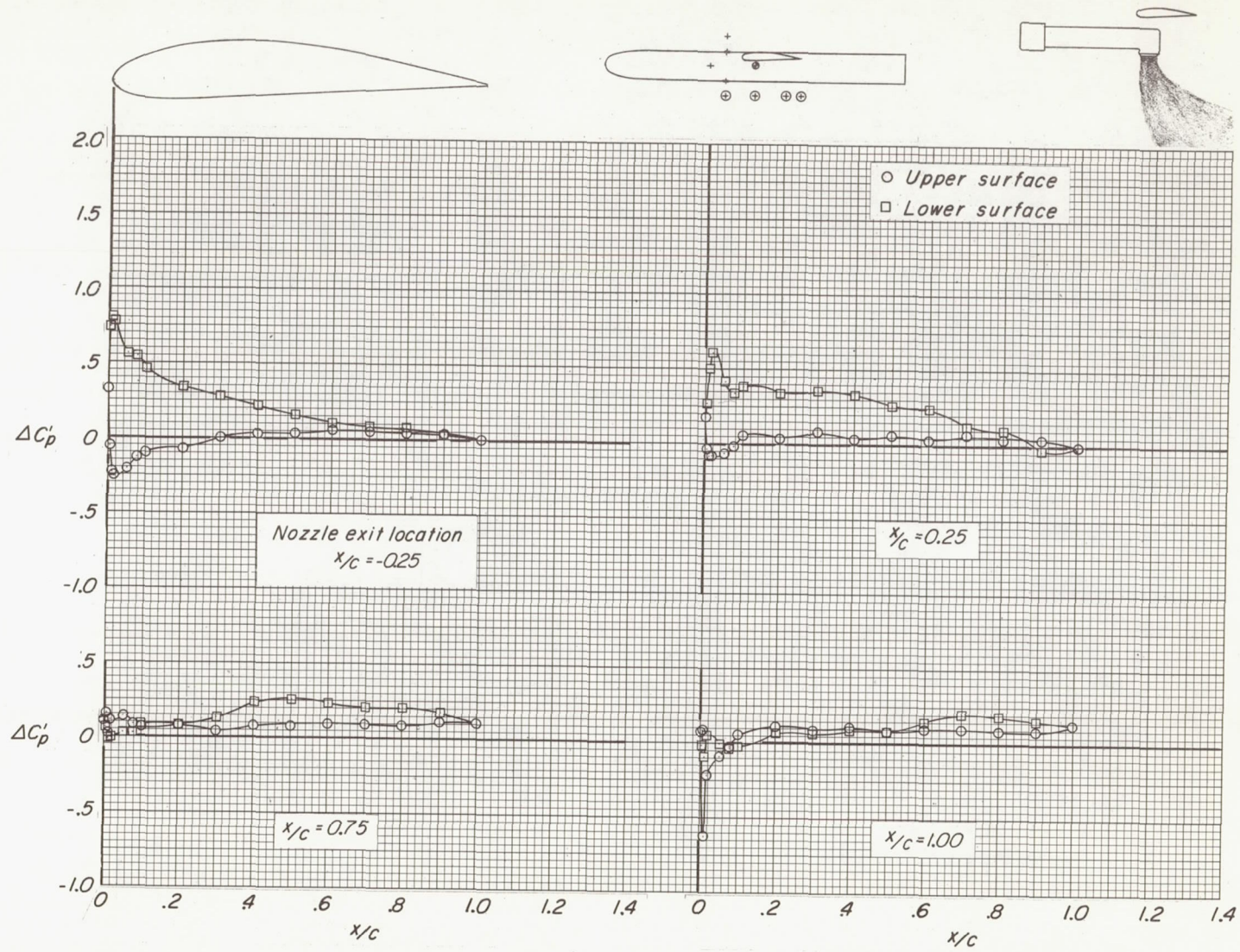

(c) $V_e \approx 0.20$.

Figure 27.- Continued.

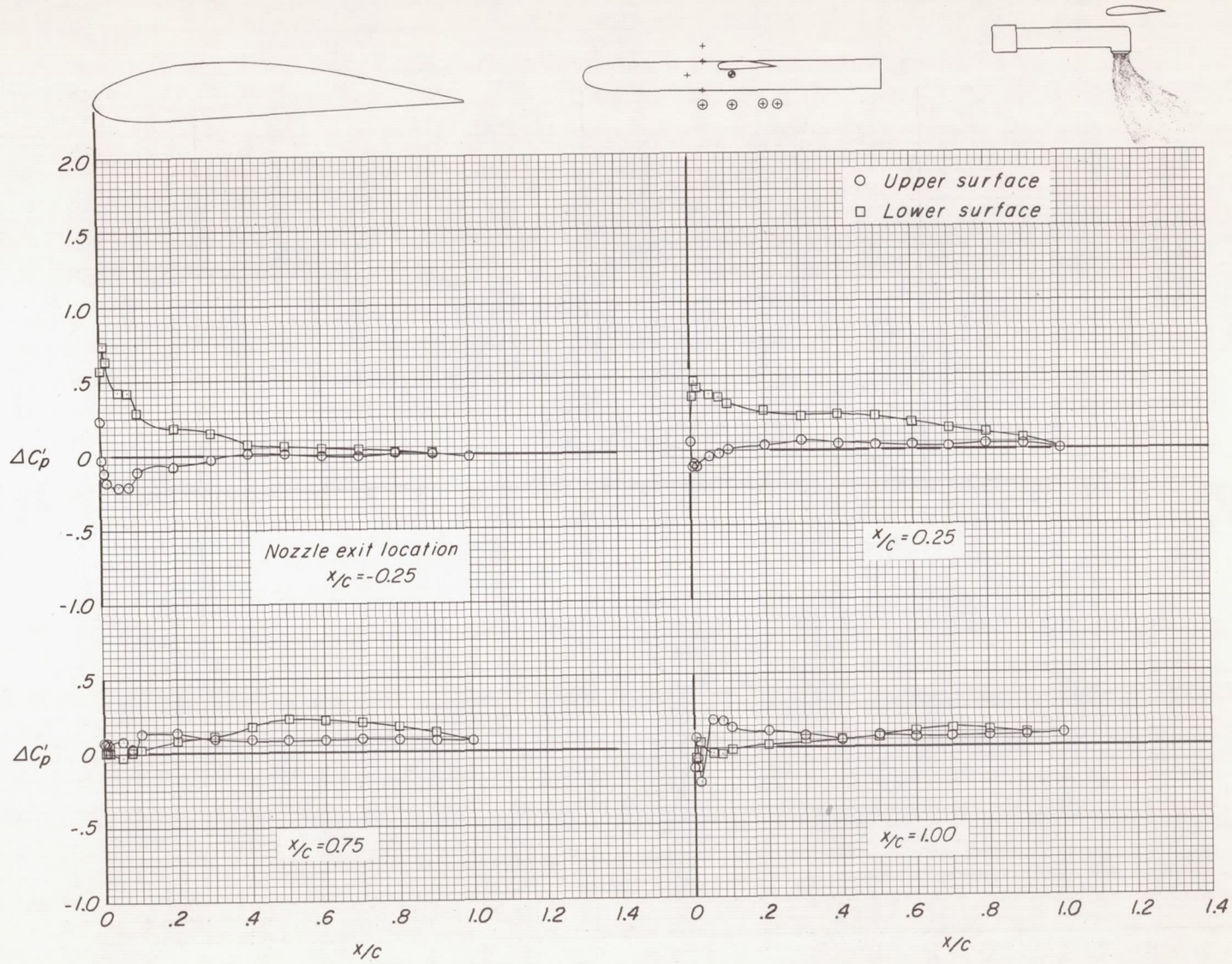

(d) $V_e \approx 0.25$.

Figure 27.- Concluded.

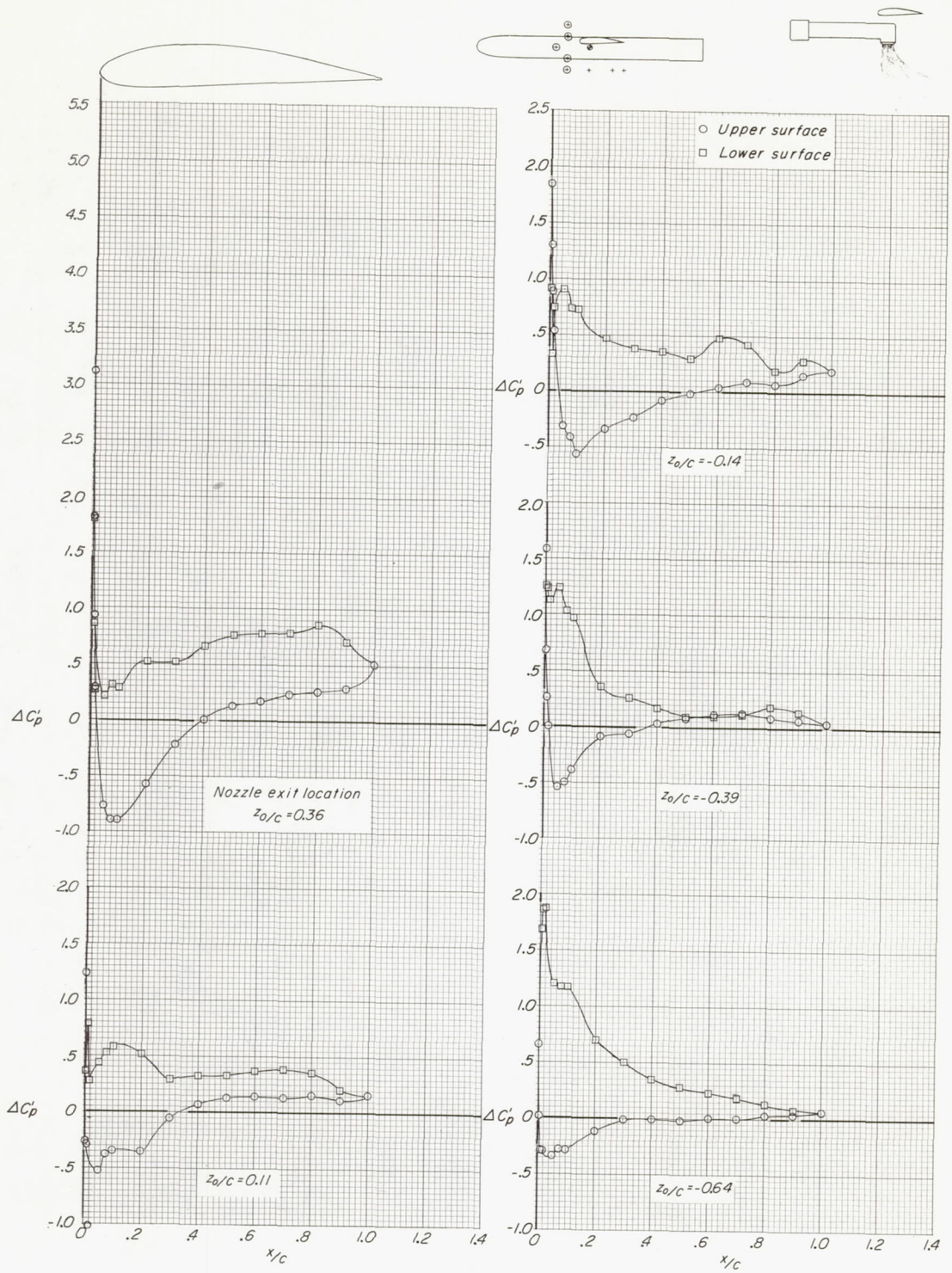

(a) $V_e \approx 0.10$.

Figure 28.- Effect of vertical location of the jet exhaust on the incremental upper- and lower-surface pressure distributions due to power. $\delta_f = 0^0$; $\delta_j = 90^0$; $x/c = -0.25$.

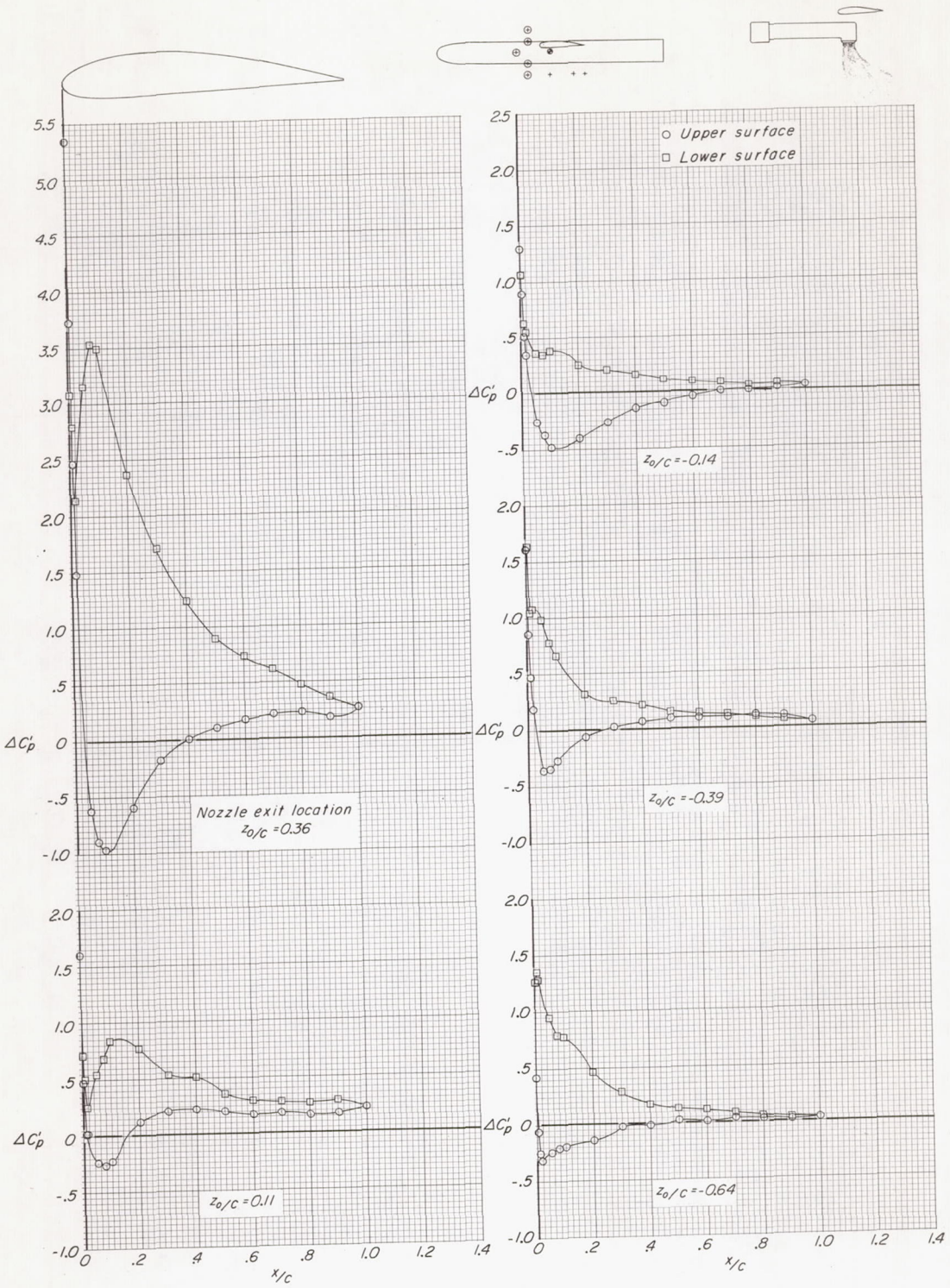

(b) $V_e \approx 0.15$.

Figure 28.- Continued.

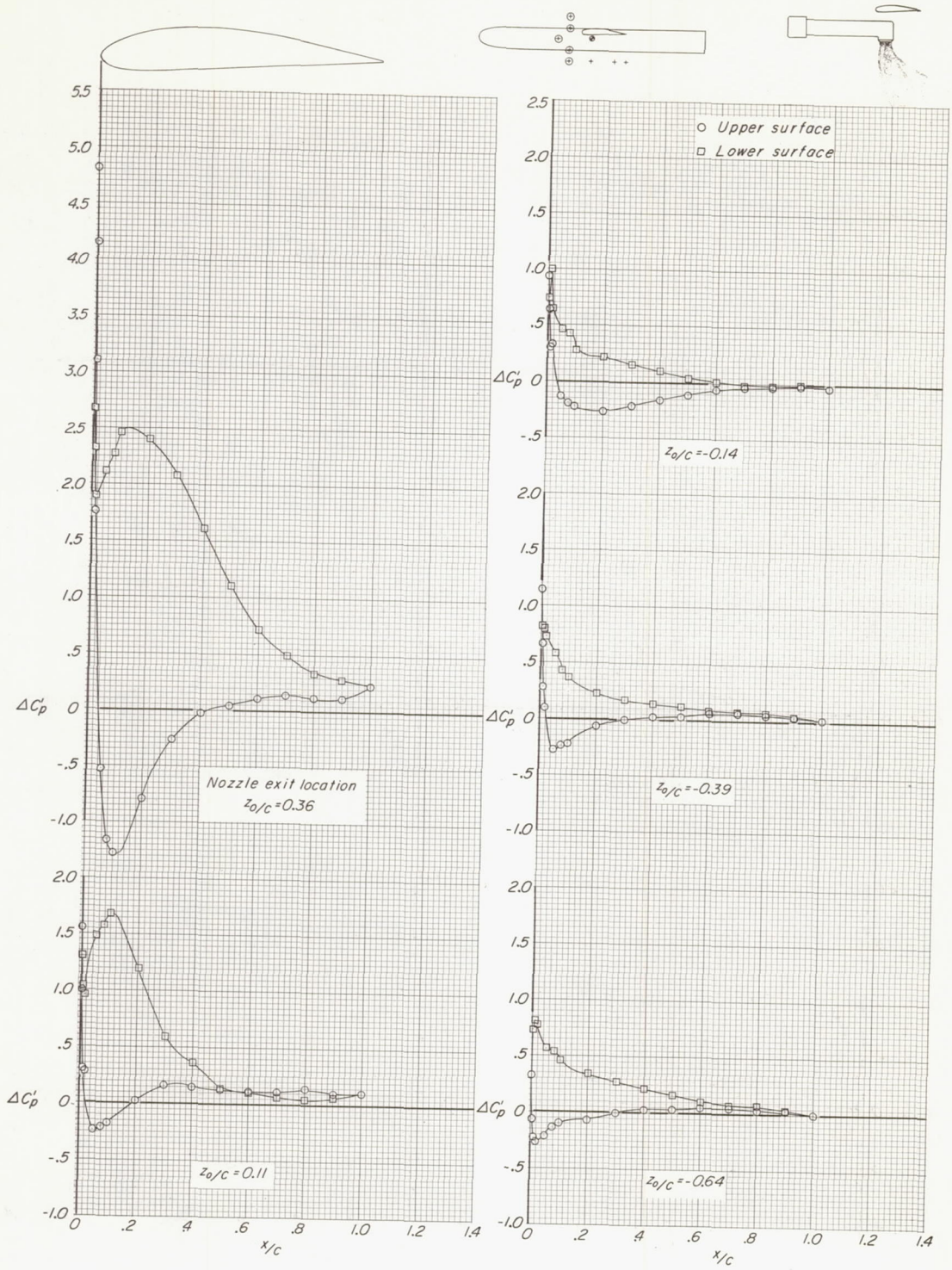

(c) $V_e \approx 0.20$.

Figure 28.- Continued.

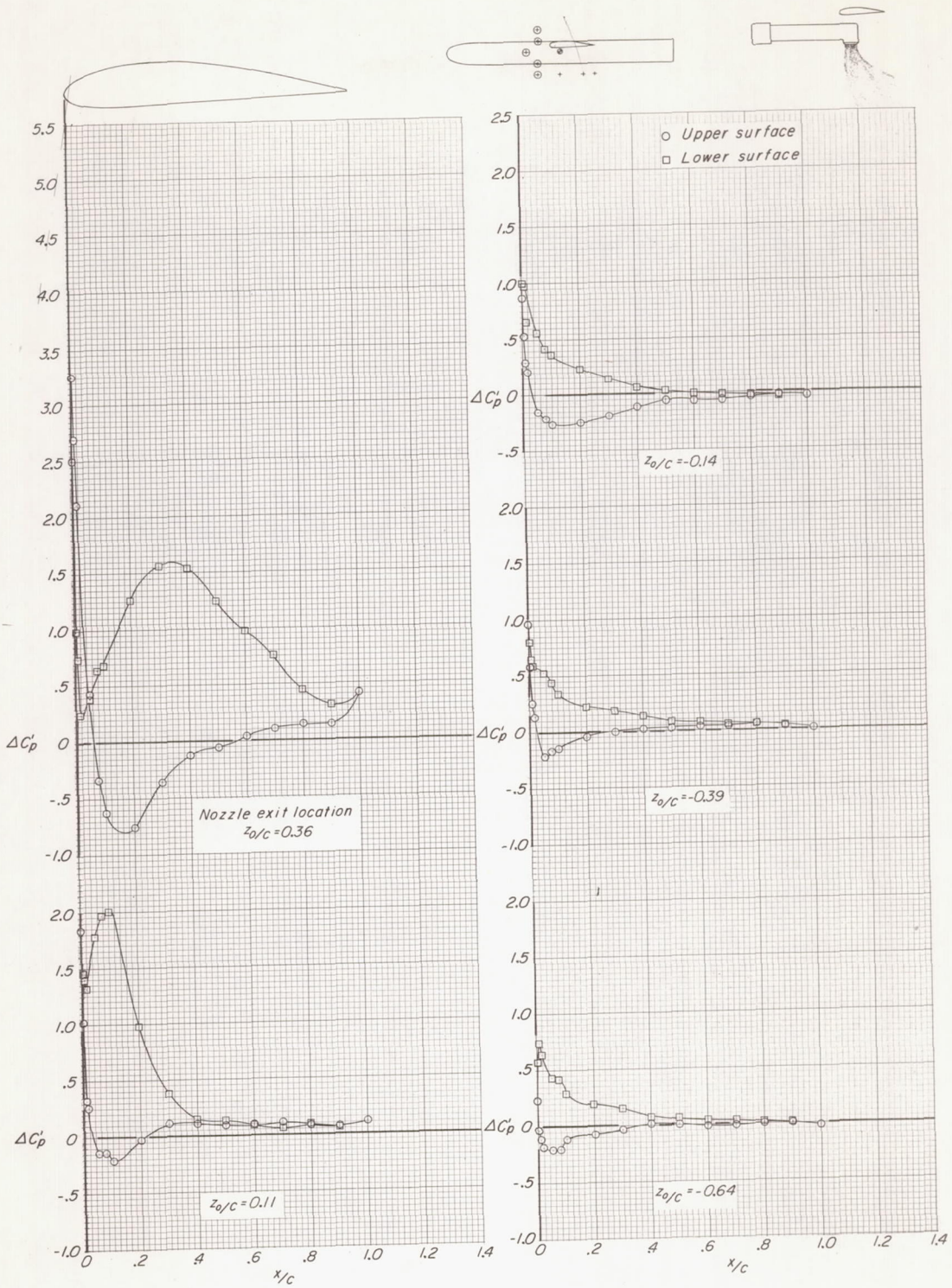

(d) $V_e \approx 0.25$.

Figure 28.- Concluded.

NASA-Langley, 1969 — 1 L-6479